

INFORMATION TO USERS

This manuscript has been reproduced from the microfilm master. UMI films the text directly from the original or copy submitted. Thus, some thesis and dissertation copies are in typewriter face, while others may be from any type of computer printer.

The quality of this reproduction is dependent upon the quality of the copy submitted. Broken or indistinct print, colored or poor quality illustrations and photographs, print bleedthrough, substandard margins, and improper alignment can adversely affect reproduction.

In the unlikely event that the author did not send UMI a complete manuscript and there are missing pages, these will be noted. Also, if unauthorized copyright material had to be removed, a note will indicate the deletion.

Oversize materials (e.g., maps, drawings, charts) are reproduced by sectioning the original, beginning at the upper left-hand corner and continuing from left to right in equal sections with small overlaps.


ProQuest Information and Learning
300 North Zeeb Road, Ann Arbor, MI 48106-1346 USA
800-521-0600

UMI[®]

University of Alberta

Electroacoustic Spectroscopy of
Water-in-Diluted Bitumen Emulsions

by

Alejandro Magual 

A thesis submitted to the Faculty of Graduate Studies and Research in partial

fulfillment of the requirements for the degree of Master of Science

in

Chemical Engineering

Department of Chemical and Materials Engineering

Edmonton, Alberta
Spring 2005



Library and
Archives Canada

Bibliothèque et
Archives Canada

0-494-08136-8

Published Heritage
Branch

Direction du
Patrimoine de l'édition

395 Wellington Street
Ottawa ON K1A 0N4
Canada

395, rue Wellington
Ottawa ON K1A 0N4
Canada

Your file *Votre référence*

ISBN:

Our file *Notre référence*

ISBN:

NOTICE:

The author has granted a non-exclusive license allowing Library and Archives Canada to reproduce, publish, archive, preserve, conserve, communicate to the public by telecommunication or on the Internet, loan, distribute and sell theses worldwide, for commercial or non-commercial purposes, in microform, paper, electronic and/or any other formats.

The author retains copyright ownership and moral rights in this thesis. Neither the thesis nor substantial extracts from it may be printed or otherwise reproduced without the author's permission.

AVIS:

L'auteur a accordé une licence non exclusive permettant à la Bibliothèque et Archives Canada de reproduire, publier, archiver, sauvegarder, conserver, transmettre au public par télécommunication ou par l'Internet, prêter, distribuer et vendre des thèses partout dans le monde, à des fins commerciales ou autres, sur support microforme, papier, électronique et/ou autres formats.

L'auteur conserve la propriété du droit d'auteur et des droits moraux qui protègent cette thèse. Ni la thèse ni des extraits substantiels de celle-ci ne doivent être imprimés ou autrement reproduits sans son autorisation.

In compliance with the Canadian Privacy Act some supporting forms may have been removed from this thesis.

Conformément à la loi canadienne sur la protection de la vie privée, quelques formulaires secondaires ont été enlevés de cette thèse.

While these forms may be included in the document page count, their removal does not represent any loss of content from the thesis.

Bien que ces formulaires aient inclus dans la pagination, il n'y aura aucun contenu manquant.


Canada

Abstract

Water-in-oil emulsions of Athabasca bitumen diluted in toluene have been studied using the latest advances in Acoustic and Electroacoustic Spectroscopy. From the sound attenuation spectra of emulsions, the water droplet size distribution is derived. The electrical surface charge density of the droplets is obtained from the colloid vibration current. In case of freshly prepared water-in-oil emulsions, the water droplet size increases while the surface charge density decreases with time. The time span of this transient behavior ranges from several hours to three days. Such long transients are probably due to the slow adsorption/desorption kinetics of bituminous components at the water-oil interface. This study illuminates the contribution of the electrostatic interactions to the stability of water-in-oil emulsions.

Acknowledgments

The author wishes to thank the many people and institutions which have directly or indirectly contributed to the realization of the present work.

I am particularly grateful to my supervisors Dr. Jacob Masliyah and Dr. Geza Horvath-Szabo for their guidance and invaluable discussions. Financial support received through the NSERC Industrial Research Chair in Oil Sands Engineering is greatly appreciated.

The support from the Machine and Instrument Shop (MIS) from our Department is also greatly appreciated. MIS manufactured a water-jacketed metallic chamber which constituted a significant improvement to the original configuration of the DT-1200 Spectrometer used in the present study.

I want to sincerely thank Dr. Yadollah Maham from our Department for facilitating the use of the density meter.

To the many colleagues and friends in the Oil Sands Group, I want to express my thanks for their encouragement and support. I am particularly grateful to Mr. James Skwarok, Ms. Leanne Swekla, Dr. Li-Yan Zhang and Mr. Robert Lopetinsky for their assistance throughout this thesis. I am also grateful to Ms. AnnMarie Brereton from our Department, for her assistance throughout my Master program.

Finally, I would like to thank Dr. Andrei Dukhin and Dr. Philip Goetz from Dispersion Technology Inc. for their technical assistance on the DT-1200 Acoustic and Electroacoustic Spectrometer.

Table of Contents

1. Introduction	1
2. Literature Review	3
2.1 Water-in-diluted bitumen emulsions in the oil sands industry	3
2.1.1 Origin, composition and industrial importance	3
2.1.2 Bitumen compounds responsible for the emulsion stability	4
2.1.3 Stabilizing mechanism of water-in-diluted bitumen emulsions	5
2.1.4 Experimental evidence for the steric stabilization mechanism	6
2.2 Electrostatic stabilization in nonaqueous media	10
2.2.1 Electrical charges in nonaqueous media	10
2.2.2 Concepts of DLVO Theory	11
2.2.3 Experimental evidence for the electrostatic stabilization in nonaqueous media	14
2.3 Electrokinetic measurements of the electro-surface properties of dispersions	16
2.4 Electroacoustic Spectroscopy	18
2.4.1 The Electroacoustic effects: CVP, CVC and ESA	18
2.4.2 Colloid Vibration Potential (CVP)	19
2.4.3 Colloid Vibration Current (CVC)	20
2.4.4 Electrokinetic Sonic Amplitude (ESA)	21
2.4.5 Theory of Electroacoustics: O'Brien's approach	22
2.4.6 Theory of Electroacoustics: Shilov's approach	29
2.5 Electroacoustic studies relevant to water-in-oil emulsions	34
2.5.1 Study of the coalescence of water-in-crude oil emulsions	34
a) Relation between the CVP signal and water concentration	35

b)	Relation between the CVP signal and water droplets coalescence	36
2.5.2	Study of the electro-surface properties of asphaltenes at toluene-water interfaces	37
2.5.3	Surface charge density measurements in nonaqueous dispersions	39
a)	Alumina dispersion in kerosene	40
b)	Water-in-kerosene emulsions	41
2.6	Acoustic Spectroscopy for particle size characterization	43
2.6.1	Phenomenon of sound attenuation in liquid dispersions	44
2.6.2	Theory of Acoustics for emulsions	45
3.	Experimental	69
3.1	Materials	69
3.2	Equipments	70
3.2.1	DT-1200 Acoustic and Electroacoustic Spectrometer	70
3.2.2	Supplementary equipment	72
3.3	Droplet size distribution measurements	73
3.3.1	Calibration of acoustic spectrometer and sound attenuation measurement	73
3.3.2	Droplet size distribution analysis	74
3.4	Droplet surface charge density measurement	76
3.4.1	Calibration of electroacoustic probe and CVC measurement	76
3.4.2	Droplet surface charge density analysis	78
3.5	Design of experiments	81
3.5.1	Selection of bitumen concentration in toluene	81
3.5.2	Diluted bitumen preparation	83
3.5.3	Emulsion preparation	84

4. Results and Discussion	95
4.1 Material properties	95
4.1.1 Material property measurements	95
4.1.2 Selection of bitumen concentration in toluene	95
4.2 Electroacoustic phenomenon in water-in-diluted bitumen emulsions	96
4.2.1 Design of experiments	97
4.2.2 CVC signal of emulsions: magnitude and transient behavior	98
4.2.3 Equilibrium versus relaxation process	100
4.2.4 Superposition of relaxations	102
4.2.5 CVC signal and the effect of water distribution in the chamber	104
4.2.6 CVC signal and the effect of solids in bitumen	105
4.2.7 CVC signal and the effect of the high speed homogenizer	106
4.2.8 Theoretical considerations	108
4.2.9 CVC and inertia effects	109
4.2.10 Volume fraction dependence of CVC	111
4.3 Surface charge density of water droplets	113
4.4 Droplet size distribution calculation	118
5. Summary and Conclusions	148
6. Recommendations	150
Bibliography	152
Appendix 1: Calculation of the drag coefficient (Kuwabara cell model)	158
Appendix 2: Measurement of diluted bitumen density and thermal expansion	160
Appendix 3: Measurement of diluted bitumen dynamic viscosity	162
Appendix 4: Water droplets sedimentation test data	163
Appendix 5: Measurement of diluted bitumen acoustic properties	167

Appendix 6: Measurement of diluted bitumen electroacoustic properties	174
Appendix 7: Measurements of diluted bitumen electric conductivity	177
Appendix 8: Measurement of heavy water acoustic properties	178

List of Tables

Table 2.1:	Surface potentials to stabilize particles as a function of radius	50
Table 2.2:	Simplified equations for attenuation coefficients	51
Table 3.1:	Summary of emulsion experiments	86
Table 4.1:	Material properties for droplet size distribution and surface charge density calculation	124
Table 4.2:	Super-imposed relaxation data for emulsion B2	125
Table 4.3:	Water distribution in chamber for emulsions B1, B2 and B3	126
Table 4.4:	Water distribution in chamber for emulsion C1	126
Table A2.1:	Diluted bitumen density measurement data (vibrating tube method)	160
Table A2.2:	Diluted bitumen thermal expansion calculation	161
Table A3.1:	Diluted bitumen dynamic viscosity measurement data (Fenske viscometer method)	162
Table A4.1:	Water sedimentation test data of 5% wt. water-in-diluted bitumen emulsions	163
Table A4.2:	Water sedimentation test data of 10% wt. water-in-diluted bitumen emulsions	165
Table A5.1:	Acoustic properties of diluted bitumen	167
Table A5.2:	Acoustic properties data for diluted bitumen stock #1	168
Table A5.3:	Acoustic properties data for diluted bitumen stock #2	171
Table A6.1:	Electroacoustic properties of diluted bitumen	174
Table A6.2:	Electroacoustic properties data for diluted bitumen stock #1	175
Table A6.3:	Electroacoustic properties data for diluted bitumen stock #2	176
Table A7.1:	Diluted bitumen electric conductivity data	177
Table A8.1:	Acoustic properties of heavy water (99% interval of confidence on the mean)	178

List of Figures

Figure 2.1:	Effect of the solvent to bitumen ratio on the emulsion stability	52
Figure 2.2:	Dynamic surface tension measurements for the determination of the kinetics of asphaltene adsorption at toluene-water interfaces	52
Figure 2.3:	Effect of the critical solvent to bitumen ratio on the interfacial film rheology	53
Figure 2.4:	Fowkes mechanism of electrostatic charging in nonaqueous media	54
Figure 2.5:	Interaction potentials for approaching particles	54
Figure 2.6:	Representation of the electrical double layer	55
Figure 2.7:	Potential energy of interaction for bitumen-in-water emulsions in the presence of NaCl and CaCl ₂	56
Figure 2.8:	Double layer distortion due to relaxation effect	56
Figure 2.9:	Alternating polarization of the electric double layer created by an acoustic wave	57
Figure 2.10:	Double layer polarization due to the relative liquid flow	57
Figure 2.11:	The definition of the dynamic electrophoretic mobility	58
Figure 2.12:	Magnitude and phase angle of inertia factor G according to O'Brien's approach	58
Figure 2.13:	Estimate of the minimum volume fraction for double layer overlap	59
Figure 2.14:	Effect of sonication time on the CVP signal for a 10% water-in-Leduc crude oil emulsion	60
Figure 2.15:	Sensitivity of CVP signal to water content in water-in-Leduc crude oil emulsions	60
Figure 2.16:	The change in CVP signal in the presence and absence of the addition of 100 ppm chemical at 4 min	61
Figure 2.17:	Sensitivity of the CVP signal to the coagulation process.	61
Figure 2.18:	Comparison of the coagulation process as determined by electroacoustic analysis and centrifugation tests	62

Figure 2.19:	Interfacial tension between a 100 ppm asphaltenes-in-toluene solution and water as a function of pH at 22 °C.	63
Figure 2.20:	ESA signal of toluene-in-water/SLS/CA emulsions, as a function of pH and asphaltene content	63
Figure 2.21:	Conductivity of alumina dispersion as a function of SPAN 80 content	64
Figure 2.22:	Surface charge density of alumina dispersion	64
Figure 2.23:	Evolution of the droplet size distribution of water-in-kerosene emulsions in time	65
Figure 2.24:	Evolution of the conductivity and surface charge density of water-in-kerosene emulsions in time	66
Figure 2.25:	Double layer restructuring due to the ion exchange between interior and exterior of the water droplet	67
Figure 2.26:	Representation of the propagation of compressional waves in a dispersion	68
Figure 3.1:	DT-1200 Acoustic and Electroacoustic Spectrometer	87
Figure 3.2:	Details of the chamber after equipment improvements	88
Figure 3.3:	DT-1200 with new water-jacketed metallic chamber for temperature control	89
Figure 3.4:	Installation of conductivity meter probe	90
Figure 3.5:	PowerGen high speed homogenizer	90
Figure 3.6:	Homogenizer probe component parts	91
Figure 3.7:	Density log-normal particle size distribution	92
Figure 3.8:	Cumulative log-normal particle size distribution	92
Figure 3.9:	Diagram of the electroacoustic probe for measuring CVC	93
Figure 3.10:	Determination of the percentage of settled water droplets in sedimentation tests	94
Figure 4.1:	Density of diluted bitumen as a function of bitumen concentration	127

Figure 4.2:	Thermal expansion of diluted bitumen as a function of bitumen concentration at 20 °C	127
Figure 4.3:	Dynamic viscosity of diluted bitumen as a function of bitumen concentration at 20 °C	128
Figure 4.4:	Percentage of settled water droplets after 24 hours at 20 °C	128
Figure 4.5:	Intrinsic attenuation coefficient of diluted bitumen (50% wt) and heavy water	129
Figure 4.6:	Conductivity of diluted bitumen (50% wt) at 20 °C	129
Figure 4.7:	Dependence of CVC on the method of water dispersion in diluted bitumen	130
Figure 4.8:	Transient behavior of CVC	131
Figure 4.9:	Emulsion B1 – 10% wt. water (no water redispersion)	132
Figure 4.10:	Emulsion B2 – 10% wt. water (3 water redispersions)	133
Figure 4.11:	Emulsion B3 – 10% wt. water (repetition experiment B2)	134
Figure 4.12:	Effect of the high speed homogenizer on diluted bitumen	135
Figure 4.13:	Emulsion C1 – 30% wt. water (water distribution without applying the high speed homogenizer)	136
Figure 4.14:	Emulsion B1 – 10% wt. water (CVC signal phase according to measurements)	137
Figure 4.15:	Emulsion B1 – 10% wt. water (CVC signal phase considering absolute value)	137
Figure 4.16:	Volume fraction dependence of CVC (2% to 30% wt. water emulsions)	138
Figure 4.17:	Emulsion D – 2% wt. water	139
Figure 4.18:	Emulsion D – 10% wt. (after water addition)	139
Figure 4.19:	Emulsion E – 20% wt. (no water redispersion)	140
Figure 4.20:	Droplet surface charge density calculation for emulsions B1, B2 and E	141

Figure 4.21:	μ_d/σ ratio as a function of droplet diameter, calculated from Shilov's theory for a 10% wt. emulsion	142
Figure 4.22:	Microscope observation of 10% wt. water emulsion after water dispersion with the high speed homogenizer	143
Figure 4.23:	Emulsion B1 – 10% wt. water (acoustic attenuation spectrum in time)	144
Figure 4.24:	Emulsion E – 20% wt. water (acoustic attenuation spectrum in time)	145
Figure 4.25:	Emulsion B2 – 10% wt. water (acoustic attenuation spectrum in time)	146
Figure 4.26:	Emulsion B1 – 10% wt. water (effect of high speed homogenizer on erratic behavior of acoustic spectrum at higher frequencies)	147

List of Symbols

a	particle or droplet radius (m)
\tilde{a}	normalized parameter (dimensionless), Kuwabara cell model
b	cell radius (m), Kuwabara cell model
\tilde{b}	normalized parameter (dimensionless), Kuwabara cell model
c_m	sound speed of liquid medium ($\text{m}\cdot\text{s}^{-1}$)
c_p	sound speed of particle or droplet ($\text{m}\cdot\text{s}^{-1}$)
c_s	sound speed of dispersion ($\text{m}\cdot\text{s}^{-1}$)
$(c_p)_m$	specific heat of liquid medium ($\text{J}\cdot\text{kg}^{-1}\cdot\text{K}^{-1}$)
$(c_p)_p$	specific heat of particle or droplet ($\text{J}\cdot\text{kg}^{-1}\cdot\text{K}^{-1}$)
C_{ant}	calibration constant electroacoustic probe
CVC	CVC signal of dispersion after background subtraction
$\text{CVC}_{\text{background}}$	CVC signal of liquid medium
$\text{CVC}_{\text{measured}}$	CVC signal of dispersion before background subtraction
$\langle\text{CVC}\rangle$	CVC normalized signal ($\text{A}\cdot\text{m}\cdot\text{Pa}^{-1}$)
$\langle\text{CVP}\rangle$	CVP normalized signal ($\text{V}\cdot\text{s}\cdot\text{m}^{-1}$ or $\text{V}\cdot\text{m}\cdot\text{Pa}^{-1}$)
d	interparticle distance (m)
d_{L_n}	mean diameter (m)
D_{eff}	diffusion coefficient of charge carriers in liquid medium ($\text{m}^2\cdot\text{s}^{-1}$)
D_u	Dukhin number (dimensionless)
e	elementary charge ($1.602\cdot 10^{-19}$ C)
$\langle\text{ESA}\rangle$	ESA normalized signal ($\text{Pa}\cdot\text{m}\cdot\text{V}^{-1}$)
f	electrodynamic factor of μ_d (dimensionless)
F	Faraday constant ($9.648\cdot 10^4$ C $\cdot\text{mol}^{-1}$)
G	inertia factor of μ_d (dimensionless)
$h_1(x)$	special function Kuwabara cell model
$h_2(x)$	special function Kuwabara cell model
i	complex number
I_{ini}	initial sound intensity ($\text{W}\cdot\text{m}^{-2}$)

I_{end}	sound intensity after traveling a distance L in the dispersion ($W \cdot m^{-2}$)
$I(x)$	special function Kuwabara cell model
$I_1(x)$	special function Kuwabara cell model
$I_2(x)$	special function Kuwabara cell model
k	Boltzmann constant ($1.381 \cdot 10^{-23} J \cdot K^{-1}$)
K^*	complex conductivity of the suspension ($S \cdot m^{-1}$)
K_m	conductivity of liquid medium ($S \cdot m^{-1}$)
K_p	conductivity of particle or droplet ($S \cdot m^{-1}$)
K^S	surface conductivity
n	integer number
$n_{i\infty}$	ionic number concentration of the i th species in the bulk solution (m^{-3})
N	number of ionic species (dimensionless)
P	pressure amplitude of the acoustic perturbation in the dispersion (Pa)
P_{ant}	pressure amplitude of the acoustic perturbation in the center electrode (Pa)
$q_r(X)$	density lognormal particle size distribution function
$Q_r(X)$	cumulative lognormal particle size distribution function
Q_1, Q_2	constants
r	particle radius (μm)
R	gas constant ($8.314 J \cdot K^{-1} \cdot mol^{-1}$)
S/B	solvent to bitumen ratio (dimensionless, weight basis)
T	temperature (K)
X	particle (or droplet) diameter in size distribution formula (m)
z_i	valency of the i th ionic species
Z	acoustic impedance of the dispersion ($Pa \cdot s \cdot m^{-1}$)
Z_{ant}	acoustic impedance of the center electrode ($Pa \cdot s \cdot m^{-1}$)
α	relative hydrodynamic frequency, ω/ω_{hd} (dimensionless)
α	total attenuation coefficient of dispersion ($dB \cdot cm^{-1} \cdot MHz^{-1}$)
$\alpha_{colloid}$	excess attenuation coefficient of dispersion ($dB \cdot cm^{-1} \cdot MHz^{-1}$)
α_{int}	intrinsic loss attenuation coefficient of dispersion ($dB \cdot cm^{-1} \cdot MHz^{-1}$)
$(\alpha_{int})_m$	intrinsic loss attenuation coefficient of liquid medium ($dB \cdot cm^{-1} \cdot MHz^{-1}$)
$(\alpha_{int})_p$	intrinsic loss attenuation coefficient of particle or droplet ($dB \cdot cm^{-1} \cdot MHz^{-1}$)

α_{sca}	scattering loss attenuation coefficient of dispersion ($\text{dB}\cdot\text{cm}^{-1}\cdot\text{MHz}^{-1}$)
α_{th}	thermal loss attenuation coefficient of dispersion ($\text{dB}\cdot\text{cm}^{-1}\cdot\text{MHz}^{-1}$)
α_{vis}	viscous loss attenuation coefficient of dispersion ($\text{dB}\cdot\text{cm}^{-1}\cdot\text{MHz}^{-1}$)
β_{m}	thermal expansion of liquid medium (K^{-1})
β_{p}	thermal expansion of particle or droplet (K^{-1})
ϵ_{m}	dielectric constant of liquid medium (dimensionless)
ϵ_{p}	dielectric constant of particle or droplet (dimensionless)
ϵ_0	permittivity of vacuum ($8.854\cdot 10^{-12} \text{ C}\cdot\text{V}^{-1}\cdot\text{m}^{-1}$)
κ	inverse Debye length (m^{-1})
ζ	zeta potential (V)
η_{m}	dynamic viscosity of liquid medium ($\text{Pa}\cdot\text{s}$)
η_{p}	dynamic viscosity of droplet ($\text{Pa}\cdot\text{s}$)
λ	wave length of the acoustic field (m)
μ	electrophoretic mobility ($\text{m}^2\cdot\text{V}^{-1}\cdot\text{s}^{-1}$)
μ_{d}	dynamic electrophoretic mobility ($\text{m}^2\cdot\text{V}^{-1}\cdot\text{s}^{-1}$)
ρ_{m}	density of liquid medium ($\text{kg}\cdot\text{m}^{-3}$)
ρ_{p}	density of particle or droplet ($\text{kg}\cdot\text{m}^{-3}$)
ρ_{s}	density of dispersion ($\text{kg}\cdot\text{m}^{-3}$)
σ	surface charge density ($\text{C}\cdot\text{m}^{-2}$)
σ_{Ln}	standard deviation (dimensionless)
τ_{m}	thermal conductivity of liquid medium ($\text{W}\cdot\text{m}^{-1}\cdot\text{K}^{-1}$)
τ_{p}	thermal conductivity of particle or droplet ($\text{W}\cdot\text{m}^{-1}\cdot\text{K}^{-1}$)
φ	volume fraction of the dispersed phase (dimensionless)
φ_{min}	minimum φ for strongly overlap of double layers (dimensionless)
Φ_0	surface potential (mV)
ω	frequency (Hz)
ω_{hd}	characteristic hydrodynamic frequency (Hz)
ω_{MW}	Maxwell-Wagner frequency (Hz)
ω'	relative Maxwell-Wagner frequency, $\omega/\omega_{\text{MW}}$ (dimensionless)
Ω	drag coefficient (dimensionless)
∇P	pressure gradient of the acoustic perturbation in the dispersion ($\text{Pa}\cdot\text{m}^{-1}$)

∇P_{ant} pressure gradient of the perturbation in the center electrode ($\text{Pa}\cdot\text{m}^{-1}$)

Chapter 1

Introduction

The stability of water-in-diluted bitumen emulsions is a subject of importance for the oil sands industry. Bitumen froth produced in commercial water-based extraction processes (a mixture of bitumen, water and solids) is diluted with organic solvent in order to reduce bitumen viscosity and thus facilitate the separation of water and solids prior to bitumen upgrading. After froth treatment, water can still remain in the diluted bitumen as a stable emulsion. Due to the presence of chlorides in the water, this residual water should be minimized. Hence, research effort to understand the mechanism of water stabilization in diluted bitumen (which has not been completely established yet) is justified.

Previous studies have revealed that asphaltenes and fine solids can stabilize water-in-diluted bitumen emulsions. It is believed that the high emulsion stability is mainly due to a steric repulsion mechanism, where interfacial material adsorbed at the water-oil interface prevents droplet coalescence. The rigidity of this interfacial adsorbed layer depends on the bitumen concentration and the paraffinic/aromatic nature of the solvent. Repulsive electrostatic interactions could also play a role in the stability of water-in-diluted bitumen emulsions. This mechanism, however, has been far less understood because of the lack of electric surface charge data of aqueous drops in organic media.

Advent of commercially available ultrasound based techniques during the past decade offers a new opportunity for studying water-in-diluted bitumen emulsions. They can provide information regarding size distribution and electro-surface properties of particles or droplets dispersed in a non-transparent and non-polar media. This technique is not invasive and it can be applied in relatively concentrated systems, which avoids the need of sample dilution previous to its characterization.

Theory of electroacoustics by Shilov and coworkers (based on measurements of the colloid vibration current) is well established for ζ -potential characterization in water dispersions. In the case of non-polar media, Shilov's theory provides the surface charge

density of the dispersed phase under the assumption of strongly overlapped double layers. These features are incorporated in the DT-1200 Spectrometer from Dispersion Technology Inc., which also evaluates the particle size distribution from measurements of the sound attenuation in the dispersion. Shilov's theory is the only one of its kind available in the electroacoustic literature which allows the study of the surface charge density of particles or droplets dispersed in low conductivity media like water-in-diluted bitumen emulsions.

The purpose of the present study is to investigate the surface charge density of water droplets dispersed in diluted bitumen by means of this novel electroacoustic technique and theory. This is the first work in the area of electroacoustics where Shilov's theory is applied to water-in-diluted bitumen emulsions. The significance of the study is that it contributes to illuminate the role of electrostatic interactions in emulsion stability.

Chapter 2

Literature Review

2.1 *Water-in-diluted bitumen emulsions in the oil sands industry*

2.1.1 Origin, composition and industrial importance

Oil sands deposits in northern Alberta are mixtures of bitumen, silica sands and fine clays. Bitumen is a form of heavy oil which needs to be upgraded to obtain commercial fuels. Oil sands ores typically contain 9% to 13% wt bitumen, which is recovered through surface mining operations, followed by a water-based extraction process (Czarnecki, 2001). At some stage of the process, the extracted bitumen is in the form of *bitumen froth*, containing about 60% bitumen, 30% water and 10% solids (Czarnecki, 2001). Water and solids must be separated from the bitumen prior to upgrading (in order to avoid serious corrosion and clogging problems in upgrading plant operations), and this is done through the addition of an organic solvent (diluent) to the bitumen froth. Such a mixture of bitumen froth diluted with organic solvent forms a water-in-oil emulsion, where the organic phase is the continuous phase. They are referred to as *water-in-diluted bitumen emulsions*.

The dilution of the bitumen froth facilitates the removal of emulsified water and suspended solids, because it lowers the density and viscosity of the oil phase (Czarnecki, 2001). Bitumen density is about the same of water and, therefore, a lighter organic solvent is used for dilution. The separation of water and solids is achieved by mechanical operations such as scroll and disk centrifuges and inclined plate settlers (Czarnecki, 2001). In some cases, chemical treatment (demulsifiers) is also implemented to enhance removal efficiency. The diluted bitumen is required to meet downstream process specification: it must contain less than 0.5% vol. total solids and water (BS&W), and it must have a viscosity of less than 350 cSt for pipelining (Long et al., 2002).

The paraffinic/aromatic nature of the organic solvent and the mass ratio of added organic solvent to bitumen (hereafter referred to as the *solvent to bitumen ratio*) are key factors to be considered in froth treatment operations, because they are directly related to

the *stability* of water-in-diluted bitumen emulsions. The term *emulsion stability* refers to the ability of the water droplets to resist coalescence, thus preventing the ultimate separation of water from the continuous phase (Isaacs & Chow, 1992). The higher the emulsion stability is, the more difficult is to break the emulsion into a water phase and a hydrocarbon phase. This is because the coalescence of water droplets is the limiting step in the demulsification process (McLean & Kilpatrick, 1997).

Naphthenic or aromatic naphthas are being used as diluent in the current commercial oil sands operations, at a solvent to bitumen ratio between 0.6 and 0.7 (Long et al., 2002). Under these operating conditions and after multistage centrifugation and demulsifier addition, the diluted bitumen product still contains water (2% – 5% wt.) and solids (0.5% - 1.0% wt.), in the form of a stable water-in-diluted bitumen emulsion with droplets less than 10 μm in diameter (Long et al., 2002). The emulsified water is then removed in a subsequent stage together with the diluent, in the solvent recovery unit. However, dissolved salts (mostly sodium chloride) and suspended solids remain in the bitumen and are carried to the upgrading process. There, chlorides are inevitably converted to corrosive hydrochloric acid (Czarnecki, 2001) and fine solids tend to obstruct hydrotreatment reactors and lower catalyst activity (Chen et al., 1999).

Therefore, the effective removal of water from diluted bitumen in froth treatment operations is a subject of importance to the oil sands industry, and this requires the understanding of the mechanism responsible for the stability of water-in-diluted bitumen emulsions.

2.1.2 Bitumen compounds responsible for the emulsion stability

Asphaltenes, fine solids and natural surfactants present in bitumen have been identified as stabilizing compounds of water-in-diluted bitumen emulsions. Among them, asphaltenes and fine solids are recognized as the main stabilizers. Experiments carried out by Yan et al. clearly support this general conclusion (Yan et al., 1999).

They studied the ability of each individual component to stabilize water-in-diluted bitumen emulsions, where a mixture of 50:50 by volume of hexane and toluene was used for dilution. A series of emulsions were prepared where the same amount of water (9%

vol.) was dispersed in different organic solutions or dispersions: diluted bitumen (with and without solids), diluted deasphalted-bitumen (with and without solids), and diluted asphaltenes/solids mixture extracted from bitumen. For consistency, all types of water-in-oil emulsions were prepared with the same equivalent bitumen concentration. The emulsion stability was determined by measuring the volume of free water decanted after 48 hours settling tests in 500 ml graduated cylinders: the higher the amount of free water, the lower the emulsion stability.

The observations of this study can be summarized as follow (Yan et al., 1999):

- I. Emulsions prepared with diluted asphaltenes/solids mixture show higher stability than those using diluted bitumen with solids. This means that the presence of deasphalted bitumen molecules lowers the ability of asphaltenes and solids to stabilize emulsions.
- II. Individually, both asphaltenes and solids are good stabilizers of water-in-diluted bitumen emulsions. However, the stabilization effect is greatest when both are present.
- III. Water-in-diluted bitumen emulsions are poorly stabilized by deasphalted bitumen, i.e. when both asphaltenes and solids have been removed from bitumen.

Another important observation made by Yan and coworkers is that only fine solids are effective stabilizers of water-in-diluted bitumen emulsions. Fine solids in this study are defined as the fraction recovered in a 0.22 μm filter paper, when highly diluted bitumen is filtered, first against a 8.0 μm filter paper (for coarse solid removal), and then against a 0.22 μm filter paper where fine solids are captured. Fine solids are typically smaller than 0.5 μm (Yan et al., 1999).

2.1.3 Stabilizing mechanism of water-in-diluted bitumen emulsions

The mechanism for the stabilization of water-in-diluted bitumen emulsions is not completely understood yet. A *mechanism* for the emulsion stability is an explanation of

the factors that prevent water droplets to approach each other and eventually flocculate or coalesce. There are two basic mechanisms that can contribute to the emulsion stability: *steric repulsion* and *electrical repulsion* (Isaacs et al., 1990). They are of different nature and both can act simultaneously.

Steric repulsion refers to physical barriers that prevent droplet coalescence. Asphaltenes, fine solids and natural surfactants present in bitumen tend to gather at the water-oil interface, resulting in a film which acts as a structural barrier to the coalescence of water droplets. Steric interactions are short-ranged (Isaacs et al., 1990). On the other hand, if water droplets have electrical surface charge, then electrical repulsive forces arise between the droplets. Electrical interactions can act at relatively longer distances than steric interactions (Isaacs et al., 1990).

Most experimental work to date suggests that the stability of water-in-diluted bitumen emulsions is mainly due to a steric repulsion mechanism. Repulsive electrical interactions might have a minor role in the emulsion stability. However, this last mechanism has been far less experimentally investigated, and no definite conclusion is available as yet.

2.1.4 Experimental evidence for the steric stabilization mechanism

The existence of a critical solvent to bitumen ratio which delimits the stability behavior of water-in-diluted bitumen emulsions is well documented in the literature. Above the critical solvent to bitumen ratio, the emulsion is unstable and water and solids can easily be removed. On the other hand, below the critical solvent to bitumen ratio, water-in-diluted bitumen emulsions are very stable (Czarnecki, 2001). The fact is that this dramatic change on the emulsion stability behavior has a clear connection with the mechanical properties and composition of the film at the water-oil interface, which supports the thesis of the predominant role of steric interactions on the emulsion stability. This has been recently demonstrated using a variety of experimental techniques, including the micropipette, colloidal particle scattering (colloidal collider), thin liquid film-pressure balance and isolation/characterization of interfacial material through water emulsification (Czarnecki, 2001; Wu, 2003).

Yang and Czarnecki have reported critical solvent to bitumen ratio about 2 for natural gas condensate-diluted bitumen, and about 4 for naphtha-diluted bitumen (Yang & Czarnecki, 2002). The effect of the critical solvent to bitumen ratio on the emulsion stability is illustrated in Figure 2.1, based on contacting experiments performed by Yang and Czarnecki (Yang & Czarnecki, 2002). Syncrude naphtha-diluted bitumen was contacted with water in a cell, avoiding mixing of the two phases by carefully placing the oil phase on top of the aqueous phase. After two days, the oil phase was removed for water content analysis. Significant water emulsification occurred below the critical solvent to bitumen ratio only ($S/B \leq 4$), as can be observed in Figure 2.1.

A similar experiment was repeated on a smaller scale; this time the two phases were contacted within a micro-slide for microscope observation, avoiding any agitation on the system (Yang & Czarnecki, 2002). Water droplets less than 3 μm in diameter were spontaneously formed inside the oil phase for solvent to bitumen concentrations below critical ($S/B \leq 4$). At higher solvent to bitumen ratios ($S/B \geq 4$), no water droplets were observed in the oil phase. It was also noticed that asphaltene precipitation occurred at $S/B \geq 4$ (Yang & Czarnecki, 2002). Apparently, the onset of asphaltene precipitation coincided with the critical solvent to bitumen ratio.

On the basis of the steric stabilization mechanism, these experiments suggest that the effect of the solvent on the emulsion stability is related to the state of solubility of asphaltenes in the oil phase (Yang & Czarnecki, 2002). Emulsions are stable below the critical solvent to bitumen ratio because asphaltenes can adsorb at the water-oil interface. On the other hand, above the critical ratio, asphaltenes are precipitated and, therefore, they are not able to adsorb at the interface. This results in unstable emulsions above the critical solvent to bitumen ratio (Yang & Czarnecki, 2002).

Further experimentation carried out by Yang and Czarnecki demonstrated that if asphaltene precipitation occurs at any solvent to bitumen ratio, maximum emulsion stability is obtained when water and diluent are added to the bitumen at the same time (Yang & Czarnecki, 2002). The emulsion stability greatly decreases if the water is added some time after the bitumen dilution (one day in their experiments). On the other hand, for any solvent to bitumen ratio where asphaltene precipitation does not occur, the order

of addition is unimportant and it does not make any difference in the emulsion stability (Yang & Czarnecki, 2002).

The aforementioned facts support further the hypothesis for the steric stabilization by asphaltenes. When bitumen dilution induces asphaltene precipitation and water is added simultaneously with the diluent, there is still a chance for asphaltenes to adsorb at the water-oil interface and stabilize the emulsion (Yang & Czarnecki, 2002). Precipitation of asphaltenes is an equilibration process that takes time to complete. On the other hand, if water is added after bitumen dilution and the oil phase has reached a new equilibrium state where asphaltenes have already precipitated, then there is a significant detrimental in the stability of the emulsion as asphaltenes are no longer available to adsorb at the interface (Yang & Czarnecki, 2002).

The adsorption process of asphaltenes and other compounds at the water-oil interface imparts time dependence characteristics to the stabilizing interfacial film. Sheu and coworkers studied the kinetics of asphaltene adsorption at toluene-water interfaces as a function of pH and asphaltene concentration (Sheu et al., 1992; Sheu et al., 1995). They measured the rate of change of interfacial tension with time (which directly correlates to the adsorption rate of asphaltenes), and they found that the adsorption kinetics are in the order of hours. This is actually much slower than the adsorption kinetics of surfactants (Sheu et al., 1992).

Figure 2.2 shows the decrease of interfacial tension with time due to asphaltene adsorption, which eventually reaches an equilibrium value after few hours. The initial decrease of the interfacial tension with time adjusts well to a *diffusion-controlled* adsorption kinetics (Sheu et al., 1992). However, as the interfacial tension approaches equilibrium, the adsorption kinetics is no longer diffusion-controlled but *reaction-controlled*, presumably because of the necessary rearrangement processes of asphaltene molecules at the adsorption layer (Sheu et al., 1992).

According to Sheu and coworkers, initially the concentration of adsorbed asphaltenes at the water-oil interface is low, and the adsorption kinetics is only controlled by diffusion of asphaltenes from the bulk of the oil phase to the interface (Sheu et al., 1992). As the concentration of adsorbed asphaltenes increases, however, asphaltenes

molecules have to rearrange themselves in order to minimize the system free energy. This rearrangement process now drives the adsorption kinetics, and it is particularly slow due to the constraints imposed by the wide structural distribution of asphaltenes (Sheu et al., 1992).

The adsorption layer thickness of water-in-diluted bitumen emulsions has been determined by Czarnecki and coworkers using the colloidal particle scattering technique (Czarnecki, 2001). This technique allows the calculation of the interaction forces between water droplets, from the analysis of collision trajectories between two micrometer-sized droplets under simple shear flow field. Two types of interaction forces were assumed: van der Waals (attractive) and steric (repulsive). The results of their experiments suggest that the steric barrier may have a thickness varying from 7 to 40 nm (Czarnecki, 2001). Further experimentation carried out by Khristov, Wasan, Czarnecki and Masliyah using the liquid film-pressure balance technique also reported large variations in the film thickness, which suggests that the steric barrier has a multilayer structure (Czarnecki, 2001).

The experimental evidence discussed so far emphasizes the role of asphaltenes on the steric stabilization of water-in-diluted bitumen emulsions. It has been discussed the relationship between the state of solubility of asphaltenes and the emulsion stability. However, this is just one of the explanations formulated to present. There is additional evidence which support the steric stabilization mechanism in emulsion systems where asphaltene precipitation does not occur. In these cases, the critical bitumen to solvent ratio is not related to the onset of asphaltene precipitation but to changes of the composition and mechanical properties of the interfacial adsorbed layer.

One example are *heptol*-diluted bitumen emulsions, where the solvent is a mixture 50:50 by volume of heptane and toluene. Wu investigated this system and determined that compositional changes of interfacial material occur at the critical solvent to bitumen ratio (Wu, 2003). Below the critical solvent to bitumen ratio (low solvent dilution), interfacial material is composed of a mixture of asphaltenes and water insoluble carboxylic salts (sodium naphthenates); above the critical ratio (high dilution by the solvent), only asphaltenes were detected (Wu, 2003).

Previous studies with heptol-diluted bitumen emulsions using the micropipette technique (Dabros et al., 1999) revealed that the critical solvent to bitumen ratio also delimits the transition between flexible interfacial films (below the critical ratio) and rigid interfacial films (above the critical ratio). As shown in Figure 2.3, deflating a large water droplet in heptol results in two different surface rheologies of the film: above the critical ratio, the surface of the droplet crumples because the film is rigid; on the other hand, below the critical ratio the surface of the droplet remains spherical but with some protrusions that eventually detach from the surface, resulting in the formation of micrometer-sized water droplets (Dabros et al., 1999). This process of emulsification through area contraction is called *budding*, and it only occurs when the interfacial film is flexible. The budding emulsification process requires low input energy, and it is believed that it contributes to the high stability of water-in-diluted bitumen emulsions below the critical solvent to bitumen ratio (Dabros et al., 1999).

2.2 *Electrostatic stabilization in nonaqueous media*

2.2.1 Electrical charges in nonaqueous media

Following Morrison's review article (Morrison, 1993), it is generally accepted that electrolytes can dissociate in nonaqueous media if there is a structure around cations and anions that keeps them apart. An *inverse micelle* is one possible structure, which can contain an ion in its core and thus separate it from counter ions in different micelles (Morrison, 1993). Large size ions (polymer macro-ions) itself can generate self-associating structures. On the other hand, ions would exist as cation-anion pairs if such structure is not available (Morrison, 1993). Equilibrium between ion pairs and the dissociated electrolyte is governed by the size of the stabilizing structure: the larger the size of the structure, the bigger the effective size of ions, and this favor dissociation because ions have enough kinetic energy to overcome electrostatic attraction (Morrison, 1993). Theoretically, a minimum diameter in the order of 30 nm is required for complete electrolyte dissociation (Morrison, 1993).

Inverse micelle formation in nonaqueous media is primarily determined by the intermolecular interactions between the hydrophilic head groups of the molecules at the

core of the micelle (Morrison, 1993). They can have a wide variety of shapes as opposed to micelle formation in aqueous media, where they tend to be spherical (Morrison, 1993). The presence of small amounts of water contributes to inverse micelle formation in nonaqueous media, because it enhances the intermolecular interactions between hydrophilic head groups. Furthermore, water molecules also facilitate the solubilization of excess ions at the core of the micelle (Morrison, 1993).

When electric surface charge develops on particles in a dispersion, an equivalent number of oppositely charged ions (hereafter referred to as *counter-ions*) exist in the liquid medium to keep the system electrically neutral. The same aforementioned stabilizing structure prevents counter-ions to combine with the charged particles and, therefore, they do not neutralize each other (Morrison & Ross, 2002).

There are at least two proposed mechanism for particle charging in nonaqueous media. Kitahara and coworkers postulate the preferential adsorption mechanism of cations or anions of a dissociated electrolyte onto the particle surface (Morrison, 1993). On the other hand, Fowkes and coworkers propose a different mechanism. They suggest that the non-dissociated electrolyte adsorbs onto the particle surface, and then acid-base (or donor-acceptor) interactions occur between surface groups and the neutral electrolyte. Finally, the charged electrolyte desorbs from the particle surface (which is now provided with electric surface charge), and it is often stabilized in an inverse micelle in the nonaqueous medium (Morrison, 1993). Figure 2.4 (Morrison & Ross, 2002) shows an example of the Fowkes mechanism, where acidic particles (with acidic sites HA) are dispersed in a nonaqueous solution of basic polymer dispersants (with basic sites B).

2.2.2 Concepts of DLVO Theory

The stability behavior of dispersions (either particles or droplets) in liquid media is governed by the balance between attractive and repulsive interactions in the system. The electrostatic stabilization of dispersions comprises the balance of two types of interactions: London dispersion forces (called van der Waals interactions) which are attractive, and electrostatic forces (called double layer interactions) which are repulsive between similarly charged particles (Masliyah, 1994).

The electrostatic stabilization of aqueous dispersions can be quantitatively predicted by means of the DLVO theory, which calculates the *net potential energy of interaction*, defined as the work required to bring two particles or droplets from infinity to a given separation distance (Masliyah, 1994). Figure 2.5 shows three possible scenarios for the stability analysis. Curve V_1 represents a stable system: at a separation distance r_1 , the potential reaches a maximum and it represents the energy barrier to be overcome for particle coagulation. On the other hand, curve V_3 represents an unstable system (the potential of interactions is always negative). Curve V_2 represents an intermediate case where particles can flocculate at the local minimum at a separation distance r_2 (Masliyah, 1994).

The role of double layer interactions is fundamental in determining the stability of an electrostatically stabilized colloidal suspension (Morrison & Ross, 2002). Variations in factors influencing double layer interactions (such as electrolyte concentration and particle surface charge) can change the net potential of interaction from V_1 (stable) to V_3 (unstable) and vice versa (Figure 2.5). As a general result, the DLVO theory predicts that electrostatic stabilization is more important the larger the particle or droplet size of a dispersion (Morrison & Ross, 2002).

The name of double layer interactions comes from the distribution of counter-ions in an *electrical double layer* in the vicinity of the charged particles. In this region, ions of opposite charge to that of the surface (counter-ions) are attracted, while ions of similar charge (co-ions) are repelled. This results in a region where there is no charge neutrality as a consequence of the prevailing presence of counter-ions over co-ions. Figure 2.6 depicts the structure of the electrical double layer (Masliyah, 1994).

The *Stern layer* defines an inner region where counter-ions are strongly attached to the particle surface (Morrison & Ross, 2002). The rest of the excess counter-ions are mobile in the liquid medium, but their spatial distribution is determined by two competitive processes. On the one hand, counter-ions tend to concentrate near the particle surface because of electrical attractive forces. On the other hand, counter-ions tend to diffuse away from the particle surface because of their thermal motion. The end result is the formation of a *diffuse layer* as shown in Figure 2.6, where the concentration of excess

counter-ions decreases with distance. The Stern layer and diffuse layer are delimited by the so called *shear plane* (Masliyah, 1994).

The diffuse double layer can be perturbed from its equilibrium distribution when the particle moves (Morrison & Ross, 2002). This is the origin of the so called *Electrokinetic phenomena*, which are discussed in sections 2.3 and 2.4 in regard to the measurement of the electro-surface properties of particles or droplets dispersed in liquid media. Such electrokinetic measurements are able to investigate the surface charge density (σ) or electric potential (ζ -potential) at the shear plane. As shown in Figure 2.6, the decrease in excess counter-ion concentration with distance from the shear plane is accompanied with a decrease in the developed electric potential in the liquid medium. The electric potential decreases from ζ with a characteristic length $1/\kappa$ called *Debye length* (Masliyah, 1994).

The DLVO theory considers the Debye length as the thickness of the diffuse layer. As shown in Equation 2.1, this parameter can be calculated from the ionic composition of the liquid medium (Masliyah, 1994). The following parameters intervene in Equation 2.1: dielectric constant of the liquid medium (ϵ_m), permittivity of vacuum (ϵ_0), Boltzmann constant (k), temperature (T), elementary charge (e), number of ionic species (N), valency (z_i) and number concentration ($n_{i\infty}$) of the i th ionic species in the bulk solution.

$$\frac{1}{\kappa} = \sqrt{\frac{\epsilon_m \epsilon_0 k T}{e^2 \sum_{i=1}^N z_i^2 n_{i\infty}}} \quad (2.1)$$

Under the assumption of equal diffusion coefficient for all charge carriers in the liquid medium, and using Einstein relationship between the diffusion coefficient and the migration mobility (Zholkovskij et al., 2002), Equation 2.2 is derived, where K_m is the conductivity of the liquid medium and D_{eff} is the diffusion coefficient of charge carriers. Equation 2.2 can be used to estimate the Debye length in dispersion systems where the ionic composition of the liquid medium is unknown, as it is the case of most nonaqueous dispersions (Dukhin & Goetz, 2002).

$$\frac{1}{\kappa} = \sqrt{\frac{\epsilon_m \epsilon_0 D_{\text{eff}}}{K_m}} \quad (2.2)$$

One interesting example of the applicability of the DLVO theory is the electrostatic stabilization of bitumen-in-water emulsions reported in reference (Isaacs & Chow, 1992), which is the mirror case for the system under study in the present work (i.e., water-in-diluted bitumen emulsions). Figure 2.7 shows the net potential energy of interaction diagram for bitumen-in-water emulsions in the presence of NaCl and CaCl₂ (Isaacs & Chow, 1992). The net potential energy of interaction is expressed in kT units.

According to reference (Isaacs & Chow, 1992), the DLVO theory predicts that an emulsion would be stable against coagulation (under the condition of no flow) considering an energy barrier of at least 15 kT. As shown in Figure 2.7, the DLVO theory predicts that in the presence of 300 mM NaCl the emulsion should flocculate (similar case to curve V₂ in Figure 2.5), and in the presence of 20 mM CaCl₂ the emulsion should coagulate (similar case to curve V₃ in Figure 2.5). Those predictions were confirmed experimentally as discussed in reference (Isaacs & Chow, 1992).

2.2.3 Experimental evidence for the electrostatic stabilization in nonaqueous media

Following van der Hoeven and Lyklema review article (van der Hoeven & Lyklema, 1992), there is a controversy about the possibility of electrostatic stabilization of nonaqueous suspensions. The common believe is that steric stabilization would be the dominant mechanism because electrostatic forces would not be high enough to stabilize colloids (van der Hoeven & Lyklema, 1992).

According to the DLVO theory, charged particles can be effectively stabilized when electrostatic repulsion forces can outweigh van der Waals attraction forces, in such a way that an energy barrier is established to prevent their coagulation. Electrostatic forces are determined by the particle charge and the interaction between the double layers surrounding the particles (van der Hoeven & Lyklema, 1992). Both factors depend on the concentration of ions and the degree of ion dissociation in the media. Nonaqueous media is characterized by very low conductivities and, therefore, low ion concentration. This is why small electrostatic repulsive forces are generally expected in nonaqueous dispersions,

and the reason for the often found skepticism about the possibility for their electrostatic stabilization (van der Hoeven & Lyklema, 1992).

Furthermore, van der Hoeven and Lyklema emphasize the role of the dielectric constant of the media (van der Hoeven & Lyklema, 1992). They affirm that electrostatic stabilization is difficult for $\epsilon_m \leq 5$ because of negligible dissociation of electrolytes (for hydrocarbons, $\epsilon_m \approx 2$). However, their argument is based on the assumption that charge screening in the media is only determined by the polarization of the solvent (van der Hoeven & Lyklema, 1992), and they do not consider in their analysis that electrolyte dissociation also depends on the availability of a stabilizing structure such as an inverse micelle or self-associating polymer macro-ions, as discussed in Morrison's review article (Morrison, 1993).

There has been, however, experimental evidence for the electrostatic stabilization of nonaqueous suspensions since the early days of the DLVO theory. The following is an extract taken from reference (van der Minne & Hermanie, 1952), which best illustrates the difficulties in accepting the electrostatic stabilization of suspensions in nonaqueous media, because of the lack of evidence of the presence of charge carriers:

"In an investigation which the authors carried out several years ago they came across the curious fact that peptization of suspensions in mineral oil of material resembling carbon black was promoted by calcium soaps and also by oil-soluble oxidation products of such an oil, but that when both these substances were added together flocculation of the suspension ensued. Only when one of the two peptizing substances was present in excess could the suspension be peptized again. When using benzene instead of the mineral oil the authors observed exactly the same phenomena; only here flocculation of the suspension takes much less time owing to the much lower viscosity. The two substances apparently did not react with each other, which would have given the easiest explanation. The explanation of such phenomena in aqueous suspensions would be simply the presence of opposite charges due to the addition of various electrolytes. A similar explanation in the case of suspensions in oil was at that time not acceptable, because, although for other reasons it was considered the most likely one, there was no evidence of charged particles."

Experimental evidence has shown that the electrostatic stabilization of colloids in nonaqueous media is particularly likely in the case of large particles, in the micron range

(Morrison, 1991). According to Morrison, this size dependence can be approximately represented by Equation 2.3, where Φ_0 is the required surface potential to stabilize the dispersion (mV), r is the particle radius (μm) and ϵ_m is the dielectric constant of the medium (Morrison, 1991). Furthermore, as pointed out by Koelmans and Overbeek (van der Hoeven & Lyklema, 1992), when small particles are considered, the electrostatic stabilization of the larger coagulates of the primary particles is more likely than that of the primary particles.

$$\Phi_0^2 > \frac{10^3}{\epsilon_m r} \quad (2.3)$$

Equation 2.3 is valid for nonconducting particles (Morrison, 1991). Furthermore, the Debye length is assumed to be larger than the interparticle distance, and the electrostatic interactions were approximated to simple Coulomb forces (Morrison, 1991). This essentially assumes that ions do not form a diffuse layer around particles, but are distributed uniformly throughout the medium (Morrison, 1991). This is the so called *strongly overlapped double layers* approximation, which is generally valid for dispersions in nonaqueous media where the ionic concentration is low. This follows from Equation 2.1, where it can be concluded that the lower the concentration of ionic species ($n_{i\infty}$), the higher the Debye length ($1/\kappa$).

The dependence of the required surface potential to stabilize nonconducting particles as a function of particle radius is presented in Table 2.1 (Morrison, 1991), considering the typical dielectric constant of hydrocarbons ($\epsilon_m = 2$). It follows from Morrison's expression (Equation 2.3), and it compares well with experimental evidence obtained from electrophoretic measurements (Morrison, 1991).

2.3 Electrokinetic measurements of the electro-surface properties of dispersions

Techniques based on the so called *Electrokinetic phenomena* can provide information on the electro-surface properties of particles (or droplets) dispersed in a liquid medium. These phenomena are associated with the relative movement between the

charged particle surface and the surrounding electrolytic medium. Only the mobile part of the electric double layer (i.e., the diffuse layer) is involved (Masliyah, 1994). Therefore, it is more appropriate to say that these techniques measure the *electrokinetic charge* (Dukhin, 1993). Measurements are usually reported in terms of a surface charge density or a surface potential (ζ -potential).

Traditional electrokinetic techniques include *particle electrophoresis*, where an electric field is applied to a suspension of particles. If the particles are charged, they migrate along the electric field, eventually reaching a steady state velocity when the hydrodynamic drag force acting on the particle balances the electric force. The ratio of the steady state particle velocity to the electric field strength is called *electrophoretic mobility* (Masliyah, 1994), and it is ultimately related to the ζ -potential of the particle.

The relationship between the electrophoretic mobility (μ) and the ζ -potential (ζ) depends on the relative thickness of the double layer, which is measured as the ratio between the particle radius and the Debye length (κa). There are two limiting cases, namely Smoluchowski and Hückel equations for *thin double layers* ($\kappa a \gg 1$, Equation 2.4) and *thick double layers* ($\kappa a \ll 1$, Equation 2.5), respectively (Masliyah, 1994). η_m is the dynamic viscosity of the liquid medium:

$$\mu = \frac{\zeta \epsilon_m \epsilon_o}{\eta_m} \quad \text{Smoluchowski equation for } \kappa a \gg 1 \quad (2.4)$$

$$\mu = \frac{2}{3} \frac{\zeta \epsilon_m \epsilon_o}{\eta_m} \quad \text{Hückel equation for } \kappa a \ll 1 \quad (2.5)$$

For the intermediate case where the double layer has a finite thickness, there is no simple relationship between the electrophoretic mobility and the ζ -potential, because the *electrophoretic relaxation effect* complicates the analysis. This effect is associated to the double layer distortion under the electric field, which creates a superposed electric field that opposes the motion of the particle as shown in Figure 2.8 (Isaacs & Chow, 1992). This effect needs to be considered for double layer thicknesses, let say in the range $1 < \kappa a < 300$ (Isaacs & Chow, 1992). In this case, the numerical solution developed by O'Brien and White would be appropriate to relate the electrophoretic mobility to the ζ -potential (Isaacs & Chow, 1992).

Commercial instruments for particle electrophoresis require the dispersion sample to be dilute and transparent to light. Particle velocity is determined either from the direct observation through a microscope or by the Doppler shift of scattered radiation from the moving particle (Isaacs & Chow, 1992). Therefore, particle electrophoresis has many limitations for the characterization of real dispersions, especially non-transparent systems such as water-in-oil emulsions. Even in the case of emulsions transparent to light (like oil-in-water emulsions), the sample would require dilution well below 1% concentration, thus altering the original distribution of components between the two phases (Hunter, 1998). The end result is that the measured ζ -potential of the diluted sample may not correspond to the real dispersion value.

There is only one electrokinetic technique that can overcome these two limitations and, therefore, it is the only one that could be applied for the study of water-in-diluted bitumen emulsions. The *electroacoustic technique* for the characterization of the electro-surface properties of particles or droplets in a liquid medium can be applied in non-transparent and relatively concentrated systems. It has been commercially available since the 1980's. It is an area of significant importance and growing interest in colloid science, because of its unique advantages over traditional electrokinetic techniques for the characterization of dispersions in their natural state.

2.4 *Electroacoustic Spectroscopy*

2.4.1 The Electroacoustic effects: CVP, CVC and ESA

The electroacoustic technique is based on the measurement of the so called *Electroacoustic phenomena*. If particles (or droplets) dispersed in a liquid medium are electrically charged, and if the densities of the particle and the liquid are different, the application of an acoustic field generates an alternating electric field in the bulk of the dispersion. Similarly, the application of an alternating electric field generates sound waves at the boundaries of the dispersion with its container. These are phenomena where acoustic and electric fields are coupled together because of the presence of charged particles in a liquid medium. Any of the two fields can act as the driving field, thus generating a response in the other field which can be measured and ultimately related to

the electro-surface properties of the particles in the dispersion (Hunter, 1998; Dukhin & Goetz, 2002).

It is pertinent to classify these phenomena in two categories, depending on the nature of the response field (Hunter, 1998; Dukhin & Goetz, 2002). The first category corresponds to the case of applied acoustic field, and the electroacoustic effect is called *Colloid Vibration Potential* (CVP) if the response is measured as an electric potential between two electrodes, or *Colloid Vibration Current* (CVC) if an electric current is measured between the two electrodes. The second category corresponds to the case of applied electric field, where the associated acoustic response is called *Electrokinetic Sonic Amplitude* (ESA). A more detailed description of the CVP, CVC and ESA effects follows.

2.4.2 Colloid Vibration Potential (CVP)

In the electroacoustic literature, this effect is also called *Ultrasonic Vibration Potential* (UVP), but the terminology CVP is preferred here because it explicitly states that the electroacoustic effect is that associated to the colloidal particles in the suspension. There is a similar electroacoustic effect associated to electrolytes in solution (i.e., the build up of electric fields due to the different motion of anions and cations in an acoustic field), which is called *Ion Vibration Potential* or IVP (Dukhin & Goetz, 2002). For clarity, therefore, the terminology Colloid Vibration Potential (CVP) will be used in the present work.

The CVP is developed because of a temporary separation of charges that arise in the suspension as a consequence of the applied acoustic field. The particle and its surrounding liquid medium have different densities and, therefore, they exhibit different inertia. When sound waves are transmitted through the suspension, the particles and their associated double layers move differently because of their different inertia (Figure 2.9). This in turn creates temporary separation between charges in the particles and its counter charges in the liquid medium, building up dipoles in the bulk of the dispersion. The sum of the separates dipole fields give rise to the Colloid Vibration Potential (Hunter, 1998). The term “vibration” refers to the fact that an alternating electric potential is induced at

the same frequency of the driving acoustic field. In fact, this is a common characteristic of all electroacoustic effects, where the applied field and the resulting response field occur at the same frequency (Hunter, 1998).

The CVP effect can be measured when two electrodes are placed in the bulk of the suspension at a separation distance which is not exactly one or more whole wave lengths. The maximum amplitude of the CVP is measured when the two electrodes are placed at a separation distance equivalent to $(2n+1)\lambda/2$, where n is an integer and λ is the wave length of the acoustic field (Hunter, 1998). There is another important condition that must be met to measure CVP and it is related to the external circuit connected to the electrodes. The impedance of the external circuit must be much higher than the impedance of the suspension between the electrodes in order to measure CVP, so the characteristics of the external circuit will not affect the measurements. This is called the *high impedance requirement* (Babchin et al., 1989).

As a side comment, it is pertinent to mention here an important result concerning the motion of a rigid spherical particle in an acoustic field. As demonstrated by Babchin (Babchin et al., 1989), when the density of the particle is higher than the density of the liquid, then the motion of the particle lags behind the fluid in amplitude and phase. This is an important observation for the discussion of the electroacoustic phenomenon (later it will be referred to as the *inertia effect*). For example, returning to Figure 2.9, it can be concluded that the motion of excess counter-ions in the double layer lag ahead the particle. In the following discussion, it is always assumed that the density of the particle is higher than the density of the liquid.

2.4.3 Colloid Vibration Current (CVC)

The CVC effect is similar to the CVP effect, with the difference that the measured quantity is the electric current instead of an electric potential. In this case, the impedance of the electric circuit connected to the electrodes must be much lower than the impedance of the suspension between the electrodes. Both effects, CVP and CVC are due to the polarization and vibration of the double layers as a consequence of the applied acoustic

field. Whether we measure an electric potential or current depend, however, on the relative impedance of the external circuit (Dukhin & Goetz, 2002).

A more thorough understanding of the CVC and CVP effects is gained when analyzing the mechanism of double layer polarization. Figure 2.10 illustrates such mechanism for a negatively charged particle (Dukhin & Goetz, 2002). As a consequence of the relative movement between the particle and its surrounding liquid (as indicated by the arrows labeled U_p-U_m), positive counter-ions accumulate at the left-side pole of the double layer, thus reducing the number of positive counter-ions at the right-side pole. Therefore, the relative motion between the particle and the liquid generates an electric current within the double layer called *hydrodynamic surface current* (I_s). The induced dipole moment, on the other hand, generates an electric field responsible for the CVP effect (Dukhin & Goetz, 2002).

However, to make the picture self consistent in Figure 2.10, it must be recognized the presence of another electric current (I_n) in the bulk of the electro-neutral solution beyond the double layer (Dukhin & Goetz, 2002). Otherwise, the double layer would never return to its equilibrium configuration after the acoustic perturbation. This current arises because of the effect of the CVP on the ions beyond the double layer (Dukhin & Goetz, 2002). The combined effect of I_s and I_n is called the *total dynamic current*. Under the condition of low impedance in the external electric circuit, the total dynamic current is measurable and it corresponds to the CVC effect (Babchin et al., 1989).

2.4.4 Electrokinetic Sonic Amplitude (ESA)

In the case of ESA, the driving field is an alternating electric field. If the particles (or droplets) in a dispersion are charged, they oscillate at the same frequency of the driving field. The movement of the particles generates an acoustic field: the particles act as acoustic dipoles radiating sound waves (Hunter, 1998). These dipoles cancel one another in the bulk of the dispersion, but such cancellations do not occur at the boundaries of the dispersion with its container (Hunter, 1998). An electrode (acoustic transducer) can be placed at the boundaries of the dispersion to sense the acoustic response (ESA). In the immediate neighborhood of the electrode surface, particles

moving in one direction cause an equal volume of liquid to move in the opposite direction. Therefore, the net momentum change per unit area in the direction normal to the electrode surface generates an alternating pressure, since the densities of the particles and liquid are different (Hunter, 1998). This alternating pressure is responsible of the acoustic response in the ESA effect.

2.4.5 Theory of Electroacoustics: O'Brien's approach

The theory of electroacoustics has been under development since 1933 when Debye first predicted this effect. Today, there are two independent theoretical approaches to electroacoustics (Dukhin & Goetz, 2002). The first approach was developed by O'Brien and the second approach was developed by Shilov, Dukhin, Ohshima and Goetz. Unfortunately, these two approaches have not merged into a unified electroacoustic theory yet (Dukhin & Goetz, 2002). They actually merge in the case of dilute suspensions, but it has not been completely established if they merge in the concentrated case. O'Brien's approach has been applied mostly to the ESA effect, while Shilov and coworkers approach has been applied to the CVC effect (Dukhin & Goetz, 2002).

The present discussion begins with O'Brien's approach because he was the first to introduce a parameter of primary importance, known as the *dynamic electrophoretic mobility*. According to O'Brien, this parameter is the analogue of the electrophoretic mobility as measured by electrophoresis (Hunter, 1998), and it incorporates the complete functional dependence of ESA, CVC or CVP on key properties of the particles like the ζ -potential (Dukhin & Goetz, 2001). Furthermore, it also incorporates the functional dependence with particle size and frequency of oscillation which arise from the non-stationary character of the phenomena (this justify the terminology of "dynamic" electrophoretic mobility).

The dynamic electrophoretic mobility is again defined as the ratio between the particle velocity and the electric field strength. However, contrary to the electrophoretic mobility, this parameter is represented by a complex number having a magnitude and a phase angle (Cannon, 1993). This can be explained by considering the ESA effect. As shown in Figure 2.11, a sinusoidal applied electric field generates a sinusoidal particle

motion at the same frequency. Both, the particle velocity and the applied electric field are characterized by amplitude and phase. Therefore, the magnitude of the dynamic electrophoretic mobility is the ratio of the particle velocity amplitude and the electric field amplitude; the phase angle, on other hand, represents the phase time lag between the particle motion and the applied electric field (Cannon, 1993).

The aforementioned explanation of the dynamic electrophoretic mobility of a particle in the frame of the ESA effect is not casual. Actually, this property is directly related to the ESA effect because, same as the electrophoretic mobility in the case of electrophoresis, it is a measure of the ability of a particle to move under the influence of an applied electric field. However, it can also be related to the other electroacoustic effects. This is done by means of a reciprocal relation derived by O'Brien which links the CVP and ESA effects through the same concept of dynamic electrophoretic mobility (O'Brien, 1988). Therefore, following O'Brien's approach, the ESA and CVP effects can be expressed as follow (O'Brien et al., 1994):

$$\langle \text{ESA} \rangle = Q_1 \varphi \left(\frac{\rho_p - \rho_m}{\rho_m} \right) \mu_d \quad (2.6)$$

$$\langle \text{CVP} \rangle = Q_2 \varphi \left(\frac{\rho_p - \rho_m}{\rho_m} \right) \frac{\mu_d}{K^*} \quad (2.7)$$

where μ_d is the dynamic electrophoretic mobility, K^* is the complex conductivity of the suspension, φ is the volume fraction of the dispersed phase, ρ_p and ρ_m are the densities of the particle and liquid medium, respectively. $\langle \text{ESA} \rangle$ and $\langle \text{CVP} \rangle$ are the electroacoustic signals normalized by the corresponding driving force. This means that $\langle \text{ESA} \rangle$ has units of pressure divided by electric field strength ($\text{Pa} \cdot \text{m} \cdot \text{V}^{-1}$). In the case of $\langle \text{CVP} \rangle$, two unit systems have been used in the literature (Dukhin & Goetz, 2002; O'Brien, 1988): $\text{V} \cdot \text{m} \cdot \text{Pa}^{-1}$ (electric potential divided by the pressure gradient of the acoustic perturbation), and $\text{V} \cdot \text{s} \cdot \text{m}^{-1}$ (electric potential divided by the velocity of the acoustic perturbation). Finally, Q_1 and Q_2 are constants that only depend on the apparatus and the geometry of the cell used for measuring the ESA and CVP effects, respectively (O'Brien et al., 1994).

From Equations 2.6 and 2.7 it can be concluded that, in principle, the measurement of any of the two electroacoustic effects (ESA or CVP) can provide the

dynamic electrophoretic mobility of the particles or droplets in a dispersion. However, the complex conductivity must be known in the case of CVP but not for ESA. This is an inherent advantage of ESA over CVP (Cannon, 1993). The complex conductivity refers to the conductivity of the dispersion measured at the same frequency of the electroacoustic effect. Same as μ_d , $\langle\text{ESA}\rangle$ and $\langle\text{CVP}\rangle$ in Equations 2.6 and 2.7, K^* is represented by a complex number. Current electroacoustic techniques work in the megahertz frequency range from 0.1 to 10 MHz, approximately (Hunter, 1998).

If measurement of the conductivity of the dispersion is not available at the aforementioned frequency range (usually, it is available at much lower frequencies), then errors will be introduced when determining the dynamic electrophoretic mobility from CVP (Cannon, 1993). This limitation, however, does not apply to measurements based on the CVC effect (Hunter, 1998). The complex conductivity relates CVC and CVP as follows (Dukhin & Goetz, 2002):

$$\langle\text{CVC}\rangle = \langle\text{CVP}\rangle \cdot K^* \quad (2.8)$$

Then, Equations 2.7 and 2.8 give the following expression for the determination of the dynamic electrophoretic mobility from the CVC effect, without the intervention of the complex conductivity.

$$\langle\text{CVC}\rangle = Q_2 \varphi \left(\frac{\rho_p - \rho_m}{\rho_m} \right) \mu_d \quad (2.9)$$

Following the terminology of O'Brien (O'Brien, 1988), Equations 2.6, 2.7 and 2.9 are the *macroscopic constitutive equations*. They allow the determination of the dynamic electrophoretic mobility from quantities which are accessible to measurement (φ , ρ_p , ρ_m , $\langle\text{ESA}\rangle$, $\langle\text{CVC}\rangle$ and $\langle\text{CVP}\rangle$). Constants Q_1 and Q_2 can be found by calibration of the equipment with a suspension of known electro-surface properties (i.e., for which μ_d is known).

It can be recognized from the above discussion that measurement of the electro-surface properties of a dispersion is a two steps process. First, the dynamic electrophoretic mobility is determined from the measured electroacoustic signal. Second, the electro-surface properties must be extracted from the measured dynamic

electrophoretic mobility using an appropriate formula (this issue will be discussed shortly). In the case of electrophoresis, the mobility is determined from the observation of the particle velocity under known electric field strength (step 1), and then the ζ -potential is determined using Hückel, Smoluchowski or O'Brien and White formulas (step 2).

The next topic to be discussed is how the electro-surface properties of the particles (or droplets) in a dispersion are extracted from the measured dynamic electrophoretic mobility (i.e., step 2 of the electroacoustic technique). O'Brien's first formula for the dynamic electrophoretic mobility (Hunter, 1998) was applicable to the case of dilute suspensions (less than 4% by volume) of spherical particles with thin double layers ($\kappa a \gg 1$). He solved classical electrokinetic equations (Poisson's equation, ion conservation equation, continuity and Navier-Stokes equations) for an isolated particle undergoing electroacoustic motion in the *long wavelength regime*, where the particle diameter is smaller than the wavelength (O'Brien, 1988). This first theoretical development of O'Brien led to the following expression for the dynamic electrophoretic mobility (Hunter, 1998):

$$\mu_d = \frac{2\varepsilon_m \varepsilon_o \zeta}{3\eta_m} \cdot G(\alpha) \cdot [1 + f(Du, \omega')] \quad \text{for } \kappa a \gg 1 \quad (2.10-A)$$

$$G(\alpha) = \frac{1 + (1+i)\sqrt{\frac{\alpha}{2}}}{1 + (1+i)\sqrt{\frac{\alpha}{2}} + i\frac{\alpha}{9} \left(3 + 2\frac{\rho_p - \rho_m}{\rho_m} \right)} \quad (2.10-B)$$

$$f(Du, \omega') = \frac{1 + i\omega' - \left(2Du + i\omega' \frac{\varepsilon_p}{\varepsilon_m} \right)}{2(1 + i\omega') + \left(2Du + i\omega' \frac{\varepsilon_p}{\varepsilon_m} \right)} \quad (2.10-C)$$

Several parameters intervene in Equations 2.10-A/B/C and they are presented in the following discussion.

Equation 2.10-A establishes the relationship between the dynamic electrophoretic mobility and the electro-surface properties of the particles (ζ -potential). It has a similar structure as compared to the Smoluchowski or Hückel equations, but two additional

factors are included: the G factor which takes into account the effect of inertia forces, and the f factor which takes into account electrodynamic effects associated to the polarization of the double layer (Dukhin & Goetz, 2002). It is important to say here that Shilov's approach uses the same general structure for the formulae of the dynamic electrophoretic mobility as shown by Equation 2.10-A. Therefore, what follows is a general explanation on the role of factors G and f which is valid for both, O'Brien and Shilov approaches.

The frequency dependence of the dynamic electrophoretic mobility is incorporated in these two factors. The values of factors G and f at the low frequency limit are (Dukhin & Goetz, 2002):

$$G(\omega \rightarrow 0) = 1 \quad (2.11)$$

$$f(\omega \rightarrow 0) = \frac{1 - 2Du}{2 + 2Du} \quad (2.12)$$

As frequency is increased, however, it will eventually get close to some critical values where the factors G and f start to significantly deviate from their low frequency limits. The corresponding critical frequencies are the *characteristic hydrodynamic frequency* (ω_{hd}) for the G factor, and the *Maxwell-Wagner frequency* (ω_{MW}) for the f factor (Dukhin & Goetz, 2002). In Equations 2.13 and 2.14, a is the particle (or droplet) radius.

$$\omega_{hd} = \frac{\eta_m}{a^2 \rho_m} \quad (2.13)$$

$$\omega_{MW} = \frac{K_m}{\epsilon_m \epsilon_o} \quad (2.14)$$

The frequency dependence of factors G and f is expressed as a function of parameters α and ω' in Equations 2.10-B and 2.10-C. Parameter α is the relative hydrodynamic frequency (defined as ω/ω_{hd}), and ω' is the relative Maxwell-Wagner frequency (defined as ω/ω_{MW}). Therefore, frequency dependence is important when $\alpha \geq 1$ or $\omega' \geq 1$.

Figure 2.12 sketches the magnitude and phase angle of the G factor with parameter α . The effect of inertia forces on the dynamic electrophoretic mobility is

important for $\alpha \geq 1$. As α increases in this range, the magnitude of the dynamic electrophoretic mobility significantly decreases and the particle motion start to lag behind the applied field (Hunter, 1998). The inertia effect is so significant that the electroacoustic signal might be too small to be measured at sufficiently high frequencies and/or for very big particles. On the other hand, the limiting value of the phase lag is 45° (Hunter, 1998).

In order to explain this inertia effect, let us consider the ESA effect. The particle moves at the same frequency of the applied electric field, and it also interacts with the surrounding liquid through transfer of momentum (viscous coupling between the particle and the liquid), which is the origin of the acoustic response. This transfer of momentum takes a time of the order $1/\omega_{hd}$ to occur; it is the *characteristic hydrodynamic time*. When the period of oscillation (i.e., the *characteristic time of oscillation*) is much larger than the characteristic hydrodynamic time ($\alpha \ll 1$), the particle tends to move in sympathy with the liquid. However, when $\alpha \approx 1$, both characteristic times are comparable, and the abovementioned effects start to manifest in the dynamic electrophoretic mobility (magnitude reduction and phase lag).

The fact that the dynamic electrophoretic mobility is sensible to the particle size gives an opportunity to employ electroacoustics for particle size measurements, in addition to the determination of the electro-surface properties of the particles (Hunter, 1998). This can be done when measuring the dynamic electrophoretic mobility within a range of frequencies, therefore generating a spectrum. This is why this technique is also known as *Electroacoustic Spectroscopy*.

The f factor in Equation 2.10-C is proportional to the tangential electric field at the particle surface (Hunter, 1998). Recalling electrophoresis, this is the component of the electric field that causes the particle motion. The f factor accounts for the electrodynamic effects that can deform the electric field at the surface of the particle, therefore affecting the dynamic electrophoretic mobility. There are two electrodynamic effects included in this factor (Dukhin & Goetz, 2002): surface conductivity (associated to the parameter Du) and Maxwell-Wagner relaxation (associated to the parameter ω').

Du is a dimensionless parameter called the *Dukhin number*, and it is defined as $Du = (K^S)/(K_m \cdot a)$, where K^S is the surface conductivity, K_m is the conductivity of the

liquid medium, and a is the particle radius (Dukhin & Goetz, 2002). The surface conductivity refers to the enhanced conductivity in the double layer relative to the conductivity in the bulk of the liquid medium (Hunter, 1998). As discussed later, there is a more general definition of the Dukhin number where the electrodynamic effects of conducting particles are considered (Dukhin & Goetz, 2004B). The present discussion on the basis of O'Brien's approach is restricted to non-conducting particles.

The effect of high surface conductivity (i.e., high Dukhin number) is to decrease the dynamic electrophoretic mobility. An explanation in the frame of the ESA effect is as follows. The polarization of the double layer set up a back field that opposes the applied electric field. In principle, the polarization of the double layer occurs because of the relative movement between the particle and liquid medium. This is shown in Figure 2.8 for a positively charged particle. However, the effect of high surface conductivity is to increase the polarization of the double layer, as more negative counter-ions migrate to the left-side pole of the double layer under the influence of the applied electric field (Figure 2.8). This means that the effect of the surface conductivity is to set up an additional contribution to the back field that opposes the applied electric field. Therefore, the net result is that the tangential electric field at the particle surface is reduced, thus decreasing the dynamic electrophoretic mobility (Hunter, 1998).

The Maxwell-Wagner relaxation effect can introduce an additional phase shift to the dynamic electrophoretic mobility. Continuing our discussion in the frame of the ESA effect, the polarization of the double layer takes a time of the order $1/\omega_{MW}$ to occur under the influence of the applied alternating electric field (Hunter, 1998). Same as the inertia effect, when the period of the oscillation is comparable to the characteristic time of the double layer polarization ($\omega' \approx 1$), an additional phase shift is introduced in the dynamic electrophoretic mobility. In the general sense, the Maxwell-Wagner relaxation accounts for the field-induced charge density variations within the double layer (Dukhin & Goetz, 2002).

So far, we have discussed O'Brien's approach to electroacoustic for thin double layers ($\kappa a \gg 1$) and dilute suspensions ($\phi < 0.04$). The latest developments of O'Brien are presented in the paper (O'Brien et al., 2003) for the concentrated case and thin double layers. This condition is generally valid for most dispersion in aqueous media. A further

simplification of the theory applies to dilute dispersions in aqueous media for low ζ -potentials, because surface conductivity has a negligible effect (Hunter, 1998). This, in addition to the fact that the ratio $\varepsilon_p/\varepsilon_m$ is also small for most water-based dispersions, lead to a f factor equal to 0.5 in Equation 2.10-A, and the formulae for the dynamic electrophoretic mobility takes the form of the Smoluchowski equation corrected only by the inertia factor G (Hunter, 1998):

$$\mu_d = \frac{\varepsilon_m \varepsilon_o \zeta}{\eta_m} \cdot G(\alpha) \quad \text{for } \kappa a \gg 1 \text{ and low } \zeta\text{-potential} \quad (2.15)$$

In the case of aqueous dispersions, Equation 2.15 not only allows for the determination of the ζ -potential, but also allows for the determination of the charge of the particles. This is done from measurements of the phase of the dynamic electrophoretic mobility. Because the frequency dependence is only concentrated on the inertia factor, the phase of the dynamic mobility varies in the range from 0° to 45° for positively charged particles, and 135° to 180° for negatively charged particles (Hunter, 1998).

In the case of dilute dispersions in non-aqueous media (low conductivity media), Equations 2.10-A or 2.15 would not be appropriate because they are valid for thin double layers. In this case, it would be more appropriate to assume thick double layers and low ζ -potential (Hunter, 1998), and the formula for the dynamic electrophoretic mobility takes the form of the Hückel equation corrected by the inertia factor (Cannon, 1993):

$$\mu_d = \frac{2\varepsilon_m \varepsilon_o \zeta}{3\eta_m} \cdot G'(\alpha) \quad \text{for } \kappa a \ll 1 \text{ and low } \zeta\text{-potential} \quad (2.16-A)$$

$$G'(\alpha) = \left\{ \left(1 + \sqrt{\frac{\alpha}{2}} \right) - i \left[\sqrt{\frac{\alpha}{2}} + \frac{\alpha}{9} \left(1 + \frac{2\rho_p}{\rho_m} \right) \right] \right\}^{-1} \quad (2.16-B)$$

2.4.6 Theory of Electroacoustics: Shilov's approach

Shilov and coworkers approach is based on the initial works of Booth and Enderby for dilute dispersions, and Marlow, Fairhurst and Pendse for concentrated dispersions (Dukhin & Goetz, 2001). This approach was developed for the CVC and CVP effects. Same as O'Brien, this approach covers the two limiting cases of thin and thick

double layers. Most of the discussion in the last section applies to Shilov's approach, but the formula for the dynamic electrophoretic mobility is different.

For thin double layers ($\kappa a \gg 1$), the following formula for the dynamic electrophoretic mobility is valid for dilute and concentrated dispersions (Dukhin & Goetz, 2002):

$$\mu_d = \frac{2\varepsilon_m \varepsilon_o \zeta (\rho_p - \rho_s) \rho_m}{3\eta_m (\rho_p - \rho_m) \rho_s} \cdot G\left(\frac{\alpha}{2}, \varphi\right) \cdot [1 + f(Du, \omega', \varphi)] \quad \text{for } \kappa a \gg 1 \quad (2.17-A)$$

$$G(\alpha, \varphi) = \frac{9\varphi \rho_s \cdot h(0.5\alpha)}{4i\varphi(1-\varphi)(0.5\alpha) \cdot I(0.5\alpha) \cdot \left\{ \rho_p - \rho_m \left[\frac{3 \cdot H(0.5\alpha)}{2 \cdot I(0.5\alpha)} + 1 \right] \right\}} \quad (2.17-B)$$

$$1 - \frac{\rho_p}{(1-\varphi) \left\{ \rho_p - \rho_m \left[\frac{3 \cdot H(0.5\alpha)}{2 \cdot I(0.5\alpha)} + 1 \right] \right\}} \cdot \varphi \cdot \left[\frac{3 \cdot H(0.5\alpha)}{2 \cdot I(0.5\alpha)} + 1 \right]$$

$$f(Du, \omega', \varphi) = \frac{(1 - 2Du)(1 - \varphi) + i\omega' \left(1 - \frac{\varepsilon_p}{\varepsilon_m} \right) (1 - \varphi)}{2(1 + Du + \varphi(0.5 - Du)) + i\omega' \left(2 + \frac{\varepsilon_p}{\varepsilon_m} + \varphi \left(1 - \frac{\varepsilon_p}{\varepsilon_m} \right) \right)} \quad (2.17-C)$$

Equations 2.17-A/B/C are valid for monodisperse systems. Similar equations have been developed for the dynamic electrophoretic mobility of polydisperse systems (with a particle size distribution) as discussed in reference (Dukhin & Goetz, 2002). ρ_s is the density of the dispersion and H, I and h are special functions which are introduced by two cell models used in the derivation: the Kuwabara cell model for describing the hydrodynamic field around the particle, and the Shilov-Zharkikh cell model for describing the electric field (Dukhin & Goetz, 2002). These functions are shown in Appendix 1.

Another important feature of Shilov's approach is that it is not restricted to the case of non-conducting particles. Equation 2.17-A can be extended to conducting particles by modifying the expression for the Dukhin number as follows (Dukhin & Goetz, 2004B):

$$Du = \frac{K_p}{K_m} + \frac{K^s}{K_m a} \quad (2.18)$$

In regard to the case of thick double layers ($\kappa a \ll 1$), Shilov's approach offers the only expression available in the electroacoustic literature for the calculation of the dynamic electrophoretic mobility which is applicable for both, dilute and concentrated dispersions (Dukhin & Goetz, 2004A; Dukhin & Goetz, 2004B). This theory is more appropriately called by their authors as the *electroacoustic theory for strongly overlapped double layers*. In section 2.2.3 it was mentioned that this condition is generally valid for dispersion in nonaqueous media where the ionic concentration is low. This results in large Debye lengths as can be concluded from Equation 2.1.

The condition of thick double layers ($\kappa a \ll 1$) corresponds to double layer thickness much larger than the particle radius. Actually, the double layer of the particle extends in a way that it overlaps with the double layers of the surrounding particles for which the condition $\kappa a \ll 1$ is also valid. When double layers overlap strongly, there is a homogeneous charge distribution in the liquid media between the particles. No effective charge screening takes place. This condition is valid for both, dilute and concentrated dispersions as long as $\kappa a \ll 1$.

However, in the concentrated case there is a more general condition for having strongly overlapped double layers, and it is not only restricted to the limiting case of thick double layers ($\kappa a \ll 1$). For a finite double layer thickness (i.e., for an intermediate value of κa), the condition of strongly overlapped double layers is achieved if the particles are close enough, so that the interparticle distance is smaller than the double layer thickness and, therefore, the distribution of ions between the particles does not significantly deviate from the homogeneous distribution (Dukhin & Goetz, 2004A). Therefore, for concentrated dispersions with a finite double layer thickness, the more general condition of strongly overlap of double layers can be expressed by $\kappa d \ll 1$, where d is the interparticle distance (Dukhin & Goetz, 2004A).

For any intermediate value of κa , there is a minimum concentration above which the condition $\kappa d \ll 1$ is satisfied and, therefore, the assumption of strongly overlapped double layers and homogeneous ion distribution is theoretically valid. According to

Shilov and coworkers, the relationship between the minimum volume fraction required for strongly overlapped double layers as a function of κa is approximately given by Equation 2.19 (Dukhin & Goetz, 2004B). This relationship is also shown in Figure 2.13 (Dukhin & Goetz, 2002).

$$\varphi_{\min} \approx \frac{0.52}{\left(1 + \frac{1}{\kappa a}\right)^3} \quad (2.19)$$

For strongly overlapped double layers and monodisperse systems, Shilov's approach provides the following formula for the dynamic electrophoretic mobility (Dukhin & Goetz, 2004B), where σ is the surface charge density of the particles or droplets, and Ω is the drag coefficient. Appendix 1 details the calculation of the drag coefficient.

$$\mu_d = \frac{2\sigma a}{3} \frac{\rho_m}{\rho_s \eta \Omega + j\omega(1-\varphi)\frac{2a^2}{9}\rho_p \rho_m} \quad \text{for } \kappa a \ll 1 \quad (2.20)$$

Equation 2.20 does not follow the same general structure of Equation 2.17-A for the dynamic electrophoretic mobility. First, it relates the dynamic electrophoretic mobility with the surface charge density of the particles (not the ζ -potential). Second, there are no electrodynamic parameters normally involved in the factor f in Equation 2.17-A, such as conductivity and dielectric permittivity of particle and liquid medium. This is because the homogeneous distribution of ions in the case of strongly overlapped double layers eliminates polarization charges induced by the liquid motion (Dukhin & Goetz, 2004B). In this case, the nature of the electroacoustic effect is not due to the polarization of double layers, but to the generation of a current associated to the oscillating motion of charged particles (Dukhin & Goetz, 2004B). Apart from the surface charge density, the generation of the CVC effect is purely hydrodynamic. This also explains why the CVC effect is directly related to the surface charge density of the particles and not to the ζ -potential (Dukhin & Goetz, 2004B).

There is a third fundamental difference between Equation 2.20 for strongly overlapped double layers and Equation 2.17 for thin double layers. The phase of the

dynamic electrophoretic mobility varies between 0° and 45° for thin double layers, but in the case of strongly overlapped double layers Shilov's theory predicts a range between 0° and 90° (Dukhin & Goetz, 2004A).

The relationship between the ζ -potential and the surface charge density in the case of strongly overlapped double layers can be derived from the condition of electro-neutrality in the dispersion (Dukhin & Goetz, 2004B). The result is given in Equation 2.21, where F is the Faraday constant and R is the universal gas constant.

$$\sigma = \frac{1}{3} \frac{RT}{F} \frac{1-\varphi}{\varphi} \varepsilon_0 \varepsilon_m a \kappa^2 \sinh\left(\frac{F\zeta}{RT}\right) \quad (2.21)$$

As pointed out in reference (Dukhin & Goetz, 2004B), the ζ -potential depends on the volume fraction of the dispersed phase for a given surface charge density. Therefore, erroneous interpretations can be made when judging the charge of the particles using the concept of ζ -potential (Dukhin & Goetz, 2004B). Furthermore, the calculation of the ζ -potential requires the knowledge of the Debye length, which is not required for the surface charge density as shown in Equation 2.20 (Dukhin & Goetz, 2004B). Therefore, the characterization of the electro-surface properties of the dispersion is best represented by the surface charge density when the condition of strongly overlap of double layers apply.

To our knowledge, Shilov and coworkers theory for strongly overlapped double layers is the only one of its kind available to date in the electroacoustic literature. It is the latest theoretical development in electroacoustic spectroscopy that allows the study of the electro-surface properties of dispersions in low conductivity media like water-in-diluted bitumen emulsions. It has been incorporated in the DT-1200 Acoustic and Electroacoustic Spectrometer from Dispersion Technology Inc. The present work study the surface charge density of water droplets dispersed in diluted bitumen using this novel electroacoustic theory and spectrometer.

Currently, Shilov's theory is under development to extend it to the case when double layers do not overlap strongly. This situation is an intermediate case between the two limiting cases of strongly overlapped double layers ($\kappa a \ll 1$ or $\kappa d \ll 1$) and thin double

layers ($\kappa a \gg 1$). No such theoretical development is available yet in the field of Electroacoustics.

2.5 *Electroacoustic studies relevant to water-in-oil emulsions*

There are few works reported in the literature regarding the study of water-in-oil emulsions using the electroacoustic technique, as can be appreciated in two recent review articles written by Hunter (Hunter, 2001; Hunter, 1998). To our best knowledge, there are only three studies that are relevant to the area of water-in-diluted bitumen emulsions and they will be discussed in the following sections.

2.5.1 Study of the coalescence of water-in-crude oil emulsions

This work represents an important contribution to the electroacoustic technique and its practical aspects for the study of the stability of water-in-oil emulsions. It was carried out by Isaacs, Babchin, Chow, Huang and Sawatzky at the Alberta Research Council (Isaacs et al., 1990; Babchin et al., 1989; Isaacs & Chow, 1992). They demonstrated that the electroacoustic technique is effective to monitor the rate and extent of coalescence in water-in-crude oil emulsions, and to evaluate the effectiveness of additives to break the emulsion and optimize dosage concentration.

They worked with the Electrokinetic Sonic Analysis System of Matec Instrument and measured the CVP effect of the emulsions at 1.0 MHz. The emulsion to be tested was circulated from the sample container to the electroacoustic cell using a peristaltic pump (Isaacs et al., 1990). Their approach was to monitor the coalescence process using the CVP signal, which in turns depends on the concentration, particle size distribution and electro-surface properties of the water droplets. The coalescence process was also independently monitored by photomicrography and by performing dewatering centrifugation tests from samples taken at various times during the experiment. Therefore, the relation between the measured CVP signal and the ongoing coalescence process could be established (Isaacs et al., 1990). The choice for measuring the CVP effect was made based on the inherent advantage of a strong CVP signal for dispersions

in low conductivity media. However, no attempt was made to determine the dynamic electrophoretic mobility or to calculate any electro-surface property of the emulsion.

The emulsion system studied was water-in-Leduc crude oil emulsions, because they were very stable with no evidence of phase separation even after standing for several days (Isaacs et al., 1990). This allowed several chemical additives to be tested as emulsion breakers. The main findings of this work are summarized in the following discussion, and they were taken from references (Isaacs et al., 1990; Babchin et al., 1989; Isaacs & Chow, 1992).

2.5.1-a Relation between the CVP signal and water concentration

Emulsions with no added chemicals were prepared by mixing crude oil and water using a magnetic stirrer for 5 minutes, followed by sonication. Figure 2.14 shows the effect of sonication time on the CVP signal for a 10% water-in-Leduc crude oil emulsion. The change of the CVP signal with time is attributed to a change in the particle size distribution of the water droplets due to sonication. After 4 minutes, the CVP signal attains a constant value, indicating that a constant state of dispersion of the water droplets has been reached (Isaacs et al., 1990).

Therefore, in order to investigate the effect of water concentration on the CVP signal, the time for sonication was set to 5 minutes. The results of this experiment are presented in Figure 2.15, where it can be seen that the CVP signal increases with the water content in an approximate linear relation. No CVP signal was detected for the crude oil in the absence of added water (Isaacs et al., 1990). This observation is in agreement with Equation 2.7, where an increase in the volume fraction of the dispersed phase results in an increase of the CVP, assuming that the dynamic electrophoretic mobilities of the water droplets is approximately the same after sonication.

The magnitude of the CVP signals in Figures 2.14 and 2.15 are not directly comparable because different electroacoustic transducers with different sensitivities were used in the two experiments (Isaacs et al., 1990).

2.5.1-b Relation between the CVP signal and water droplets coalescence

Emulsions were prepared following the standard procedure of 5 minutes crude oil and water mixing under magnetic stirring, followed by 5 minutes sonication. In the absence of added chemical demulsifier, the CVP signal was almost stable and it only marginally decreased with time as shown in Figure 2.16, probably because of small amount of coalescence due to emulsion agitation promoted by the pumping action through the electroacoustic cell. However, when a highly effective emulsion breaker is added, there is a sharp decrease in the CVP signal. This is shown in Figure 2.16 for Duomeen C (AKZO Chemicals), where the CVP signal is reduced in 58% when 100 ppm of the chemical is added (Isaacs et al., 1990).

Figure 2.17 shows the comparison between the CVP signal with photomicrography tests, showing that the sharp decrease in the CVP is associated to the increase of the droplet size after the addition of 100 ppm of Duomeen C (Isaacs et al., 1990). This observation can be explained on the basis of the inertia effect of water droplets on the CVP: the higher the water droplet size, the lower the dynamic electrophoretic mobility, and thus the lower the CVP signal (Equation 2.7). Another important observation in Figure 2.17 is that the CVP signal never decreased to zero after the addition of Duomeen C. This is probably due to the fact that small water droplets can still be observed and remain unchanged (do not coalesce), which might be responsible for the remaining signal (Isaacs et al., 1990).

The size dependence of the CVP signal or any other electroacoustic effect (ESA or CVC) could be exploited (as done by Isaacs and coworkers) to monitor the kinetic of coalescence of water-in-oil emulsions. However, this interpretation of the CVP signal in Isaacs and coworker experiments is valid only under the assumption that the electro-surface properties of the water droplets remain the same (or approximately the same) before and after the addition of the chemical demulsifier. It is clear that this is not necessarily true in the general case.

The comparison of the CVP signal and dewatering centrifugation tests illustrates the aforementioned issue. Water-in-Leduc crude oil emulsions were prepared at two water concentrations (6% and 10% vol.) and Duomeen C was added at different concentrations

in the range 0 – 500 ppm. The different emulsions were compared on the basis of the measured CVP signal 20 minutes after the chemical addition, and also on the basis of the volume of free water recorded under standardized centrifugation tests at 2000 RPM. For consistency, the volume of all emulsions was kept constant. Figure 2.18 shows the results of these experiments (Isaacs et al., 1990).

Dewatering tests by centrifugation also provide information regarding the coalescence of water droplets in water-in-oil emulsions: the higher is the volume of separated water after centrifugation, the higher is the droplet size and the extent of the coalescence process promoted by Duomeen C. However, as can be seen in Figure 2.18, the CVP signal only correlates with the extent of coalescence at low concentration of Duomeen C, where the CVP decreases as the volume of recovered water after centrifugation increases. The CVP shows a minimum and then increases with increasing Duomeen C concentration. This increase of the CVP signal is likely due to adsorption of the Duomeen C at the water-oil interface, to an extent that the electro-surface properties are significantly altered (Isaacs et al., 1990).

In conclusion, these experiments suggest that the raw electroacoustic signal (whether ESA, CVP or CVI) might be useful for the study of the kinetics of coalescence and stability analysis of water-in-oil emulsions. However, the electroacoustic effect depends not only on the droplet size but also on its electro-surface properties, and this could lead to wrong interpretations. A complete analysis for the interpretation of the electroacoustic signal involves the calculation of the size and electro-surface properties of the water droplets, using a suitable model for the dynamic electrophoretic mobility for the system under study.

2.5.2 Study of the electro-surface properties of asphaltenes at toluene-water interfaces

This work was carried out by do Carmo Marques, de Oliveira and González at PETROBRAS Research and Development Center (do Carmo Marques et al., 1997). Similar to the study of Isaacs and coworkers, they worked with the raw electroacoustic signal (ESA in this case), to establish a direct relationship between the ESA signal and

the asphaltene content of toluene-in-water miniemulsions (Hunter, 2001). Most importantly, their work shows evidence of the electrical charging of water-oil interfaces due to asphaltene adsorption.

One evidence of the amphoteric nature of asphaltenes is that they are polar molecules which can reduce the interfacial tension of the oil-water interface at extreme pH values. Figure 2.19 shows this fact for the interfacial tension of a 100 ppm asphaltene-in-toluene solution and water as a function of pH (do Carmo Marques et al., 1997). This fact suggests that asphaltenes play a role in determining the electro-surface properties of water-oil interfaces.

The electric charging of toluene droplets due to asphaltenes was investigated using the Electrokinetic Sonic Analysis System of Matec Instruments. They measured the magnitude of the ESA effect of toluene-in-water miniemulsions, and investigated the relation between the ESA signal and the asphaltene content under different conditions of pH and volume fraction of the organic phase. Their ultimate objective was to investigate the role of asphaltenes on the emulsion stability from the perspective of the ζ -potential of the toluene droplets (do Carmo Marques et al., 1997). Similar to Isaacs and coworkers, they only measured the electroacoustic effect but they did not calculate the electro-surface properties. They assumed that the ESA signal had a direct relationship with the ζ -potential in their experiments.

0.01 mol/L of sodium lauryl sulphate (SLS) and 0.01 mol/L of cetyl alcohol (CA) were dissolved in the aqueous phase at two pH levels (7 and 13). On the other hand, asphaltenes were dissolved in toluene in the concentration range from 0 to 5500 ppm. The emulsions were prepared at several toluene concentrations, ranging from 5% to 20% by volume. Figure 2.20 shows the magnitude of the ESA signal as a function of asphaltene content, pH and toluene concentration. It can be seen that the addition of asphaltenes always increased the magnitude of the ESA signal of the emulsion.

According to do Carmo Marques and coworkers, the increase in the ESA signal is due to an increase in the surface charge of toluene droplets. Previous work performed by Goetz and El-Aasser demonstrated that toluene-in-water emulsions prepared with SLS and CA have negatively charged droplets, and the droplet size is below 0.5 μm (Goetz &

El-Aasser, 1992). Furthermore, they claim that inertia effects can be neglected and, therefore, the ESA signal can only increase because of an increase in the dispersed phase concentration and/or an increase of the surface charge of toluene droplets (Goetz & El-Aasser, 1992).

Therefore, these experiments suggest that asphaltenes are negatively charged species at neutral and alkaline pH, and also suggests that asphaltenes show a higher degree of ionization as the pH increases (do Carmo Marques et al., 1997). This hypothesis would explain the increase of the magnitude of the ESA signal when asphaltenes are dissolved in toluene-in-water emulsions with SLS and CA. On the other hand, the amphoteric nature of asphaltenes suggests that oil droplets would be positively charged at low pH. Most importantly, these experiments demonstrates that asphaltenes plays a role in determining the surface charge of oil-water interfaces and, therefore, the contribution of asphaltenes to the emulsion stability is based, in principle, on both mechanisms: steric and electrostatic.

Oil-in-water emulsions are often stabilized by electrostatic forces, and they can be destabilized through the addition of electrolyte. An example was discussed in section 2.2.2 and Figure 2.7. In the case of water-in-oil emulsions, evidence to date points toward the predominant role of steric repulsive forces in the emulsion stability. As discussed before, the question still remains on the role of electrostatic forces. Undoubtedly, further developments in the electroacoustic technique will contribute to the clarification of this issue.

2.5.3 Surface charge density measurements in nonaqueous dispersions

Shilov and coworkers electroacoustic theory is well established for the characterization of aqueous dispersions (for which the condition of thin double layers applies). An extensive list of experimental studies reported in the literature is available in reference (Dukhin & Goetz, 2002). As previously discussed, Shilov's theory for strongly overlapped double layers is the only one available in the literature for the determination of the surface charge density of nonaqueous dispersions. The latest theoretical developments are incorporated in the DT-1200 Acoustic and Electroacoustic

Spectrometer from Dispersion Technology Inc. The first experimental work using this theory has been published very recently by Dukhin and Goetz. They measured the surface charge density of two nonaqueous systems: alumina dispersion in kerosene/SPAN 80 (Dukhin & Goetz, 2004A) and water-in-kerosene/SPAN 80 emulsions (Dukhin & Goetz, 2004B).

2.5.3-a Alumina dispersion in kerosene

In this study, the surface charge density of 0.3 μm alumina particles in kerosene was investigated. Non-ionic surfactant Sorbitan mono-oleate (SPAN 80 by Fluka) was added to the organic phase at several concentrations and its effect on the surface charge density of alumina particles was investigated (Dukhin & Goetz, 2004A). Conductivity and electroacoustic measurements were performed to determine the surface charge density of alumina particles and the extent of adsorption of surfactant on the alumina particles. The sign of the measured surface charge density of the alumina particles was independently confirmed by micro-electrophoresis. Figures 2.21 and 2.22 show the results of this study (Dukhin & Goetz, 2004A).

Figure 2.21 shows the conductivity of kerosene-SPAN 80 solutions with no added alumina particles. The conductivity increases with surfactant concentration indicating that SPAN 80 produces charge carriers in the organic media, either because SPAN 80 molecules dissociate forming inverse micelles, or probably because SPAN 80 stabilizes ions originally present in Kerosene as impurities in the form of ion pairs (Dukhin & Goetz, 2004A). When alumina particles are added, the conductivity of the dispersion becomes substantially lower than the conductivity of the kerosene-SPAN 80 solution for surfactant concentrations below 1% wt. On the other hand, the conductivity of the dispersion follows the same trend as the conductivity of kerosene-SPAN 80 solution above 1% wt. surfactant content. These results suggest that surfactant molecules adsorb on the alumina particles, and a saturation point is reached when the surfactant content is approximately 1% wt. The electroacoustic determination of the surface charge density of the alumina particles (Figure 2.22) reveals that a saturation point is indeed reached

between 1% and 2% wt. of surfactant content in the dispersion (Dukhin & Goetz, 2004A).

2.5.3-b Water-in-kerosene emulsions

The stability behavior of water-in-kerosene emulsions with SPAN 80 surfactant was investigated. Acoustic spectroscopy provided the droplet size distribution evolution in time. Simultaneously, electroacoustic spectroscopy provided the surface charge density of the water droplets. Conductivity measurements were also performed because of the demonstrated ability of SPAN 80 surfactant to produce charge carriers in kerosene (Dukhin & Goetz, 2004B). This system showed an evolution from an emulsion state to a mini-emulsion state in a time span of 40 hours. 5% by volume water-in-kerosene emulsions were prepared using distilled water and 1% wt. surfactant content in the organic phase; samples were sonicated for 2 minutes after water addition, and then kept under agitation in the DT-1200 spectrometer chamber in order to prevent water sedimentation during measurements (Dukhin & Goetz, 2004B).

Figure 2.23 shows the evolution of the droplet size distribution in time measured by acoustic spectroscopy. Right after sonication of the emulsion, the mean water droplet size is 0.4 μm and it steadily increases in time during the next 10 hours up to 2 μm , revealing that water droplets are coalescing. At this point, a second fraction with a mean droplet size of 25 nm appears, and the droplet size distribution is now bimodal (Dukhin & Goetz, 2004B). During the next 30 hours, the micrometer size water droplets continue to coalesce, and the content of the nanometer size fraction increases. After 40 hours, the emulsion converts completely to the nanometer size state (mini-emulsion state) with no further change of size with time (Dukhin & Goetz, 2004B).

Electroacoustic measurements revealed that the magnitude of the CVC signal of the emulsion steadily decreases with time during the first 10 hours, eventually leveling off close to the noise level of the signal. This means that only micrometer droplets (i.e., the emulsion fraction) contribute to the CVC signal of the dispersion (Dukhin & Goetz, 2004B). Figure 2.24 shows the calculated surface charge density for the coalescing water droplets obtained from CVC using Shilov and coworkers electroacoustic theory for

strongly overlapped double layers. The conductivity of the emulsion and the relative double layer thickness calculated from conductivity is also shown in Figure 2.24. It can be seen that the surface charge density of the water droplets rapidly decreases with time during the first 10 hours (Dukhin & Goetz, 2004B).

The sign of the surface charge density in Figure 2.24 is not specified in the paper, and no independent confirmation was performed as it was the case for the alumina dispersion study (section 2.5.3-a). Therefore, it is assumed that Figure 2.24 shows the magnitude of the surface charge density without specifying the sign of the electric charge.

According to Dukhin and Goetz, one possible explanation to these observations is based on the ion-exchange model between the water and kerosene phases. They assumed that the adsorption of SPAN 80 surfactant molecules at the water-kerosene interface is responsible for the surface charge of the water droplets (Dukhin & Goetz, 2004B). They also assumed local thermodynamic equilibrium at the water-kerosene interface, which means that the time dependence characteristics of the surface charge density cannot be attributed to the kinetic of adsorption or restructuring of SPAN 80 surfactant molecules at the interface (local equilibrium would imply that such adsorption process is much faster than the rate of change of the surface charge density).

The ion-exchange model contemplates ion diffusion from the interior of the water droplets to the kerosene phase, which results in the neutralization of counter-ion electric charge in the double layer (Dukhin & Goetz, 2004B). More precisely, this means that an internal double layer is created in the interior of the water droplets (initially electro neutral), as ions diffuse to the organic phase to neutralize counter-ion charge. Eventually, the external double layer collapse and disappear. Figure 2.25 illustrates the ion-exchange model (Dukhin & Goetz, 2004B).

The decrease in the surface charge density of water drops can be explained in the frame of the ion-exchange model, as electric charge associated to the internal double layers screens the electric charge associated to the adsorbed surfactant molecules at the interface (Dukhin & Goetz, 2004B). According to this model, charging of the interior double layer is more energy efficient than the exterior double layer, and this represent the

driving force for ion diffusion from the water droplets to the kerosene phase (Dukhin & Goetz, 2004B).

Dukhin and Goetz recognized that the ion-exchange model is not the only possible explanation to these observations. However, they postulated this mechanism because it can explain the apparent discrepancy between the decreasing surface charge density of the water droplets and the increasing emulsion conductivity. Increasing conductivity would result from ions being released from the water droplets into the kerosene phase (Dukhin & Goetz, 2004B).

2.6 Acoustic Spectroscopy for particle size characterization

Advent of commercially available ultrasound based techniques during the past decade offers a new opportunity for the characterization of dispersions in liquid media. Ultrasound based techniques have two inherent advantages: they can be applied to opaque systems and moderately concentrated dispersions. This is the case of Electroacoustic Spectroscopy for the characterization of the electro-surface properties of particles or droplets in a dispersion.

The determination of the ζ -potential or surface charge density from electroacoustics requires the knowledge of the particle size distribution. In principle, the size distribution can be obtained from the electroacoustic signal itself. For example, considering Equation 2.20, this would require the measurement of μ_d within a range of frequencies, and the best fit of the data with the two adjustable parameters σ and a would provide the particle radius in addition to its surface charge density. However, as pointed out by Dukhin and Goetz (Dukhin & Goetz, 2001), it is more appropriate to determine the size distribution independently from electroacoustics. The two most important reasons are (Dukhin & Goetz, 2001): 1) the size distribution of uncharged particles cannot be obtained from electroacoustics, and 2) particle size analysis with electroacoustics depends on the assumption made in regard to the particle double layers ($\kappa a \ll 1$ or $\kappa a \gg 1$).

Commercial light-scattering based techniques for particle sizing are widely spread, but they fail in opaque and concentrated dispersions. *Acoustic Spectroscopy* is an alternative technique which can provide the particle size distribution based on

measurements of sound attenuation. It is a well established technique with an extensive list of applications reported in the literature, including slurries (cement, ceramics, coal, etc), nanosized dispersions, nonaqueous dispersions, emulsions and microemulsions (Dukhin & Goetz, 2002). Size measurements can be made in the range from 0.01 to 1000 μm (Morrison & Ross, 2002). The major disadvantage of acoustic spectroscopy, however, is that it requires the knowledge of several thermo-physical properties of the materials of the dispersion, and also the concentration of the dispersed phase (Morrison & Ross, 2002).

The theoretical aspects of acoustic spectroscopy are briefly discussed in the next sections. Emphasis is made on the determination of the droplet size distribution of emulsions with the DT-1200 Acoustic and Electroacoustic Spectrometer from Dispersion Technology Inc.

2.6.1 Phenomenon of sound attenuation in liquid dispersions

Low intensity compressional waves are used for the non-destructive characterization of dispersions in liquid media (McClements, 1991). As compressional waves pass through the dispersion, successive compressions and expansions occur in the material, and particles are displaced from their equilibrium position and oscillate in the acoustic field. This is illustrated in Figure 2.26 (McClements, 1991). Depending on the compressibility of the particles, they also deform (expand and contract) under the influence of the acoustic field, just as the liquid medium does.

The fact is that sound intensity weakens as acoustic waves propagate through the dispersion, as illustrated by the decreasing amplitude of the particle displacement in Figure 2.26. The loss in sound intensity is called *sound attenuation* (McClements, 1991). Sound attenuation is quantitatively described by the *attenuation coefficient* defined in Equation 2.22, where I_{ini} is the initial sound intensity, I_{end} is the sound intensity after traveling a distance L in the dispersion, and ω is the sound frequency (Dukhin & Goetz, 2002). The attenuation coefficient is usually expressed in $\text{dB}\cdot\text{cm}^{-1}\cdot\text{MHz}^{-1}$ units.

$$\alpha = \frac{20}{\omega} \frac{\log_{10} \left(\frac{I_{ini}}{I_{end}} \right)}{L} \quad (2.22)$$

The term *sound attenuation* characterizes the loss of power of a sound beam as it propagates through a dispersion (Dukhin & Goetz, 2002). There are two fundamental mechanisms of sound attenuation (McClements, 1991): *sound absorption* (dissipation of mechanical energy of the sound wave into heat), and *sound scattering* or α_{sca} (an incident sound wave upon an interface is scattered in different directions, and so does the mechanical energy of the sound wave). In regard to sound absorption, there are three relevant mechanisms (Dukhin et al., 2000): viscous (α_{vis}), thermal (α_{th}) and intrinsic (α_{int}). They are discussed below.

The relative movement between the particle and its surrounding liquid in the acoustic field generates shear waves which dissipate acoustic energy due to friction. This is the mechanism of *viscous loss* (Dukhin & Goetz, 2002). On the other hand, the difference in thermal expansion of particles and liquid medium generates temperature gradients near the particle surface. Temperature gradients are created when the particle and liquid medium expand and contract due to the alternating pressure of the acoustic wave. Their different thermal expansion coefficients lead to different temperatures. Acoustic energy is dissipated due to the resulting heat conduction. This is the mechanism of *thermal loss* (Dukhin & Goetz, 2002). Finally, the *intrinsic loss* mechanism refers to the dissipation of acoustic energy on a molecular level associated to the particles and liquid medium as homogeneous phases (Dukhin & Goetz, 2002).

2.6.2 Theory of Acoustics for emulsions

The theoretical treatment of the attenuation coefficient and its relation to the particle size distribution of a dispersion is simplified in what is called the *long wavelength regime of acoustics* (also called the *Rayleigh limit*), where the particle size is much smaller than the wavelength of sound (Babick et al., 2000). Here, the attenuation coefficient is assumed to be the sum of the individual attenuation mechanisms (Babick et al., 2000; Dukhin & Goetz, 2002):

$$\alpha = \alpha_{\text{int}} + \alpha_{\text{th}} + \alpha_{\text{vis}} + \alpha_{\text{sca}} \quad (2.23)$$

In the long wavelength regime, sound attenuation is mainly due to the adsorption mechanisms (Babick et al., 2000). Scattering loss is often negligible (Babick et al., 2000), and it must only be considered at the upper limit of the long wavelength regime (i.e., when the particle size is of the same order of the sound wavelength). In the case of emulsions, the dominant mechanism of sound attenuation is thermal loss. This is because the thermal expansion of water and organic compounds are significantly different. On the other hand, the viscous loss mechanism is negligible because of the relative small density contrast between the continuous and dispersed phases of emulsions (Babick et al., 2000; Dukhin & Goetz, 2002). Finally, the intrinsic loss mechanism might contribute significantly to sound attenuation, especially if a high viscous oil is involved in the emulsion (Dukhin & Goetz, 2002). Therefore, Equation 2.23 can be rewritten for emulsions as follows:

$$\alpha = \alpha_{\text{int}} + \alpha_{\text{th}} + \alpha_{\text{sca}} \quad (2.24)$$

There are two basic theoretical approaches for the calculation of the individual attenuation coefficients: the ECAH theory and the coupled-phase model (Babick et al., 2000). The details of these complex theoretical treatments are beyond the scope of the present work which focuses on Electroacoustics rather than Acoustics. The complete theoretical treatment is discussed in reference (Dukhin & Goetz, 2002) and it has been incorporated in the DT-1200 Spectrometer from Dispersion Technology Inc. However, some simplified formulas are presented in the following discussion in order to explain the most important ideas behind the particle size distribution analysis from sound attenuation measurements. These formulas are presented in Table 2.2.

As can be concluded from Table 2.2, the different sound attenuation mechanisms show different functional relationship with droplet size and sound frequency. This opens an opportunity for the qualitative interpretation of the experimental data when the attenuation coefficient is determined at several frequencies, thus generating an *acoustic spectrum*. The DT-1200 spectrometer generates an acoustic spectrum at 18 frequencies within the 3 to 100 MHz range, taken in logarithmic steps (Dukhin & Goetz, 2002).

From Table 2.2 it can be observed that the intrinsic loss of the dispersion does not depend on the droplet size. It only depends on the material properties and the volume fraction of the dispersion, and also on frequency. On the other hand, thermal and scattering losses do depend on the droplet size distribution. Therefore, it should be noticed that the intrinsic loss constitutes the base line of the acoustic spectrum, because any *excess attenuation* from this level is the part of the spectrum which is truly related to the droplet size distribution. This excess attenuation is also known as the *colloid loss* (α_{colloid}). Therefore, for emulsions:

$$\alpha_{\text{colloid}} = \alpha_{\text{th}} + \alpha_{\text{sca}} \quad (2.25)$$

From the two mechanisms that contribute to the excess attenuation, the thermal loss is the only one that shows up in the entire frequency range from 3 to 100 MHz (Dukhin & Goetz, 2002). Table 2.2 presents two simplified formulae for the asymptotic approximation of the thermal loss coefficient at the low and high frequency limits, respectively (Babick et al., 2000). At the lower frequencies, α_{th} is proportional to a^2 , and at the higher frequencies it is proportional to a^{-1} . Consequently, thermal losses due to large droplets (micrometer size) would cause excess attenuation at the lower frequencies. On the other hand, very small droplets (nanometer size) would cause attenuation at the higher frequencies.

The situation is different for the scattering loss mechanism. As shown in Table 2.2, scattering loss is a strong function of droplet size, and particularly of frequency. As shown in Table 2.2, frequency is raised to the power of four and the droplet radius is raised to the power of three. Consequently, scattering loss shows up at the higher frequencies only, and it is important for large droplets (micrometer size). According to reference (Dukhin & Goetz, 2001), scattering is not important for droplet diameter below 1 micron in the 3 - 100 MHz frequency range.

The above discussion brings a point of fundamental importance for the analysis of the acoustic spectrum. Both, very small (nanometer size) and very large droplets (micrometer size) show increasing attenuation at the higher frequencies. They are different only at the lower frequencies (Dispersion Technology, 2003). According to Dukhin and Goetz, if there is excess attenuation at frequencies below 10 MHz, this is an

indication that large droplets (micrometer size) are present in the emulsion. On the other hand, if only very small droplets are present in the emulsion (less than 100 nm), there should not be excess attenuation at the lower frequencies (Dispersion Technology, 2003). This test helps in a qualitative interpretation of the acoustic spectrum.

The DT-1200 analysis software calculates the droplet size distribution from the best fit between the prediction theory and the measured acoustic spectrum. The standard analysis is made in the whole frequency range (3 – 100 MHz). However, the long wavelength limit might impose a restriction on the frequency range in the case of large droplets. According to Dukhin and Goetz, the highest frequency for analysis should be restricted down to at least 30 MHz if the droplet size exceeds 10 microns (Dispersion Technology, 2003). The theory would simply not apply at higher frequencies for droplet size calculation purposes.

In the above discussion, it has been assumed that we are dealing with emulsions which follow a unimodal droplet size distribution. However, what if the emulsion follows a bimodal size distribution with two very different size fractions? For example, let us consider the case of one fraction being in the order of 50 nm and the other fraction being in the order of 30 μm . In such a case, the highest frequency should be restricted down to at least 30 MHz, but in doing so the smaller fraction would be ruled out from the analysis as they do not contribute to the excess attenuation at such low frequencies.

In view of this fact, it seems that the restriction imposed by the long wavelength regime would prevent the analysis of the size distribution of bimodal dispersions with a large size fraction. Actually, the ability of acoustic spectroscopy to recognize and analyze bimodal dispersions has been investigated with model systems where the particle size distribution of a bimodal dispersion is known independently. An interesting study is presented in reference (Dukhin & Goetz, 1999). Also, various emulsion systems with bimodal size distribution have been successfully characterized with acoustic spectroscopy; these include: oil-in-water and water-in-oil emulsions (Fairhurst et al., 2001), hetape/water/AOT emulsions (Wines et al., 1999), and water-in-kerosene emulsions (Dukhin & Goetz, 2004B). The general conclusion is that acoustic spectroscopy is able to recognize and analyze bimodal droplet size distributions in the

whole 3-100 MHz range when the larger size fraction does not exceed 10 microns, approximately.

To finalize this section, it is important to mention that the prediction theory works well for moderately concentrated emulsions, with dispersed phase concentrations up to, at least 10% by volume. This is shown in reference (Dukhin & Goetz, 2001), where it is mentioned some experimental work which demonstrated almost perfect correlation between theory and experiments for 10% hexadecane emulsions, 20% toluene emulsions, and even 30% for polystyrene latex dispersions. This last system is not an emulsion (polystyrene latex), but it is relevant to the acoustic theory of emulsions because thermal loss is the dominant attenuation mechanism (Dukhin & Goetz, 2002).

Particle radius (μm)	Surface potential (mV)
0.01	224
0.05	100
0.1	71
0.3	41
0.5	32
0.75	26
1.0	22
5.0	10

Table 2.1: Surface potentials to stabilize particles as a function of radius.
(Reference: Morrison, 1991)

Attenuation mechanism	Formula
Intrinsic	$\alpha_{int} = \frac{(1-\phi)(\alpha_{int})_m \rho_p c_p + \phi(\alpha_{int})_p \rho_m c_m}{\sqrt{(1-\phi)\rho_p^2 c_p^2 + \phi\rho_p \rho_m c_m^2}} \sqrt{\frac{\rho_s}{\rho_m}}$
Scattering	$\alpha_{sca} = \frac{\phi\omega^4 a^3}{2c_m^4} \left[\frac{1}{3} \left(1 - \frac{\rho_m c_m^2}{\rho_p c_p^2} \right)^2 + \left(\frac{\rho_p - \rho_m}{2\rho_p + \rho_m} \right)^2 \right]$
Thermal	$\alpha_{th} = \frac{1}{30} \phi a^2 \omega^2 T c_m \rho_m \rho_p^2 (c_p)_p \frac{\tau_m + 5\tau_p}{\tau_m^2} \left(\frac{\beta_p}{\rho_p (c_p)_p} - \frac{\beta_m}{\rho_m (c_p)_m} \right)^2$ (low frequency limit within the long wavelength regime)
	$\alpha_{th} = \frac{3}{4} \frac{\phi\sqrt{2\omega}}{a} T c_m \rho_m \frac{\sqrt{\tau_p \tau_m \rho_p \rho_m (c_p)_p (c_p)_m}}{\sqrt{\tau_p \rho_p (c_p)_p + \tau_m \rho_m (c_p)_m}} \left(\frac{\beta_p}{\rho_p (c_p)_p} - \frac{\beta_m}{\rho_m (c_p)_m} \right)^2$ (high frequency limit within the long wavelength regime)
ϕ ω c ρ (c_p)	volume fraction dispersed phase frequency of sound sound speed density specific heat
a T τ β (α_{int})	particle (droplet) radius temperature thermal conductivity thermal expansion intrinsic loss of material
Sub-indexes: m (liquid medium) / p (droplet) / s (suspension)	

Table 2.2: Simplified equations for attenuation coefficients.

(Adapted from: Babick et al., 2000 ; Dukhin et al., 1996)

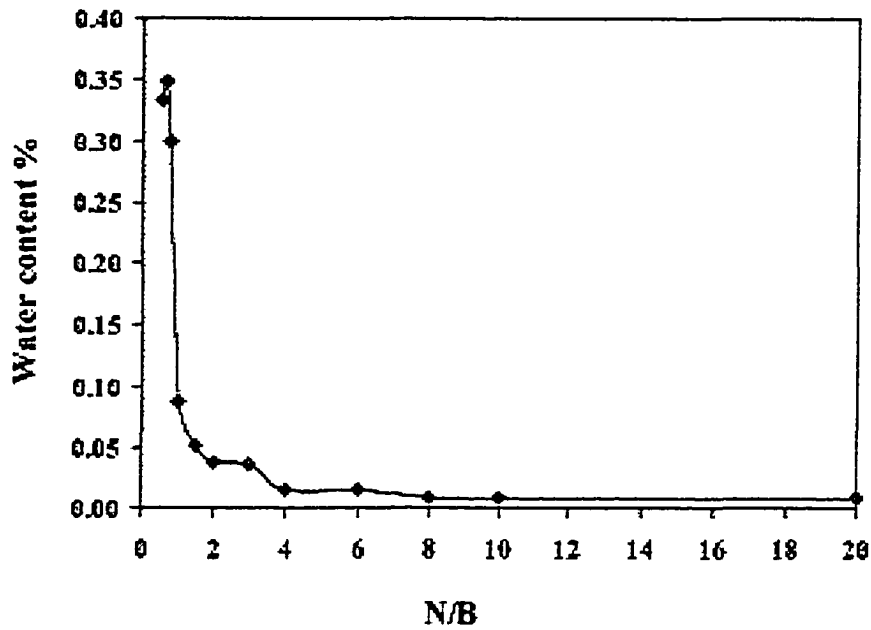


Figure 2.1: Effect of the solvent to bitumen ratio on the emulsion stability.
(Reference: Yang & Czarnecki, 2002)

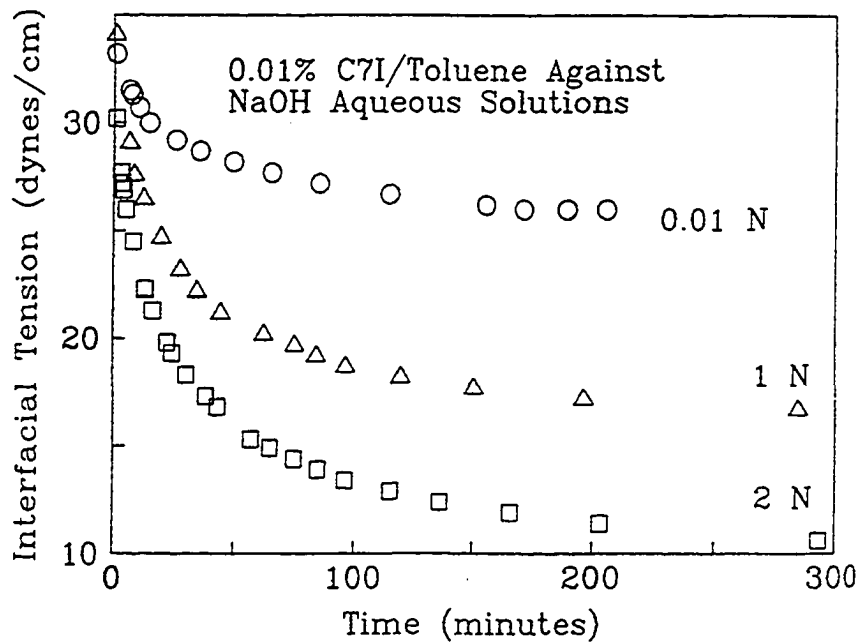


Figure 2.2: Dynamic surface tension measurements for the determination of the kinetics of asphaltene adsorption at toluene-water interfaces.
(Reference: Sheu et al., 1992)

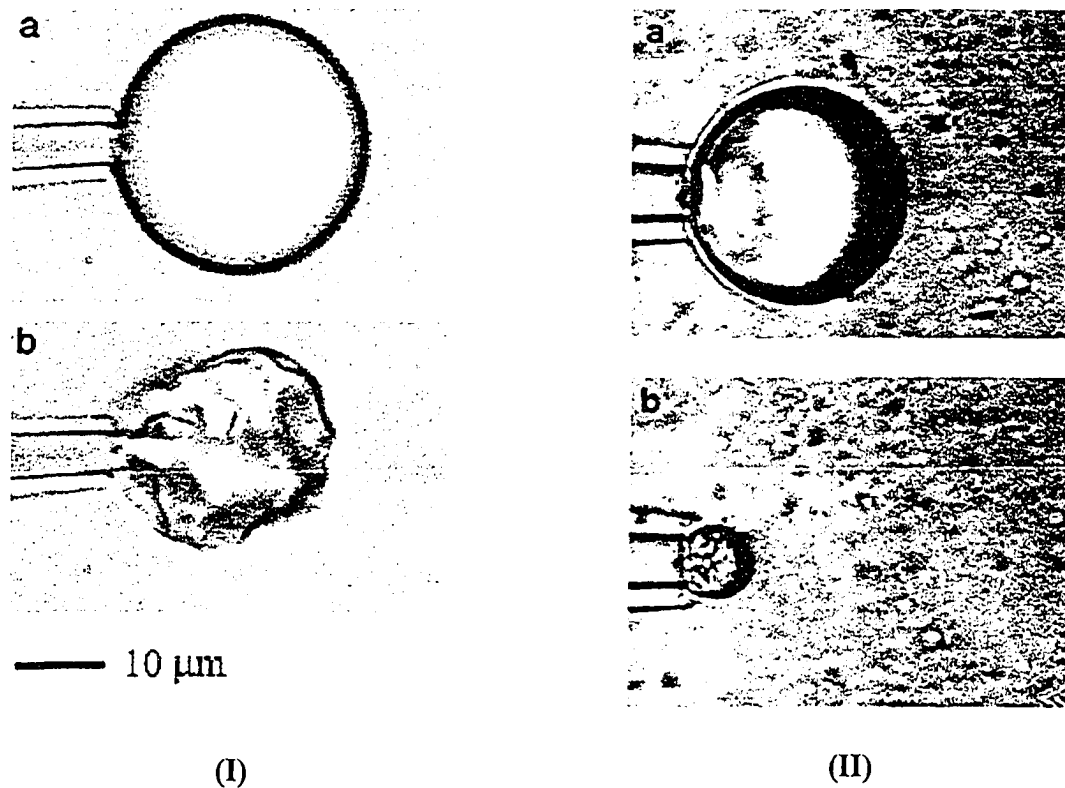


Figure 2.3: Effect of the critical solvent to bitumen ratio on the interfacial film rheology.

(I) Above the critical ratio (rigid film)

(II) Below the critical ratio (flexible film)

(Reference: Dabros et al., 1999)

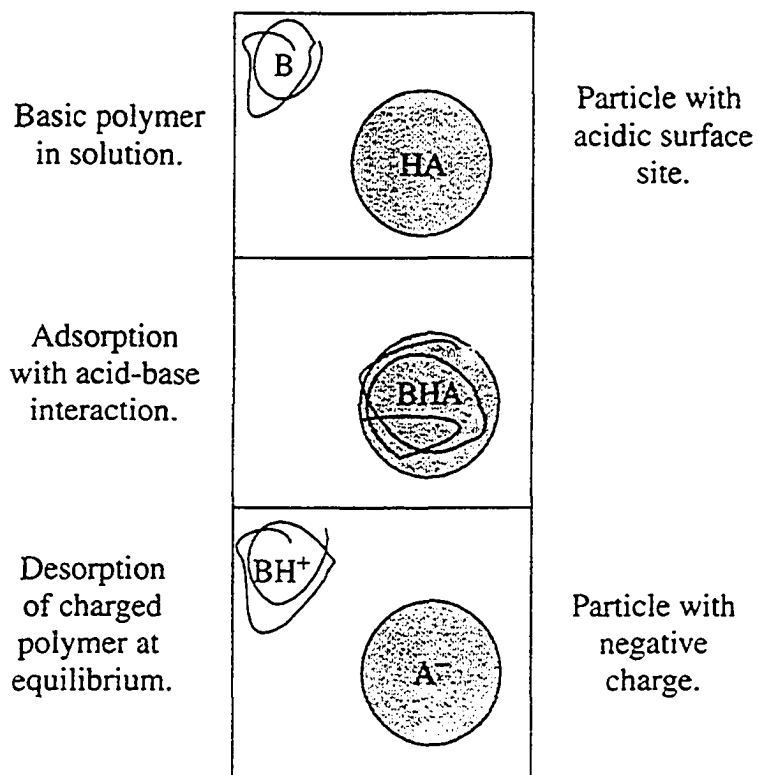


Figure 2.4: Fowkes mechanism of electrostatic charging in nonaqueous media.
(*Reference: Morrison & Ross, 2002*)

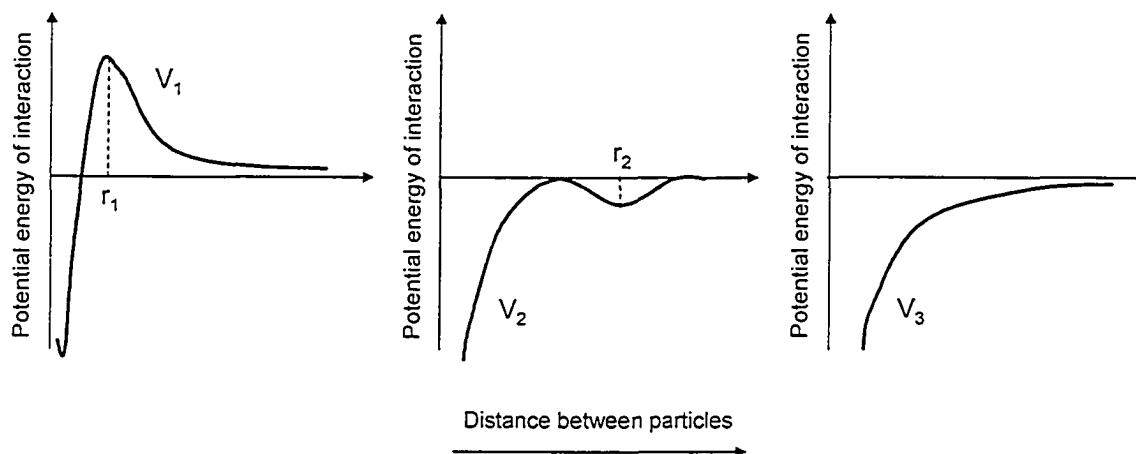


Figure 2.5: Interaction potentials for approaching particles.
(*Adapted from: Masliyah, 1994*)

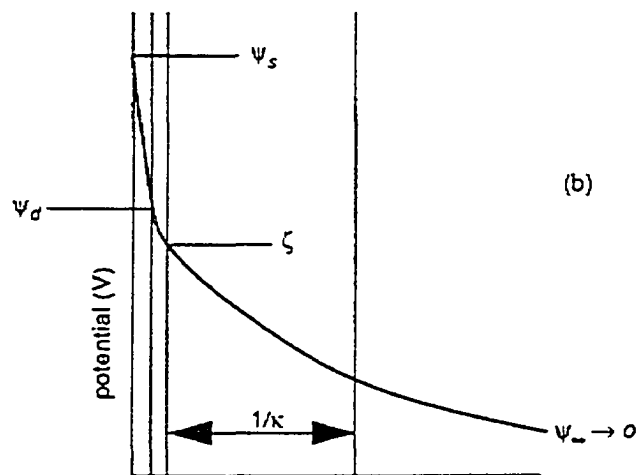
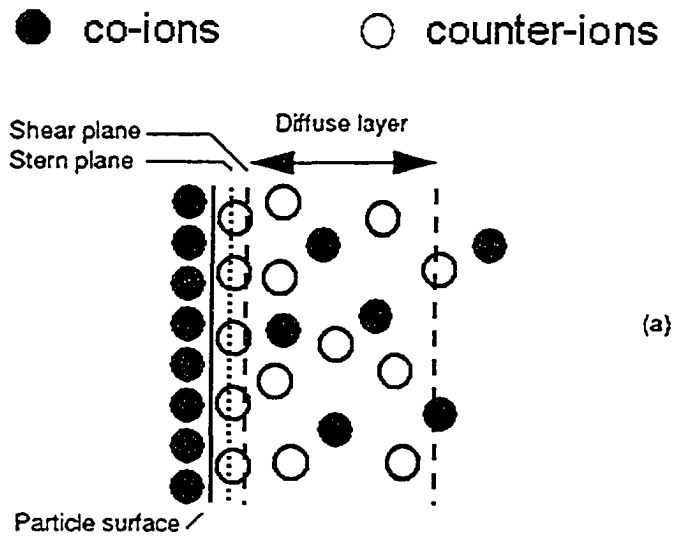


Figure 2.6: Representation of the electric double layer.

- (a) Structure of the double layer
- (b) Decay in the electric potential

(Reference: Masliyah, 1994)

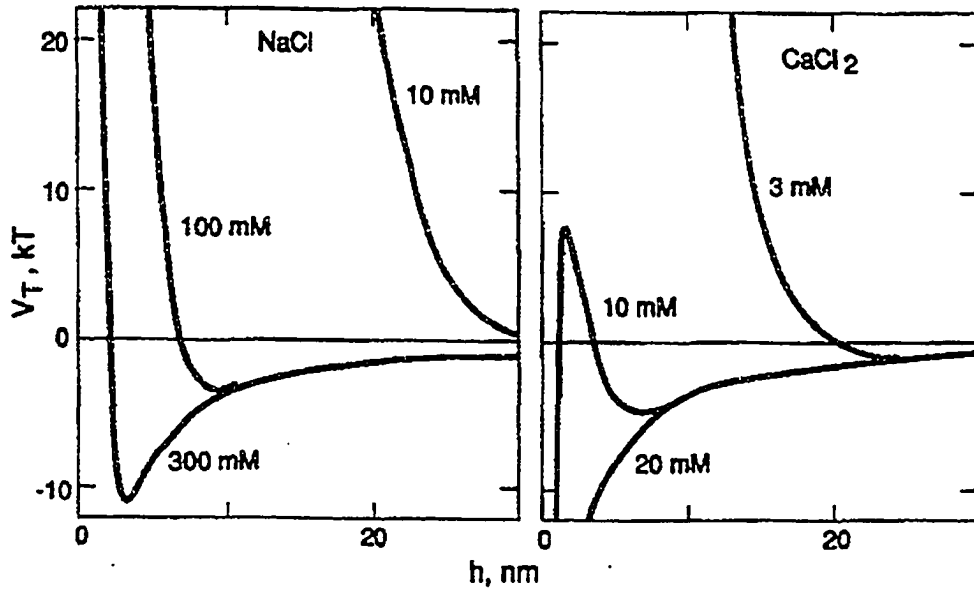


Figure 2.7: Potential energy of interaction for bitumen-in-water emulsions in the presence of NaCl and CaCl₂.

(Reference: Isaacs & Chow, 1992)

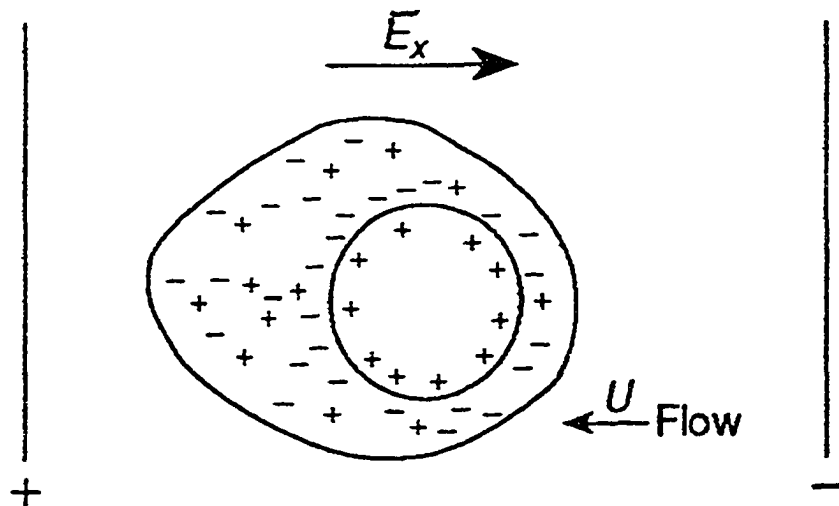


Figure 2.8: Double layer distortion due to relaxation effect.

(Reference: Masliyah, 1994)

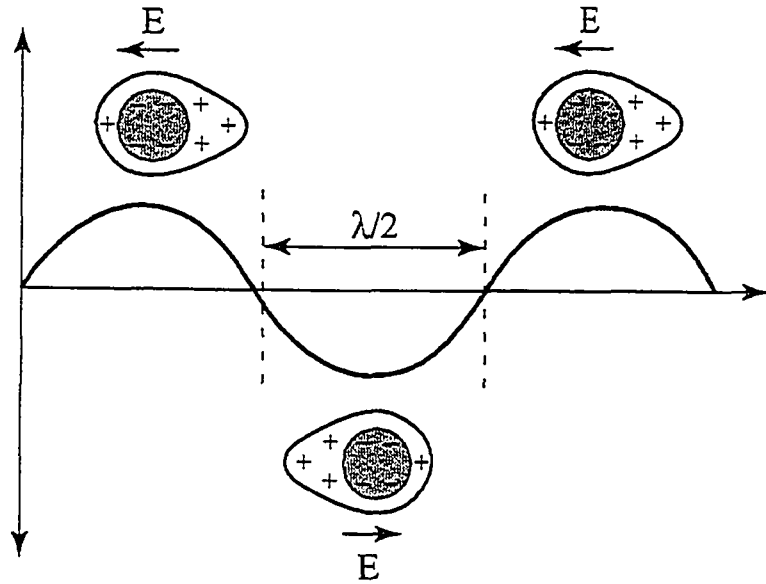


Figure 2.9: Alternating polarization of the electric double layer created by an acoustic wave.
 (Reference: Morrison & Ross, 2002)

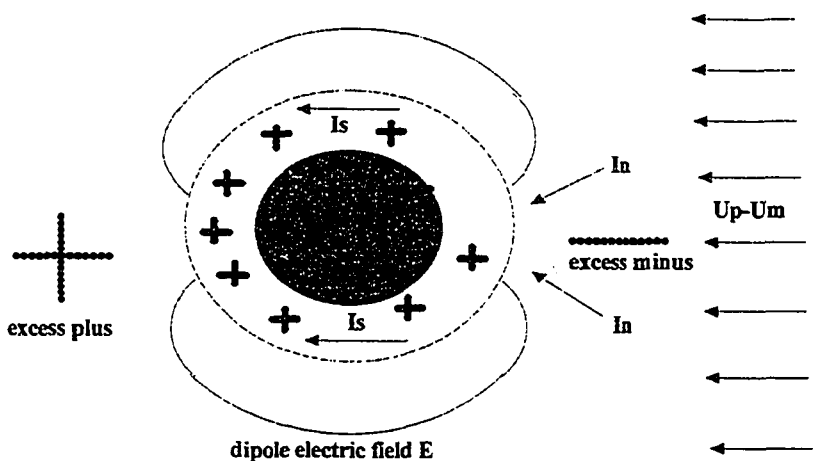


Figure 2.10: Double layer polarization due to the relative liquid flow.
 (Reference: Dukhin & Goetz, 2002)

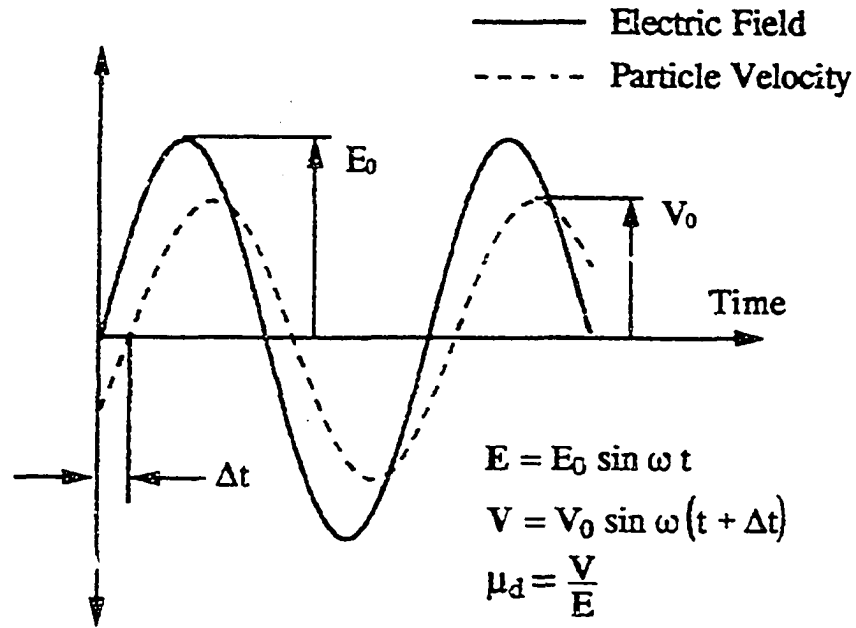


Figure 2.11: The definition of the dynamic electrophoretic mobility.

(Reference: Cannon, 1993)

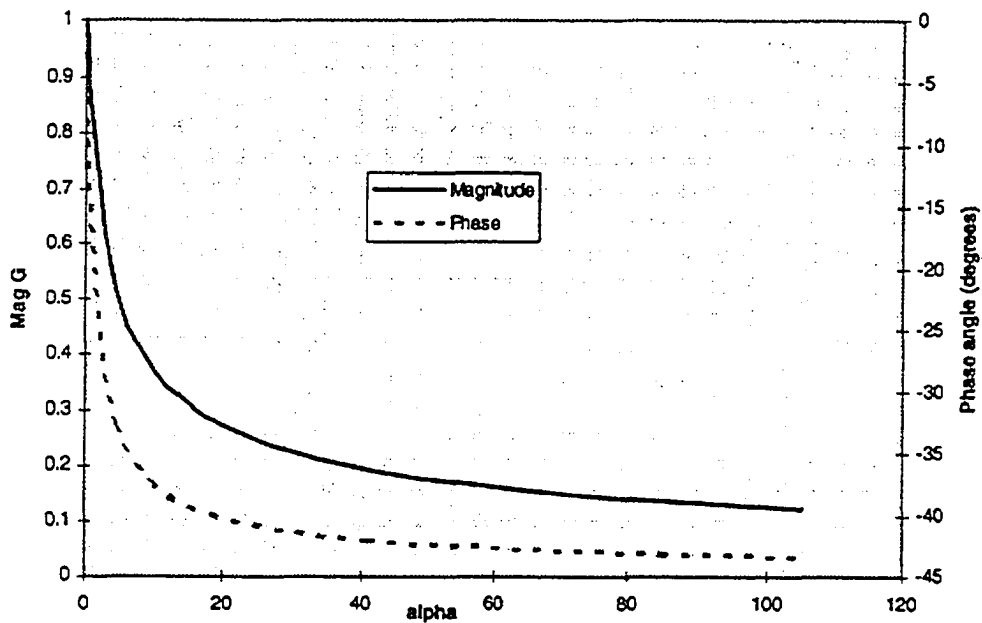


Figure 2.12: Magnitude and phase angle of inertia factor G according to O'Brien's approach (calculated for $\rho_p = 2\rho_m$).

(Reference: Hunter, 1998)

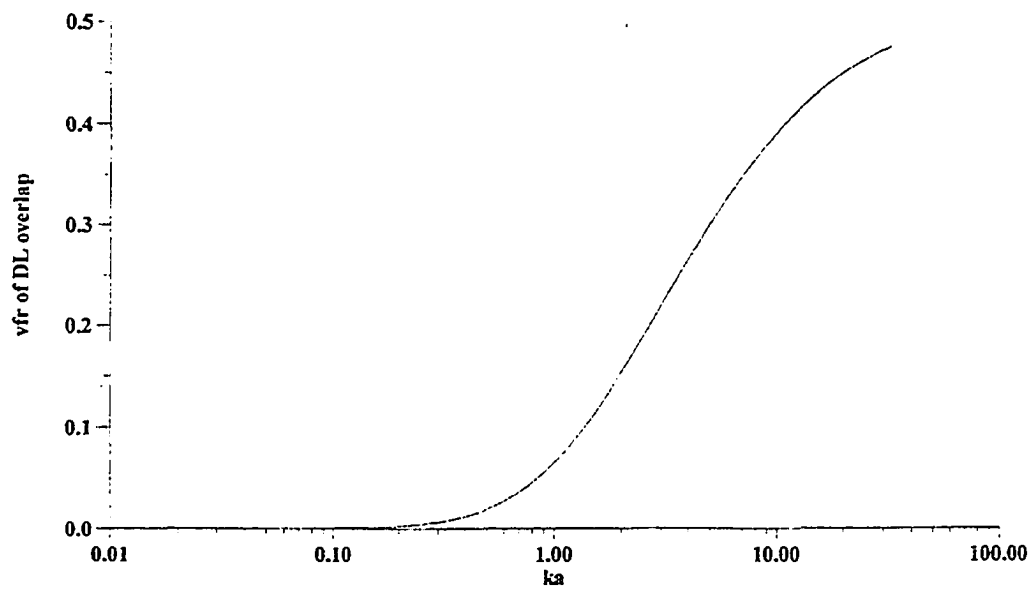


Figure 2.13: Estimate of the minimum volume fraction for double layer overlap.
(Reference: Dukhin & Goetz, 2002)

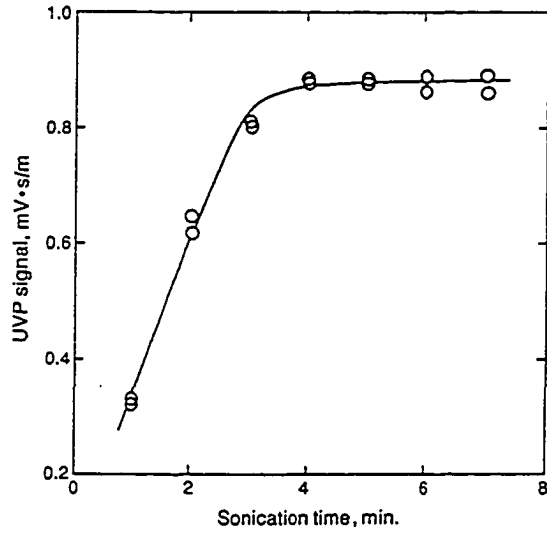


Figure 2.14: Effect of sonication time on the CVP signal for a 10% water-in-Leduc crude oil emulsions.

(Reference: Isaacs et al., 1990)

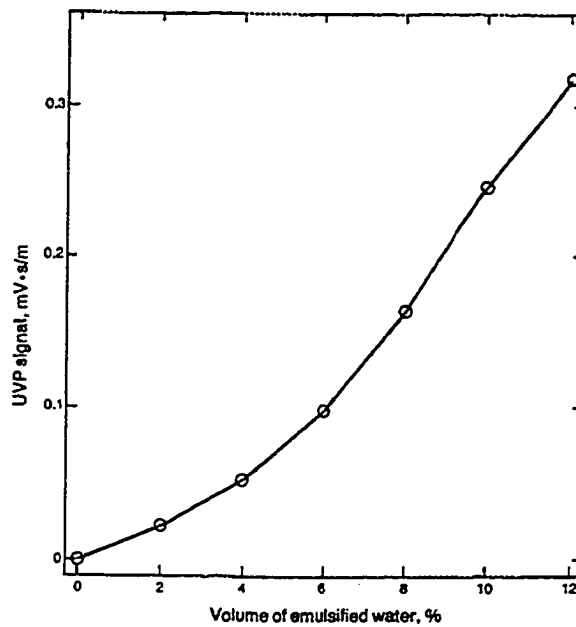


Figure 2.15: Sensitivity of CVP signal to water content in water-in-Leduc crude oil emulsions.

(Reference: Isaacs & Chow, 1992)

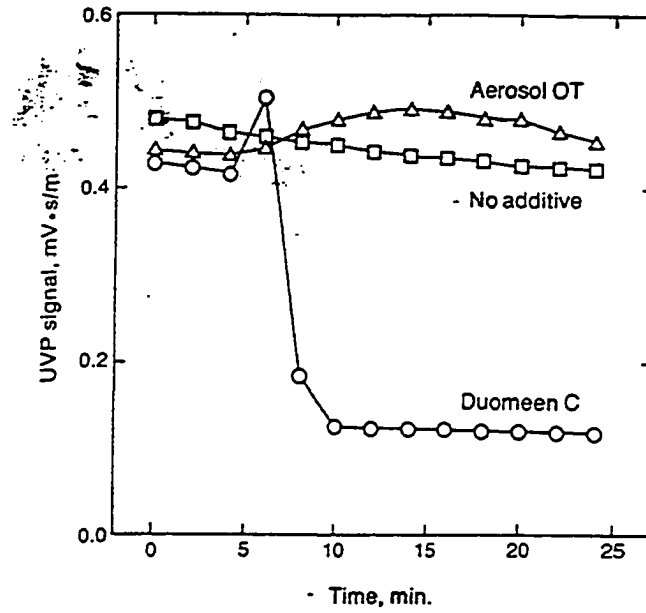


Figure 2.16: The change in CVP signal in the presence and absence of the addition of 100 ppm chemical at 4 min.

(Reference: Isaacs et al., 1990)

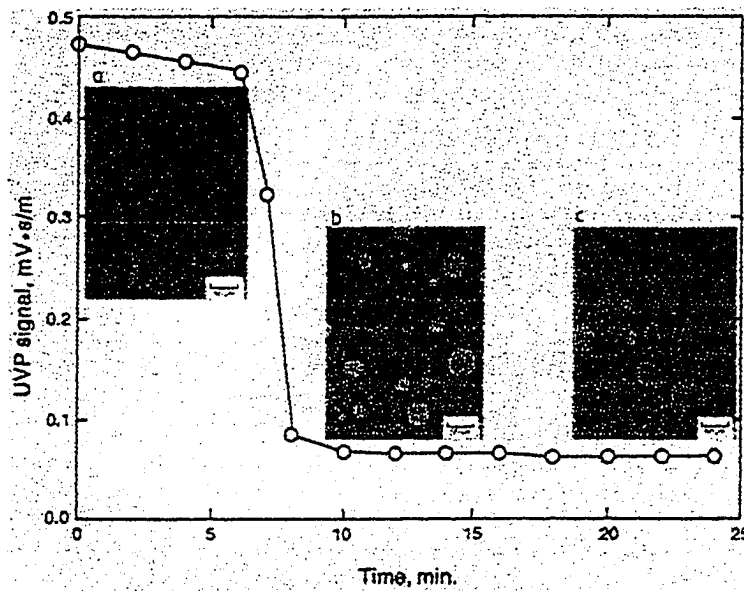


Figure 2.17: Sensitivity of the CVP signal to the coagulation process (photographs taken at 3, 12 and 24 min).

(Reference: Isaacs et al., 1990)

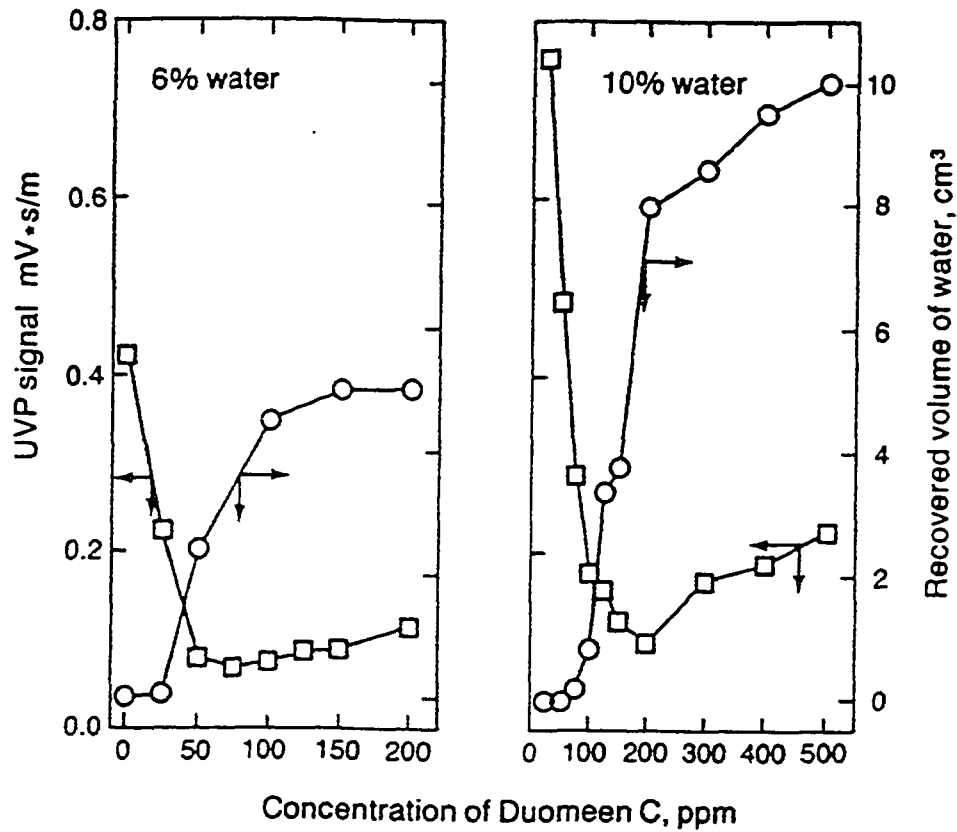


Figure 2.18: Comparison of the coagulation process as determined by electroacoustic analysis (□) and centrifugation tests (○)

(Reference: Isaacs et al., 1990)

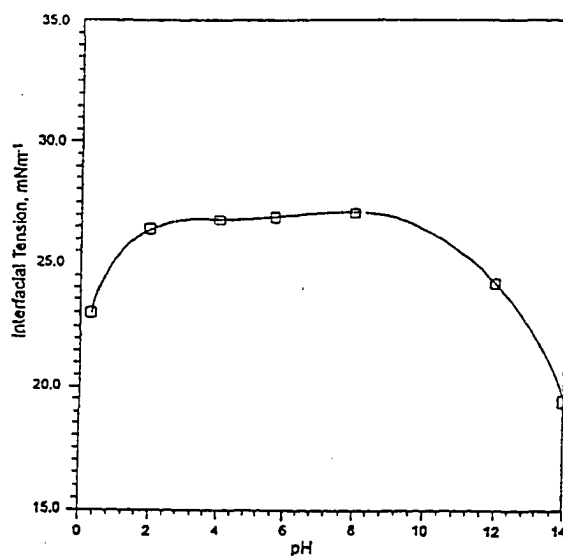


Figure 2.19: Interfacial tension between a 100 ppm asphaltenes-in-toluene solution and water as a function of pH at 22 °C.

(Reference: do Carmo Marques et al., 1997)

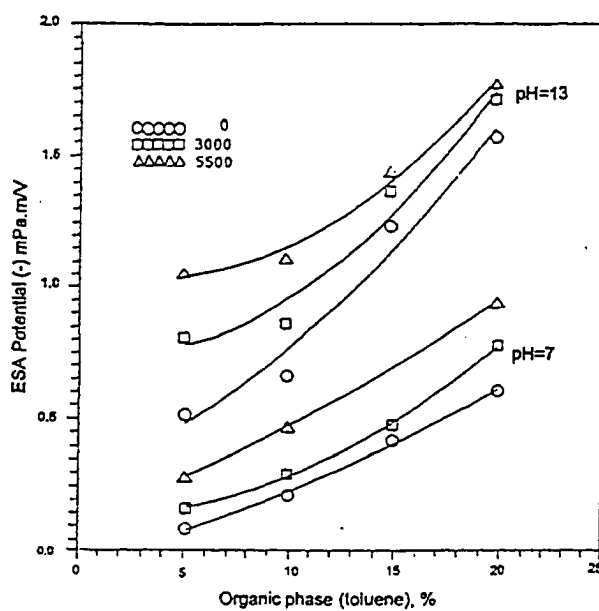


Figure 2.20: ESA signal of toluene-in-water/SLS/CA emulsions, as a function of pH and asphaltene content.

(Reference: do Carmo Marques et al., 1997)

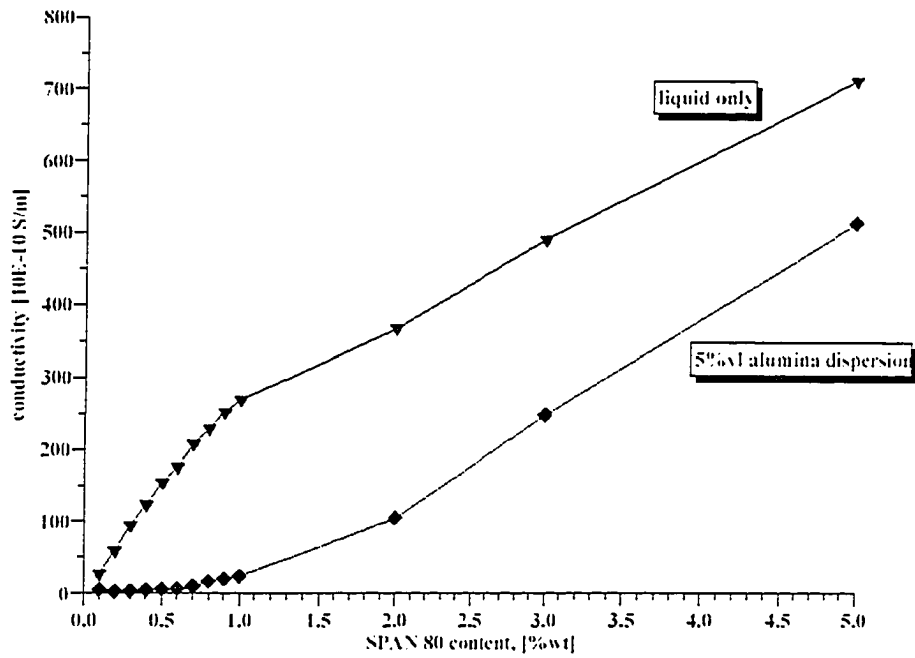


Figure 2.21: Conductivity of alumina dispersion as a function of SPAN 80 content.
(Reference: Dukhin & Goetz, 2004A)

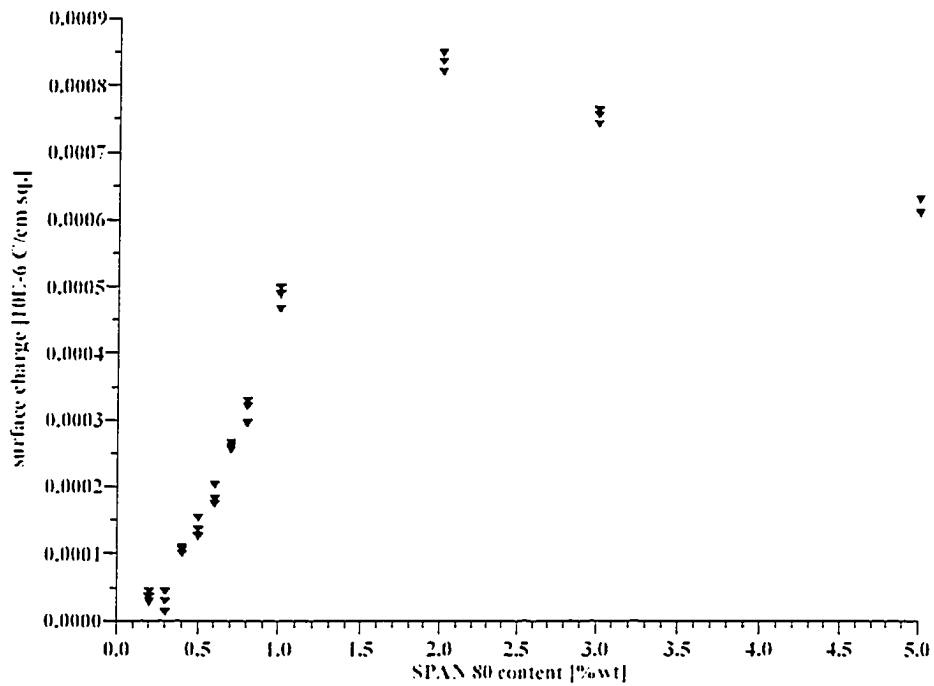


Figure 2.22: Surface charge density of alumina dispersion.
(Reference: Dukhin & Goetz, 2004A)

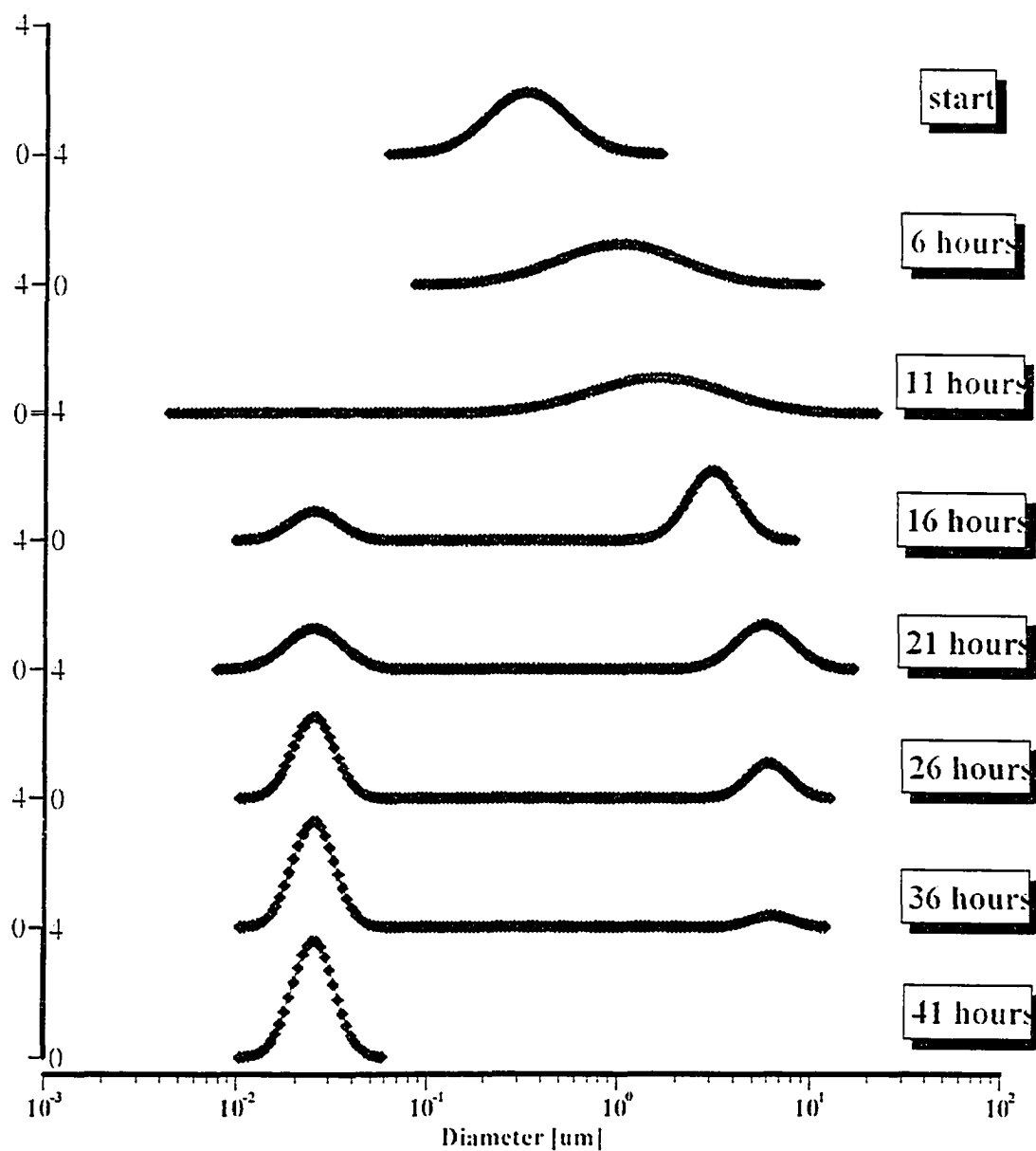


Figure 2.23: Evolution of the droplet size distribution of water-in-kerosene emulsions in time.

(Reference: Dukhin & Goetz, 2004B)

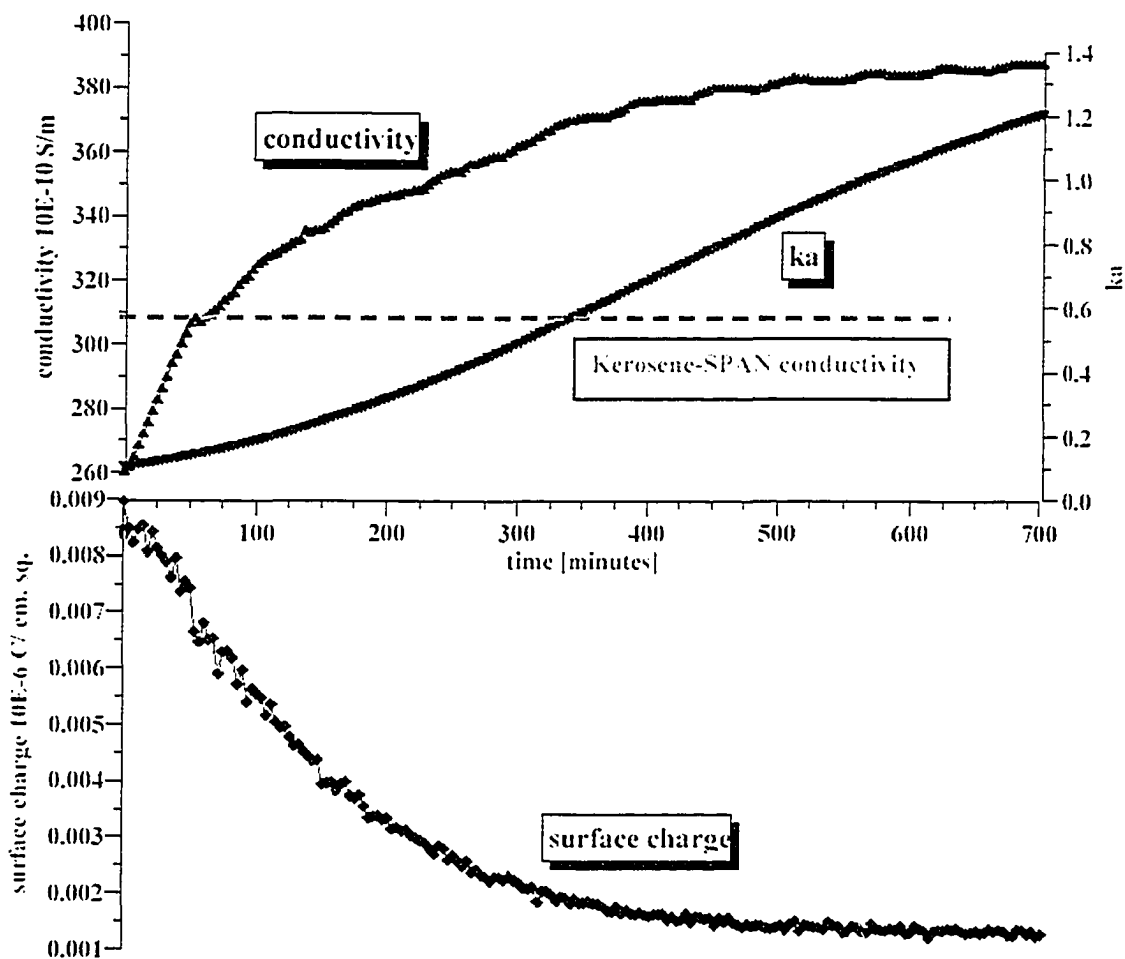


Figure 2.24: Evolution of the conductivity and surface charge density of water-in-kerosene emulsions in time.

(Reference: Dukhin & Goetz, 2004B)

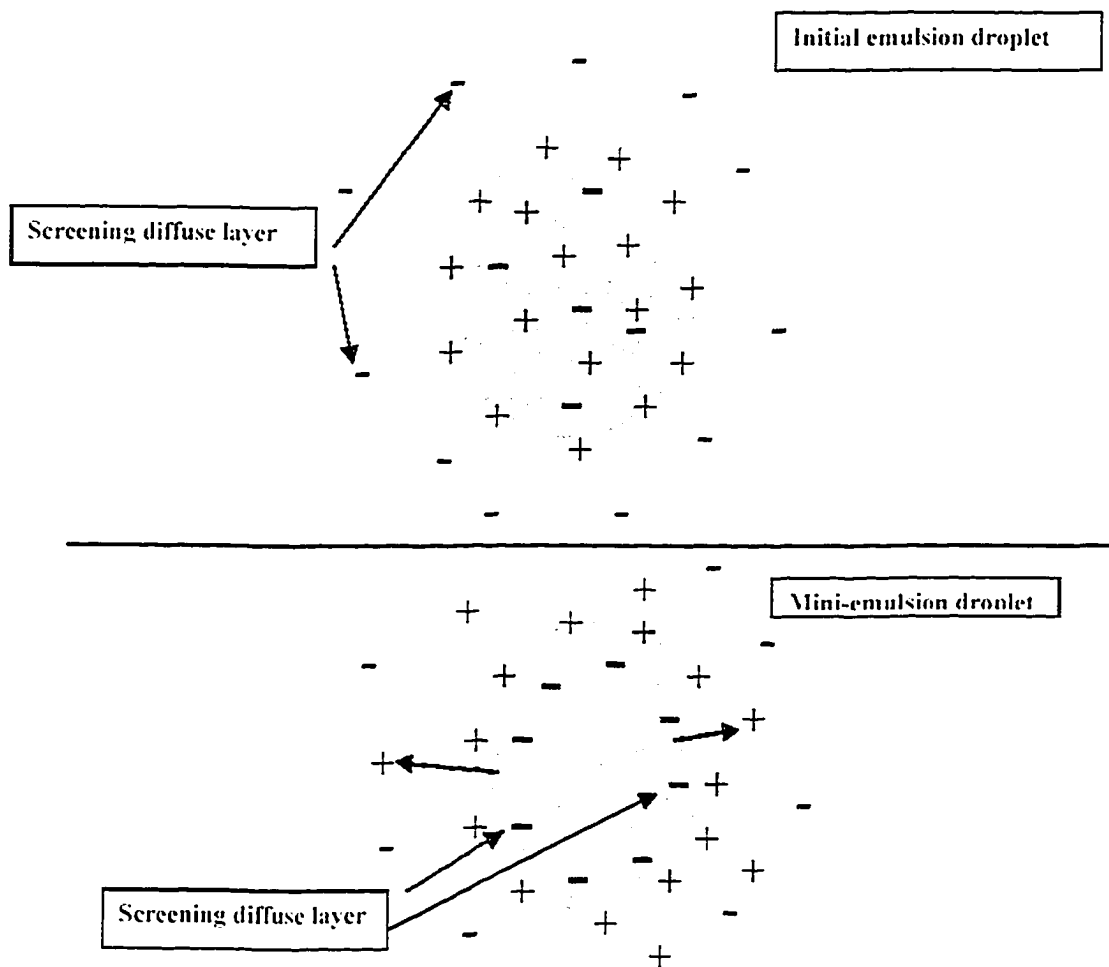


Figure 2.25: Double layer restructuring due to the ion exchange between interior and exterior of the water droplet.

(Reference: Dukhin & Goetz, 2004B)

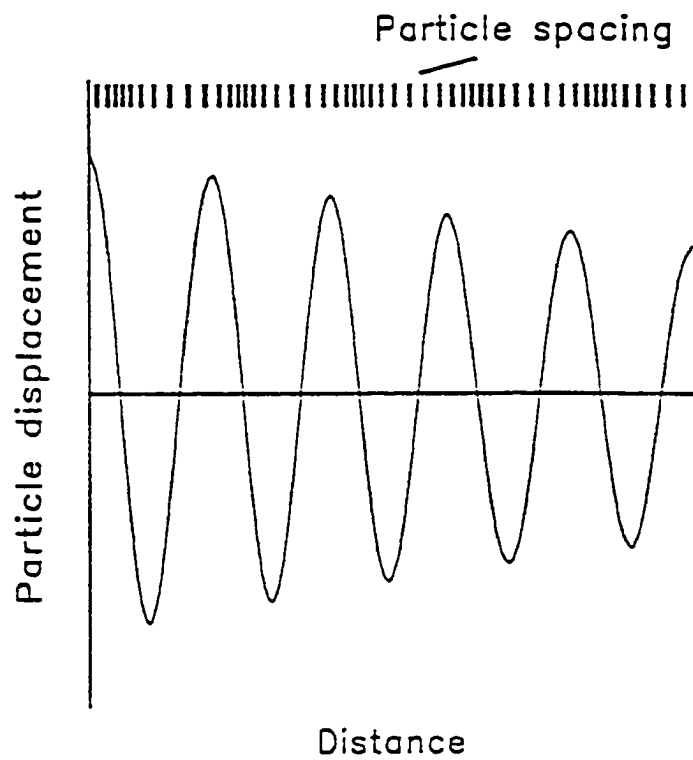


Figure 2.26: Representation of the propagation of compressional waves in a dispersion.
(Reference: McClements, 1991)

Chapter 3

Experimental

3.1 *Materials*

Materials for the preparation of water-in-diluted bitumen emulsions include: Athabasca diluted bitumen (Suncor Energy Inc.), toluene HPLC grade (Fisher Scientific), and deuterium oxide 99.8% atom D (Fisher Scientific). We will refer to Suncor diluted bitumen as being “bitumen”.

Naphtha diluted bitumen was used as received from Suncor Energy Ltd in the emulsion preparation. The asphaltene content of Suncor bitumen is 12% wt. The procedure for the asphaltene determination is as follows. A mass of 10 g of diluted bitumen was diluted with toluene (10% wt. bitumen concentration). Solids were removed by centrifugation at 20,000 g and 21 °C, and the toluene diluted bitumen sample was then kept in a fume hood for 10 days for natural evaporation of the organic solvent. The solvent-free bitumen was diluted with n-heptane HPLC grade (Fisher Scientific) at a solvent to bitumen ratio of 40:1 by weight. The sample was shaken for 2 hours and then kept settling for 24 hours. The sample was filtered using a 0.2 micron PTFE membrane filter (Whatman). The filter cake was washed with n-heptane and then put in an oven at 100 °C for 2 hours. Finally, the filter cake was weighted and the asphaltene content was calculated.

Calibration of the Electroacoustic Spectrometer was made with an aqueous dispersion of known ζ -potential, prepared with Silica Ludox TM-50 dispersion (50% wt) provided by Dispersion Technology Inc., distilled water (passed through a Millipore filter system), potassium chloride ACS reagent (Sigma-Aldrich), and potassium hydroxide ACS reagent (BDH).

Toluene certified ACS (Fisher Scientific) and 2-propanol HPLC grade (Fisher Scientific) were used for cleaning the spectrometer chamber.

3.2 Equipments

3.2.1 DT-1200 Acoustic and Electroacoustic Spectrometer

Figure 3.1 shows the DT-1200 Acoustic and Electroacoustic Spectrometer. Figure 3.2 details the components of the spectrometer chamber after equipment improvements were made.

The Spectrometer is provided with a rectangular chamber where approximately 125 ml of a sample can be fed. A magnetic stirrer device is connected to the bottom of the chamber. The stirring bar acts as a vortex stirrer and also as a centrifugal pump to circulate fluid from bottom to top of the chamber through the recirculation line (Dispersion Technology, 2003). The speed of the stirring bar is adjusted to keep the dispersion well mixed and prevent possible sample sedimentation. There are 6 preset stirring speeds.

The upper part of the chamber is attached to the acoustic sensors, where two piezoelectric transducers are placed over opposite lateral walls in the chamber. The transmitting transducer (on the right hand side in Figure 3.1) is fixed. The receiving transducer (on the left hand side) is movable. The gap between the transducers can be controlled by a stepping motor from 0.15 to 20 mm (Dukhin & Goetz, 2002). Sound pulses are transmitted through the sample dispersion and the resulting sound attenuation between the two acoustic transducers is measured at 18 frequencies (within the 3 to 100 MHz range) and 21 gaps (Dukhin & Goetz, 2002). An acoustic spectrum is generated (sound attenuation coefficient versus frequency) from which the particle size distribution is then calculated.

The Electroacoustic probe is inserted into the lower part of the chamber. Both, the transmitting and receiving transducers are mounted in the same probe. The transmitting transducer emits sound pulses at a frequency of 3 MHz (Dukhin & Goetz, 2002). The receiving transducer consists of a two-element antenna. The electric field response due to the electroacoustic effect changes the potential of one of the element with respect to the other, causing a current flow in the antenna which is referred to as the Colloid Vibration Current signal or *CVC signal* (Dukhin & Goetz, 2002).

The present work implemented the following equipment improvements to the DT-1200 spectrometer. The original chamber is composed of two blocks made of plastic material, tightly joined by thumbscrews (this is illustrated by the two blocks shown in Figure 3.2). The upper block is attached to the acoustic sensor. The lower block (where the electroacoustic probe is installed) is removable by unscrewing the thumbscrews. This lower block was replaced by a water-jacketed metallic chamber (Figure 3.3), which allowed temperature control of the emulsion sample (around 20.7 ± 0.2 °C) by means of a circulating water bath (Fisher Scientific - Isotemp 3016). The Spectrometer includes a temperature probe in the chamber for continuous monitoring of the sample temperature. The metallic chamber also functioned as a Faraday shield to the electroacoustic probe, as an attempt to reduce the noise of the CVC signal. The metallic chamber was grounded to the stainless steel shell of the electroacoustic probe.

Another equipment improvement was the installation of a conductivity meter (Scientifica - model 627), provided with a stainless steel flow-through probe which was connected to the recirculation line as shown in Figure 3.4. The conductivity probe could not be installed in the main recirculation line because it caused significant restriction to flow. Therefore, it was installed on a side connection (previously used for chamber drainage). Sample was drawn into the conductivity probe by means of a 3 ml Teflon syringe (Braun Injekt). In order to get a representative sample, normally 30 strokes were performed to expose the probe to fresh sample before conductivity reading. The full scale of the conductivity meter is 38 to 38,000 picosiemens/cm with an accuracy of 2%. Conductivity is measured at 18 Hz with an applied voltage of 5 volts rms, approximately (Scientifica, 2003).

Finally, a high speed homogenizer (Fisher Scientific - PowerGen Homogenizer, 125 watt and 30,000 rpm variable speed) was mounted at the top of the chamber in order to disperse water in diluted bitumen directly within the chamber. It was removed from the chamber before starting measurements with the spectrometer. Figure 3.5 and 3.6 show the homogenizer probe component parts. Figure 3.2 shows the positioning of the homogenizer probe relative to the chamber geometry.

3.2.2 Supplementary equipment

An Anton Paar DMA 45 density meter based on the vibrating tube technique was used for high precision density measurements of diluted bitumen (with an accuracy of 10^{-4} g/ml) at 15 °C, 20 °C and 25 °C \pm 0.01 °C.

A Cannon-Fenske viscometer size 100 was used for the determination of the kinematic viscosity of diluted bitumen and heavy water at 20 °C \pm 0.1 °C.

In order to rule out emulsified water sedimentation in the chamber, emulsion samples were taken with a 200 μ L Hamilton syringe at three levels in the chamber (top, medium and bottom). The water content of emulsion samples were measured with a G.R. Scientific Ltd. Karl Fisher titrator model Cou-Lo 2000 (measuring range 1 μ g - 10 mg water). A correction factor of 1.111 applies when determining heavy water content.

Equipment for diluted bitumen and emulsion preparation include: Sartorius semi-analytic and analytic balances, high speed shaker (200 per minute), 1 liter glass bottles for diluted bitumen preparation, and 250 ml Teflon bottles for diluted bitumen storage at 4 °C.

Emulsified water drops sedimentation tests were performed to investigate the emulsion stability as a function of bitumen concentration. Supplementary equipment for performing these tests include: 10 ml Kimax conical-bottom glass centrifuge tubes (graduated 0.1 ml), Lindberg thermal bath at 20 °C, low speed shaker (30 per minute) and vortex maxi mix plus agitator (3,000 rpm).

A sonication bath (Fisher Scientific Ultrasonic Cleaner FS-30) was used to investigate the effect of water dispersion by sonication on the electroacoustic phenomenon of water-in-diluted bitumen emulsions.

Finally, an Accumet AR50 pH meter was used for adjusting the pH of the Silica Ludox sample used for the calibration of the electroacoustic spectrometer.

3.3 Droplet size distribution measurements

3.3.1 Calibration of acoustic spectrometer and sound attenuation measurement

The Acoustic Spectrometer does not require calibration using a colloid sample with known particle size (Dukhin & Goetz, 2001). It only requires the precise measurement of the attenuation coefficient of the sample (α_{sample}) in order to calculate the droplet size distribution using a suitable predictive theory, as discussed in section 2.6. The DT-1200 spectrometer electronics include a precision fixed 40 dB reference attenuator. For every attenuation measurement, the signal of the sample is compared with the signal level from the 40 dB reference attenuator (Dukhin & Goetz, 2002). This allows the precise measurement of the attenuation coefficient of any sample.

Measurement of the sound attenuation is performed by a transmission variable gap technique involving two transducers (transmitter and receiver). The main advantage of a variable gap technique is that it allows the measurement of the attenuation coefficient over a wide range of values, at several frequencies. This is normally not possible in a fixed gap technique (Dukhin & Goetz, 2002). This means that different samples might require different gaps between transducers, and the variable gap technique should handle this requirement.

Equation 2.22 shows the calculation of the attenuation coefficient of the sample. For clarity in the following explanation, let us recap Equation 2.22 and the meaning of the variables involved: I_{ini} is the initial sound intensity, I_{end} is the sound intensity after traveling a distance L in the sample, and ω is the frequency of the sound pulse.

$$\alpha = \frac{20}{\omega} \frac{\log_{10} \left(\frac{I_{\text{ini}}}{I_{\text{end}}} \right)}{L} \quad (3.1)$$

The DT-1200 spectrometer measures the attenuation coefficient at the following 18 frequencies: 3.0, 3.7, 4.5, 5.6, 6.8, 8.4, 10.3, 12.7, 15.6, 19.2, 23.5, 28.9, 35.5, 43.7, 53.6, 65.9, 81.0 and 99.5 MHz. For each frequency, the ratio $I_{\text{ini}}/I_{\text{end}}$ is determined at 21 gaps from 0.15 to 0.20 mm taken in logarithmic steps (Dukhin & Goetz, 2002). Minimum 800 pulses are averaged for every $I_{\text{ini}}/I_{\text{end}}$ measurement in order to achieve a satisfactory signal to noise ratio of at least 40 db. The attenuation coefficient is then calculated from a

regression analysis of I_{ini}/I_{end} versus L for each frequency (Dukhin & Goetz, 2002). Finally, the acoustic spectrum is generated (attenuation coefficient versus frequency), and the droplet size distribution is calculated. In the present study, this process required between 5 to 7 minutes to be completed for each droplet size distribution measurement.

The details of the electronics of the DT-1200 Spectrometer for the determination of I_{ini}/I_{end} and regression analysis are given in reference (Dukhin & Goetz, 2002).

3.3.2 Droplet size distribution analysis

The predictive theory for droplet size calculation was briefly discussed in section 2.6.2. It was presented some simplified equations which relate the attenuation coefficient with the material properties of the emulsion and the droplet size distribution. Such simplified equations were presented in order to explain the relationship between the measured acoustic spectrum and the droplet size distribution in the easiest way possible. Such analysis allows interpreting the acoustic spectrum qualitatively. The complete theoretical treatment is very complex and it is presented in reference (Dukhin & Goetz, 2002).

The DT-1200 analysis software includes an optimization algorithm which finds the droplet size distribution that best fit the experimentally measured acoustic spectrum, based on the aforementioned predictive theory. The following information is required for the calculation of the droplet size distribution, in addition to the acoustic spectrum (Dukhin & Goetz, 2002):

- i) Concentration of the dispersed phase
- ii) Thermodynamic properties
 - { Density
 - { Thermal expansion
 - { Specific heat
- iii) Transport properties
 - { Viscosity
 - { Thermal conductivity
- iv) Acoustic properties
 - { Intrinsic attenuation coefficient
 - { Sound speed

As discussed in (Dukhin & Goetz, 2002) and section 2.6, emulsions belong to the category of soft particle dispersion where thermal loss is the dominant mechanism of sound attenuation. In this case, in addition to the volume fraction, the most important properties needed to be known with accuracy are the density, thermal expansion, intrinsic attenuation coefficient and sound speed of both phases (Dukhin & Goetz, 2002). All material properties were determined at 20 °C.

The characterization of diluted bitumen required high precision density measurements at three different temperatures: 15 °C, 20 °C and 25 °C. This allowed the calculation of the thermal expansion of diluted bitumen at 20 °C as follows:

$$\beta \approx \rho_{20^{\circ}\text{C}} \cdot \left(\frac{\frac{1}{\rho_{25^{\circ}\text{C}}} - \frac{1}{\rho_{15^{\circ}\text{C}}}}{10} \right) \quad (3.2)$$

The density of diluted bitumen was determined at several bitumen concentrations in toluene (from 0% to 70% by weight), because this information is required for performing emulsified water drops sedimentation tests (section 3.5.1).

The thermal expansion of heavy water was determined using the same formula with density data obtained from reference (CRC Handbook, 2003). These are 1.1056 g/ml (15 °C), 1.105 g/ml (20 °C), and 1.1044 g/ml (25 °C).

The intrinsic attenuation coefficients (within the 3 – 100 MHz range) and sound speeds of diluted bitumen and heavy water were determined using the DT-1200 Spectrometer.

The specific heat and thermal conductivity of diluted bitumen and heavy water were approximated to those reported in the DT-1200 material property database for toluene and water, respectively. The dynamic viscosity of diluted bitumen and heavy water were derived from kinematic viscosity measurements with the Cannon-Fenske viscometer at 20 °C.

The dynamic viscosity of diluted bitumen was also determined at several bitumen concentrations in toluene (from 0% to 70% by weight), because this information is

required for interpreting emulsified water drops sedimentation tests, as discussed later in section 3.5.1.

In general, the complexity of real droplet size distributions can be satisfactorily represented by a *log-normal distribution*, or by a *bimodal distribution*. These are the two statistically representative distributions considered in the DT-1200 analysis software. The results are reported based on the type of distribution that minimizes the fitting error of the prediction theory to the measured acoustic spectrum (Dukhin & Goetz, 2002).

A log-normal distribution (Figure 3.7) is characterized by two adjustable parameters: mean diameter (d_{Ln}) and standard deviation (σ_{Ln}). Equation 3.3 provides the density function for this distribution, in terms of these two adjustable parameters and the droplet diameter (X). The standard deviation is defined as the ratio of the droplet size at two specified points in the cumulative droplet size distribution curve (Figure 3.8), as shown in Equation 3.4 (Dukhin & Goetz, 2002).

$$q_r(X) = \frac{1}{\sqrt{2\pi}\text{Ln}(\sigma_{Ln})} \cdot \exp\left\{-\left[\frac{\text{Ln}\left(\frac{X}{d_{Ln}}\right)}{\sqrt{2}\text{Ln}(\sigma_{Ln})}\right]^2\right\} \quad (3.3)$$

$$\sigma_{Ln} = \frac{X(15.87\%)}{X(50\%)} \quad \text{or equivalently} \quad \sigma_{Ln} = \frac{X(50\%)}{X(84.13\%)} \quad (3.4)$$

The bimodal distribution is defined as the superposition of two lognormal distributions with the same standard deviation, and it is characterized by four adjustable parameters: two mean diameters, standard deviation and the relative weight of modes (Dukhin & Goetz, 2002).

3.4 Droplet surface charge density measurement

3.4.1 Calibration of electroacoustic probe and CVC measurement

The Electroacoustic Spectrometer requires calibration using a colloidal dispersion with known ζ -potential. Following the manufacture's instructions, Silica Luddox TM-50

dispersion 10% by weight was used for this purpose. This calibration colloid is prepared by diluting a concentrated Silica sample (50% by weight, provided by Dispersion Technology) with 0.01 mol/L KCl solution adjusted to pH 10 with potassium hydroxide (Dispersion Technology, 2003). Such Silica suspension has a ζ -potential of -38 mV (Dukhin & Goetz, 2002).

Figure 3.9 details the component parts of the electroacoustic probe used for CVC measurements. Both, the transmitting and receiving transducers are mounted in the same probe. The transmitting transducer is described next. The electronics of the spectrometer generates 1 Watt radio frequency pulses which are routed to the piezoelectric device. Here, the electric pulses are converted to sound pulses at 3 MHz, which are then partially transmitted through the quartz delay rod, then through the Rexolite (buffer) delay rod, and finally through the dispersion sample facing the probe, creating the driving acoustic field of the electroacoustic phenomenon (Dukhin & Goetz, 2001; Dukhin & Goetz, 2002).

The receiving transducer consists of a two element antenna immersed in the sample. The end of the Rexolite (buffer) delay rod is coated with gold. This provides an electrode which can sense the change in electric potential in the suspension due to the electroacoustic effect. This is called the *center electrode* in Figure 3.9. On the other hand, the stainless steel shell which protects the electroacoustic probe constitutes the *outer electrode* which remains at a reference electric potential. Both electrodes are connected to the spectrometer measuring circuit through a coaxial cable. The center electrode is connected to the center conductor of the coaxial cable. The shield of the coaxial cable makes connection with the stainless steel shell (outer electrode). Both electrodes are separated by a ceramic material in the probe (Dukhin & Goetz, 2002).

Under the condition of low impedance of the measuring circuit (section 2.4.3), the antenna senses an electric current which is carried by the coaxial cable. This is referred to as the Colloid Vibration Current (CVC). The magnitude and phase of this current is available in the DT-1200 software, and it is referred to as the *CVC signal*. The CVC phase refers to the phase lag between current and the acoustic perturbation. The unit of such a current is not available to the user. In the present work, it will be referred to as the CVC signal expressed in *absolute units*, following the terminology used in reference (Dukhin & Goetz, 2004B). The important message here is that the CVC signal is a

number which is proportional to the CVC current being measured. The calculation of the surface charge density or ζ -potential is derived from the CVC signal after equipment calibration, as discussed in the next section.

Same as for acoustics, a minimum of 800 pulses measurements are averaged in order to achieve a high signal to noise ratio in CVC measurements. Indeed, CVC measurements in low conductivity media require the averaging of millions of pulses (Dukhin & Goetz, 2001). There are several options in the DT-1200 spectrometer for controlling the number of pulses during CVC measurements. In the present work, only two options were considered. They will be referred to as the *short integration time* and *long integration time* modes for CVC measurement. Approximately 1.6 million pulses are averaged in the short integration time mode, and every CVC measurement requires from 3 to 4 minutes to be completed. The long integration time mode collects 8 million pulses, approximately, and every measurement takes between 30 to 35 minutes to be completed.

3.4.2 Droplet surface charge density analysis

Equations 2.9 and 2.20 are the fundamental expressions for the calculation of the droplet surface charge density of water-in-diluted bitumen emulsions from CVC measurements. For clarity in the following explanation, let us recap these equations:

$$\langle \text{CVC} \rangle = Q_2 \varphi \left(\frac{\rho_p - \rho_m}{\rho_m} \right) \mu_d \quad (3.5)$$

$$\mu_d = \frac{2\sigma a}{3} \frac{\rho_m}{\rho_s \eta \Omega + j\omega(1-\varphi) \frac{2a^2}{9} \rho_p \rho_m} \quad \text{for } ka \ll 1 \quad (3.6)$$

As mentioned in section 2.4.5, $\langle \text{CVC} \rangle$ refers to the CVC signal (CVC) normalized by the pressure gradient of the acoustic perturbation in the dispersion (∇P). Therefore:

$$\langle \text{CVC} \rangle = \frac{\text{CVC}}{\nabla P} \quad (3.7)$$

As mentioned in the last section, the output of the electroacoustic probe is the CVC signal (CVC), and not the normalized CVC (<CVC>). Therefore, from Equation 3.5 and 3.7:

$$\text{CVC} = \nabla P \cdot Q_2 \varphi \left(\frac{\rho_p - \rho_m}{\rho_m} \right) \mu_d \quad (3.8)$$

As mentioned in section 2.4.5, constant Q_2 depends on the apparatus and the geometry of the electroacoustic probe used for the measurement of CVC. The value of Q_2 can be found by calibration with a dispersion of known properties (as mentioned in the last section). However, first it is still necessary to modify Equation 3.8 as follows (Dukhin & Goetz, 2001, Dukhin & Goetz, 2002):

$$\text{CVC} = (\nabla P_{\text{ant}}) \cdot \frac{2Z}{Z_{\text{ant}} + Z} Q_2 \varphi \left(\frac{\rho_p - \rho_m}{\rho_m} \right) \mu_d \quad (3.9)$$

The reason is the following. In Equation 3.8, ∇P is the pressure gradient of the acoustic perturbation in the dispersion, and it is not a constant. The design of the electroacoustic probe guaranties constant pressure amplitude at the center electrode (Figure 3.9). But when the sound pulse is transmitted from the center electrode to the dispersion, there is a loss in pressure amplitude which depends on the properties of the dispersion. Therefore, ∇P is not a constant in Equation 3.8.

A relationship between the pressure amplitude in the dispersion (P) and the pressure amplitude at the center electrode (P_{ant}) can be established based on the concept of acoustic impedance (Z), defined as the ratio between pressure amplitude and sound velocity (Dukhin & Goetz, 2002):

$$\frac{P}{P_{\text{ant}}} = \frac{2Z}{Z_{\text{ant}} + Z} \quad (3.10)$$

Z is the acoustic impedance of the dispersion, and Z_{ant} is the acoustic impedance of the center electrode. A similar expression to Equation 3.10 applies for ∇P and ∇P_{ant} , from which Equation 3.9 is derived.

The advantage of Equation 3.9 is that ∇P_{ant} and Q_2 can be combined in a single constant (C_{ant}), which can be determined by calibration (Dukhin & Goetz, 2001):

$$\text{CVC} = C_{\text{ant}} \frac{2Z}{Z_{\text{ant}} + Z} \varphi \left(\frac{\rho_p - \rho_m}{\rho_m} \right) \mu_d \quad (3.11)$$

The volume fraction, ζ -potential, particle size and materials properties are known for the Silica Ludox dispersion for calibration. This means that μ_d can be calculated for such dispersion (Equation 2.17). The acoustic impedance of the antenna is known and the acoustic impedance of the dispersion can be calculated from the density and sound velocity of the dispersion (Dukhin & Goetz, 2002):

$$Z = \rho_s c_s \quad (3.12)$$

Therefore, C_{ant} can be determined from the measurement of the CVC of the Silica Ludox dispersion.

Finally, the surface charge density of droplets in water-in-diluted bitumen emulsions can be calculated from CVC measurements after equipment calibration. This is done following the 2 steps procedure discussed in section 2.4.5. First, the dynamic electrophoretic mobility (μ_d) is determined from CVC (Equation 3.11), and then the surface charge density (σ) is derived from Equation 3.6.

The calculation of the surface charge density requires the same input information for the droplet size distribution calculation (section 3.3.2). Additionally, it is also required to know the CVC signal of the liquid medium of the dispersion. This is called the *background CVC signal* ($\text{CVC}_{\text{background}}$). The CVC signal that is considered in Equation 3.11 is the difference of the measured CVC signal for the dispersion ($\text{CVC}_{\text{measured}}$) and this background CVC signal:

$$\text{CVC} = \text{CVC}_{\text{measured}} - \text{CVC}_{\text{background}} \quad (3.13)$$

The CVC signal has a magnitude and a phase. Therefore, Equation 3.13 should be interpreted as a vectorial subtraction. The Spectrometer software can perform this subtraction automatically when measuring the CVC signal of the dispersion.

3.5 *Design of experiments*

3.5.1 Selection of the bitumen concentration in toluene

Selection of the bitumen concentration in toluene is primarily based on the stability of the resulting emulsion. The aim of the present study is to investigate the water droplet surface charge density of emulsions which show high stability. As discussed earlier in section 2.1.1, the industrial practice is to operate at solvent to bitumen ratios between 0.6 and 0.7, which corresponds to a bitumen concentration of about 60% wt. At this concentration range, water-in-diluted bitumen emulsions show high stability, which is the cause of the residual emulsified water content in the diluted bitumen product after froth treatment operations. Therefore, in principle, a bitumen concentration of 60% wt. would be appropriate for the experimental work.

One important issue regarding the selection of the bitumen concentration is the viscosity of the diluted bitumen. Care must be taken to select a bitumen concentration that would not result in unsatisfactory circulation and mixing of the emulsion sample in the chamber, which is primarily governed by the viscosity of diluted bitumen. To address this issue, the viscosity of diluted bitumen was measured at 20° C, for various bitumen concentrations in toluene (from 0% to 70% wt.). The ability of diluted bitumen to circulate easily in the chamber was then verified for bitumen concentrations in toluene about 60% (from 50% to 70% wt.). These observations provided the necessary information for the final selection of the bitumen concentration in toluene.

Supplementary water sedimentation tests were also conducted at several bitumen concentrations to observe the emulsion stability. The presence of free water after sedimentation is an indication that the emulsion is unstable. On the other hand, the absence of free water after sedimentation is an indication that the emulsion is stable, because the emulsified water droplets are not able to coalesce and produce a separate water phase. These observations provided the necessary information to confirm that the selected bitumen concentration in toluene results in a stable water-in-diluted bitumen emulsion as previously defined.

Water sedimentation tests were performed for 24 hours at 20° C. The bitumen content was varied from 2.5% to 70% wt. Two water concentrations were considered for

each bitumen concentration: 5% and 10% wt. Distilled water (passed through a Millipore filter system) was used in these experiments. The detailed procedure for water sedimentation tests follows:

1. Eleven stock diluted bitumen samples were prepared in 50 ml teflon tubes, one for each bitumen concentration being considered (ranging from 2.5% to 70% by weight).
2. In order to have bitumen and toluene well mixed before emulsion preparation, each sample tube was mixed with a vortex mixer (maxi mix plus agitator) for 2 minutes, and then shaken for two hours at low speed (30 per minute). Finally, the tubes were put in a refrigerator for 24 hours at 4 °C.
3. The weights of diluted bitumen and water required to prepare 8 ml emulsion samples were calculated.
4. Emulsion samples were prepared by adding diluted bitumen and water into 10 ml conical bottom glass centrifuge tubes. Sedimentation of solids was observed in stock diluted bitumen tubes. Therefore, they were shaken with the vortex mixer for 2 minutes before taking the diluted bitumen sample for the emulsion preparation.
5. Water was dispersed, first by shaking each conical bottom glass tube with the vortex mixer for 30 seconds, and then by applying the homogenizer at minimum speed (5,000 RPM) for 2 minutes.
6. Immediately after water dispersion, the emulsion sample was placed into a thermal bath for 24 hours at 20 °C.
7. Finally, each emulsion sample was carefully removed from the thermal bath after 24 hours for inspection and further analysis (percentage of settled water droplets as described next).

In the case of stable emulsions, water droplet sedimentation leads to the formation of a concentrated emulsion at the bottom of the tube, and a hydrocarbon supernatant lying above the settled emulsified water droplets. The percentage of settled water droplets after

24 hours sedimentation is of practical interest, because it provides information regarding the easiness of water dispersion in the diluted bitumen sample. In the present study, the criterion for determining the percentage of settled water droplets is based on an experimental procedure designed by Horvath-Szabo in the Oil Sands Research Group (Horvath-Szabo, 2004).

As shown in Figure 3.10, five emulsion samples are taken from each conical bottom glass tube for water content analysis. Each sample is taken with a Hamilton syringe calibrated to a fixed volume of 50 μL , approximately. The syringe's needle point is initially positioned at the liquid meniscus level. The syringe is firmly supported on a movable arm, and the point of the syringe can be moved downwards. The first sample is taken $\frac{1}{2}$ cm below the meniscus level. The following four samples are taken by 1 cm steps downwards. These five emulsion samples scan approximately 75% of the emulsion sample volume from top to bottom. This volume is considered to contain the supernatant. The water content of the supernatant is then calculated as the mean average of the 5 measurements. Finally, the percentage of settled water droplets is calculated as follows:

$$\% \text{ SETTLED WATER DROPLETS} = 100 \cdot \left(\frac{(\% \text{wt})_{\text{EMULSION}} - (\% \text{wt})_{\text{SUPERNATANT}}}{(\% \text{wt})_{\text{EMULSION}}} \right) \quad (3.14)$$

3.5.2 Diluted bitumen preparation

Two stock diluted bitumen samples (700 ml each, approximately) with identical bitumen concentration were prepared for performing emulsion experiments. Each stock solution provides sufficient diluted bitumen to conduct 5 emulsion experiments, for a total of 10. As will be discussed in section 4.1.2, the selected bitumen concentration in toluene is 50% wt. for the present study.

The purpose of preparing two stock solutions is to facilitate the diluted bitumen preparation. Each stock solution was prepared in a one liter glass bottle, which can be safely placed in a high speed shaker (200 per minute) for 4 hours of mixing. Just after mixing is stopped, the 700 ml diluted bitumen is immediately split into 5 teflon bottles in approximate equal volumes. This is done just after mixing is stopped to avoid solid

sedimentation in the glass bottle, thus obtaining 5 equally representative diluted bitumen samples per stock solution. All diluted bitumen samples were stored at 4 °C for later use.

3.5.3 Emulsion preparation

The bitumen concentration in toluene was fixed at 50% wt. for all emulsions. Heavy water was used instead of water with the aim of maximizing the density contrast between the continuous and dispersed phases. The higher the density contrast, the higher the magnitude of the CVC signal (Equation 2.9), thus improving the chances for its detection. Indeed, the choice of heavy water allowed doubling the density difference that exists between the two phases when normal water is used (181 kg/m³ for the heavy water option versus 81 kg/m³ for the water option).

This study assumes that the chemistry of water and heavy water are essentially the same in the diluted bitumen. Consequently, the measurement of the electro-surface properties of the emulsion should reflect the behavior of the real system found in industrial practice.

The concentration of heavy water in the emulsion was determined from mass balance, as known weights of heavy water and diluted bitumen were added to the chamber. A fixed magnetic stirrer speed was chosen in order to keep the emulsion well dispersed in the chamber at all times during measurements. The 4th agitation speed in the scale from 1st (minimum) to 6th (maximum) was the choice for all experiments. This state of well dispersion could be experimentally verified by sampling the top, medium and bottom portions of the chamber and measuring the water content by Karl Fisher analysis.

In the present study, eight emulsion experiments were performed with the DT-1200 Spectrometer in order to investigate the surface charge density of water droplets dispersed in diluted bitumen. The details for the planning of each experiment are presented in Chapter 4, in conjunction with their results and discussion. The present work is eminently experimental; the results of one experiment inspired the planning of later experiments. There is a thread of logic among the different experiments presented in this work, and the discussion is greatly facilitated by concentrating on all the relevant information in Chapter 4.

Nevertheless, Table 3.1 is provided in order to facilitate the follow up of the discussion regarding these eight emulsion experiments. It summarizes the most relevant information: emulsion name, heavy water concentration, and a brief description of the experiment.

Emulsion name	Heavy water (% wt.)	Brief description
A	10%	<ul style="list-style-type: none"> ▪ Water dispersed by sonication (90 minutes) ✓ <i>CVC shows transient behavior (section 4.2.2)</i>
B1	10%	<ul style="list-style-type: none"> ▪ Water dispersed using homogenizer (3 minutes) ✓ <i>The effect of water dispersion method on CVC is identified (section 4.2.2)</i> ✓ <i>The dependence of CVC on the droplet size distribution is demonstrated (section 4.2.3)</i>
B2	10%	<ul style="list-style-type: none"> ▪ Water dispersed using homogenizer (3 minutes) ▪ Followed by 3 redispersion with homogenizer (every 24 hours) ✓ <i>Two relaxations are identified in the CVC transient behavior (section 4.2.4)</i>
B3	10%	<ul style="list-style-type: none"> ▪ Repetition of experiment B2 ✓ <i>Existence of the two relaxations for CVC transient behavior is reproducible (section 4.2.4)</i>
C1	30%	<ul style="list-style-type: none"> ▪ Water dispersed only by magnetic stirring in chamber (without the high speed homogenizer) ✓ <i>CVC is not necessarily linked to the use of high intensity water dispersion methods only, such as the homogenizer and sonication (section 4.2.7)</i>
C2	30%	<ul style="list-style-type: none"> ▪ Water dispersed using homogenizer (3 minutes) ✓ <i>Effect of volume fraction increase on CVC is studied (section 4.2.10)</i>
D	2%	<ul style="list-style-type: none"> ▪ Water dispersed using homogenizer (3 minutes) ✓ <i>The CVC effect cannot be detected for water concentration below 10%, approx. (section 4.2.10)</i>
E	20%	<ul style="list-style-type: none"> ▪ Water dispersed using homogenizer (3 minutes) ✓ <i>Effect of volume fraction increase on CVC is studied (section 4.2.10)</i>
<p>Note:</p> <ul style="list-style-type: none"> ▪ This bullet identify information regarding the emulsion preparation ✓ This bullet identify relevant results from the experiment, in regard to the study of the electroacoustic phenomenon of emulsions (section 4.2) 		

Table 3.1: Summary of emulsion experiments.

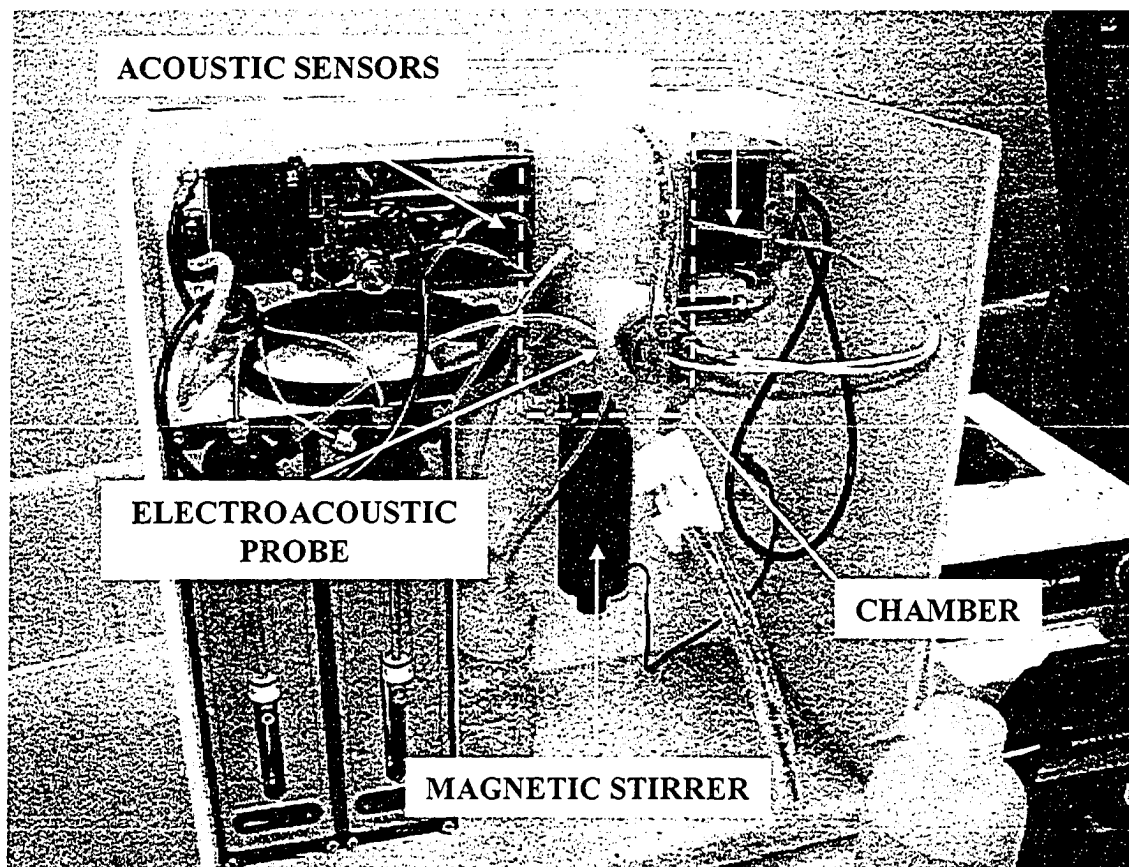


Figure 3.1: DT-1200 Acoustic and Electroacoustic Spectrometer.

(Reference: Dispersion Technology, 2003)

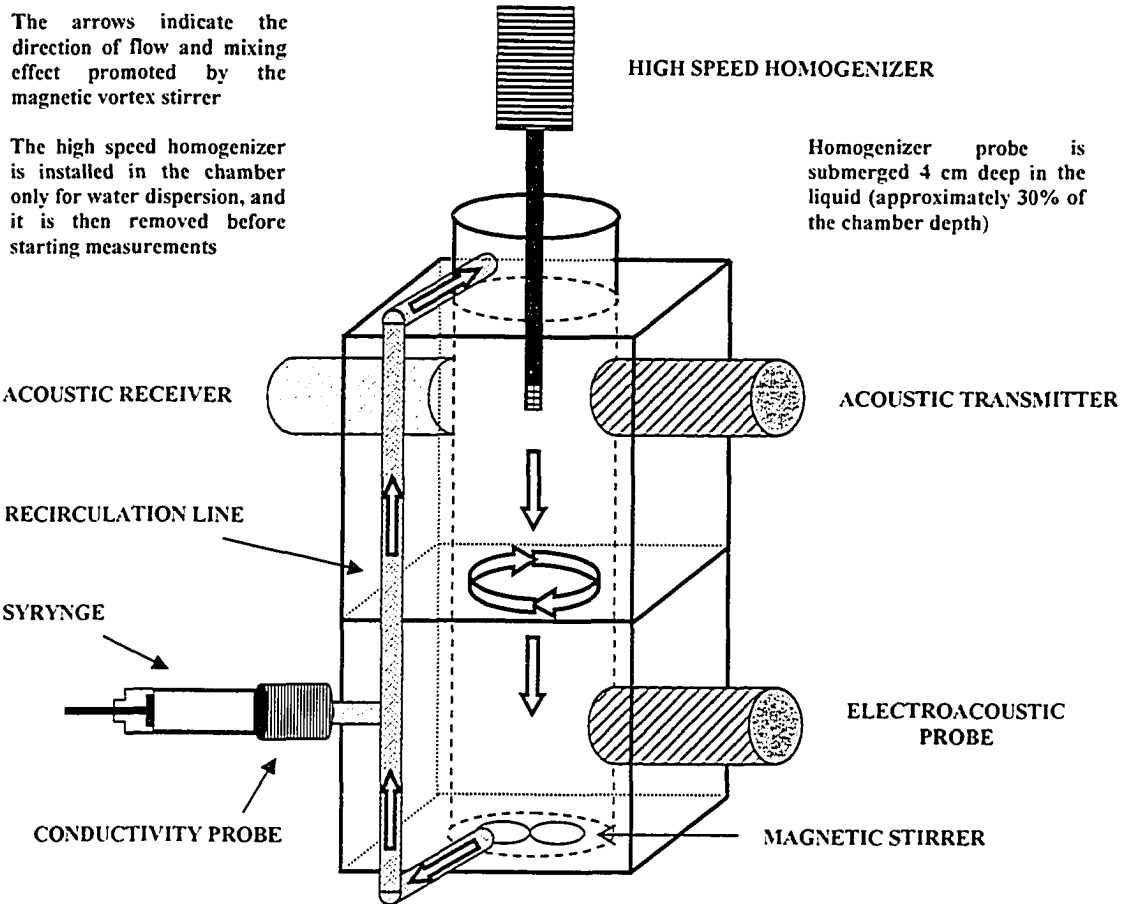


Figure 3.2: Details of the chamber after equipment improvements.

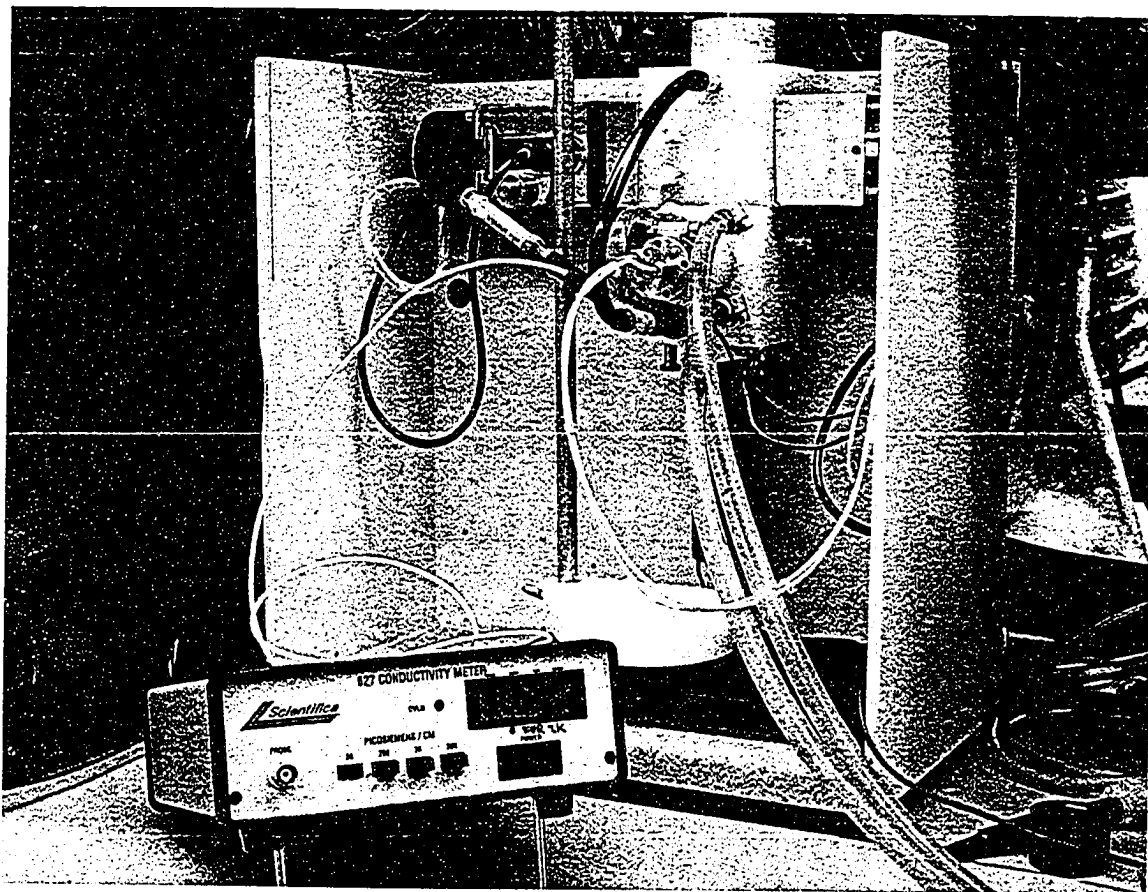


Figure 3.3: DT-1200 with new water-jacketed metallic chamber for temperature control.

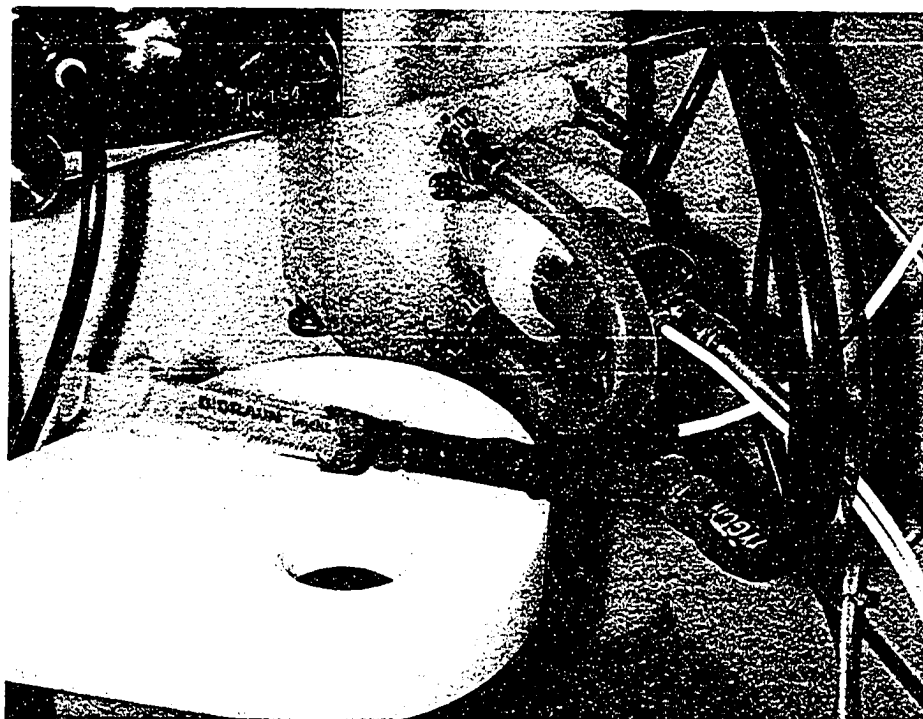


Figure 3.4: Installation of conductivity meter probe.

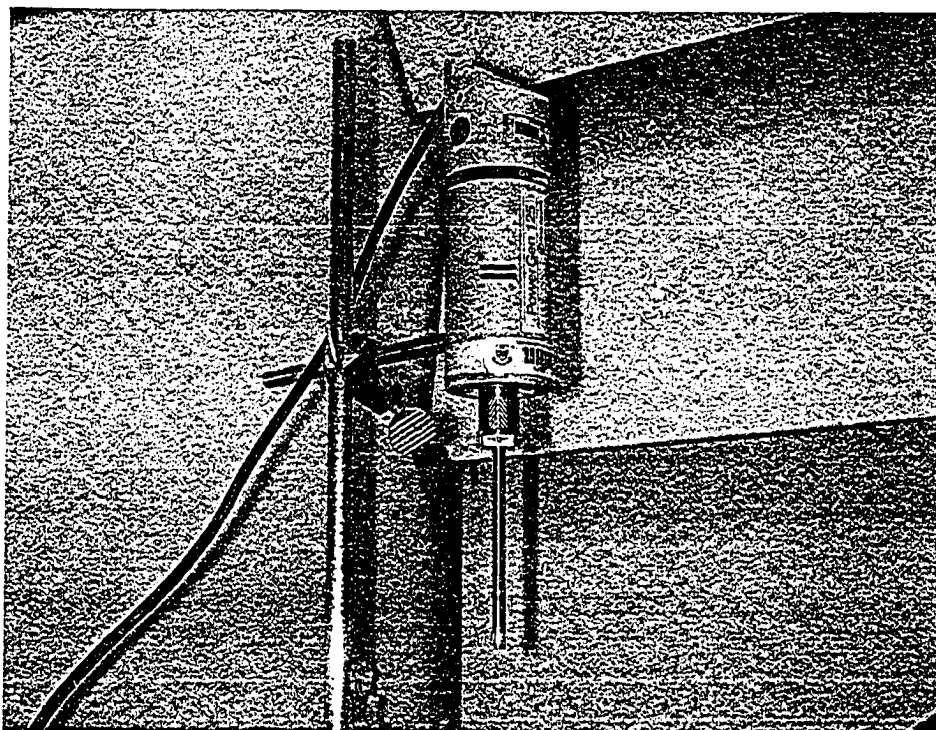


Figure 3.5: PowerGen high speed homogenizer

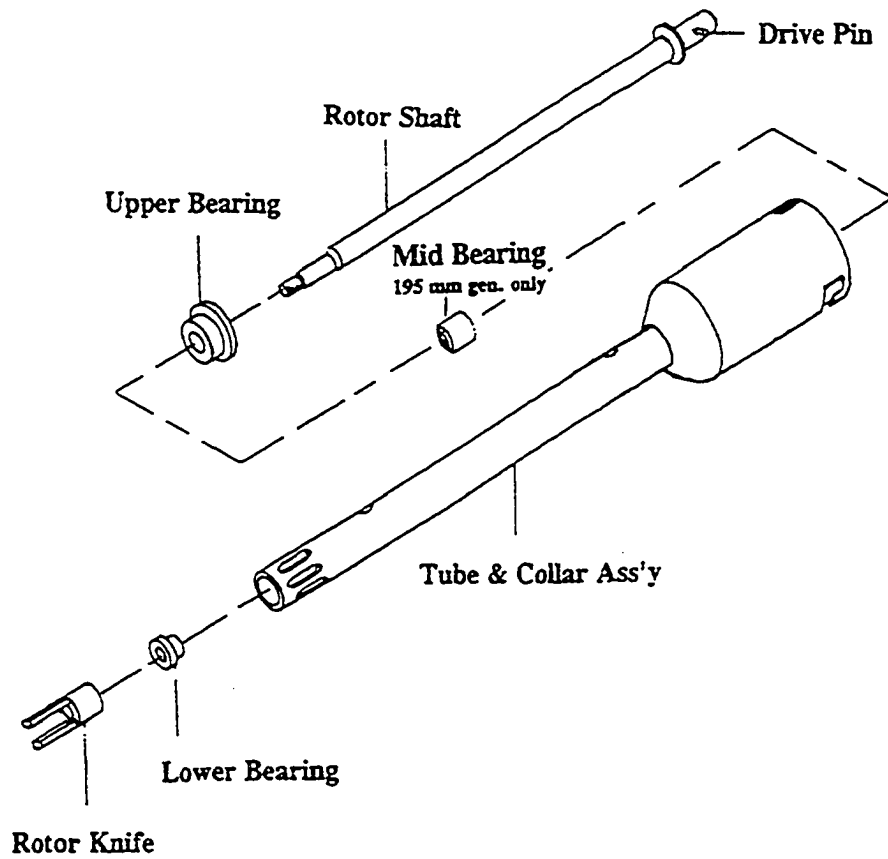


Figure 3.6: Homogenizer probe component parts.

(Reference: PowerGen Homogenizer Operating Manual)

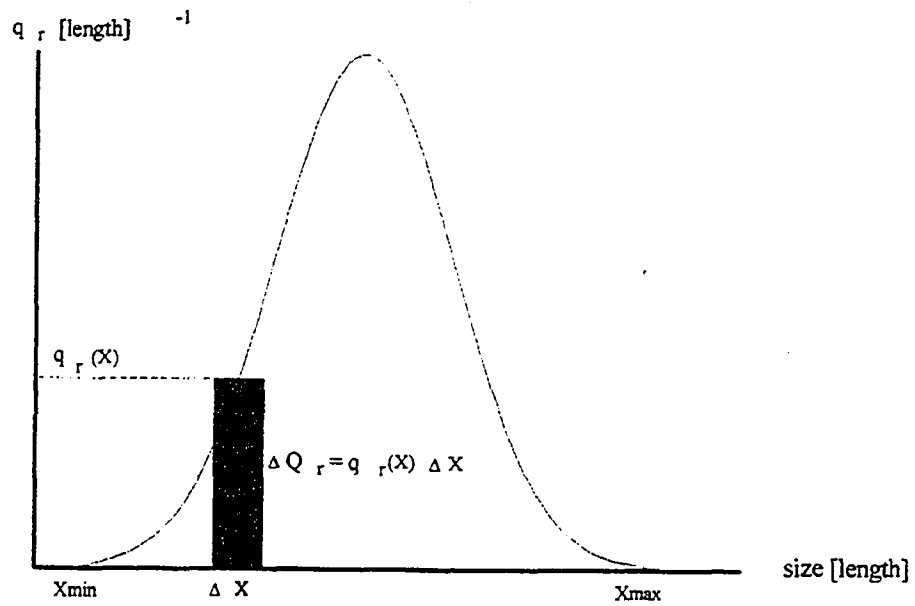


Figure 3.7: Density log-normal particle size distribution.
(Reference: Dukhin & Goetz, 2002)

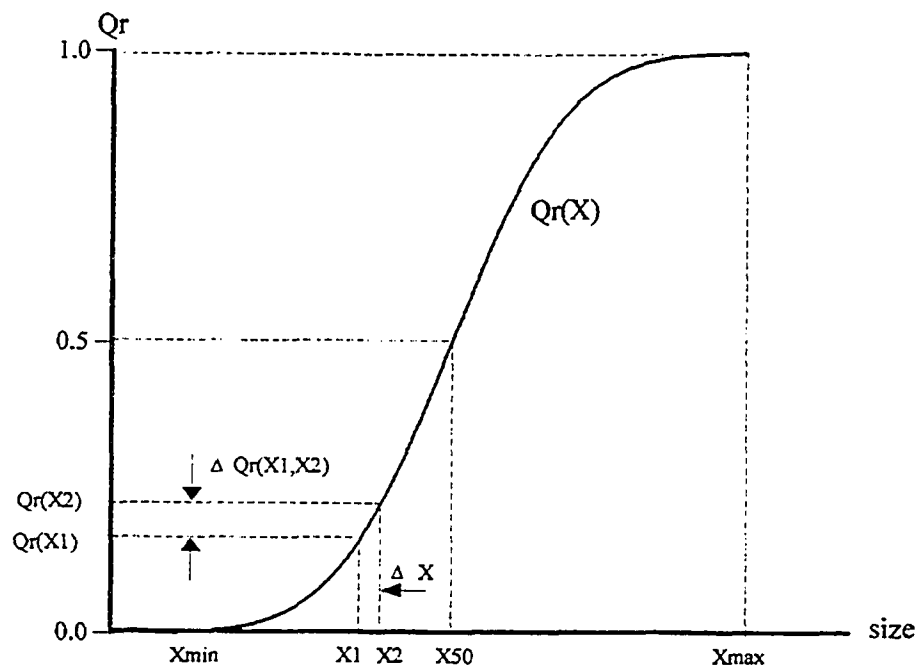


Figure 3.8: Cumulative log-normal particle size distribution.
(Reference: Dukhin & Goetz, 2002)

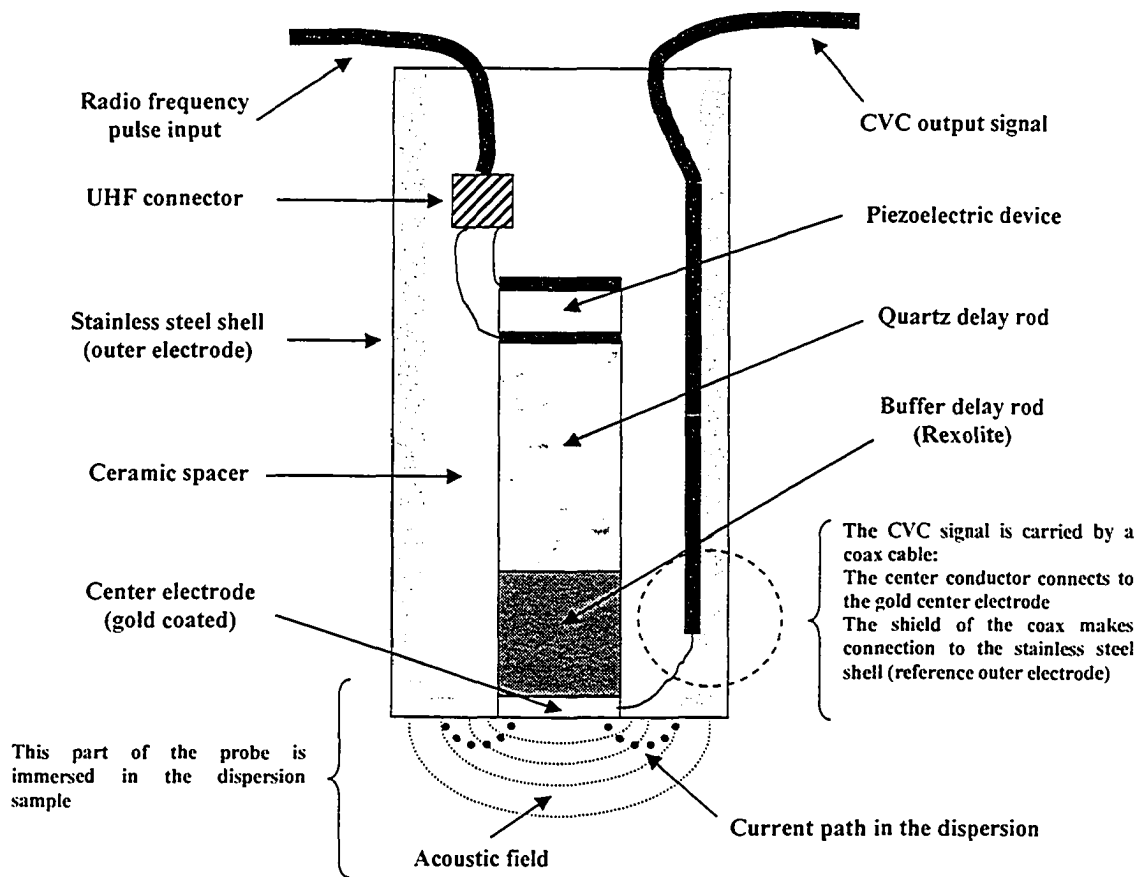


Figure 3.9: Diagram of the electroacoustic probe for measuring CVC.
(Adapted from: Dukhin & Goetz, 2002)

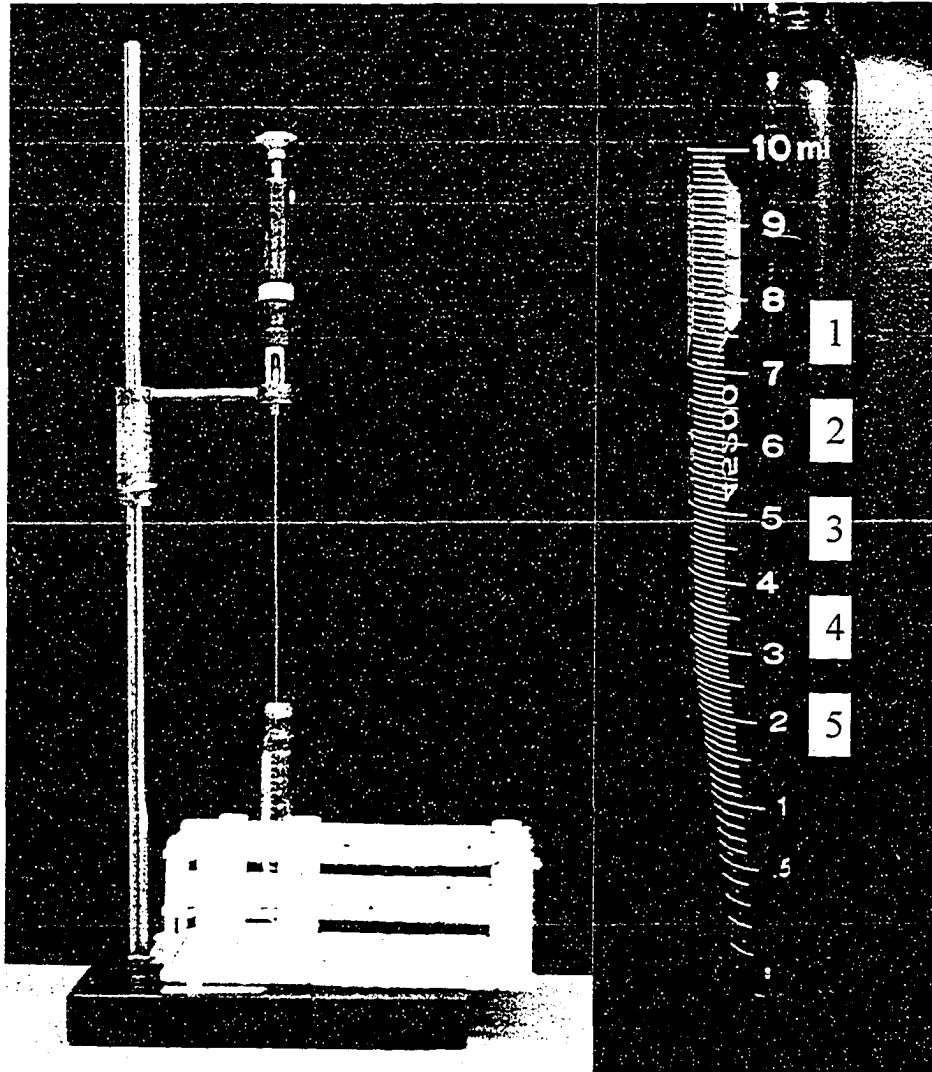


Figure 3.10: Determination of the percentage of settled water droplets in sedimentation tests.

Chapter 4

Results and Discussion

4.1 *Material properties*

4.1.1 **Material property measurements**

Table 4.1 summarizes the material properties of diluted bitumen and heavy water required for droplet size distribution and droplet surface charge density calculations. The selected bitumen concentration in toluene is 50% wt. (this is justified in the next section).

Additional information regarding these material properties is presented as figures and appendices. Figure 4.1 shows the results of diluted bitumen density measurements as a function of bitumen concentration. This information is required for performing water drops sedimentation tests (section 4.1.2). Thermal expansion of diluted bitumen was derived from density data (Figure 4.2). Diluted bitumen dynamic viscosity was also determined as a function of bitumen concentration (Figure 4.3). The intrinsic attenuation coefficient of diluted bitumen (50% wt.) and heavy water are presented in Figure 4.5. Additional data related to these measurements is presented in the appendices.

Finally, Figure 4.6 shows electric conductivity measurements for diluted bitumen (50% wt.). Electric conductivity is not required for the calculation of the droplet size distribution or droplet surface charge density. However, it is an important variable in the present study for the investigation of the electroacoustic phenomenon of water-in-diluted bitumen emulsions (section 4.2).

4.1.2 **Selection of bitumen concentration in toluene**

Satisfactory circulation of diluted bitumen in the spectrometer chamber was achieved for a bitumen concentration in toluene of 50% wt. Visual inspection of the discharge flow of diluted bitumen from the recirculation line into the chamber was an indicative of satisfactory circulation. At higher bitumen concentrations (60% and 70% wt.), the circulation was not satisfactory due to the higher viscosity, especially at 70% wt.

The dynamic viscosity of diluted bitumen at 20° C (Figure 4.3) increases five times when the bitumen concentration is increased from 50% wt (4.9 mPas) to 70% wt (24.4 mPas). A bitumen concentration of 50% wt. is still close to the industrial practice in froth treatment operations (\approx 60% wt.). For the aforementioned reasons, 50% wt. was the selected concentration for the preparation of diluted bitumen.

Water sedimentation tests revealed that emulsions prepared with the selected diluted bitumen (50% wt.) are stable, as free water was never observed after 24 hours sedimentation. Indeed, free water was not observed at any other bitumen concentration within the 2.5% - 70% wt. range. The state of the separated water is in the form of a concentrated water-in-oil emulsion (physically, it resembles a brownish sludge at the bottom of the conical tubes).

Figure 4.4 presents the results of water sedimentation tests in terms of the percentage of settled water droplets. Clearly, the dynamic viscosity of diluted bitumen (Figure 4.3) has an important effect on the percentage of settled water droplets, particularly at bitumen concentrations within the 50% - 70% wt. range, where the viscosity increases 5 times. This explains the sharp decrease in the percentage of settled water droplets above 50% wt. bitumen. It is expected that emulsions prepared with the selected bitumen concentration of 50% wt would be easily kept dispersed in the chamber because they do not show fast settling behavior. Fast settling behavior would be a problem for dispersing water at bitumen concentrations below 20% wt, approximately, because the percentage of separated water is nearly 100% in this region.

4.2 Electroacoustic phenomenon in water-in-diluted bitumen emulsions

When the present research was initially started, there was no previous study in the area of water-in-diluted bitumen emulsions using the electroacoustic technique based on the CVC effect. Therefore, the study of the surface charge density of water-in-diluted bitumen emulsions required, in the first place, the investigation of the electroacoustic phenomenon for this particular system, in order to answer the following fundamental questions:

- *Can the electroacoustic phenomenon based on the Colloid Vibration Current (CVC) be measured for water-in-diluted bitumen emulsions?*
- *If it is measurable, does the electroacoustic phenomenon exhibit the general characteristics expected from theoretical considerations?*

Answering these two questions is essential to determine if the measured electroacoustic signal is reliable for further analysis using Shilov and coworkers theory for strongly overlapped double layers. This section discusses the experimental work carried out to accomplish this task.

For conciseness, the following discussion will refer to the disperse phase as “water”, with the understanding that emulsion experiments were performed using heavy water as mentioned before in chapter 3. The rationale for using heavy water was explained in section 3.5.3.

4.2.1 Design of experiments

From the discussion presented in the literature review, it can be said that the Colloid Vibration Current signal (hereafter referred to as the CVC signal) of water-in-diluted bitumen emulsions depends on the following five factors:

- Density difference between water and diluted bitumen
- Concentration of the dispersed phase (water)
- Water droplet size distribution
- Nature and concentration of charge carriers in diluted bitumen
- Electro-surface properties of water droplets (surface charge density)

The first two factors (density difference between the phases and water concentration) were under control in all experiments. The next two factors were measured simultaneously to the CVC signal: water droplet size distribution was determined by Acoustic Spectroscopy, and the conductivity of the emulsion was measured as an indication of the concentration of charge carriers in the medium. Finally, the surface

charge density is the target of the study, and it cannot be measured independently but calculated from the CVC signal using Shilov's electroacoustic theory. This is the subject of section 4.3.

4.2.2 CVC signal of emulsions: magnitude and transient behavior

As will be shown throughout section 4.2, the CVC electroacoustic effect is indeed measurable for water-in-diluted bitumen emulsions, provided that the water concentration is sufficiently high. However, as a general observation, the CVC effect always exhibits time dependence behavior, and the magnitude of the CVC effect strongly depends on the method of preparation of the emulsion; more specifically, on the intensity of water dispersion in diluted bitumen.

Figure 4.7 illustrates this point where two 10% wt. water-in-diluted bitumen emulsions were prepared following different methods for water dispersion. Emulsion "A" was prepared dispersing water first with the high speed homogenizer for 3 minutes, followed by 90 minutes sonication. Emulsion "B1" was prepared dispersing water only with the high speed homogenizer for 3 minutes. Measurements were started 2 minutes after water dispersion in both cases, and the CVC signal magnitude is shown in Figure 4.7 for the next 24 hours. The CVC signal magnitude for diluted bitumen with no added water corresponds to the noise level of the CVC signal expected for any emulsion, and it is also shown in Figure 4.7 measured in a similar time span.

From this experiment, it is evident that the CVC signal depends on the method of water dispersion, which was much more intense for emulsion "A" as the sample was sonicated for a long period of time. Correspondingly, emulsion "A" showed a higher CVC signal magnitude compared to emulsion "B1". On the other hand, independently from the method of preparation, the CVC signal magnitude decreases with time. The initial peak value certainly depends on the method of preparation, but then the CVC signal rapidly decreases, and after one day it is relatively close to the noise level.

One important question is whether or not the CVC signal eventually reaches the noise level. To answer this, it would be necessary to measure the CVC effect for a longer period of time (in the order of days). This is actually the case for emulsion "B1" where

the CVC signal was measured for four days as shown in Figure 4.8. For all practical purposes, the CVC signal of the emulsion does reach the noise level after 3 days, approximately.

These observations suggest that the CVC electroacoustic effect is measurable for water-in-diluted bitumen emulsions, but it is still necessary to demonstrate that the measured signal is clearly associated to the creation of the emulsion and not to a different phenomenon. For example, it is reasonable to think that emulsions “A” and “B1” had very different states of water dispersion because of the radically different methods followed for the emulsion preparation. The CVC signal depends (among other factors) on the droplet size, and the difference in the signal magnitude for these two emulsions might well reflect their different states of dispersion. Moreover, the transient behavior of the CVC signal could reflect the change of droplet size and electro-surface properties with time.

However, it is also possible to think that the measured CVC signal is not closely related, or even not related at all to the creation of the emulsion. For water-in-diluted bitumen emulsions, the following issues are of concern when analyzing the electroacoustic effect:

- A decreasing CVC signal (which eventually reaches the noise level) could be associated to an ongoing equilibration process in the system (such as phase equilibrium of bituminous components between the water and oil phases), and not to the creation of the emulsion itself.
- Even if the CVC signal is associated to the creation of the emulsion, the observed transient behavior might be a consequence of improper agitation in the chamber that would lead to water droplets sedimentation. This in turn would cause the CVC signal to decrease with time because it is proportional to the water concentration (Equation 2.9).
- Solids present in the diluted bitumen might be responsible for the electroacoustic signal by their own.

- The possibility that the CVC signal is a consequence of the action of the high speed homogenizer or sonication on the sample and not to the creation of the emulsion by itself. This include the possibility of a CVC effect due to entrapped air bubbles after dispersion, or the electrical charging of water droplets or air microbubbles due to the high shear rate.

4.2.3 Equilibrium versus relaxation process

The most fundamental issue to be resolved is whether or not the observed CVC signal is associated to an ongoing equilibration process in the system. The state of water dispersion in water-in-diluted bitumen emulsions is driven by processes such as flocculation or coalescence, which in turn depend (among other factors) on the rate of water droplet collision, and on the magnitude and extent of repulsive forces between droplets (steric and electric). Therefore, the state of water dispersion is driven by the kinetics of droplet motion, which depends on external forces such as, for example, gravity, viscous drag of liquid motion induced by stirring, or pressure waves induced by sonication (Morrison & Ross, 2002). In this regard, water-in-diluted bitumen emulsions are different to microemulsions which are thermodynamically stable and show the typical phase-equilibrium behavior.

If the observed CVC electroacoustic effect is indeed related to the creation of the emulsion, it is expected that it will also show the same dynamic behavior of the emulsion and not an equilibrium behavior where the CVC signal cannot be recovered after a certain period of time. Any change in the state of water dispersion has to influence the measured CVC signal. In other words, a clear relationship must exist between the measured CVC effect and the state of water dispersion. For example, should the droplet size distribution change in time after water dispersion, it might be expected that the CVC effect also changes with the same time scale. On the other hand, if the emulsion is redispersed by applying the high speed homogenizer again, then a corresponding qualitative change in the CVC signal might also be expected.

Such observations would firmly support the fact that the measured CVC signal is related to the creation of the emulsion and not to a different phenomenon. Most

importantly, because the CVC effect is primarily related to the electro-surface properties of the dispersed phase, then by extension the observed CVC effect for the emulsion would indicate that the water droplets are indeed charged, and that this charge might be calculated by means of a suitable electroacoustic theory.

This issue was investigated by studying the CVC signal and the droplet size distribution simultaneously for two 10% wt. emulsions (emulsions “B1” and “B2”). The emulsion conductivity was also investigated; it could also depend on the droplet size distribution if surface conductivity effects are important (Morrison & Ross, 2002). Emulsion “B1” was described before: water was dispersed with the high speed homogenizer for 3 minutes and then studied for 4 days. Emulsion “B2” was prepared in the same way, but the high speed homogenizer was applied again three times, every 24 hours. Measurements of CVC, droplet size distribution and conductivity were started 2 minutes after the initial water dispersion in both experiments. Figures 4.9 and 4.10 show the results.

As expected, the droplet size distribution changed with time for both emulsions. However, the most important observation is that the CVC signal and the emulsion conductivity also changed with the same time scale as the droplet size did. Evidently, a connection can be established between the CVC signal and emulsion conductivity with the state of water dispersion as given by the droplet size distribution. The higher the droplet size, the lower the CVC signal and the higher the emulsion conductivity. The second important observation is that the reiterative application of the high speed homogenizer in emulsion “B2” always brings the system back to the same state of dispersion, with an associated partial recovery of the CVC signal. A similar effect is observed for the emulsion conductivity.

In reference to emulsion “B1” (Figure 4.9), the steady increase in the droplet mean size indicates that water droplets start to coalesce or flocculate immediately after the application of the high speed homogenizer. This behavior is, however, dynamic and after two days the mean droplet size levels off. One interpretation could be that the rate of aggregation or coalescence of water droplets is equal to the rate of destruction of the aggregates or droplet breakup. Both effects are associated to the fact that the emulsion is under permanent agitation in the chamber to prevent settling, and eventually a dynamic

equilibrium is established between aggregation and/or coalescence due to droplet collision, and droplet breakup and/or aggregate disjoin due to shearing. The reiterative application of the high speed homogenizer causes an abrupt change in the state of water dispersion, but the system always relaxes again towards this condition of dynamic equilibrium.

These facts firmly support the concept that the CVC effect is associated to the presence of the emulsion. The transient behavior of the CVC signal is driven by kinetic factors; it does not correspond to an equilibration process in the thermodynamic sense. From now, the transient behavior of the CVC effect will be referred to as *relaxation*, to emphasize the dependence of this phenomenon on kinetic factors of the system.

4.2.4 Superposition of relaxations

As was discussed in the previous section, the transient behavior or relaxation of the CVC signal and emulsion conductivity are strongly influenced by the droplet size distribution. This is clearly observed for emulsion “B1” where the homogenizer is applied only once (Figure 4.9). However, when the homogenizer is applied consecutive times as for emulsion “B2”, the transient behavior of the CVC effect and emulsion conductivity cannot be explained only in terms of the droplet size evolution in time. Indeed, a superposition of two types of relaxations can be distinguished:

- 1st relaxation (or relaxation in the droplet size)
- 2nd relaxation (or super-imposed relaxation due to yet unknown factor)

The existence of a super-imposed relaxation is evident from the partial recovery of the CVC signal and emulsion conductivity after water redispersion, and it is shown in Figure 4.10 by a segment line. Certainly, this super-imposed relaxation cannot be explained in terms of the droplet size. The 1st relaxation contemplates that the effect of an increase in the droplet size is to decrease the CVC signal and increase the emulsion conductivity. However, when the super-imposed relaxation is analyzed by comparing the first measurement just after every water redispersion, the opposite effect is observed as shown in Table 4.2.

The observation of a super-imposed relaxation in the CVC signal and emulsion conductivity is a remarkable result of the present study. The fact that the emulsion conductivity changes with droplet size may well reflect changes occurring at the water-oil interface. As mentioned by (Morrison & Ross, 2002), the emulsion conductivity can change with the droplet size when surface conductivity effects are important. On the other hand, the CVC effect is related to the electro-surface properties of the emulsion besides its droplet size distribution. Therefore, the super-imposed relaxation of CVC might also be related to the same phenomenon at the water-oil interface.

The segment lines in Figure 4.10 suggest that the super-imposed relaxation corresponds to a phenomenon that continues for several hours before it apparently stabilizes. Following the hypothesis that this behavior reflects changes at the water-oil interface, it can be attributed to the slow adsorption/desorption kinetics of bituminous components at the water-oil interface. There are strong backgrounds to support this hypothesis. As discussed in the literature review, work performed by Sheu and coworkers confirmed the time dependence characteristics of the adsorbed layer and revealed its relationship with the slow kinetic of adsorption of asphaltenes at the water-oil interface (section 2.1.4). Work performed by do Carmo Marques and coworkers showed that asphaltenes adsorbed at the water-oil interface contribute to the surface charge of water droplets (section 2.5.2). On the basis of these facts, it is reasonable to postulate that the super-imposed relaxation of the CVC effect and emulsion conductivity is connected to the interfacial adsorption process.

The implications of this observation will be analyzed in section 4.3 when discussing the surface charge density of the emulsified water. However, it is still important to confirm if such a fact is indeed reproducible. For this reason, a new experiment similar to emulsion “B2” was conducted again, and the results are shown in Figure 4.11. This new emulsion (emulsion “B3”) was again prepared dispersing 10% wt. water, following the same standard procedure (water was dispersed with the high speed homogenizer for three minutes, and measurements were started 2 minutes after water dispersion).

Qualitatively, the results are the same as a super-imposed relaxation was again observed. It is indicated with segment lines in Figure 4.11. In this case, emulsion “B3”

showed a higher increase in conductivity as compared to emulsion “B2”. On the other hand, the droplet size distribution behaviors of both emulsions were identical for all practical purposes. The important fact is that the observation of a super-imposed relaxation is reproducible.

4.2.5 CVC signal and the effect of water distribution in the chamber

So far, we have discussed the facts that link the observed CVC effect with the creation of the emulsion. In order to answer the question regarding whether or not the CVC effect can be measured for water-in-diluted bitumen emulsions, it is still necessary to rule out the possibility that the observed CVC signal is related to other factors extraneous to the emulsion creation as mentioned in section 4.2.2. This will be the subject of sections 4.2.5 to 4.2.7. In the present section, the effect of water distribution in the chamber is examined.

One possible alternative explanation for the decreasing CVC signal behavior is the possibility of water droplets sedimentation in the chamber due to insufficient agitation velocity. In this case, it is assumed that the CVC effect is due to the emulsion creation, but a decreasing CVC signal would result from a decreasing effective water concentration at the electroacoustic probe zone. The CVC signal is expected to be proportional to the water concentration, for a fixed surface charge and droplet size (Equation 2.9). To rule out this possibility, the water content was measured at three different positions in the chamber (top, medium and bottom) in order to confirm that the agitation speed with the magnetic stirrer was strong enough to maintain the water well dispersed. Table 4.3 summarizes the water content analysis for the three 10% wt. emulsions previously discussed (emulsions “B1”, “B2”, and “B3”, corresponding to Figures 4.9, 4.10 and 4.11, respectively).

Water was well dispersed in emulsion “B1” (where the homogenizer was applied only once) 3 days after its initial dispersion; by this time the CVC signal has already dropped to the noise level (Figure 4.9). Similarly, water was well dispersed at all times for emulsions “B2” and “B3”. These observations reveal that the decreasing CVC signal cannot be attributed to water droplets sedimentation in the chamber.

As a side comment, it is important to observe that the measured water content does not match exactly 10% wt., which is known by mass balance when preparing the emulsion. For example, the standard deviation of the nine measurements performed on emulsion “B2” is 0.37. This fact reflects the inherent difficulties associated to sampling emulsions for Karl Fisher analysis. The total volume of the emulsion in the chamber is 125 ml, approximately. The average volume of emulsion sample taken for every Karl Fisher analysis is 0.032 ml, which represents a 0.025 % of the emulsion volume. Deviations in the water content from the mass balance value occur locally in the emulsion, because it is a heterogeneous system. Such deviations can be detected when the sample volume for analysis is very small compared to the system volume. This is the most likely explanation for the variation in the data in Table 4.3.

4.2.6 CVC signal and the effect of solids in bitumen

Fine solids present in the bitumen play an important role in the stability of water-diluted bitumen emulsions as demonstrated by Yan and coworkers (section 2.1.2). Besides asphaltenes and natural surfactants, fine solids reside at the water-oil interface forming the stabilizing film. Therefore, it is expected that they might contribute to the CVC signal should they play a role in determining the surface charge of water droplets. On the other hand, the coarse fraction of solids in the diluted bitumen plays a minor role in the emulsion stability. As the present study is concerned with the surface charge of the real emulsion system found in industrial practice, solids were not removed from diluted bitumen in our experiments.

However, a different question is whether or not these solids might be responsible by their own on the observed CVC signal for the emulsion. As discussed in the paper (Chen et al., 1999), toluene can remove natural surfactants adsorbed on fine solids, making them more hydrophilic. This “washing” effect could be strengthened by the vigorous agitation achieved with the high speed homogenizer or even sonication. Therefore, it is reasonable to think about the possibility of measuring a CVC effect arising from the electro-surface properties of solids dispersed in diluted bitumen by themselves.

To rule out this possibility, the high speed homogenizer was applied to diluted bitumen only (with no added water) to note if a CVC signal can be observed above the noise level. The results are shown in Figure 4.12, where the homogenizer was applied three times following the standard procedure of 3 minutes dispersion + 2 minutes delay to start CVC measurements.

First, it is necessary to quantitatively define the noise level for CVC. Appendix 6 shows 72 measurements of CVC for diluted bitumen. The average value is 3633. The standard deviation is 544. If the spread of the distribution of CVC measurements is taken as three times the standard deviation (which would include the 95% of a normal distribution), then the noise level of CVC is about 5,000. Therefore, for the purposes of the present work, any CVC signal below 5000 is considered to be within the noise level range.

It can be seen in Figure 4.12 that the CVC signal remains within the noise level even one hour after every application of the homogenizer. For a 10% wt. emulsion, the CVC signal is above the noise level immediately after the application of the homogenizer. Therefore, it is concluded that the CVC signal observed for the emulsion cannot be attributed to the solids by themselves, but in overall to the emulsion creation which, clearly, involves not only the solids but also the other species present in diluted bitumen interacting with the water droplets. This test has other implications which are analyzed in the next section.

4.2.7 CVC signal and the effect of the high speed homogenizer

Another possible explanation to the observed CVC effect of the emulsion is the introduction of air bubbles after sample dispersion with the homogenizer. As discussed in the paper (Goetz et al., 1992), same as water droplets, entrapped air microbubbles can acquire surface charge by the adsorption of natural surfactants present in the bitumen at the air-oil interface. The electroacoustic phenomenon associated to the air bubbles could be larger than the one associated to the water droplets because of the larger density contrast existing between air and diluted bitumen.

The introduction of air bubbles does occur when a sample is being dispersed with the high speed homogenizer. The design of the homogenizer, however, minimizes this effect as the rotor shaft spins inside a static tube (stator), and the rotating knife can be positioned at the medium portion of the chamber, deep inside the sample liquid (see Figures 3.5 and 3.6). This prevents the formation of a curved liquid surface at the top of the chamber which would otherwise facilitate the introduction of air. As part of the standard procedure, an attempt was made to dislodge any air bubbles in the chamber by stopping the magnetic stirrer for 5 seconds after the sample has been already dispersed. This is done twice within the 2 minutes delay for CVC measurements after dispersion with the homogenizer.

The facts discussed in section 4.2.6 (Figure 4.12) allow us to rule out the possibility that the observed CVC effect for the emulsion might be associated to the presence of air microbubbles in the system. The high speed homogenizer was applied to diluted bitumen in the same way that it is applied to the emulsion, and no CVC signal could be detected above the noise level. Indeed, the third time the homogenizer was applied to diluted bitumen in Figure 4.12, the magnetic stirrer was not stopped as an attempt for dislodging air bubbles, and still no CVC effect could be detected.

There is another factor that needs to be ruled out regarding the effect of the high speed homogenizer, and it is the possibility of electrical charging of water droplets due to the intense shear exerted by the homogenizer. This would mean that the observed CVC effect certainly arises from the fact that water droplets are charged, but such fact would not be related to the creation of the emulsion by itself but to the intense friction between the rotating knife and the liquid sample. The best way to resolve this issue is to investigate if any CVC effect can be detected for a water-in-diluted bitumen emulsion prepared without using the homogenizer. This is actually the case as it was experimentally verified for higher water content emulsions.

Figure 4.13 shows the observed CVC effect when adding water up to 30% wt. to diluted bitumen (emulsion "C1") under maximum magnetic stirring speed in the chamber. The high speed homogenizer was not used to disperse water. The CVC signal was studied for 3 days. During the first 8 hours the signal quickly increased from the noise level up to a peak value in the order of 50,000 (which reflects the dispersion of

water in diluted bitumen). Then, the signal started to slowly decrease. Water was well dispersed in the chamber as can be concluded from water content analysis done at the third day (Table 4.4).

It was pointed out at the beginning of this chapter that the observed CVC effect strongly depends on the method of water dispersion in the diluted bitumen: the higher the intensity of water dispersion, the higher the initial CVC signal. This was shown in Figure 4.7 when two powerful dispersing techniques were used (homogenizer and sonication). The possibility of electrical charging cannot be disregarded, but the experimental evidence suggests that the observance of the CVC effect for the emulsion is not necessarily linked to the use of the high speed homogenizer. This experimental evidence supports further the thesis that the observed CVC effect is related to the creation of the emulsion. The role of the homogenizer is to effectively disperse water in diluted bitumen and to reduce the droplet size, and this would be reflected in the CVC signal as it not only depends on the surface charge but also on the state of water dispersion.

4.2.8 Theoretical considerations

So far, it has been discussed the experimental facts that demonstrate that the CVC effect is measurable for water-in-diluted bitumen emulsions. The approach has been purely experimental in order to reveal the intimate relationship between the electroacoustic signal and the state of dispersion of the emulsion. The relaxation of the CVC signal has been explained on the basis of the kinetic factors that govern the emulsion behavior, in terms of its droplet size distribution and electro-surface properties.

Prior to the calculation of the surface charge density, it is still necessary to discuss how these experimental findings adapt to the theory of electroacoustics as formulated by Shilov and coworkers. This would further support the fact that the observed CVC effect is not only related to the creation of the emulsion, but it is also reliable for analysis using Shilov's theory. There are only two aspects that are accessible for verification as discussed below:

- i) Inertia effects: Shilov's theory predicts that the CVC signal would depend on the droplet size if the frequency of the driving acoustic field is higher than the characteristic hydrodynamic frequency (Equation 2.13).
- ii) Volume fraction of the dispersed phase: Shilov's theory predicts that the CVC signal is approximately proportional to the volume fraction of the dispersed phase (Equation 2.9 and 2.20), considering the same state of water dispersion.

These two issues are discussed in sections 4.2.9 and 4.2.10.

4.2.9 CVC and inertia effects

It has been discussed already the experimental observations that relate the CVC signal to the droplet size of the emulsion. It will be shown that such droplet size dependence is in accordance with theoretical considerations. In the following discussion, the measurements with emulsion "B1" will be considered, where the high speed homogenizer was applied only once to disperse a 10% wt. emulsion (Figure 4.9).

The frequency of the driving acoustic field for CVC measurements is 3 MHz. On the other hand, the hydrodynamic characteristic frequency of the system (ω_{hd}) depends on the droplet size (Equation 2.13). For $\omega_{hd} = 3$ MHz, the corresponding droplet diameter is 2.7 microns. This is the critical diameter above which inertia effects are important to the CVC effect, as the frequency of the acoustic field (3 MHz) would be higher than ω_{hd} . The droplet size distribution measurement confirms that the droplet diameter was above this critical value. The droplet mean diameter after dispersion was 7.8 μm (Figure 4.9). Considering a standard deviation of 0.25, it can be said that the majority of water droplets were in the size range between 2 and 30 μm in diameter (the sizes at 15.87% and 84.13% in the cumulative size distribution curve, respectively). Two days after water dispersion, the droplet mean size leveled off at 16 μm , approximately, and the majority of the water droplets were between 4 and 60 μm . Therefore, inertia effects are important and droplet size dependence is to be expected for the CVC effect.

The experimental results presented in Figure 4.9 are in agreement with this theoretical prediction. In fact, the CVC signal magnitude shows an apparent strong

dependence on the droplet size. Actually, this is the case for the other emulsion experiments discussed so far. Definitely, the inertia effect is very important in water-in-diluted bitumen emulsion systems, because any increase in the droplet size contributes to the reduction of the observed CVC signal magnitude. Therefore, a direct correlation between the CVC signal magnitude and the droplet surface charge density is not expected. The target of Shilov's theory is to screen the effect of droplet inertia from the measured CVC signal in order to calculate the droplet surface charge density. This is the subject of section 4.3.

There is another important observation, this time regarding the CVC signal phase. As discussed in the literature review (section 2.4.6), when inertia effects are important, any increase in the droplet size makes the droplets less susceptible to move in sympathy with the driving acoustic field. The end result is that inertia effects reduce the magnitude of the dynamic electrophoretic mobility (μ_d) and increase the phase lag. The same effects occur in the CVC signal (Equation 2.9) as it directly relates to μ_d .

Shilov's theory predicts that the phase lag is between 0° and 90° for positively charged droplets (Dukhin & Goetz, 2004A). Although not explicitly mentioned in reference (Dukhin & Goetz, 2004A), the phase lag should vary between 180° and 270° for negatively charged droplets (this comes from the fact that positively and negatively charged droplets generate currents in opposite directions). However, the experimental results are not in accordance with this prediction. Figure 4.14 shows the measured CVC signal phase for emulsion "B1". The CVC signal phase oscillates around -20° (equivalent to 340° in the $0^\circ - 360^\circ$ range). As the droplet size increases, the amplitude of this oscillation also increases. On the other hand, it is curious that the magnitude of the CVC signal phase does keep within the 0° to 90° degrees (Figure 4.15).

Unfortunately, this discrepancy between theory and experiments prevents us to rely on measurements of the CVC signal phase in order to determine the sign of electric charge of droplets. One possible explanation for this fact is discussed in section 4.3.

4.2.10 Volume fraction dependence of CVC

Shilov electroacoustic theory predicts that the magnitude of the CVC effect is approximately proportional to the volume fraction of the dispersed phase, considering the same state of water dispersion (droplet size distribution) and electro-surface properties. Experimentally, this is very difficult to confirm as neither the droplet size nor the surface charge density are under control in our experiments.

There is an additional difficulty for investigating the volume fraction dependence of CVC. Shilov's theory assumes that the double layers overlap strongly (Equation 2.19). It has been explained earlier that the condition of strongly overlapped double layers is generally valid for dispersions in low conductivity media (section 2.2.3). However, if the condition of double layer overlap is determined by the interparticle distance ($\kappa d \ll 1$), it is also true that the lower the volume fraction of the dispersed phase, the lower the degree of double layer overlap. Therefore, the analysis with Shilov's theory might be restricted to a minimum volume fraction when the condition $\kappa d \ll 1$ applies.

The calculation of the minimum volume fraction expected from theory for strongly overlap of double layers (Equation 2.19) requires the knowledge of the Debye length. In principle, the Debye length can be calculated if the electrolyte concentration and nature of ionic species in the liquid media are known (Equation 2.1), or it can be estimated from conductivity measurements and knowledge of the diffusion coefficient of the charge carriers (Equation 2.2). However, the nature and concentration of the charge carriers in diluted bitumen is not completely understood yet. Unfortunately, there is no reliable information for estimating the Debye length in bitumen systems, and hence for the calculation of the minimum theoretical volume fraction for strongly double layer overlap.

In spite of these limitations, the present study investigated the volume fraction dependence of CVC of water-in-diluted bitumen emulsions in the concentration range of 2% to 30% by weight (1.7% to 26.4% by volume). Water was always dispersed with the high speed homogenizer following the standardized procedure (3 minutes homogenizer + 2 minutes delay for starting CVC measurements). The results are presented in Figure 4.16. It is interesting to note that although the transient behavior of the CVC effect, there

is a direct correlation between the CVC magnitude and the water content as expected from theoretical considerations. The higher the water content is, the higher is the magnitude of the CVC effect, considering that all the emulsions were subjected to the same standardized water dispersion procedure.

Special attention is directed to the study of the electroacoustic phenomenon for the 2% wt. emulsion (emulsion "D"). As can be seen in Figure 4.16, a CVC signal above the noise level (5,000) could not be detected after water dispersion with the high speed homogenizer. In view of this fact, the homogenizer was applied for a second time 24 hours after the initial dispersion, but again the observed CVC signal kept within its noise level. The details are shown in Figure 4.17. In order to best interpret these observations, the water content was increased further from 2% wt. to 10% wt. It was expected that the redispersion of this new emulsion would result in a CVC signal above its noise level, based on previous observations (emulsions "B1", "B2" and "B3"). This was actually the case, as can be seen in Figure 4.18. The CVC signal showed the same general characteristics previously observed for 10% wt emulsions: it was transient and it started from a similar initial peak value (in the order of 30,000).

The CVC signal for emulsion "D" (2% wt. water) should be below the limit of detection of the electroacoustic probe. Therefore, future research in the area of water-in-diluted bitumen emulsions based on the CVC effect should be conducted at a concentration of at least 10% wt. water.

Finally, Figure 4.16 demonstrates that the electroacoustic phenomenon exhibits the same transient behavior observed for 10% wt. emulsions at higher water concentrations. For example, Figure 4.19 details the behavior of the 20% wt. emulsion (emulsion "E"). This emulsion was studied for three days after water dispersion with the high speed homogenizer following the standardized procedure. Same as previously observed for 10% wt. emulsions (Figure 4.9), the CVC signal decreased while the droplet size and emulsion conductivity increased. These observations reveal once again the intimate relationship between the electroacoustic signal and emulsion conductivity with the state of water dispersion. The characteristic times for CVC and emulsion conductivity are similar. In this case, the calculated droplet size distribution does not suggest that a

state of dynamic equilibrium has been reached as the droplet size keeps increasing on the third day.

4.3 Surface charge density of water droplets

At this point, it is important to summarize the findings discussed in section 4.2 as follow:

- The electroacoustic phenomenon based on the Colloid Vibration Current (CVC) can be measured for water-in-diluted bitumen emulsions.
- Inertia effects are important, and the CVC signal strongly depends on the droplet size (relaxation in the droplet size). This fact has been demonstrated both, experimentally and theoretically.
- From theory, it is known that the CVC signal also depends on the electro-surface properties of the water droplets. Experimentally, a super-imposed relaxation with a characteristic time of several hours was identified. It was postulated that such super-imposed relaxation might be related to the adsorption/desorption process of bituminous components at the water-oil interface, which in turn govern the electro-surface properties at the interface.

Shilov's theory allows screening the inertia effect on the CVC signal and then calculating the surface charge density of the water droplets. This is done for the three relevant emulsion experiments discussed in section 4.2 as described below:

- Emulsion "B1": 10% wt. emulsion experiment which revealed the relaxation in the droplet size (Figure 4.9)
- Emulsion "B2": 10% wt. emulsion experiment which revealed the superposed relaxation (Figure 4.10)
- Emulsion "E": 20% wt. emulsion which revealed the effect of increasing the water concentration (Figure 4.19)

The calculation of the droplet surface charge density for these three emulsion experiments are shown in Figure 4.20. Same as the CVC signal magnitude, the calculated droplet surface charge density shows a transient behavior after water dispersion: it decreases while the droplet size and emulsion conductivity increases with time. These results suggest that inertia effects are not solely responsible for the decrease in the magnitude of the electroacoustic signal of the emulsion. There is an additional contribution due to the decrease in the surface charge density of the water droplets with time.

Figure 4.21 helps to discuss further this last point, where the ratio of the dynamic electrophoretic mobility to surface charge density (μ_d/σ) is plotted as a function of droplet diameter, as given by Shilov's theory (Equation 2.20). The plot covers sizes above the critical droplet diameter of 2.7 μm where inertia effects are important (this was discussed in section 4.2.9). Considering for example the emulsion experiment "B1", the CVC signal magnitude decreases from an initial peak value of 28,000 to a noise level of 5,000 in a time span of 3 days (Figure 4.9). This means that CVC decreases 5.6 times from its initial peak value. However, the reduction on CVC due only to inertia is 1.6 times, as can be concluded from Figure 4.21. Clearly, according to Shilov's theory, the additional reduction in CVC is attributed to a decrease in the surface charge density.

The theoretical reduction due to inertia is calculated from Figure 4.21 by dividing the μ_d/σ ratios read at the initial and final droplet mean sizes for emulsion "B1" (8 μm just after water dispersion and 16 μm when the droplet size leveled off after 3 days). To analyze the effect of inertia expected from theory, σ is assumed constant and it cancels out in the division. This gives a reduction ratio of 1.6 for the CVC signal. However, it is important to mention here that the effect of inertia might be in reality more pronounced (i.e., a reduction ratio higher than 1.6). This follows from the fact that Shilov's theory for strongly overlapped double layers has been formulated for monodisperse systems only. The real emulsion is polydisperse in size, with a significant fraction of water droplets with sizes close to the critical diameter as discussed in section 4.2.9. Probably, this fact is also associated with the discrepancy found between theory and experiments for the CVC signal phase.

Regardless of this limitation of Shilov's theory, the conclusion of a decreasing surface charge density for freshly dispersed emulsions or redispersed emulsions is conclusive. Experimentally, it has been identified a super-imposed relaxation behavior for the decreasing CVC related to the electro-surface properties of the emulsion. Shilov's theory which is the most suitable theory available at present for water-in-oil emulsions, predicts that the observed CVC cannot only decrease because of inertia effects. The remainder of the present discussion is devoted to a possible explanation for the droplet surface charge density behavior, which follows from the hypothesis based on the slow adsorption/desorption kinetics of bituminous components at the water-oil interface previously mentioned.

Recalling the work of Sheu and coworkers (Sheu et al., 1995), they studied the micellization kinetics of asphaltenes, and the adsorption-desorption kinetics of asphaltenes at water-toluene interfaces. They demonstrated that the micellization kinetics of asphaltenes is in the order of hours, which is much slower than those of surfactants (in the order of seconds or even milliseconds). The same applies to the kinetics of asphaltene adsorption at water-toluene interfaces as discussed in section 2.1.4. Sheu has stressed that the wide molecular weight distribution and structural distribution of asphaltenes differentiate them from surfactant molecules (which are far less polydisperse in structure), and this fact can explain the slow kinetics of micellization and adsorption of asphaltenes (Sheu, 1996).

From all bituminous components that eventually adsorb at the water-oil interface, it is expected that low molar mass components would be the first to be adsorbed as they diffuse faster to the interface. This includes natural surfactants present in bitumen such as carboxylic salts (sodium naphthenates). However, in a time scale of hours, asphaltenes also tend to adsorb at the interface, giving rise to a competitive adsorption process. This is in agreement with the experimental observations of Wu discussed in section 2.1.4 (Wu, 2003). He demonstrated that the interfacial film is composed of a mixture of asphaltenes and carboxylic salts for solvent to bitumen ratios below critical, where emulsions show high stability.

This competitive adsorption process can be visualized as an adsorption-desorption process where low molar mass components are desorbed and high molar mass

components are adsorbed, which would result in a stabilizing film composed by a mixture of surfactants and asphaltenes. This tendency can also be explained based on the discussion presented in section 2.1.2. Asphaltenes are good emulsion stabilizers and they would tend to gather at the water-oil interface, which in turn could lead to desorption of poor emulsion stabilizers as natural surfactants.

These facts suggest one possible explanation for the behavior of the droplet surface charge density of freshly dispersed emulsions. The decrease of the surface charge density might be a manifestation of the ongoing adsorption-desorption process of bituminous components at the water-oil interface as described before. The peak value of the surface charge density might reflect the initial adsorption of natural surfactants at the interface. In a time scale of hours, the competitive adsorption of asphaltenes and natural surfactants might be responsible for the decrease in the droplet surface charge density with time.

When the emulsion is redispersed with the high speed homogenizer, the creation of new interfacial area associated to the reduction in the droplet size would give the opportunity for natural surfactants to be re-adsorbed, and this could be the explanation of why the surface charge density increases just after water redispersion. However, the recovery of the surface charge density is partial because it is not a freshly dispersed emulsion. It is reasonable to think that the interfacial film that has been created already can resist water redispersion to some extent. The competitive adsorption process following redispersion would not start from the same state as for a freshly dispersed emulsion.

It is important to stress here that this is just one possible explanation for the experimental observations regarding the surface charge density, but not the only possible one. It has been proposed because it is based on key experimental observations well documented in the literature as to the slow kinetics of adsorption of asphaltenes onto water-oil interfaces, and the fact that asphaltenes also play a role in determining the electric charge associated to water-oil interfaces as discussed in section 2.5.2, regarding the work of do Carmo Marques and coworkers (do Carmo Marques et al., 1997).

There is, however, one additional reason for postulating the hypothesis of competitive adsorption as a possible explanation for the behavior of the droplet surface charge density. In fact, it could also give an explanation as to why the conductivity of the emulsion increases with time for freshly dispersed or redispersed emulsions. The competitive adsorption process of asphaltenes and natural surfactants result in an “exchange” of low and high molar mass components between the water-oil interface and the bulk of the oil phase. Considering that both, low and high molar mass components are the charge carriers in the oil phase (or alternatively, they can stabilize charge in the oil phase), then this “exchange process” can explain the trend in the emulsion conductivity.

It is reasonable to think that low molar mass components (natural surfactants) should be the charge carriers with the highest equivalent conductance in the oil phase. In contrast, high molar mass charge carriers (asphaltenes) should have the lowest. The competitive adsorption process would result in a release of components with high equivalent conductance to the oil phase, and the withdrawal of components with low equivalent conductance from the oil phase in order to be adsorbed onto the interface. The overall effect would be an increase in the emulsion conductivity. In this analysis, it has been assumed that the emulsion conductivity is primarily determined from the conductivity of the oil phase. This is actually the case as the conductivity of the emulsion is of the same order of magnitude as the conductivity of diluted bitumen.

To finalize this section, it is important to recall the experimental work discussed in section 2.5.3, where the droplet surface charge density of water-in-kerosene emulsions with SPAN 80 surfactant was investigated using the same electroacoustic technique (Dukhin & Goetz, 2004B). Similarly to the present study, Dukhin and Goetz also observed that the surface charge density decreases as the droplet size and emulsion conductivity increase in their emulsion system (Figure 2.24). However, their explanation to these experimental facts is different.

As discussed in section 2.5.3, they propose that ions diffuse from the interior of the water droplets to the kerosene phase, resulting in the neutralization of counter ion electric charge in the double layer (Dukhin & Goetz, 2004B). As ions diffuse, an internal double layer is created within the water droplets. Simultaneously, the external double layer disappears as the counter charge is neutralized (Figure 2.25). Such a process is

thermodynamically driven as the charging of the interior double layer is more energy efficient than the external double layer (Dukhin & Goetz, 2004B).

This hypothesis would certainly explain the decrease in the droplet surface charge density and the increase in the emulsion conductivity, as discussed in section 2.5.3. However, it implies that such processes are driven by thermodynamic equilibrium and not by the kinetic factors that govern the emulsion behavior, as it has been demonstrated for water-in-diluted bitumen emulsions in the present study. By no means it is being suggested here that the explanation of Dukhin and Goetz is invalid. It just not adapt to the observations in the present study with water-in-diluted bitumen emulsions in this fundamental aspect.

On the other hand, there is another similarity between the experimental results of both studies. The magnitude of the droplet surface charge densities are of the same order of magnitude in both emulsions systems. For water-in-diluted bitumen emulsions, the peak value measured after dispersion is approximately $0.004 \mu\text{C}/\text{cm}^2$. For water-in-toluene emulsions with SPAN 80 surfactant, the peak value is $0.009 \mu\text{C}/\text{cm}^2$ (Dukhin & Goetz, 2004B).

4.4 Droplet size distribution calculation

To our best knowledge, there is no previous published work in the literature dealing with the determination of the droplet size distribution of water-in-diluted bitumen emulsions using the DT-1200 acoustic spectrometer. Published work covers oil-in-water and water-in-oil cosmetic emulsions (Fairhurst et al., 2001), heptane/water/AOT microemulsions (Wines et al., 1999) and water-in-kerosene emulsions (Dukhin & Goetz, 2004B). Based on the results of the present study, this section discusses important aspects that specifically apply for the acoustic determination of the droplet size distribution of water-in-diluted bitumen emulsions, thus setting a new background on this area in view of lack of related information in the literature.

As discussed by (Dukhin & Goetz, 1999), there are two levels for interpreting the acoustic attenuation spectrum that apply to this study. In the first level, the acoustic attenuation spectrum can be used just to test whether the droplet size distribution changes

with time or not. After all, a change in attenuation reflects variation in the state of the dispersion. In the second level, there is the more advanced stage of analysis where a predictive theory is applied to calculate the droplet size distribution from the attenuation spectrum. However, as any other predictive theory, it is based on specific assumptions and care must be taken to verify that such assumptions apply to the system under study.

Starting with the more advanced level of interpretation of the acoustic attenuation spectrum, the two more important assumptions to be considered in the predictive theory for droplet size calculations are: 1) the wavelength of the sound wave must be larger than the size of the water droplets (long wavelength requirement), and 2) the predictive theory has been verified to be valid for moderately concentrated dispersions (up to at least 10% by volume for emulsion systems). This was discussed in section 2.6.2.

In order to comply with these two requirements, the following conditions were considered in planning the experiments and analyzing the data: 1) the attenuation spectra was measured in the full frequency range of capability of the DT-1200 (i.e., from 3 to 100 MHz), but only the data within the frequency range from 3 to 30 MHz was used for droplet size distribution calculation; and 2) droplet size distribution measurements were limited to emulsions with a maximum water content of 10% by weight (8.49% by volume).

The frequency range for droplet size analysis was reduced to 30 MHz in order to comply with the long wavelength requirement. Emulsion samples were taken from the spectrometer chamber during experiments for observation under a microscope (Figure 4.22). Qualitatively, it can be said that the vast majority of the observed water droplets never reached a size above 50 μm . Although the mean droplet size was never determined using any visualization technique, it is obvious that it was below 50 μm during experiments. Considering that the sound speed through the emulsion system was in the order of 1380 m/s for all emulsion considered in the present study, a wavelength of 50 μm corresponds to a frequency of approximately 27.6 MHz. This means that any frequency range below 30 MHz is expected to satisfy the long wavelength requirement.

However, as discussed in the literature review (section 2.6.2), there is one fundamental limitation when cutting the frequency range down to 30 MHz. Very small

water droplets (with sizes in the range of nanometers) do not attenuate sound at low frequencies; only large water droplets do (in the order of micrometers). This means that if a fraction of nanometer size water droplets exists, it would be missed in the calculation. As shown in section 4.2, the calculated droplet size distribution that best fit the experimental data was unimodal (log-normal distribution) with droplet size in the micrometer range. The logical question is whether a second fraction in the nanometer range was present or not. The answer to this important question is no, and the rest of this section is devoted to the rationale of the provided answer.

The question regarding the possibility of missing a nanometer size fraction in the analysis can be answered considering the first level of interpretation of the acoustic attenuation spectrum (i.e., the qualitative interpretation analysis). This supports the thesis of unimodal droplet size distribution in the micrometer size to be correct in our experiments. Figure 4.23 shows the attenuation spectrum as a function of time, corresponding to the droplet size distribution calculation of emulsion “B1” (shown in Figure 4.9). As mentioned earlier, a 10% wt. emulsion was studied for 4 days, where the high speed homogenizer was applied only once at the beginning, and then the emulsion was kept under continuous agitation in the chamber for measurements. Each line in Figure 4.23 (upper graph) corresponds to the attenuation at a specific frequency; there are 18 frequencies in total increasing from bottom to top, from 3 to 100 MHz. The lower graph in Figure 4.23 shows the same attenuation spectrum as a function of frequency; only 5 measurements are shown with one day interval in-between. The intrinsic attenuation of the emulsion is also shown.

It can be observed that the attenuation in the whole frequency range changes smoothly with time during the first 3 days. Particularly, the attenuation in the 3 to 30 MHz frequency range used for droplet size calculation changes with time during the first 40 hours, and then stabilizes. However, after 3 days, the attenuation at the higher frequencies (> 65 MHz) suddenly increases and shows an erratic behavior. It is important to observe that this erratic behavior continues during the next 24 hours until the end of the experiment. Also, it is important to note that the erratic behavior first appears at the higher frequencies (> 65 MHz), and then seems to propagate to the intermediate frequencies (> 43 MHz). The same behavior for the higher frequencies attenuation was

observed every time an emulsion was studied for a relatively long period of time; for example, Figure 4.24 shows the attenuation spectrum “E” (20% wt water emulsion), corresponding to the droplet size distribution calculation shown in Figure 4.19. In this case, the erratic behavior appeared earlier and continued during the next 2 days until the experiment was stopped.

The qualitative interpretation of these spectra is as follows. As discussed in section 2.6.2, there are three major sources of sound attenuation in emulsion systems: 1) intrinsic loss, 2) thermal loss, and 3) scattering loss (Babick et al., 2000). The intrinsic attenuation constitutes the base line of the acoustic spectrum, and it is shown in Figures 4.23 and 4.24. Any attenuation in excess to the intrinsic attenuation (called *excess attenuation*) is due to thermal or scattering losses, which are due to the presence of the water droplets in the system. As discussed previously, both attenuation mechanisms show different functional relationship with droplet size and sound frequency, which allows the interpretation of the attenuation spectrum in a qualitative manner.

As can be observed in Figures 4.23 and 4.24, there is excess attenuation in the whole frequency range (3 to 100 MHz). At low frequencies, it is certainly due to large droplets in the micrometer size range. However, excess attenuation at the higher frequencies could be explained, in principle, by the large droplets itself (should scattering be responsible of high frequency attenuation), or by the presence of a second fraction of nanometer size droplets (should thermal losses be responsible of high frequency attenuation). There are three reasons to believe that high frequency attenuation is due to large droplets and not to the presence of a fraction of very small droplets.

In the first place, the erratic behavior observed for the higher frequency attenuation could be explained in terms of scattering. This erratic behavior occurs one or more days after water dispersion with the high speed homogenizer, when the droplet mean size has apparently leveled off. As discussed in the previous sections, it is reasonable to think that a dynamic equilibrium has been reached where the rate of aggregation or coalescence of water droplets is comparable to the rate of droplet breakup or aggregate disjoin. Attenuation due to scattering is very sensitive to droplet size, and the oscillatory nature of the high frequency attenuation could reflect the behavior of the larger water droplets in the size distribution. At times, they can coalesce or aggregate due to

droplet collision, thus increasing their effective size. However, they eventually reach a critical size where shearing forces causes droplet breakup or aggregate disjoin, thus decreasing their effective size again. This behavior would be reflected as an erratic oscillation of the high frequency attenuation.

A second reason to believe that high frequency attenuation is due to scattering is the fact that the observed erratic behavior occurs first at the higher frequencies within the 3 to 100 MHz range, which is in agreement with the strong frequency dependence of the scattering mechanism. Furthermore, the fact that it starts one or more days after water dispersion is in agreement with the calculated droplet size evolution in time. First, the water droplet size is reduced by the effect of the homogenizer. Then, immediately after the application of the homogenizer the water droplet size starts to increase. It would be reasonable to think that the erratic attenuation behavior will not occur immediately after the high speed homogenizer is applied but with some considerable time delay (several hours), because it would take time for the droplet size to increase until a significant population of large droplets is formed that would start to scatter sound significantly. Probably, this concept could also explain the fact that, the higher is the water content in the emulsion, the earlier the erratic behavior appears (Figures 4.23 and 4.24). It is expected that the higher water content case would correspond to a faster increase in droplet size, because there is more chance for droplets collision as the water content increases, keeping the agitation intensity the same.

A third reason supporting the thesis of scattering losses is the effect of the high speed homogenizer at the higher frequencies. Let us first consider Figure 4.25, where it is shown the attenuation spectra as a function of time corresponding to emulsion "B2" (the droplet size calculation is shown in Figure 4.10). In this experiment, the high speed homogenizer was applied every 24 hours to a 10% wt. emulsion for 4 days. It can be seen that the attenuation at all frequencies (not only within the 3 to 30 MHz range) qualitatively shows the same pattern after every application of the homogenizer. It was mentioned previously that approximately 40 hours are needed for the erratic behavior to appear for a 10% emulsion (Figure 4.23). For this reason, the erratic behavior was not observed in emulsion experiment "B2", as there was only 24 hours between successive redispersions. It can be concluded that the same pattern observed for the attenuation in the

whole frequency range well reflects the trend of the droplet size calculation obtained from the 3 to 30 MHz spectra analysis, as shown in Figure 4.10.

Having said the above, it would be interesting to analyze the effect of the high speed homogenizer on the attenuation spectrum after the erratic behavior has already started at the higher frequencies. It is expected that the application of the high speed homogenizer would eliminate this erratic behavior in the attenuation, as large water droplets which are able to scatter sound significantly and erratically would no longer exist immediately after redispersion. Many observations in the present work demonstrated that it is actually the case. For example, referring again to the emulsion experiment "B1" (Figure 4.9 and 4.23), the high speed homogenizer was applied before ending the experiment, when the erratic behavior had been showing up for 1 day. Figure 4.26 shows the attenuation spectra before and after the application of the high speed homogenizer. It can be observed that the attenuation changes smoothly with time as expected after the redispersion of the emulsion. Measurements before the application of the high speed homogenizer were made with time intervals of 40 minutes because the CVC signal was also being measured, in addition to sound attenuation.

Finally, some words have to be said in regard to the possibility of thermal losses and not scattering losses to be the cause of excess attenuation at the higher frequencies. In the first place, thermal losses would imply the presence of a second fraction in the nanometer size range that could be a microemulsion (typically when the droplet diameter is less than 100 nm). Microemulsions are thermodynamically stable. In other words, a microemulsion shows the characteristics of phase equilibrium. This is clearly not the case in our experiments, where the system does not reach equilibrium in the thermodynamic sense. Relaxation experiments where the emulsion could be repeatedly perturbed by means of the high speed homogenizer support this point. Furthermore, an erratic pattern at the higher frequencies would be contrary to the idea of a state of equilibrium of such a small size fraction.

In conclusion, the qualitative interpretation of the attenuation spectra supports the thesis of scattering losses to be the most likely cause of excess attenuation at the higher frequencies, thus confirming that the calculated unimodal droplet size distribution in the micrometer size range obtained from the 3 to 30 MHz analysis is correct.

Properties	Diluted bitumen		Heavy water	
Density [Kg·m ³]	ρ_m	919	ρ_p	1,100
Thermal expansion [K ⁻¹]	β_m	$10.8 \cdot 10^{-4}$	β_p	$1.09 \cdot 10^{-4}$
Specific heat [J·kg ⁻¹ ·K ⁻¹]	$(c_p)_m$	$1.63 \cdot 10^3$	$(c_p)_p$	$4.179 \cdot 10^3$
Dynamic viscosity [Pa·s]	η_m	$4.9 \cdot 10^{-3}$	η_p	$1.32 \cdot 10^{-3}$
Thermal conductivity [W·m ⁻¹ ·K ⁻¹]	τ_m	0.14	τ_p	0.6098
Sound speed [m·s ⁻¹]	c_m	1,378.0	c_p	1,386.6
Intrinsic attenuation coefficient [dB·cm ⁻¹ ·MHz ⁻¹]	$(\alpha_{int})_m$ 3.0 MHz	0.181	$(\alpha_{int})_p$ 3.0 MHz	0.028
	$(\alpha_{int})_m$ 3.7 MHz	0.192	$(\alpha_{int})_p$ 3.7 MHz	0.015
	$(\alpha_{int})_m$ 4.5 MHz	0.191	$(\alpha_{int})_p$ 4.5 MHz	0.004
	$(\alpha_{int})_m$ 5.6 MHz	0.215	$(\alpha_{int})_p$ 5.6 MHz	0.013
	$(\alpha_{int})_m$ 6.8 MHz	0.247	$(\alpha_{int})_p$ 6.8 MHz	0.025
	$(\alpha_{int})_m$ 8.4 MHz	0.260	$(\alpha_{int})_p$ 8.4 MHz	0.028
	$(\alpha_{int})_m$ 10.3 MHz	0.293	$(\alpha_{int})_p$ 10.3 MHz	0.033
	$(\alpha_{int})_m$ 12.7 MHz	0.327	$(\alpha_{int})_p$ 12.7 MHz	0.041
	$(\alpha_{int})_m$ 15.6 MHz	0.363	$(\alpha_{int})_p$ 15.6 MHz	0.049
	$(\alpha_{int})_m$ 19.2 MHz	0.408	$(\alpha_{int})_p$ 19.2 MHz	0.0606
	$(\alpha_{int})_m$ 23.5 MHz	0.456	$(\alpha_{int})_p$ 23.5 MHz	0.0714
	$(\alpha_{int})_m$ 28.9 MHz	0.517	$(\alpha_{int})_p$ 28.9 MHz	0.0880
	$(\alpha_{int})_m$ 35.5 MHz	0.590	$(\alpha_{int})_p$ 35.5 MHz	0.1069
	$(\alpha_{int})_m$ 43.7 MHz	0.678	$(\alpha_{int})_p$ 43.7 MHz	0.1321
	$(\alpha_{int})_m$ 53.6 MHz	0.781	$(\alpha_{int})_p$ 53.6 MHz	0.1625
	$(\alpha_{int})_m$ 65.9 MHz	0.898	$(\alpha_{int})_p$ 65.9 MHz	0.1975
$(\alpha_{int})_m$ 81.0 MHz	1.043	$(\alpha_{int})_p$ 81.0 MHz	0.2455	
$(\alpha_{int})_m$ 99.5 MHz	1.210	$(\alpha_{int})_p$ 99.5 MHz	0.301	
Measured electroacoustic signal (Eq. 3.13)	$CVC_{measured}$ (magnitude)	$164 \cdot 10^2$		
	$CVC_{measured}$ (phase)	142		
Conductivity [S·m ⁻¹]	K_m	$9.4 \cdot 10^{-7}$		
Notes:				
1) Thermal expansion and specific heat of diluted bitumen and heavy water were approximated to those of toluene and water reported on the DT-1200 materials database, respectively.				
2) Conductivity of diluted bitumen is not required for droplet size distribution or surface charge density calculation.				

Table 4.1: Material properties for droplet size distribution and surface charge density calculation.

Measurement	Mean droplet diameter (μm)	CVC signal magnitude	Emulsion conductivity ($\times 10^{-7}$ S/m)
After initial dispersion	7.00	29961	9.06
After 1 st redispersion	6.88	27275	9.69
After 2 nd redispersion	5.98	22184	10.20
After 3 rd redispersion	5.82	23843	10.37

Table 4.2: Super-imposed relaxation data for emulsion “B2” (10% wt. water emulsion with 3 water redispersions).

Measurement	Water content analysis (% wt)			
	Top	Medium	Bottom	Average
Emulsion B1				
After 3 rd Day	9.63	9.82	9.74	9.73
Emulsion B2				
After 1 st Day	9.96	9.62	9.03	9.54
After 2 nd Day	10.14	9.86	9.33	9.78
After 3 rd Day	10.12	9.76	9.52	9.80
Emulsion B3				
After 1 st Day	10.23	9.79	9.43	9.82
After 2 nd Day	10.14	9.67	9.40	9.74
After 3 rd Day	10.03	9.94	9.67	9.88
<p>Note: For emulsions B2 and B3, the water content analysis was performed before every redispersion with the high speed homogenizer</p>				

Table 4.3: Water distribution in chamber for emulsions B1, B2 and B3.

Measurement	Water content analysis (% wt)			
	Top	Medium	Bottom	Average
After 3 rd Day	29.77	29.89	29.73	29.80

Table 4.4: Water distribution in chamber for emulsion C1.

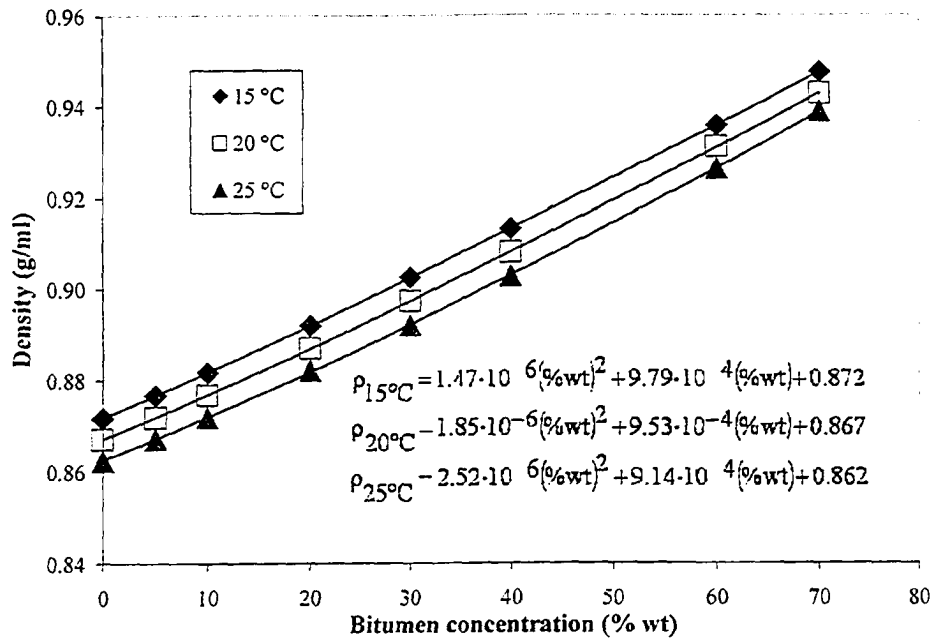


Figure 4.1: Density of diluted bitumen as a function of bitumen concentration.

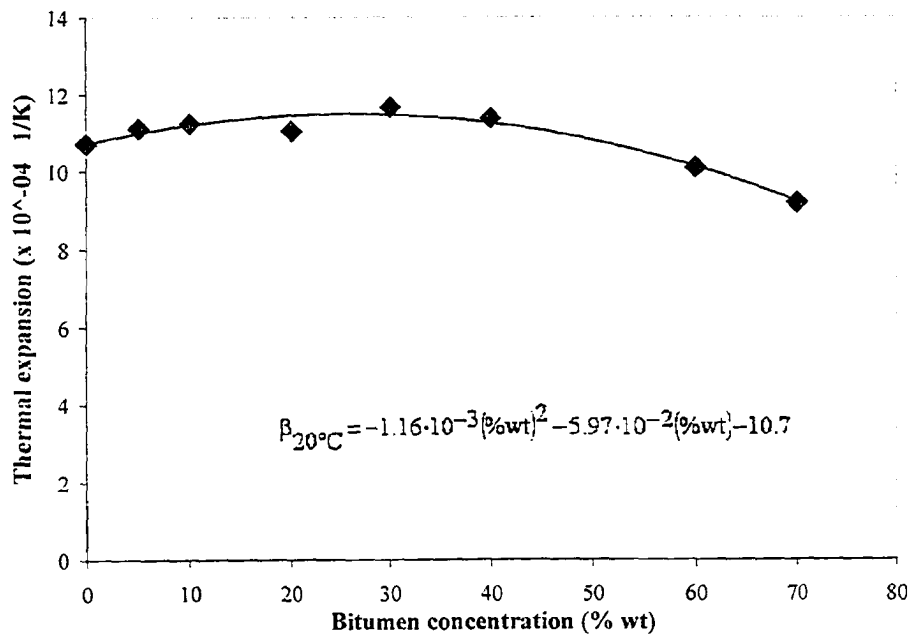


Figure 4.2: Thermal expansion of diluted bitumen as a function of bitumen concentration at 20 °C.

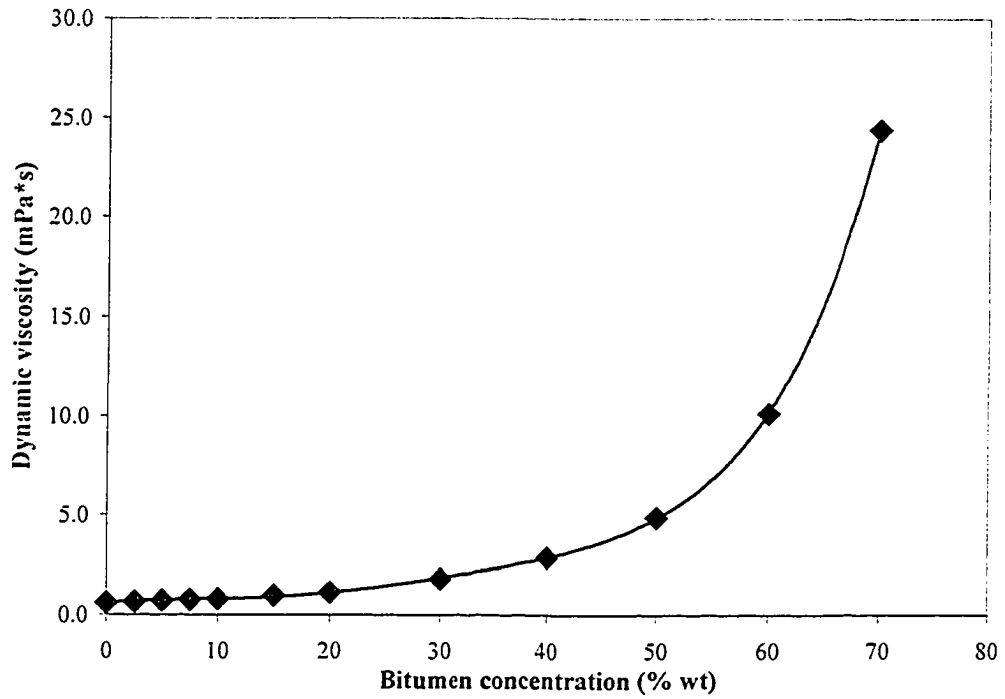


Figure 4.3: Dynamic viscosity of diluted bitumen as a function of bitumen concentration at 20 °C.

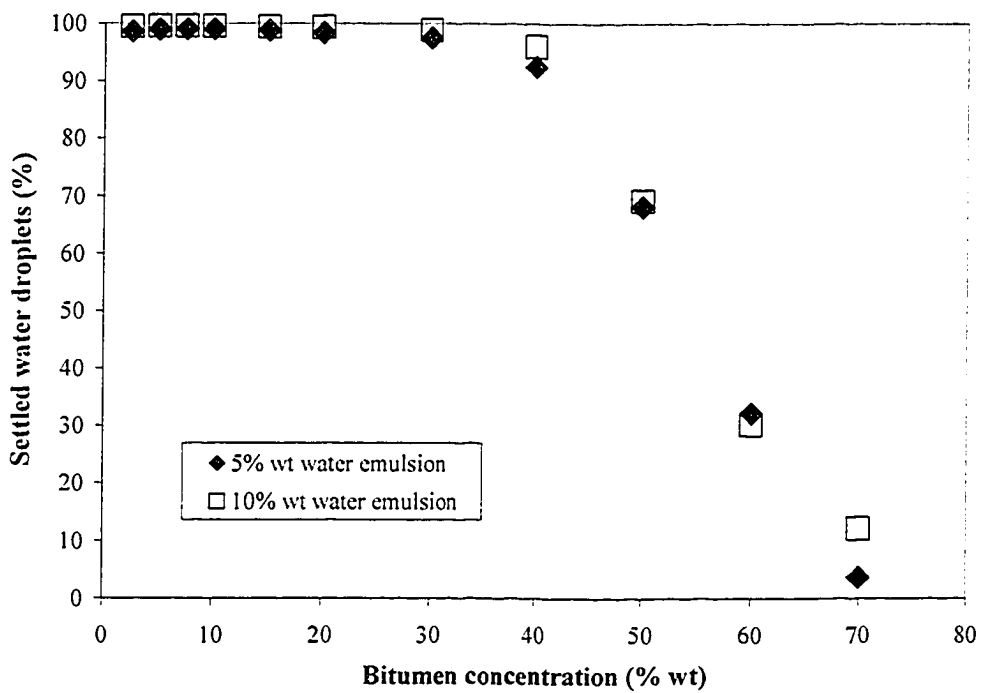


Figure 4.4: Percentage of settled water droplets after 24 hours at 20 °C.

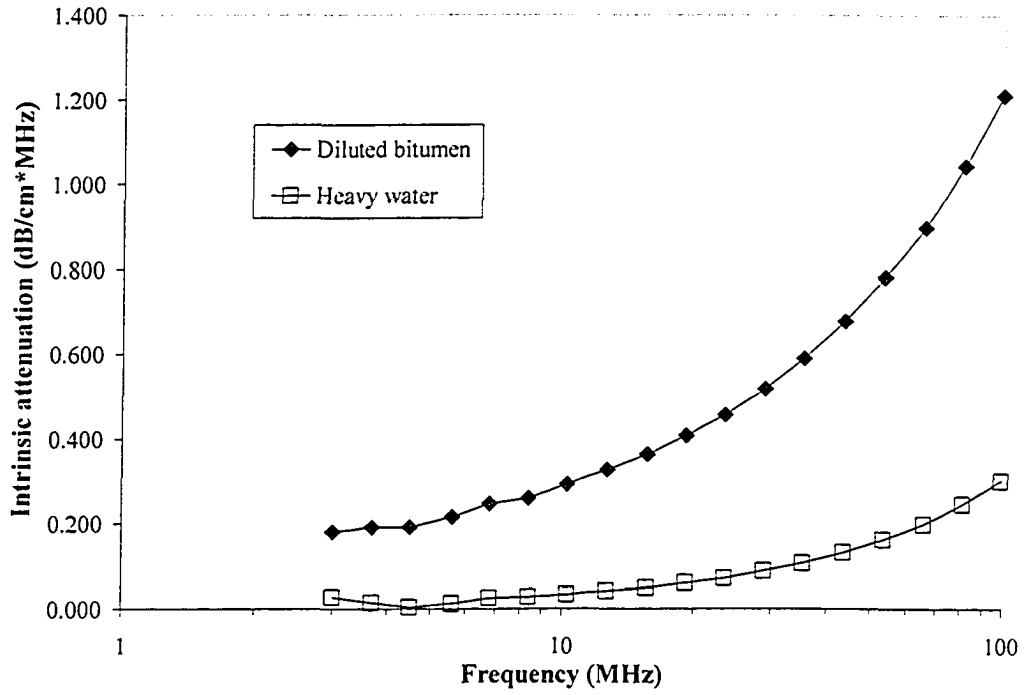


Figure 4.5: Intrinsic attenuation coefficient of diluted bitumen (50% wt.) and heavy water.

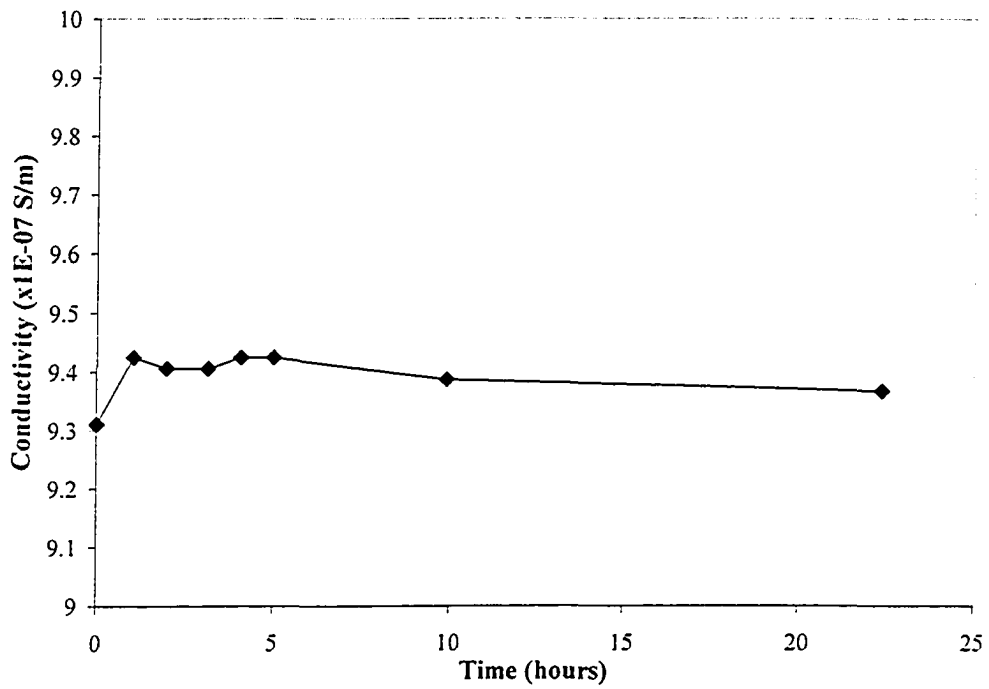


Figure 4.6: Conductivity of diluted bitumen (50% wt.) at 20 °C.

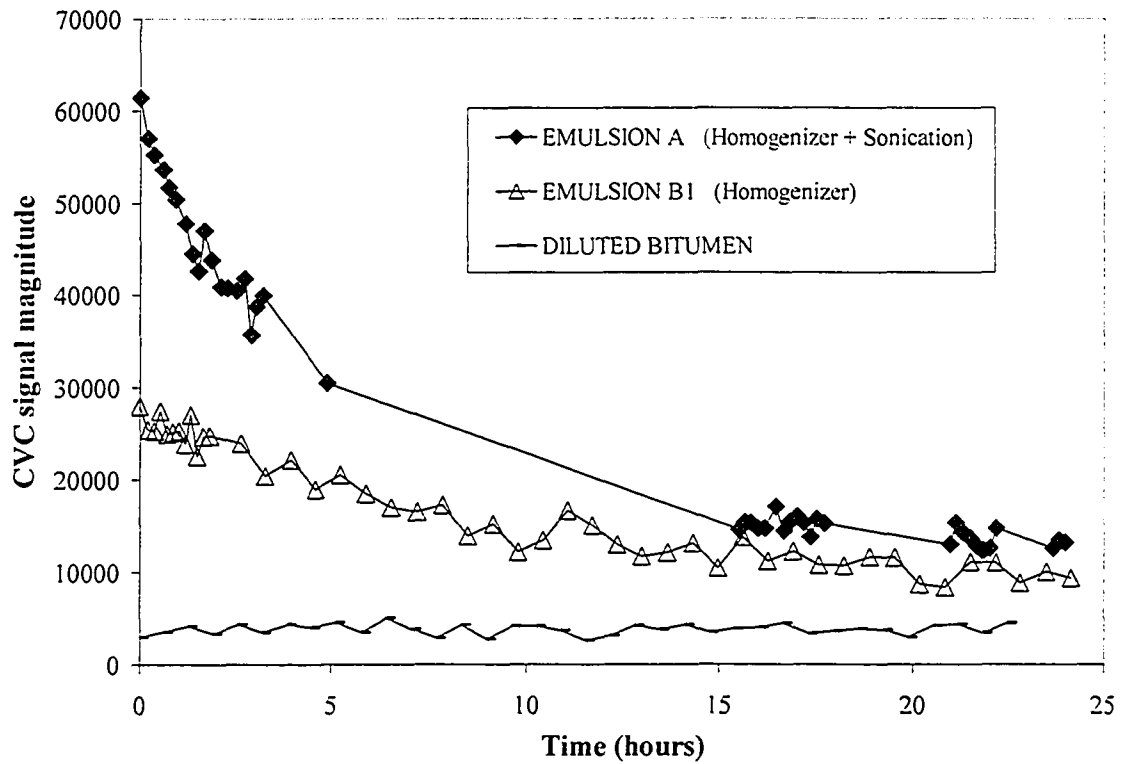


Figure 4.7: Dependence of CVC on the method of water dispersion in diluted bitumen (10% wt. water emulsions).

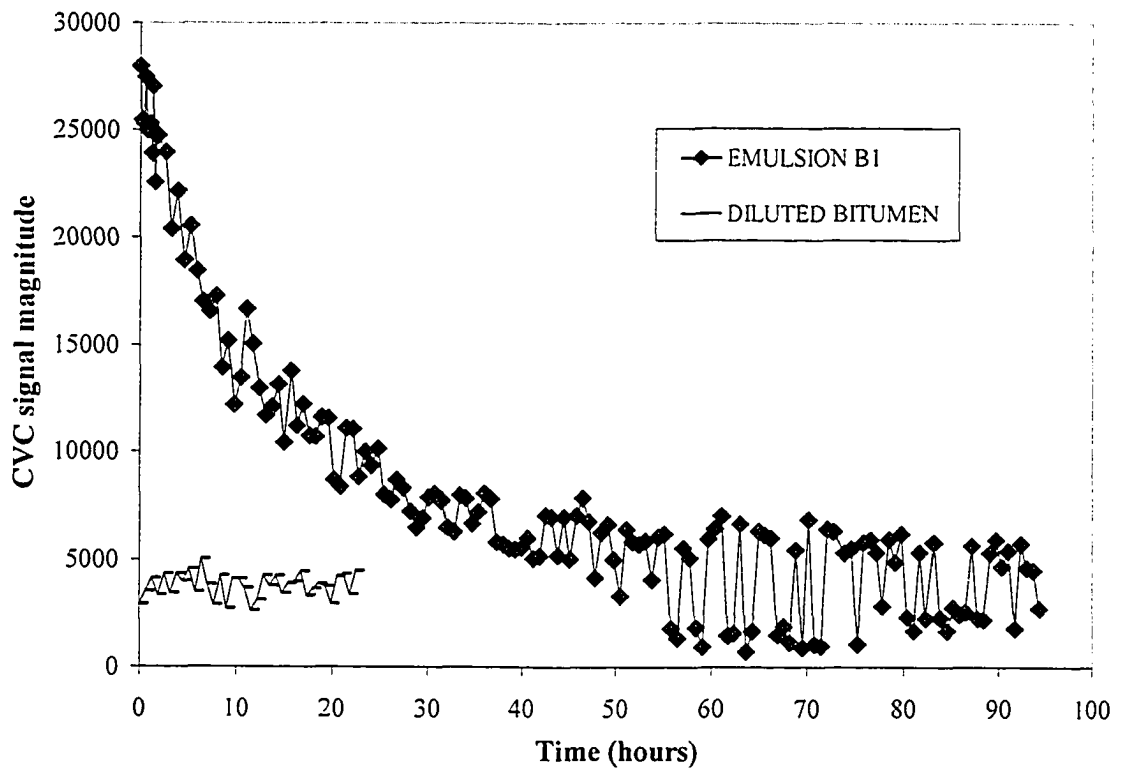


Figure 4.8: Transient behavior of CVC (10% wt. water emulsion).

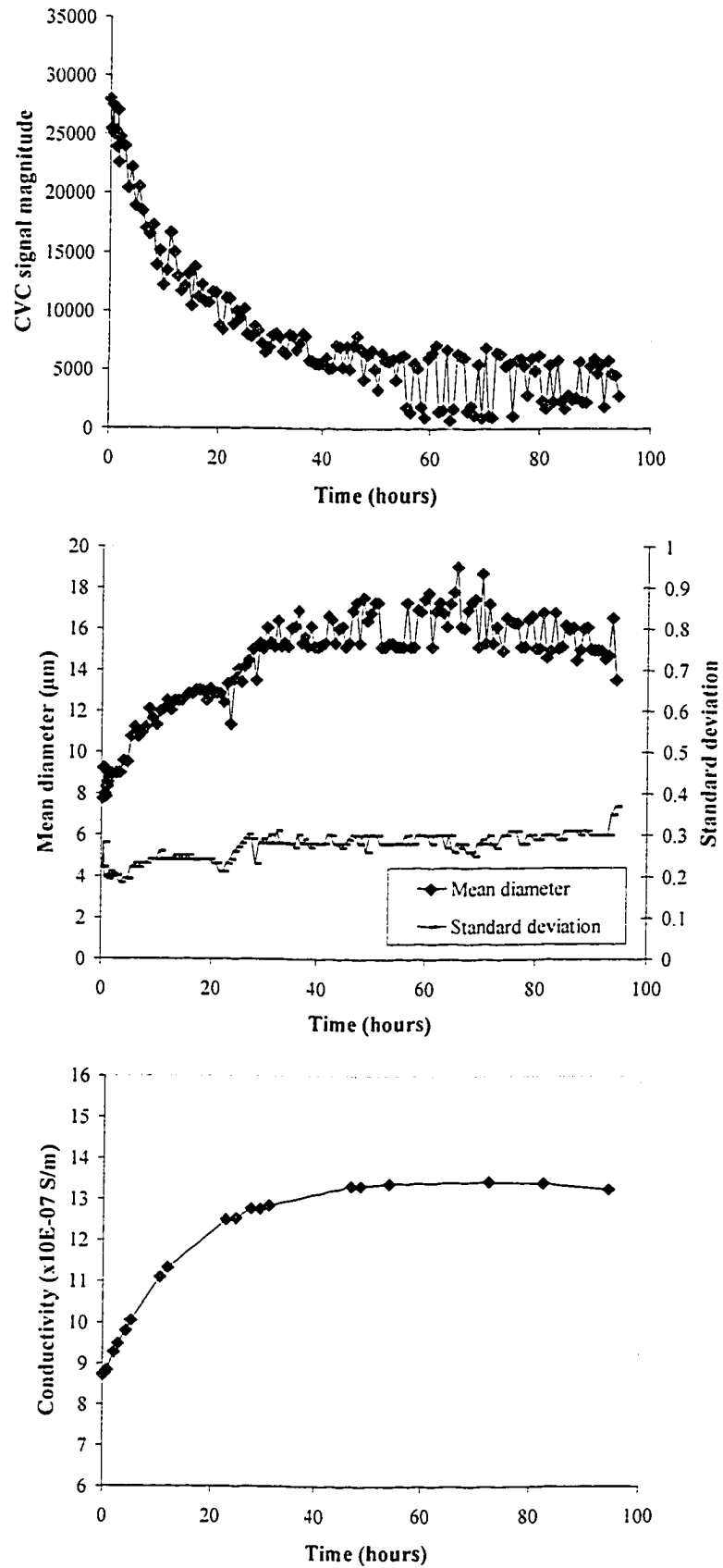


Figure 4.9: Emulsion B1 – 10% wt. water (no water redispersion).

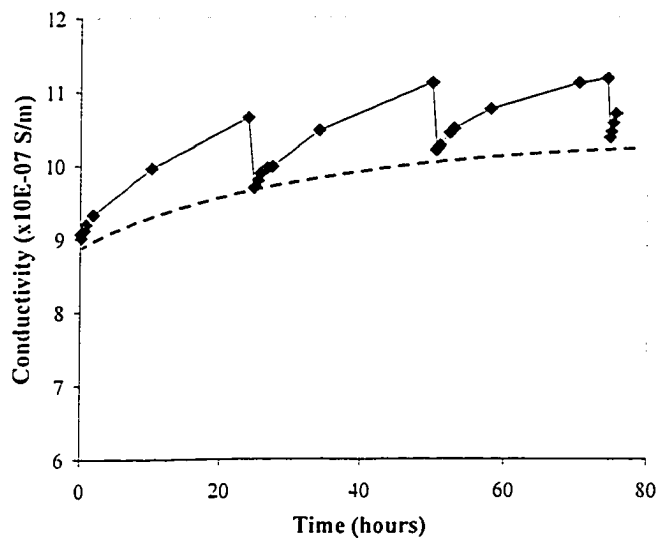
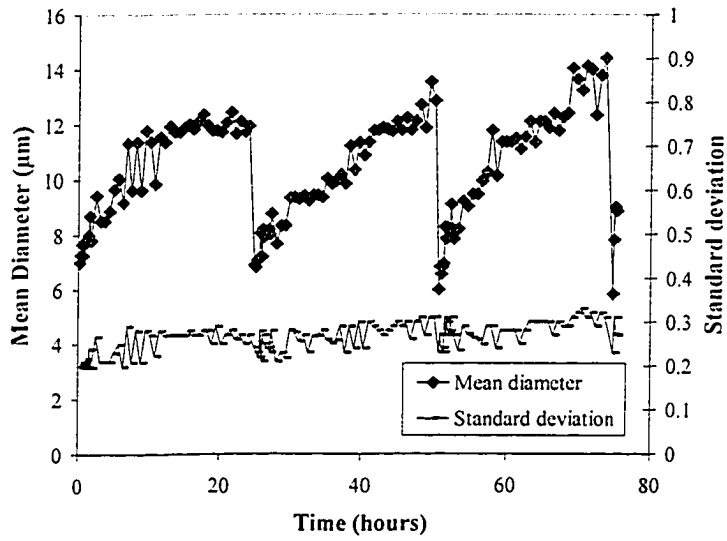
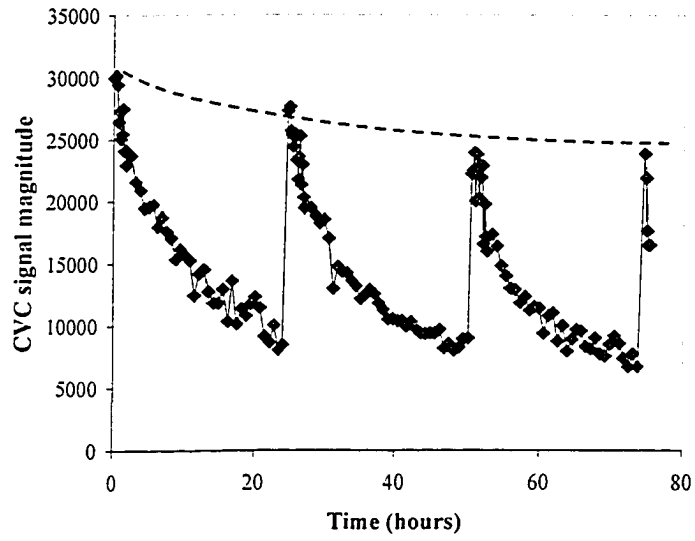


Figure 4.10: Emulsion B2 – 10% wt. water (3 water redispersions)

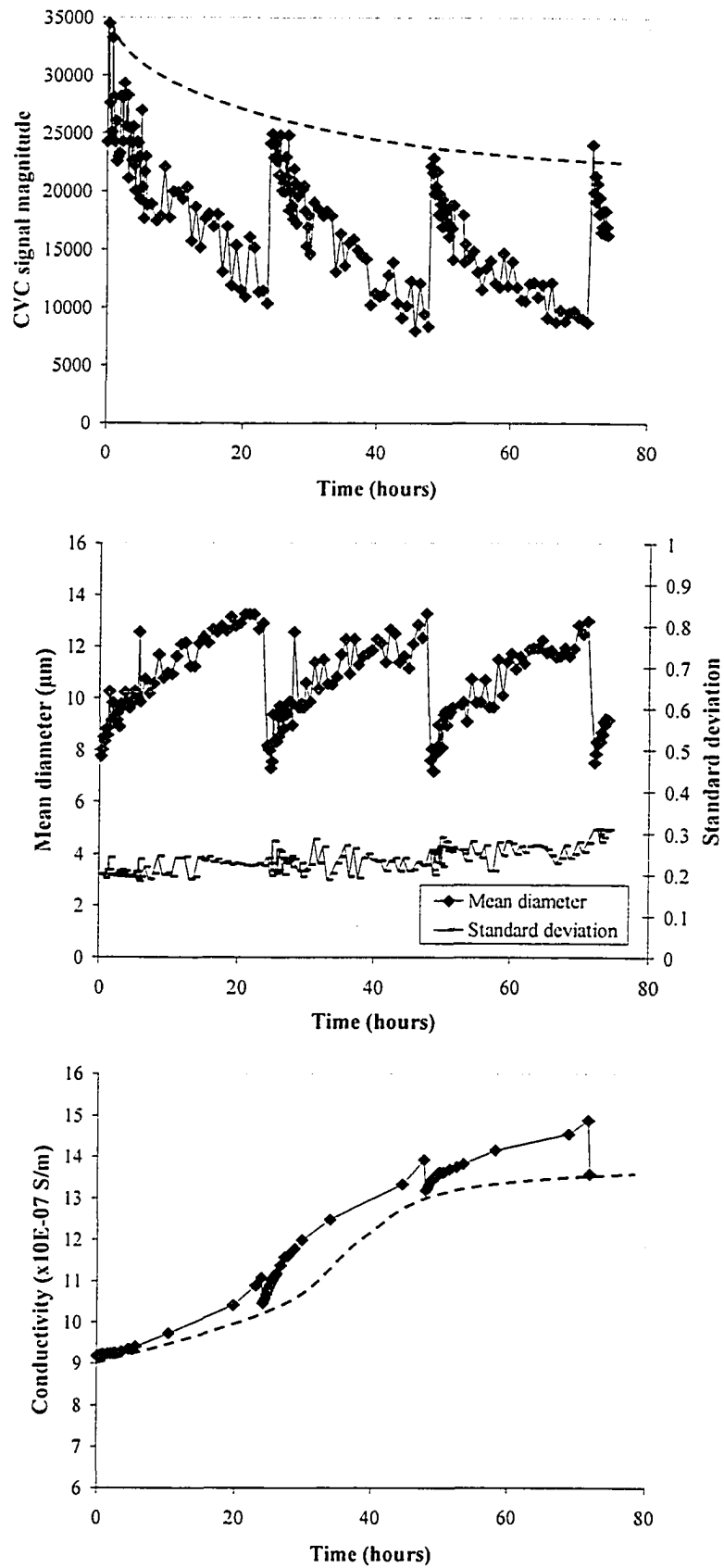


Figure 4.11: Emulsion B3 – 10% wt. water (repetition experiment B2).

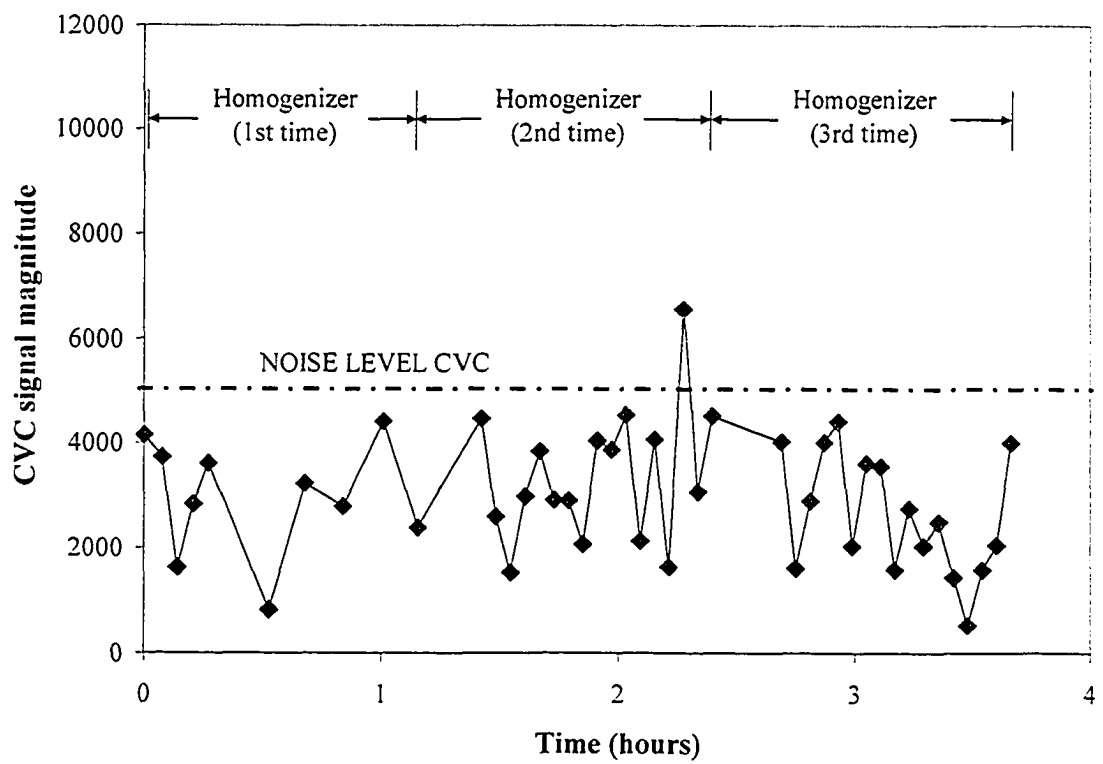


Figure 4.12: Effect of the high speed homogenizer on diluted bitumen.

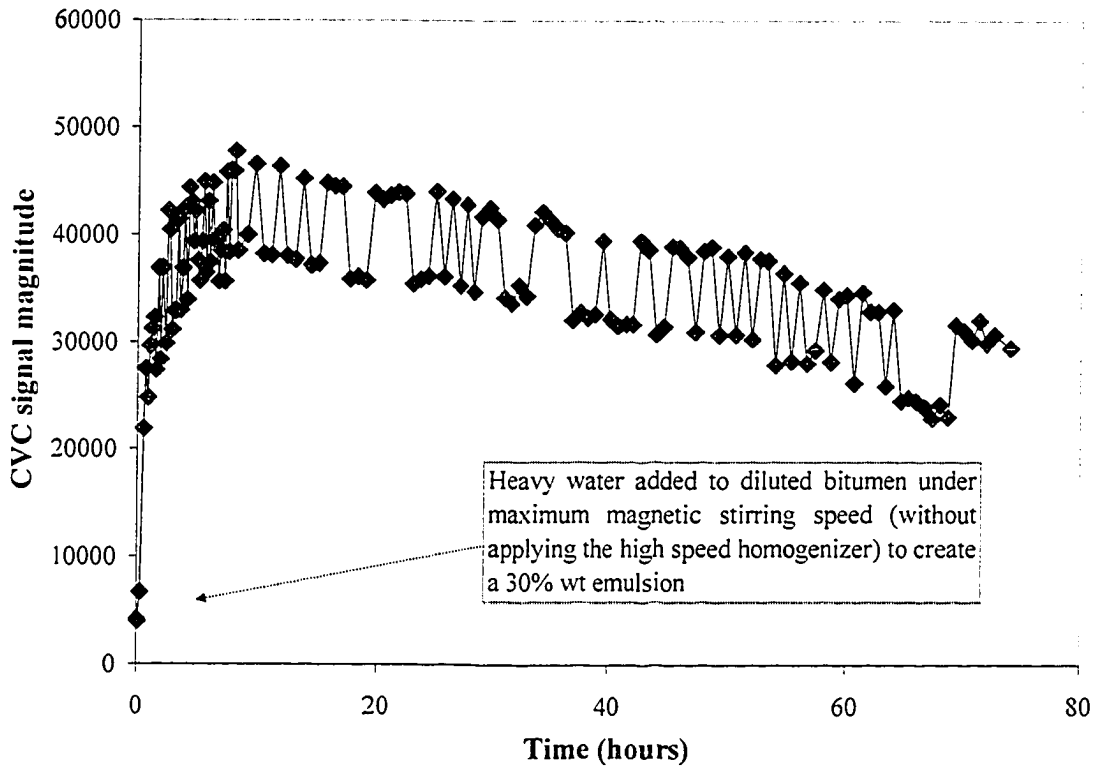


Figure 4.13: Emulsion C1 – 30% wt. water (water distribution without applying high speed homogenizer).

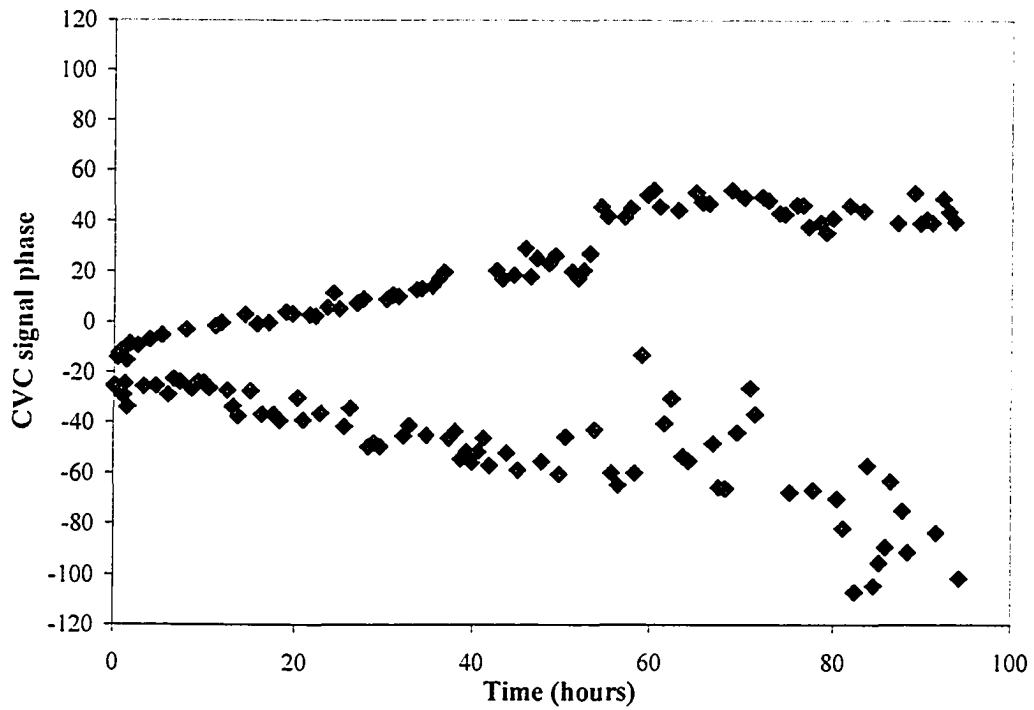


Figure 4.14: Emulsion B1 – 10% wt. water (CVC signal phase according to measurements).

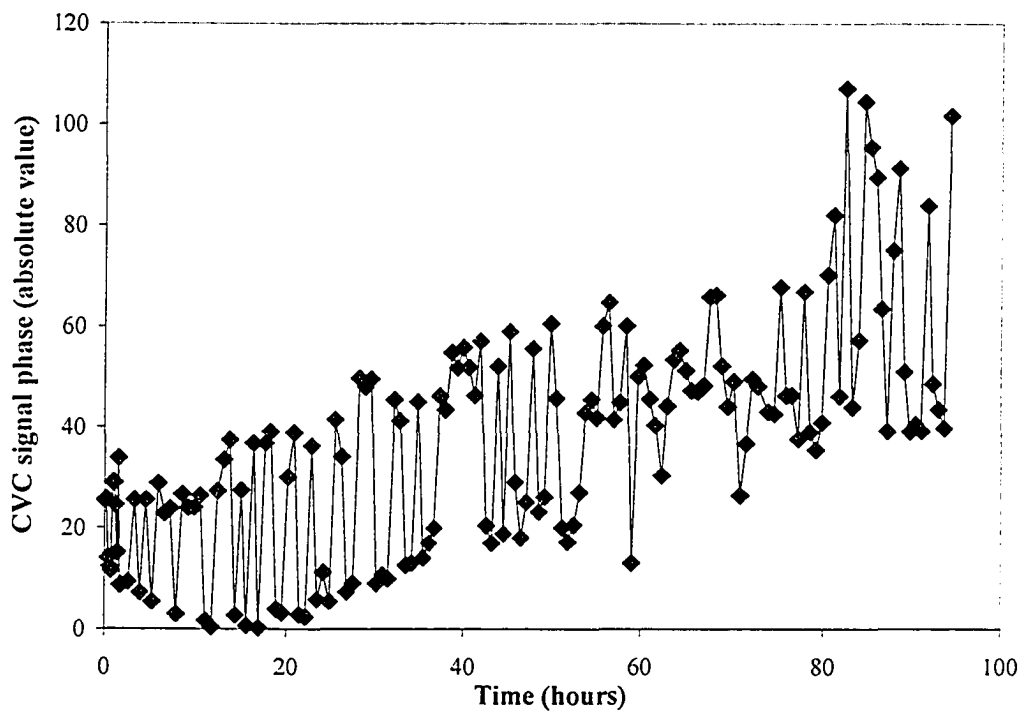


Figure 4.15: Emulsion B1 – 10% wt. water (CVC signal phase considering absolute value).

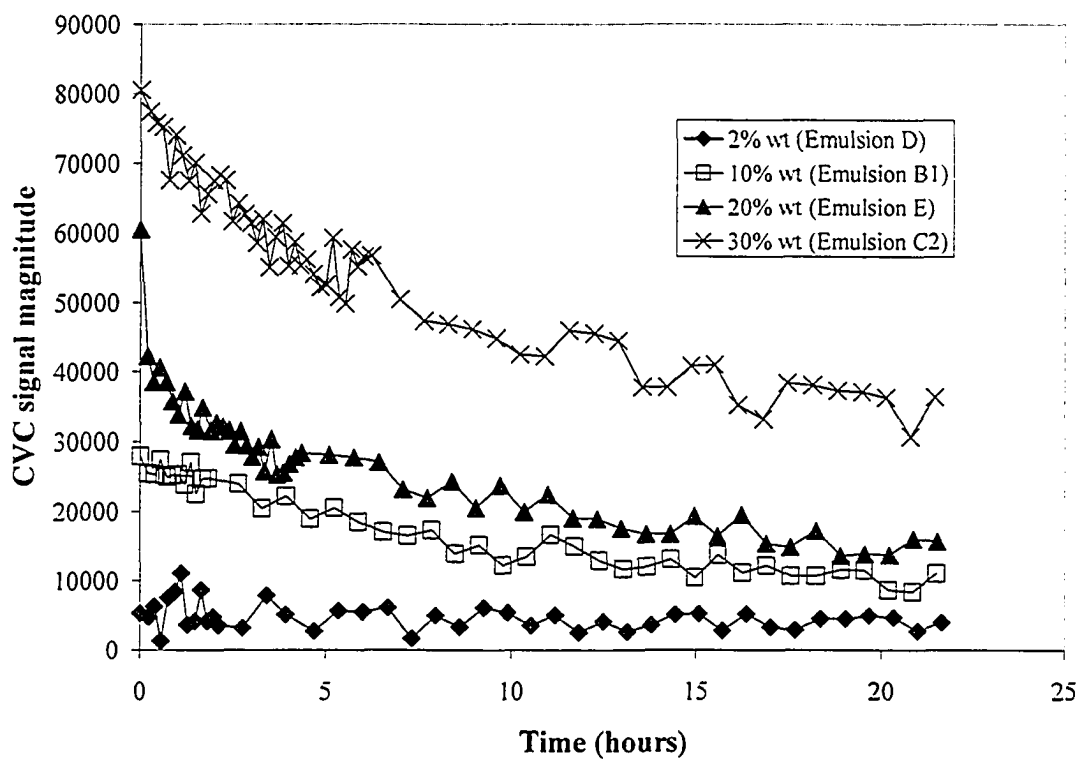


Figure 4.16: Volume fraction dependence of CVC (2% to 30% wt. water emulsions).

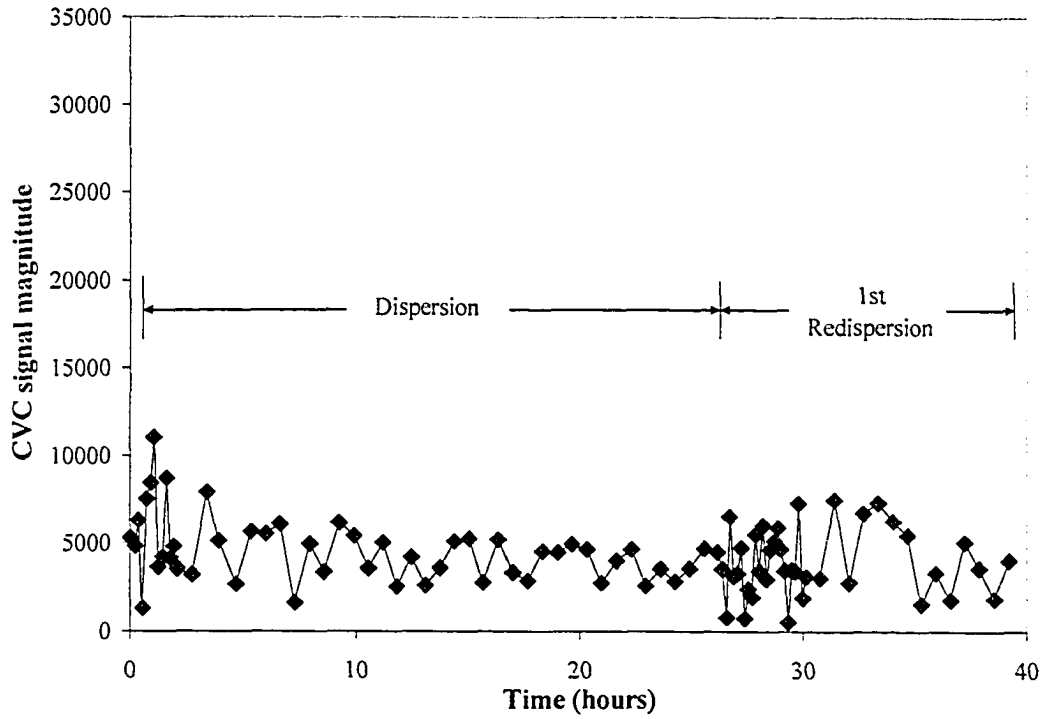


Figure 4.17: Emulsion D – 2% wt. water (one water redispersion).

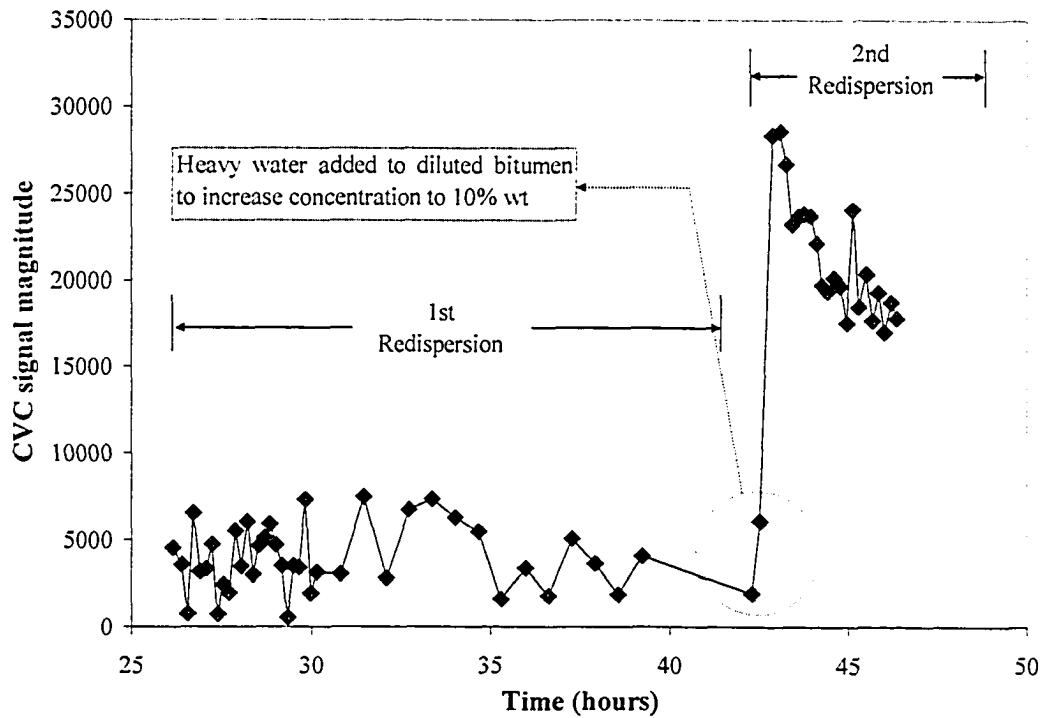


Figure 4.18: Emulsion D – 10% wt. water (after water addition).

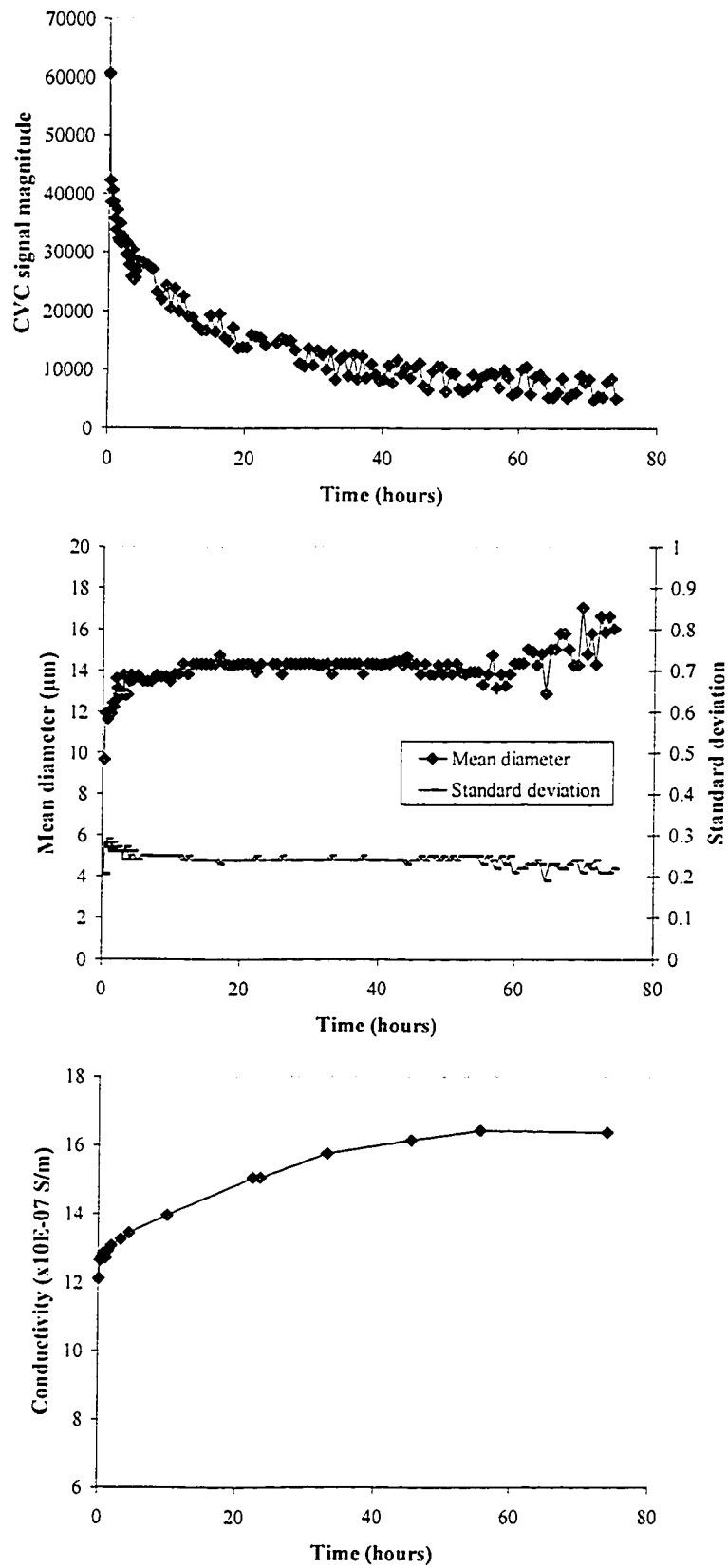


Figure 4.19: Emulsion E – 20% wt. water (no water redispersion).

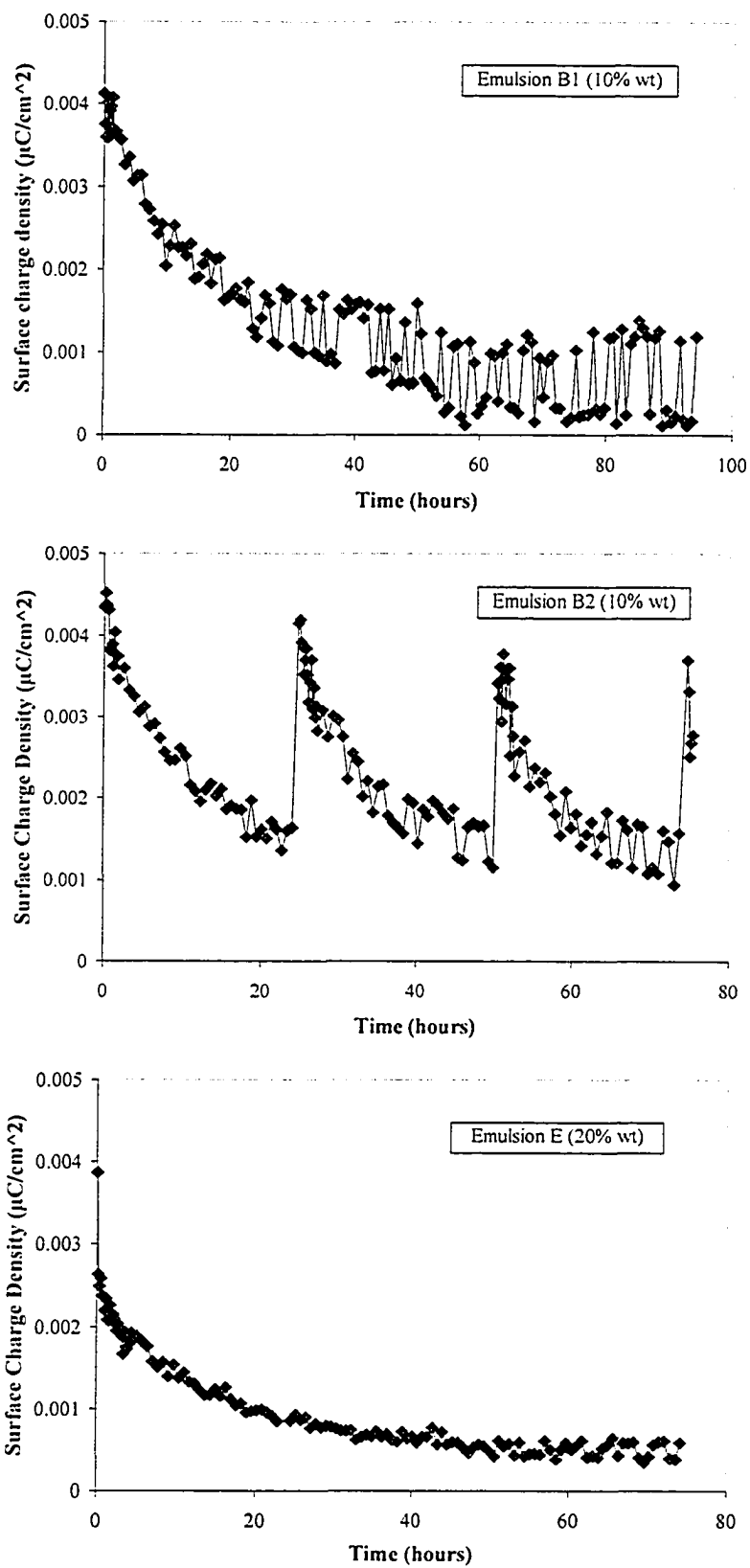


Figure 4.20: Droplet surface charge density calculation for emulsions B1, B2 and E.

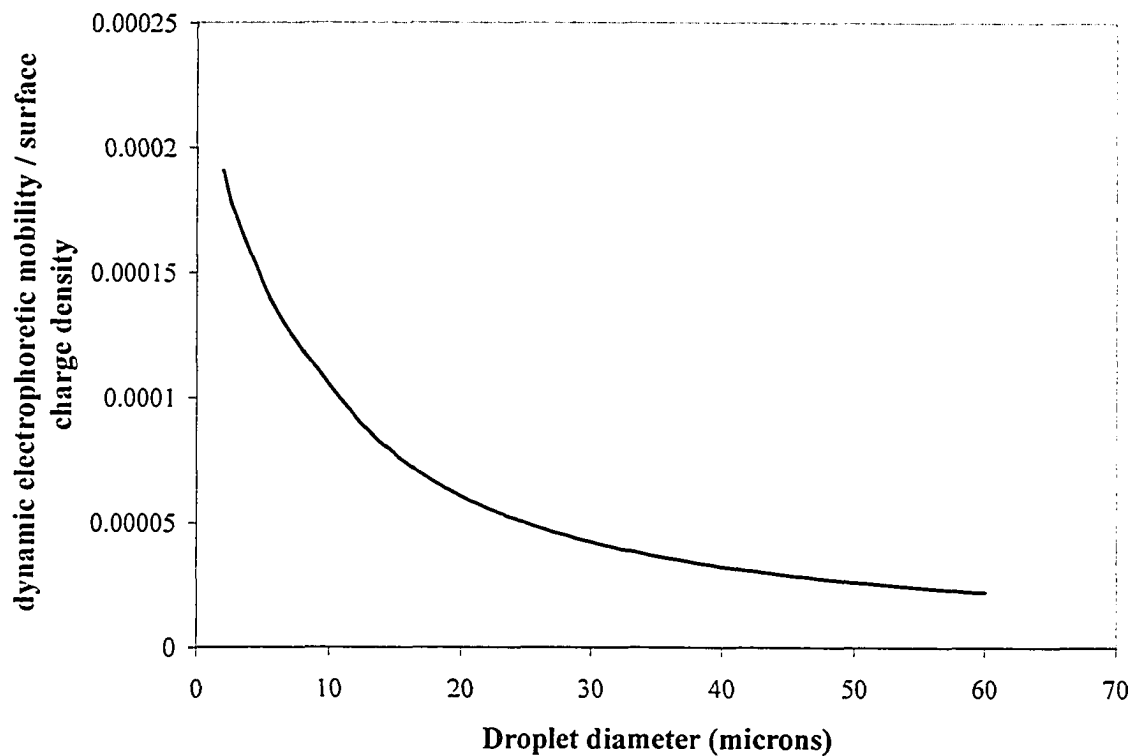


Figure 4.21: μ_d/σ ratio as a function of droplet diameter, calculated from Shilov's theory for a 10% wt. water emulsion.

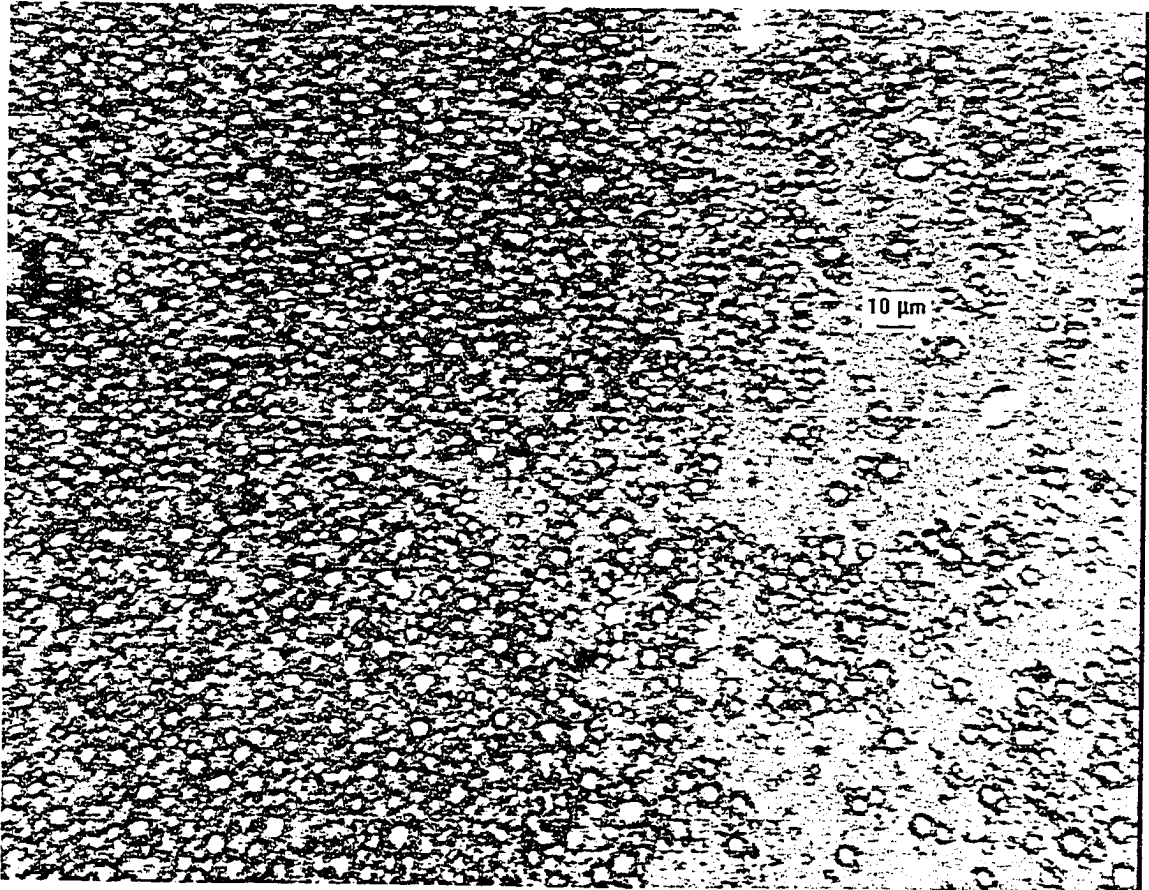


Figure 4.22: Microscope observation of 10% wt. water emulsion after water dispersion with the high speed homogenizer.

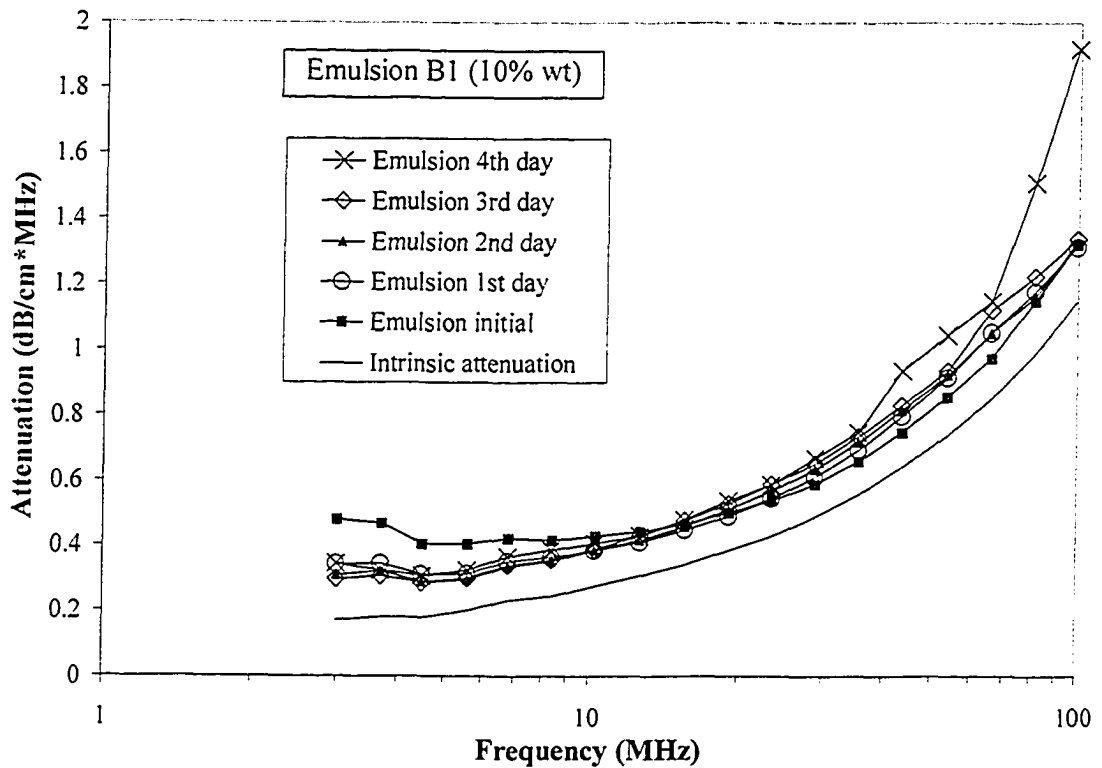
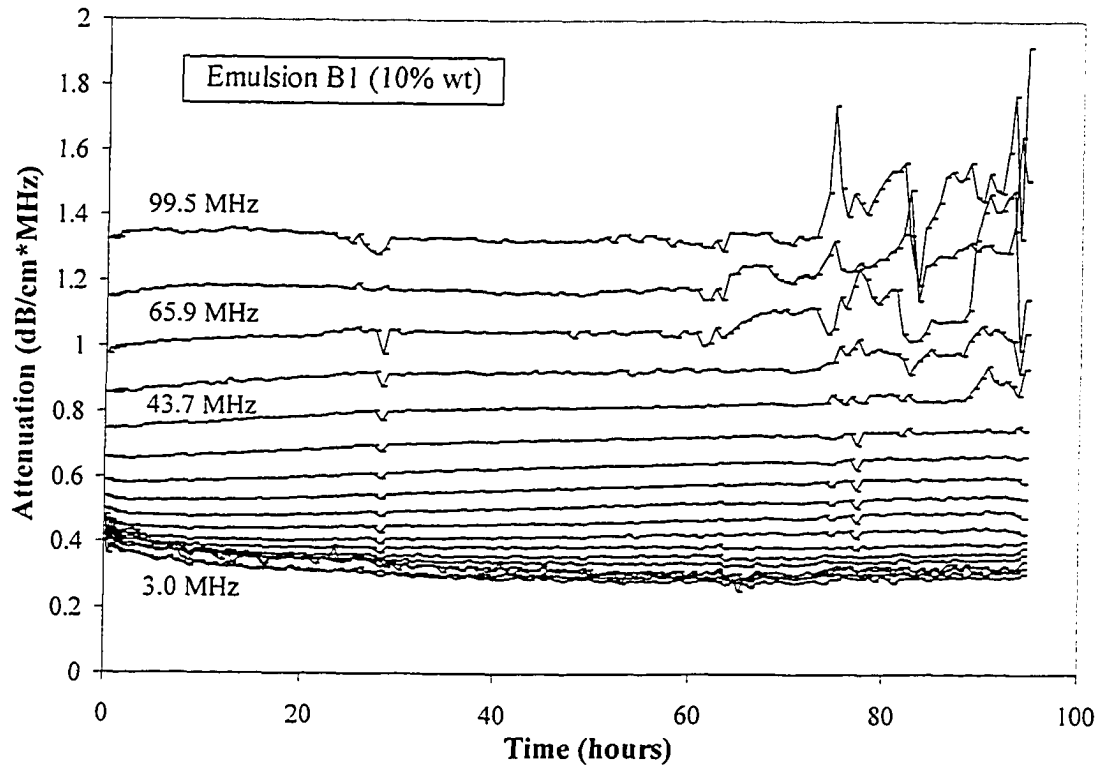


Figure 4.23: Emulsion B1 – 10% wt. water (acoustic attenuation spectrum in time).

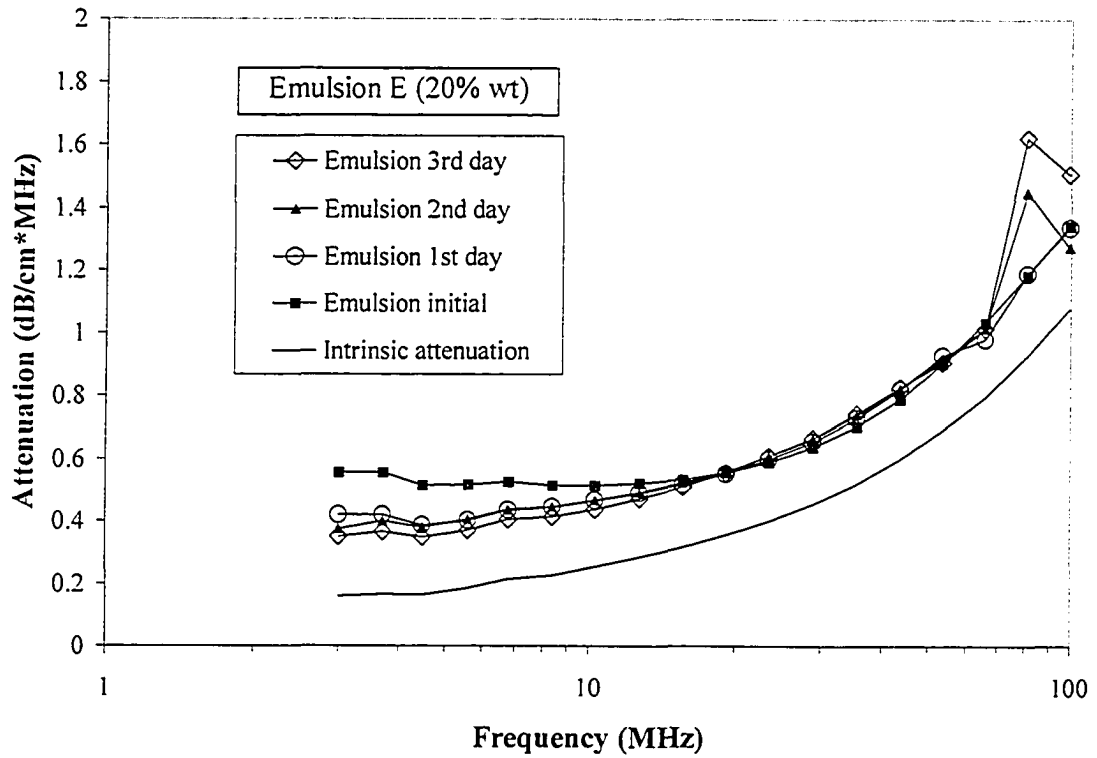
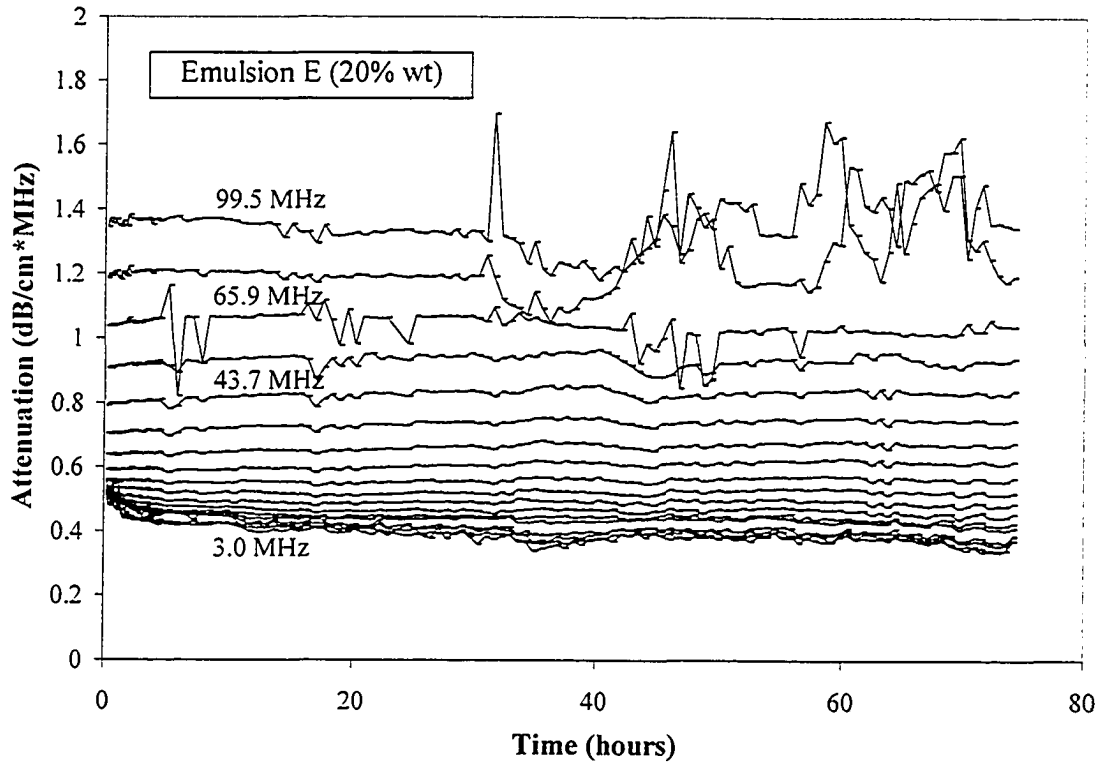


Figure 4.24: Emulsion E – 20% wt. water (acoustic attenuation spectrum in time).

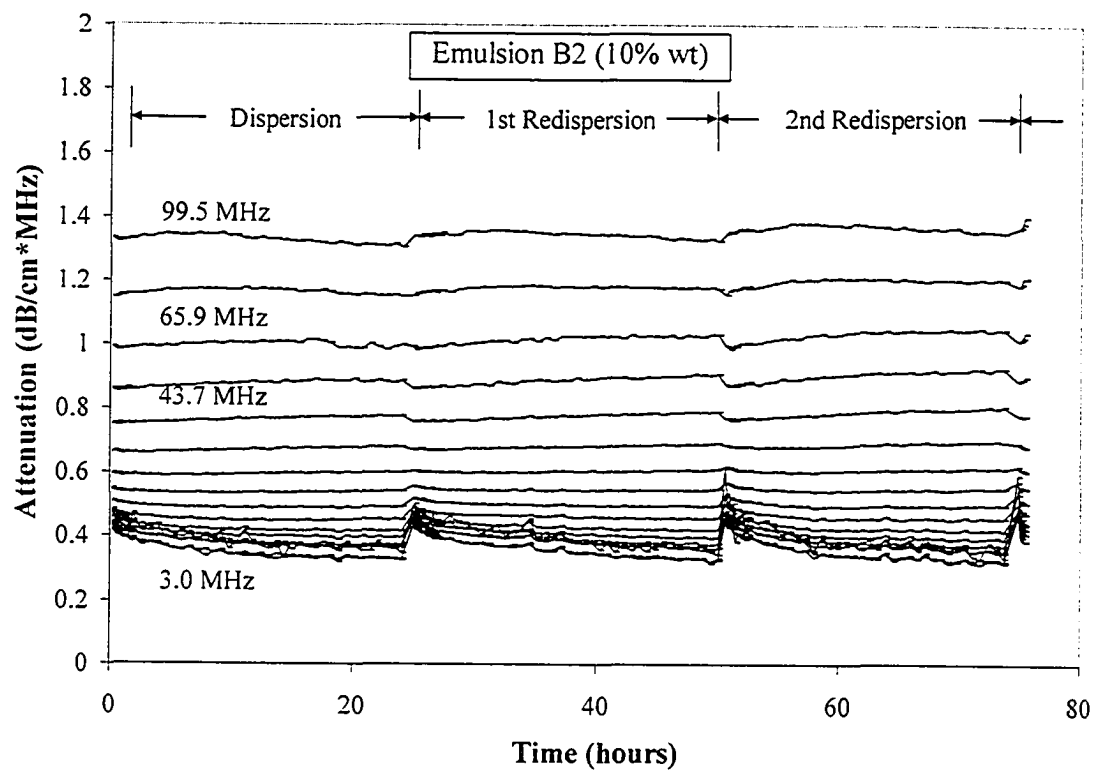


Figure 4.25: Emulsion B2 – 10% wt. water (acoustic attenuation spectrum in time).

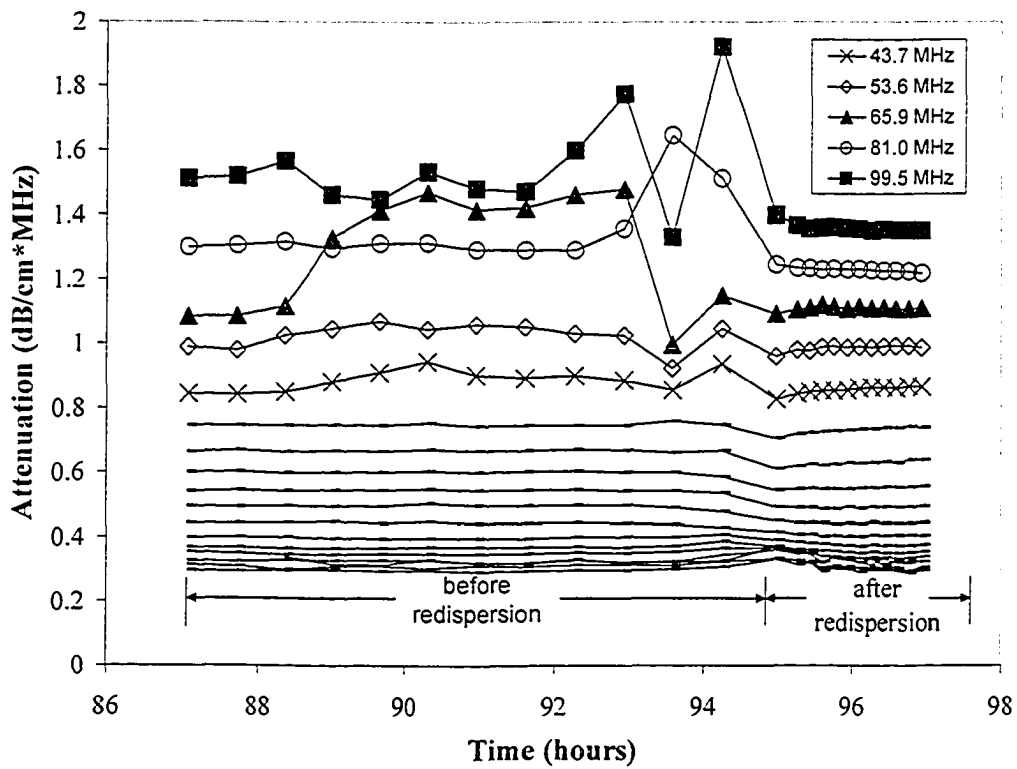


Figure 4.26: Emulsion B1 – 10% wt. water (effect of high speed homogenizer on the erratic behavior of acoustic spectrum at higher frequencies).

Chapter 5

Summary and Conclusions

In the present study, the latest developments in Acoustic and Electroacoustic Spectroscopy have been used to investigate the surface charge density of water droplets dispersed in diluted bitumen. The aim of the study is to contribute to the clarification of the role of electrostatic interactions in the stability of water-in-diluted bitumen emulsions, which is a subject of importance for the oil sands industry in Alberta. This is the first work in the field of Electroacoustics which investigates the electro-surface properties of water-in-diluted bitumen emulsions using the recent Shilov and coworkers Electroacoustic Theory, suitable for dispersions in low conductivity media.

Emulsions were prepared with Athabasca diluted bitumen from Suncor Energy Inc. Bitumen was further diluted with toluene prior to the emulsion preparation. The bitumen concentration in toluene was fixed at 50% wt., which is similar to the dilution practice in bitumen froth operations. Heavy water was used to maximize the density contrast between the continuous and dispersed phases, with the aim of increasing the magnitude of the electroacoustic signal and improve the chances for its detection during emulsion experiments. In this study, the water concentration was varied from 2% to 30% wt.

The standard procedure for the emulsion preparation consisted in the addition of known weights of diluted bitumen and water into the Spectrometer chamber, followed by water dispersion for 3 minutes by means of a high speed homogenizer. The emulsion was then kept under gentle stirring in the chamber to prevent water droplets sedimentation during measurements. Experiments were carried out at a constant temperature of 20.7 ± 0.2 °C.

Acoustic Spectroscopy provided the droplet size distribution based on measurements of sound attenuation in the emulsion sample. Electroacoustic Spectroscopy provided the surface charge density of droplets based on measurements of the colloid vibration current (CVC). The emulsion conductivity was also measured at 18 Hz with an

applied voltage of 5 V rms. The emulsion was monitored for several hours (up to four days) in order to best interpret the experimental data in view of the dynamic behavior of the emulsion.

The following conclusions can be drawn based on the experimental findings of the present study:

1. The CVC electroacoustic phenomenon is measurable for water-in-diluted bitumen emulsions, provided that the water concentration is sufficiently high (at least 10% wt.).
2. The CVC effect always exhibit time dependence behavior with a characteristic time of several hours. Experimentally, two relaxation behaviors were identified: a relaxation in the droplet size, and a super-imposed relaxation.
3. The relaxation in the droplet size revealed the dependence of the CVC effect on the kinetic factors that determines the state of water dispersion. The CVC magnitude decreases as the droplet size increases. This experimental observation is in agreement with electroacoustic theory, which predicts that inertia effects are important for the droplet size range measured for the emulsion.
4. The super-imposed relaxation cannot be explained in terms of the droplet size evolution in time. It reflects the dependence of the CVC effect on the surface charge density of the water droplets, and the nature and concentration of charge carriers in diluted bitumen.
5. The analysis of the CVC effect in terms of Shilov's electroacoustic theory for strongly overlapped double layers results in a decreasing surface charge density of droplets for freshly dispersed water in diluted bitumen.

Chapter 6

Recommendations

Future work is encouraged to elucidate the mechanism responsible for the decrease in the droplet surface charge density of freshly dispersed water-in-diluted bitumen emulsions. The present work has offered just one possible explanation based on the well known adsorption-desorption process of bituminous components at the water-oil interface. However, additional research is required to prove this hypothesis.

To elucidate the decrease in the surface charge density would require conducting research at a more fundamental level. Future work using the electroacoustic technique should focus on studying the role of asphaltenes and fine solids on the droplet surface charge density. They are recognized as the main stabilizers of water-in-diluted bitumen emulsions, based on the steric repulsion mechanism. Such research would shed more light on their role from the perspective of the electrical repulsion mechanism. Another factor that deserves attention for future work is the role of the organic solvent aromaticity on the droplet surface charge density.

This investigation would require the partial or total removal of asphaltenes or fine solids from diluted bitumen. The stability of the resulting emulsion would decrease significantly, and so the amount of water that remains dispersed in diluted bitumen. A potential problem is that the water concentration might be too low for measuring CVC. One alternative could be to follow an experimental procedure similar to the work of do Carmo Marques and coworkers, who studied the role of asphaltenes in oil-in-water emulsions stabilized with surfactants. The drawback of such a procedure is that surfactants extraneous to the bitumen system are introduced in the sample. Another alternative that is different to the use of surfactants would be to conduct the investigation using the original bitumen system but measuring CVP instead of CVC. The CVP signal is particularly strong in nonaqueous systems, as demonstrated by the work of Babchin and coworkers. However, this would require the measurement of the emulsion conductivity at

the same frequency of the electroacoustic effect. Unfortunately, this alternative based on CVP is not yet available in the DT-1200 Spectrometer.

Bibliography

- Babchin, A. J., Chow, R. S., and Sawatzky, R. P. (1989). "Electrokinetic measurements by electroacoustical methods", *Advances in Colloid and Interface Science*, **30**, 111-151.
- Babick, F., Hinze, F. and Ripperger, S. (2000). "Dependence of ultrasonic attenuation on the material properties", *Colloids and Surfaces A: Physicochemical and Engineering Aspects*, **172**, 33-46.
- Cannon, D. W. (1993). "Electroacoustics for Characterization of Particulates and Suspensions", *NIST Special Publication 856 - National Institute of Standards and Technology*. Edited by Malghan, S. B., Washington, DC. 40-66.
- CRC Handbook of Chemistry and Physics. (2003). David R. Lide (Editor). 83rd Edition.
- Chen, F., Finch, J. A., Xu, Z. and Czarnecki, J. (1999). "Wettability of fine solids extracted from bitumen froth", *Journal of Adhesion Science and Technology*, Vol. **13** (10), 1209-1224.
- Czarnecki, J. (2001). "Water-in-Oil Emulsions in Recovery of Hydrocarbons from Oil Sands". *Encyclopedic Handbook of Emulsion Technology*. Edited by Johan Sjöblom. New York: Marcel Dekker.
- Dabros, T., Yeung, A., Masliyah, J. and Czarnecki, J. (1999). "Emulsification through area contraction", *Journal of Colloid and Interface Science*, **210**, 222-224.

Dispersion Technology Inc. DT-1200 Operating and Maintenance Manual. October, 2003. 364 Adams Street, Bedford Hills, NY 10507.

do Carmo Marques, L. C., de Oliveira, J. F., and González, G. (1997). "Investigation on the role of asphaltenes as stabilizers for toluene-in-water miniemulsions using an electrosonic analysis (ESA) method", *Journal of Dispersion Science and Technology*, **18** (5), 477-488.

Dukhin, S. S. (1993). "Non-equilibrium electric surface phenomena", *Advances in Colloid and Interface Science*, **44**, 1-134.

Dukhin, A. S., Goetz, P. J. and Hamlet, C. W. (1996). "Acoustic spectroscopy for concentrated polydisperse colloids with low density contrast". *Langmuir*, **12**, 4998-5003.

Dukhin, A. S. and Goetz, P. J. (1999). "Characterization of Mixed Dispersions by means of Acoustic Spectroscopy", *Dispersion Technology Inc. Newsletter*, www.dispersion.com

Dukhin, A. S., Goetz, P. J., Wines, T. H., and Somasundaran, P. (2000). "Acoustic and electroacoustic spectroscopy", *Colloids and Surfaces A: Physicochemical and Engineering Aspects*, **173**, 127-158.

Dukhin, A. S., and Goetz, P. J. (2001). "New developments in acoustic and electroacoustic spectroscopy for characterizing concentrated dispersions", *Colloids and Surfaces A: Physicochemical and Engineering Aspects*, **192**, 267-306.

Dukhin, A. S., and Goetz, P. J. (2002). "Ultrasound for Characterizing Colloids: Particle Sizing, Zeta Potential, Rheology". Elsevier. USA.

Dukhin, A. S. and Goetz, P. J. (2004A). "Ionic properties of so-called "non-ionic" surfactants in non-polar liquids", *Dispersion Technology Inc. Newsletter*, www.dispersion.com

Dukhin, A. S. and Goetz, P. J. (2004B). "Evolution of water-in-oil emulsion controlled by droplet-bulk ion exchange. Acoustic, electroacoustic, conductivity and image analysis", *Dispersion Technology Inc. Newsletter*, www.dispersion.com

Fairhurst, D., Dukhin, A. S. and Klein, K. (2001). "A new way to characterize stability and performance of cosmetic emulsions and suspensions", *Dispersion Technology Inc. Newsletter*, www.dispersion.com

Goetz, R. J, and El-Aasser, M. S. (1992). "Effects of Dispersion Concentration on the Electroacoustic Potentials of o/w Miniemulsions", *Journal of Colloid and Interface Science*, Vol. **150** (2), 436-452.

Horvath-Szabo, G. (2004). Private communication.

Hunter, R. J. (1998). "Review: Recent developments in the electroacoustic characterization of colloidal suspensions and emulsions", *Colloids and Surfaces A: Physicochemical and Engineering Aspects*, **141**, 37-65.

- Hunter, R. J. (2001). "Electroacoustic Characterization of Emulsions". Encyclopedic Handbook of Emulsion Technology. Edited by Johan Sjöblom. New York: Marcel Dekker.
- Isaacs, E. E., Huang, H., Babchin, A. J. and Chow, R. S. (1990). "Electroacoustic Method for Monitoring the Coalescence of Water-in-Oil Emulsions", *Colloids and Surfaces*, **46**, 177-192.
- Isaacs, E. E. and Chow, R. S. (1992). "Practical Aspects of Emulsion Stability", *Advances in Chemistry Series*, Vol. **231**, 51-77.
- Long, Y., Dabros, T. and Hamza, H. (2002). "Stability and settling characteristics of solvent-diluted bitumen emulsions", *Fuel*, **81**, 1945-1952.
- Masliyah, J. (1994). "Electrokinetic Transport Phenomena". Alberta Oil Sands Technology and Research Authority (AOSTRA). Edmonton, Alberta, Canada.
- McLean, J. D. and Kilpatrick, P. K. (1997). "Effects of Asphaltene Solvency on Stability of Water-in-Crude-Oil Emulsions", *Journal of Colloid and Interface Science*, **189**, 242-253.
- McClements, D. J. (1991). "Ultrasonic characterization of emulsions and suspensions", *Advances in Colloid and Interface Science*, **37**, 33-72.
- Morrison, I. D. (1991). "Criterion for Electrostatic Stability of Dispersions at Low Ionic Strength", *Langmuir*, **7**, 1920-1922.

- Morrison, I. D. (1993). "Electrical charges in nonaqueous media", *Colloids and Surfaces A: Physicochemical and Engineering Aspects*, **71**, 1-37.
- Morrison, I. D. and Ross, R. (2002). "Colloidal Dispersions: Suspensions, Emulsions and Foams". USA: Wiley-Interscience.
- O'Brien, R. W. (1988). "Electro-acoustic effects in a dilute suspension of spherical particles", *Journal of Fluid Mechanics*, **190**, 71-86.
- O'Brien, R. W., Garside, P., and Hunter, R. J. (1994). "The Electroacoustic Reciprocal Relation", *Langmuir*, **10**, 931-935.
- O'Brien, R. W., Jones, A. and Rowlands, W. N. (2003). "A new formula for the dynamic mobility in a concentrated colloid", *Colloids and Surfaces A: Physicochemical and Engineering Aspects*, **218**, 89-101.
- van der Hoeven, P. H. C. and Lyklema, J. (1992). "Electrostatic Stabilization in Non-Aqueous Media", *Advances in Colloid and Interface Science*, **42**, 205-277.
- van der Minne, J. L. and Hermanie, P. H. J. (1952). "Electrophoresis measurements in benzene – Correlation with stability. (I. Development of method)", *Journal of Colloid Science*, **7**, 600-614.
- Scientifica. (2003). Operator's Manual Conductivity Meter Model 627. 160 Autumn Hill RD. Princeton, NJ 08540.

- Sheu, E. Y., De Tar, M. M. and Storm, D. A. (1992). "Interfacial properties of asphaltenes", *Fuel*, **71** (11), 1277-1281.
- Sheu, E. Y., Storm, D. A. and Shields, M. B. (1995). "Adsorption kinetics of asphaltenes at toluene/acid solution interface", *Fuel*, **74** (10), 1475-1479.
- Sheu, E. Y. (1996). "Physics of asphaltene micelles and microemulsions – theory and experiment", *Journal of Physics: Condensed Matter*, **8**, A125-A141.
- Wines, T. H., Dukhin, A. S. and Somasundaran, P. (1999). "Acoustic Spectroscopy for Characterizing Heptane/H₂O/AOT Reverse Microemulsions", *Journal of Colloids and Interface Science*, **216**, 303-308.
- Wu, X. (2003). "Investigating the Stability Mechanism of Water-in-Diluted Bitumen Emulsions through Isolation and Characterization of the Stabilizing Materials at the Interface", *Energy & Fuels*, **17**, 179-190.
- Yan, Z., Elliott, J. A. W. and Masliyah, J. (1999). "Roles of Various Bitumen Components in the Stability of Water-in-Diluted-Bitumen Emulsions", *Journal of Colloid and Interface Science*, **220**, 329-337.
- Yang, X. and Czarnecki, J. (2002). "The effect of naphtha to bitumen ratio on properties of water in diluted bitumen emulsions", *Colloids and Surfaces A: Physicochemical and Engineering Aspects*, **211**, 213-222.
- Zholkovskij, E., Masliyah, J. and Czarnecki, J. (2002). "An electrokinetic model of drop deformation in an electric field", *Journal of Fluid Mechanics*, **472**, 1-27.

Appendix 1

Calculation of the drag coefficient (Kuwabara cell model)

The Kuwabara cell model is used in Shilov's electroacoustic theory for the calculation of the drag coefficient (Ω), necessary for the modeling of inertia effects in Equation 2.20. The input information required for the calculation of the drag coefficient includes: volume fraction of the dispersed phase (φ), frequency of the electroacoustic phenomenon (ω), radius of particle or droplet (a), and the density (ρ_m) and dynamic viscosity (η_m) of the liquid medium. The following equations were taken from reference (Dukhin & Goetz, 2002).

$$b = \frac{a}{\sqrt[3]{\varphi}} \quad (\text{A1.1})$$

$$\tilde{a} = \sqrt{\frac{a^2 \omega \rho_m}{2\eta_m}} \quad (\text{A1.2})$$

$$\tilde{b} = \frac{b\tilde{a}}{a} \quad (\text{A1.3})$$

$$h_1(x) = \frac{\exp(-x)}{x} \left[\frac{x+1}{x} \sin x - \cos x + i \left(\frac{x+1}{x} \cos x + \sin x \right) \right] \quad (\text{A1.4})$$

$$h_2(x) = \frac{\exp(x)}{x} \left[\frac{x-1}{x} \sin x + \cos x + i \left(\frac{1-x}{x} \cos x + \sin x \right) \right] \quad (\text{A1.5})$$

$$I(x) = I_1(x) - I_2(x) \quad (\text{A1.6})$$

$$I_1(x) = -h_1(\tilde{b}) \exp(x(1+i)) \left\{ \frac{3(1-x)}{2(\tilde{b})^3} + i \left(\frac{x^2}{(\tilde{b})^3} - \frac{3x}{2(\tilde{b})^3} - \frac{1}{x} \right) \right\} \quad (\text{A1.7})$$

$$I_2(x) = h_2(\tilde{b}) \exp(-x(1+i)) \left\{ \frac{3(1+x)}{2(\tilde{b})^3} + i \left(\frac{x^2}{(\tilde{b})^3} + \frac{3x}{2(\tilde{b})^3} - \frac{1}{x} \right) \right\} \quad (\text{A1.8})$$

$$C_1 = \frac{h_2(\tilde{b})}{I(\tilde{b}) - I(\tilde{a})} \quad (\text{A1.9})$$

$$C_2 = -\frac{h_1(\tilde{b})}{I(\tilde{b}) - I(\tilde{a})} \quad (\text{A1.10})$$

$$\Omega = -\frac{(\tilde{a})^2}{3} \left[\frac{d(C_1 h_1(x) + C_2 h_2(x))}{dx} + \frac{C_1 h_1(x) + C_2 h_2(x)}{\tilde{a}} \right]_{x=\tilde{a}} - i \frac{4(\tilde{a})^2}{9} \quad (\text{A1.11})$$

Appendix 2

Measurement of diluted bitumen density and thermal expansion

Bitumen concentration (% wt)	Temperature (°C)	Meter reading for air	Meter reading for water	Meter reading for sample	Sample density (g/ml)
0	15	4.1804	5.5537	5.3979	0.8717
	20	4.1786	5.5505	5.3901	0.8671
	25	4.1770	5.5474	5.3826	0.8624
5	15	4.1804	5.5536	5.4040	0.8767
	20	4.1786	5.5505	5.3960	0.8719
	25	4.1770	5.5474	5.3883	0.8670
10	15	4.1804	5.5536	5.4102	0.8817
	20	4.1786	5.5505	5.4020	0.8767
	25	4.1770	5.5474	5.3943	0.8719
20	15	4.1804	5.5536	5.4229	0.8920
	20	4.1786	5.5505	5.4147	0.8870
	25	4.1770	5.5474	5.4071	0.8822
30	15	4.1804	5.5536	5.4359	0.9025
	20	4.1787	5.5506	5.4276	0.8973
	25	4.1769	5.5474	5.4193	0.8921
40	15	4.1805	5.5536	5.4490	0.9132
	20	4.1787	5.5506	5.4408	0.9081
	25	4.1769	5.5474	5.4326	0.9029
60	15	4.1805	5.5536	5.4767	0.9358
	20	4.1790	5.5508	5.4693	0.9311
	25	4.1772	5.5475	5.4616	0.9264
70	15	4.1805	5.5536	5.4911	0.9476
	20	4.1790	5.5508	5.4836	0.9428
	25	4.1772	5.5475	5.4769	0.9389

Calibration:
Density of air: 0.001225 g/ml (15 °C) ; 0.001204 g/ml (20 °C) ; 0.001184 g/ml (25 °C)
Density of water: 0.999099 g/ml (15 °C) ; 0.998204 g/ml (20 °C) ; 0.997045 g/ml (25 °C)

Table A2.1: Diluted bitumen density measurement data (vibrating tube method).

Bitumen concentration (% wt)	0	5	10	20	30	40	60	70
Thermal expansion ($\times 10^{-4} \text{ K}^{-1}$)	10.72	11.12	11.25	11.05	11.67	11.37	10.10	9.20

Table A2.2: Diluted bitumen thermal expansion calculation.

The equations used for the density calculation using the Anton Paar DMA 45 density meter are the following:

$$A = \frac{(T_{\text{WATER}})^2 - (T_{\text{AIR}})^2}{\rho_{\text{WATER}} - \rho_{\text{AIR}}} \quad (\text{A2.1})$$

$$B = (T_{\text{AIR}})^2 - \rho_{\text{AIR}} \cdot A \quad (\text{A2.2})$$

$$\rho_{\text{SAMPLE}} = \frac{(T_{\text{SAMPLE}})^2 - B}{A} \quad (\text{A2.3})$$

T_{WATER} and T_{AIR} are the meter readings for water and air, respectively, which are used for calculating constants **A** and **B**. The thermal expansion, on the other hand, is calculated from density data using Equation 3.2 (section 3.3.2).

Appendix 3

Measurement of diluted bitumen dynamic viscosity

Bitumen Concentration (% wt)	Drainage time (s)	Average drainage time (s)	Kinematic viscosity at 20 °C (cSt)	Density at 20 °C (g/ml)	Dynamic viscosity at 20 °C (mPa*s)
0.0	45.31	45.35	0.70	0.8671	0.60
	45.37				
	45.38				
2.5	49.45	49.49	0.76	0.8695	0.66
	49.50				
	49.51				
5.0	52.44	53.55	0.82	0.8719	0.72
	54.00				
	54.20				
7.5	56.44	56.19	0.86	0.8743	0.75
	56.08				
	56.06				
10.0	58.87	58.99	0.91	0.8768	0.79
	58.96				
	59.15				
15.0	71.31	71.23	1.09	0.8818	0.96
	71.32				
	71.06				
20.0	83.38	83.29	1.28	0.8869	1.13
	83.31				
	83.18				
30.0	129.49	129.42	1.99	0.8973	1.78
	129.79				
	128.99				
40.0	205.46	206.28	3.17	0.9082	2.88
	206.05				
	207.33				
50.0	346.62	347.10	5.33	0.9194	4.90
	347.56				
	347.13				
60.0	706.98	709.95	10.90	0.9309	10.15
	707.91				
	714.96				
70.0	1686.23	1684.18	25.87	0.9429	24.39
	1692.49				
	1673.83				

Fenske viscometer constant: 0.01536

Table A3.1: Diluted bitumen dynamic viscosity measurement data (Cannon-Fenske viscometer method).

Appendix 4

Water droplets sedimentation test data

Bitumen concentration (% wt)	Sampling position	Mass sample (g)	Mass water (μg)	Water concentration (% wt)	Average water concentration (% wt)	Settled water droplets (%)
2.5	1	0.0526	26.1	0.0496	0.0705	98.59
	2	0.0708	59.3	0.0838		
	3	0.0701	50.2	0.0716		
	4	0.0716	48.7	0.0680		
	5	0.0731	58.2	0.0796		
5.0	1	0.0738	35.9	0.0486	0.0528	98.94
	2	0.0728	36.5	0.0501		
	3	0.0729	38.5	0.0528		
	4	0.0703	36.1	0.0514		
	5	0.0730	44.5	0.0610		
7.5	1	0.0694	27.8	0.0401	0.0484	99.03
	2	0.0745	34.2	0.0459		
	3	0.0730	32.9	0.0451		
	4	0.0698	33.2	0.0476		
	5	0.0735	46.6	0.0634		
10.0	1	0.0705	28.1	0.0399	0.0478	99.04
	2	0.0744	36.8	0.0495		
	3	0.0730	32.0	0.0438		
	4	0.0742	42.7	0.0575		
	5	0.0719	34.8	0.0484		
15.0	1	0.0704	30.0	0.0426	0.0570	98.86
	2	0.0712	35.5	0.0499		
	3	0.0721	41.2	0.0571		
	4	0.0745	57.3	0.0769		
	5	0.0752	44.0	0.0585		
20.0	1	0.0757	55.7	0.0736	0.0788	98.42
	2	0.0740	51.3	0.0693		
	3	0.0727	56.1	0.0772		
	4	0.0758	67.3	0.0888		
	5	0.0751	63.8	0.0850		
30.0	1	0.0769	62.1	0.0808	0.1257	97.49
	2	0.0785	77.1	0.0982		
	3	0.0774	86.2	0.1114		
	4	0.0769	118.8	0.1545		
	5	0.0778	142.8	0.1835		
40.0	1	0.0752	135.2	0.1798	0.3730	92.54
	2	0.0798	184.8	0.2316		
	3	0.0768	194.3	0.2530		
	4	0.0791	438.2	0.5540		
	5	0.0807	522.0	0.6468		

Table A4.1: Water sedimentation test data of 5% wt. water-in-diluted bitumen emulsions (24 hours sedimentation at 20 °C).

Bitumen concentration (% wt)	Sampling position	Mass sample (g)	Mass water (μg)	Water concentration (% wt)	Average water concentration (% wt)	Settled water droplets (%)
50.0	1	0.0771	353.0	0.4578	1.5900	68.20
	2	0.0796	688.7	0.8652		
	3	0.0796	1101.0	1.3832		
	4	0.0813	1800.8	2.2150		
	5	0.0332	1005.5	3.0286		
60.0	1	0.0812	758.1	0.9336	3.3910	32.18
	2	0.0304	884.8	2.9105		
	3	0.0333	1255.4	3.7700		
	4	0.0313	1402.7	4.4815		
	5	0.0317	1540.4	4.8593		
70.0	1	0.0593	2344.1	3.9530	4.8168	3.66
	2	0.0283	1401.7	4.9530		
	3	0.0300	1519.3	5.0643		
	4	0.0294	1440.5	4.8997		
	5	0.0268	1397.3	5.2138		

Table A4.1: Water sedimentation test data of 5% wt. water-in-diluted bitumen emulsions (24 hours sedimentation at 20 °C).
(continuation)

Bitumen concentration (% wt)	Sampling position	Mass sample (g)	Mass water (μg)	Water concentration (% wt)	Average water concentration (% wt)	Settled water droplets (%)
2.5	1	0.0698	35.3	0.0506	0.0538	99.46
	2	0.0727	40.3	0.0554		
	3	0.0684	33.8	0.0494		
	4	0.0730	36.5	0.0500		
	5	0.0715	45.6	0.0638		
5.0	1	0.0709	29.3	0.0413	0.0455	99.54
	2	0.0736	38.3	0.0520		
	3	0.0707	29.2	0.0413		
	4	0.0726	34.1	0.0470		
	5	0.0729	33.5	0.0460		
7.5	1	0.0704	27.3	0.0388	0.0421	99.58
	2	0.0714	28.5	0.0399		
	3	0.0744	35.0	0.0470		
	4	0.0733	30.5	0.0416		
	5	0.0730	31.5	0.0432		
10.0	1	0.0705	28.0	0.0397	0.0470	99.53
	2	0.0737	33.5	0.0455		
	3	0.0743	37.9	0.0510		
	4	0.0710	32.3	0.0455		
	5	0.0745	39.8	0.0534		
15.0	1	0.0707	36.0	0.0509	0.0562	99.44
	2	0.0728	39.0	0.0536		
	3	0.0745	44.6	0.0599		
	4	0.0749	44.3	0.0591		
	5	0.0751	43.3	0.0577		
20.0	1	0.0739	37.7	0.0510	0.0618	99.38
	2	0.0747	40.3	0.0539		
	3	0.0756	53.2	0.0704		
	4	0.0752	45.7	0.0608		
	5	0.0751	54.8	0.0730		
30.0	1	0.0790	63.8	0.0808	0.1135	98.86
	2	0.0793	74.0	0.0933		
	3	0.0789	90.6	0.1148		
	4	0.0779	101.6	0.1304		
	5	0.0788	116.8	0.1482		
40.0	1	0.0749	131.8	0.1760	0.3925	96.07
	2	0.0789	276.3	0.3502		
	3	0.0808	268.7	0.3325		
	4	0.0774	289.3	0.3738		
	5	0.0801	584.9	0.7302		

Table A4.2: Water sedimentation test data of 10% wt. water-in-diluted bitumen emulsions (24 hours sedimentation at 20 °C).

Bitumen concentration (% wt)	Sampling position	Mass sample (g)	Mass water (μg)	Water concentration (% wt)	Average water concentration (% wt)	Settled water droplets (%)
50.0	1	0.0735	245.9	0.3346	3.0824	69.18
	2	0.0793	583.0	0.7352		
	3	0.0808	1956.8	2.4218		
	4	0.0345	1449.1	4.2003		
	5	0.0323	2493.7	7.7204		
60.0	1	0.0762	996.3	1.3075	6.9807	30.19
	2	0.0307	1908.0	6.2150		
	3	0.0328	2667.3	8.1320		
	4	0.0152	1421.8	9.3539		
	5	0.0126	1246.8	9.8952		
70.0	1	0.0615	4074.4	6.6250	8.7865	12.14
	2	0.0244	2202.0	9.0246		
	3	0.0279	2646.0	9.4839		
	4	0.0295	2716.9	9.2098		
	5	0.0325	3116.4	9.5889		

Table A4.2: Water sedimentation test data of 10% wt. water-in-diluted bitumen emulsions (24 hours sedimentation at 20 °C).
(continuation)

Appendix 5

Measurement of diluted bitumen acoustic properties

The intrinsic attenuation coefficient ($(\alpha_{int})_m$) and sound speed (c_m) were measured for each of the two stock diluted bitumen samples (section 3.5.2). 36 measurements were performed for each stock sample. 99% interval of confidence on the mean are calculated (Table A5.1). The experimental data for each stock sample is also presented (Tables A5.2 and A5.3). The attenuation coefficient is expressed in dB·cm·MHz units.

Property	Stock 1	Stock 2	Overall
c_m (m/s)	1377.8 ± 0.2	1378.2 ± 0.2	1378.0 ± 0.2
$(\alpha_{int})_m$ 3.0 MHz	0.195 ± 0.005	0.166 ± 0.005	0.181 ± 0.006
$(\alpha_{int})_m$ 3.7 MHz	0.214 ± 0.003	0.169 ± 0.003	0.192 ± 0.007
$(\alpha_{int})_m$ 4.5 MHz	0.188 ± 0.002	0.194 ± 0.001	0.191 ± 0.001
$(\alpha_{int})_m$ 5.6 MHz	0.214 ± 0.002	0.215 ± 0.002	0.215 ± 0.001
$(\alpha_{int})_m$ 6.8 MHz	0.254 ± 0.001	0.240 ± 0.001	0.247 ± 0.002
$(\alpha_{int})_m$ 8.4 MHz	0.264 ± 0.001	0.255 ± 0.001	0.260 ± 0.002
$(\alpha_{int})_m$ 10.3 MHz	0.296 ± 0.001	0.289 ± 0.001	0.293 ± 0.001
$(\alpha_{int})_m$ 12.7 MHz	0.328 ± 0.001	0.3256 ± 0.0005	0.327 ± 0.001
$(\alpha_{int})_m$ 15.6 MHz	0.365 ± 0.001	0.361 ± 0.001	0.363 ± 0.001
$(\alpha_{int})_m$ 19.2 MHz	0.409 ± 0.002	0.406 ± 0.001	0.408 ± 0.001
$(\alpha_{int})_m$ 23.5 MHz	0.458 ± 0.001	0.455 ± 0.001	0.456 ± 0.001
$(\alpha_{int})_m$ 28.9 MHz	0.520 ± 0.002	0.514 ± 0.001	0.517 ± 0.001
$(\alpha_{int})_m$ 35.5 MHz	0.595 ± 0.002	0.586 ± 0.001	0.590 ± 0.002
$(\alpha_{int})_m$ 43.7 MHz	0.684 ± 0.003	0.673 ± 0.001	0.678 ± 0.002
$(\alpha_{int})_m$ 53.6 MHz	0.786 ± 0.003	0.775 ± 0.002	0.781 ± 0.002
$(\alpha_{int})_m$ 65.9 MHz	0.900 ± 0.002	0.895 ± 0.002	0.898 ± 0.002
$(\alpha_{int})_m$ 81.0 MHz	1.052 ± 0.003	1.033 ± 0.004	1.043 ± 0.004
$(\alpha_{int})_m$ 99.5 MHz	1.217 ± 0.003	1.203 ± 0.001	1.210 ± 0.003

Table A5.1: Acoustic properties of diluted bitumen (99% interval of confidence on the mean)

#	T (°C)	c_m (m/s)	$(\alpha_{int})_m$ 3.0 MHz	$(\alpha_{int})_m$ 3.7 MHz	$(\alpha_{int})_m$ 4.5 MHz	$(\alpha_{int})_m$ 5.6 MHz	$(\alpha_{int})_m$ 6.8 MHz	$(\alpha_{int})_m$ 8.4 MHz	$(\alpha_{int})_m$ 10.3 MHz	$(\alpha_{int})_m$ 12.7 MHz
1	20.8	1378.127	0.19405	0.21526	0.18456	0.21321	0.25409	0.26441	0.29679	0.32878
2	20.8	1378.795	0.18919	0.21295	0.18682	0.21132	0.25656	0.26608	0.29816	0.32983
3	20.8	1378.491	0.19057	0.21498	0.18483	0.21119	0.25621	0.26554	0.29753	0.32862
4	20.8	1377.678	0.18967	0.20264	0.19136	0.21194	0.25407	0.26559	0.29981	0.33052
5	20.8	1378.575	0.19577	0.21551	0.18660	0.21027	0.25766	0.26524	0.29786	0.33059
6	20.8	1378.078	0.19869	0.21033	0.18938	0.21751	0.25581	0.26571	0.29459	0.33045
7	20.8	1378.101	0.16784	0.21157	0.18294	0.20884	0.25216	0.26577	0.29313	0.32836
8	20.8	1377.757	0.19768	0.21948	0.18717	0.21488	0.25420	0.26326	0.29896	0.32927
9	20.8	1377.387	0.17138	0.20446	0.17976	0.20958	0.25162	0.26219	0.29767	0.32764
10	20.8	1377.975	0.19096	0.21628	0.18813	0.21395	0.25589	0.26464	0.29565	0.32990
11	20.8	1377.898	0.20101	0.21180	0.18813	0.22025	0.26071	0.26808	0.30220	0.33339
12	20.8	1378.387	0.18623	0.21306	0.18893	0.21107	0.25213	0.26131	0.29730	0.32944

#	$(\alpha_{int})_m$ 15.6 MHz	$(\alpha_{int})_m$ 19.2 MHz	$(\alpha_{int})_m$ 23.5 MHz	$(\alpha_{int})_m$ 28.9 MHz	$(\alpha_{int})_m$ 35.5 MHz	$(\alpha_{int})_m$ 43.7 MHz	$(\alpha_{int})_m$ 53.6 MHz	$(\alpha_{int})_m$ 65.9 MHz	$(\alpha_{int})_m$ 81.0 MHz	$(\alpha_{int})_m$ 99.5 MHz
1	0.36956	0.41326	0.46216	0.52471	0.60117	0.69146	0.79440	0.90331	1.06168	1.22481
2	0.36926	0.41266	0.46223	0.52528	0.60150	0.69266	0.79205	0.90817	1.06032	1.22721
3	0.36901	0.41413	0.46093	0.52396	0.60126	0.69195	0.79216	0.90419	1.06136	1.22210
4	0.36756	0.41298	0.46117	0.52484	0.60140	0.69287	0.79192	0.90431	1.05969	1.22744
5	0.36938	0.41360	0.46014	0.52422	0.60112	0.69187	0.79286	0.90069	1.06137	1.22552
6	0.36743	0.41174	0.46320	0.52404	0.60041	0.68903	0.79256	0.90653	1.06010	1.22398
7	0.36612	0.41254	0.46066	0.52364	0.59954	0.68963	0.79424	0.90020	1.05860	1.22638
8	0.36700	0.41119	0.45951	0.52369	0.59913	0.68882	0.79153	0.90407	1.05901	1.22007
9	0.36493	0.40859	0.45902	0.52358	0.59776	0.68835	0.79148	0.90180	1.05570	1.22129
10	0.36728	0.41330	0.46107	0.52550	0.59914	0.68889	0.79108	0.90499	1.05538	1.22295
11	0.36929	0.41160	0.45988	0.52258	0.59848	0.69001	0.79250	0.89795	1.05516	1.22658
12	0.36638	0.41269	0.45856	0.52264	0.59917	0.68824	0.79230	0.90313	1.05204	1.22184

Table A5.2: Acoustic properties data for diluted bitumen stock #1.

#	T (°C)	c_m (m/s)	$(\alpha_{int})_m$ 3.0 MHz	$(\alpha_{int})_m$ 3.7 MHz	$(\alpha_{int})_m$ 4.5 MHz	$(\alpha_{int})_m$ 5.6 MHz	$(\alpha_{int})_m$ 6.8 MHz	$(\alpha_{int})_m$ 8.4 MHz	$(\alpha_{int})_m$ 10.3 MHz	$(\alpha_{int})_m$ 12.7 MHz
13	20.8	1377.582	0.19488	0.21040	0.19062	0.21237	0.25456	0.26342	0.29789	0.32876
14	20.8	1378.104	0.19062	0.21394	0.19133	0.21668	0.25719	0.26687	0.29978	0.33021
15	20.8	1377.406	0.20111	0.21326	0.18895	0.21506	0.25394	0.26452	0.29630	0.33163
16	20.8	1378.159	0.22047	0.21539	0.18938	0.21376	0.25546	0.26555	0.29679	0.32882
17	20.8	1378.014	0.17973	0.21055	0.18613	0.21362	0.25557	0.26038	0.29690	0.32990
18	20.8	1377.795	0.19285	0.21241	0.19091	0.21474	0.25646	0.26590	0.29793	0.33126
19	20.8	1378.073	0.18713	0.21416	0.18708	0.21257	0.25476	0.26569	0.29642	0.32941
20	20.8	1377.583	0.18464	0.21375	0.18841	0.21166	0.25650	0.26223	0.29559	0.32512
21	20.8	1377.640	0.19465	0.21595	0.18805	0.21573	0.25675	0.26274	0.29670	0.32891
22	20.8	1376.119	0.18861	0.22142	0.19448	0.22208	0.25106	0.26908	0.30134	0.32981
23	20.8	1377.739	0.21628	0.22600	0.19700	0.21979	0.25546	0.26816	0.30036	0.33090
24	20.8	1377.965	0.19856	0.23021	0.19631	0.22026	0.25911	0.26704	0.29642	0.32907

#	$(\alpha_{int})_m$ 15.6 MHz	$(\alpha_{int})_m$ 19.2 MHz	$(\alpha_{int})_m$ 23.5 MHz	$(\alpha_{int})_m$ 28.9 MHz	$(\alpha_{int})_m$ 35.5 MHz	$(\alpha_{int})_m$ 43.7 MHz	$(\alpha_{int})_m$ 53.6 MHz	$(\alpha_{int})_m$ 65.9 MHz	$(\alpha_{int})_m$ 81.0 MHz	$(\alpha_{int})_m$ 99.5 MHz
13	0.36659	0.41051	0.46175	0.52340	0.59706	0.68778	0.79296	0.89871	1.05335	1.21760
14	0.36698	0.41244	0.46035	0.52280	0.59576	0.68756	0.79095	0.89639	1.05221	1.22210
15	0.36611	0.41088	0.45906	0.52272	0.59769	0.68474	0.78748	0.89961	1.05021	1.22079
16	0.36610	0.41163	0.45881	0.52310	0.59631	0.68592	0.79039	0.90157	1.05351	1.21569
17	0.36590	0.41085	0.45877	0.52051	0.59666	0.68465	0.78852	0.89570	1.04167	1.21250
18	0.36587	0.41023	0.45721	0.51943	0.59575	0.68589	0.78602	0.90030	1.05200	1.21909
19	0.36708	0.40972	0.45740	0.52084	0.59500	0.68768	0.78560	0.90259	1.05253	1.21274
20	0.36286	0.40719	0.45641	0.51981	0.59122	0.68062	0.78175	0.91045	1.04764	1.21478
21	0.36564	0.40636	0.45574	0.51799	0.59120	0.68135	0.78061	0.90394	1.05138	1.22010
22	0.36460	0.40659	0.45786	0.51838	0.59298	0.68282	0.78634	0.90829	1.04953	1.21843
23	0.36536	0.40805	0.45584	0.51872	0.59130	0.68098	0.78184	0.91411	1.04643	1.21973
24	0.36538	0.40774	0.45607	0.51937	0.59095	0.67766	0.78357	0.90101	1.04073	1.22132

Table A5.2: Acoustic properties data for diluted bitumen stock #1 (continuation).

#	T (°C)	c_m (m/s)	$(\alpha_{int})_m$ 3.0 MHz	$(\alpha_{int})_m$ 3.7 MHz	$(\alpha_{int})_m$ 4.5 MHz	$(\alpha_{int})_m$ 5.6 MHz	$(\alpha_{int})_m$ 6.8 MHz	$(\alpha_{int})_m$ 8.4 MHz	$(\alpha_{int})_m$ 10.3 MHz	$(\alpha_{int})_m$ 12.7 MHz
25	20.8	1377.763	0.20784	0.21616	0.18750	0.21053	0.25574	0.26435	0.29719	0.32900
26	20.7	1378.118	0.19771	0.20101	0.18480	0.21466	0.25419	0.26273	0.29365	0.32476
27	20.7	1376.890	0.19639	0.20391	0.18452	0.20785	0.24970	0.26145	0.29238	0.32572
28	20.7	1377.617	0.20201	0.20409	0.18315	0.21071	0.25519	0.26298	0.28812	0.32481
29	20.7	1378.197	0.20895	0.22768	0.19140	0.21159	0.25067	0.26033	0.29667	0.32591
30	20.7	1377.058	0.20200	0.22260	0.19470	0.21653	0.25314	0.26530	0.29519	0.32738
31	20.6	1377.450	0.21388	0.21879	0.19212	0.21446	0.25367	0.26577	0.29542	0.32785
32	20.6	1377.570	0.18046	0.21139	0.18714	0.21261	0.25257	0.25998	0.29358	0.32676
33	20.6	1376.934	0.20098	0.21769	0.18549	0.21735	0.25299	0.26303	0.29439	0.32462
34	20.6	1377.239	0.19390	0.20986	0.18621	0.21024	0.24989	0.25860	0.29049	0.32376
35	20.6	1377.479	0.20264	0.21087	0.18634	0.20947	0.25225	0.26038	0.29306	0.32544
36	20.7	1377.706	0.19580	0.21631	0.18076	0.21247	0.24983	0.26192	0.29259	0.32347

#	$(\alpha_{int})_m$ 15.6 MHz	$(\alpha_{int})_m$ 19.2 MHz	$(\alpha_{int})_m$ 23.5 MHz	$(\alpha_{int})_m$ 28.9 MHz	$(\alpha_{int})_m$ 35.5 MHz	$(\alpha_{int})_m$ 43.7 MHz	$(\alpha_{int})_m$ 53.6 MHz	$(\alpha_{int})_m$ 65.9 MHz	$(\alpha_{int})_m$ 81.0 MHz	$(\alpha_{int})_m$ 99.5 MHz
25	0.36387	0.40686	0.45620	0.51772	0.59074	0.67794	0.77763	0.89118	1.04436	1.21586
26	0.36145	0.40649	0.45360	0.51713	0.59130	0.67946	0.78462	0.88854	1.03130	1.21937
27	0.36384	0.40456	0.45476	0.51622	0.59388	0.68038	0.78058	0.89318	1.03857	1.21272
28	0.36255	0.40567	0.45361	0.51602	0.59136	0.67993	0.78129	0.89544	1.05979	1.20594
29	0.36141	0.40506	0.45296	0.51744	0.59183	0.67881	0.77987	0.89617	1.05124	1.20662
30	0.36232	0.40560	0.45379	0.51734	0.58861	0.67924	0.78099	0.89492	1.06068	1.20575
31	0.36258	0.40531	0.45687	0.51831	0.59405	0.67968	0.78275	0.89734	1.06138	1.20408
32	0.36028	0.40696	0.45385	0.51606	0.58867	0.67801	0.77876	0.89350	1.04722	1.21046
33	0.36283	0.40489	0.45735	0.51988	0.59110	0.67605	0.78036	0.89621	1.05889	1.20476
34	0.36097	0.40539	0.45279	0.51541	0.58972	0.67764	0.77804	0.90127	1.04928	1.21204
35	0.35733	0.40344	0.45369	0.51497	0.58814	0.67454	0.77652	0.89619	1.04599	1.21190
36	0.35907	0.40143	0.45225	0.51329	0.58712	0.67266	0.77789	0.90035	1.03969	1.21343

Table A5.2: Acoustic properties data for diluted bitumen stock #1 (continuation).

#	T (°C)	c_m (m/s)	$(\alpha_{int})_m$ 3.0 MHz	$(\alpha_{int})_m$ 3.7 MHz	$(\alpha_{int})_m$ 4.5 MHz	$(\alpha_{int})_m$ 5.6 MHz	$(\alpha_{int})_m$ 6.8 MHz	$(\alpha_{int})_m$ 8.4 MHz	$(\alpha_{int})_m$ 10.3 MHz	$(\alpha_{int})_m$ 12.7 MHz
1	20.8	1378.321	0.18195	0.16582	0.19502	0.21266	0.23732	0.25685	0.28875	0.32699
2	20.8	1379.101	0.16624	0.17019	0.19628	0.21336	0.24356	0.25699	0.28651	0.32645
3	20.7	1377.977	0.17080	0.16850	0.19066	0.21055	0.23821	0.25403	0.28906	0.32373
4	20.8	1378.651	0.17126	0.16862	0.19551	0.21217	0.24286	0.25379	0.29012	0.32642
5	20.7	1378.55	0.17162	0.17028	0.19390	0.21136	0.23750	0.24885	0.29067	0.32485
6	20.7	1378.619	0.15111	0.16990	0.19318	0.21369	0.24170	0.25517	0.29042	0.32650
7	20.7	1379.264	0.17257	0.15446	0.19146	0.21087	0.23673	0.25369	0.28842	0.32579
8	20.7	1378.62	0.17191	0.17328	0.19537	0.21252	0.23853	0.25611	0.28937	0.32573
9	20.7	1377.385	0.17970	0.17013	0.19345	0.21304	0.23941	0.25238	0.28887	0.32595
10	20.8	1377.978	0.17435	0.17534	0.19339	0.21332	0.23679	0.25316	0.28373	0.32537
11	20.8	1378.523	0.17371	0.16294	0.18819	0.21160	0.24192	0.25302	0.28610	0.32528
12	20.8	1377.946	0.15283	0.16692	0.18994	0.21074	0.23717	0.25299	0.28798	0.32454

#	$(\alpha_{int})_m$ 15.6 MHz	$(\alpha_{int})_m$ 19.2 MHz	$(\alpha_{int})_m$ 23.5 MHz	$(\alpha_{int})_m$ 28.9 MHz	$(\alpha_{int})_m$ 35.5 MHz	$(\alpha_{int})_m$ 43.7 MHz	$(\alpha_{int})_m$ 53.6 MHz	$(\alpha_{int})_m$ 65.9 MHz	$(\alpha_{int})_m$ 81.0 MHz	$(\alpha_{int})_m$ 99.5 MHz
1	0.36204	0.40486	0.45663	0.51882	0.58928	0.67777	0.78186	0.89087	1.04708	1.20790
2	0.36191	0.40990	0.45501	0.51695	0.58908	0.67734	0.77789	0.89302	1.04040	1.20568
3	0.36175	0.40910	0.45598	0.51846	0.58820	0.67582	0.77898	0.89865	1.04647	1.20674
4	0.36151	0.40877	0.45535	0.51849	0.58846	0.67434	0.77784	0.89780	1.04652	1.20649
5	0.36138	0.40916	0.45474	0.51615	0.58839	0.67480	0.77924	0.88950	1.05135	1.20509
6	0.36084	0.40699	0.45532	0.51667	0.58661	0.67327	0.77971	0.89574	1.05321	1.20577
7	0.36141	0.40942	0.45405	0.51816	0.58884	0.67482	0.77672	0.89206	1.04293	1.20493
8	0.36132	0.40675	0.45429	0.51600	0.58821	0.67532	0.77855	0.89024	1.04188	1.20183
9	0.36058	0.40693	0.45462	0.51558	0.58870	0.67560	0.77774	0.90013	1.04260	1.20333
10	0.36079	0.40504	0.45512	0.51542	0.58597	0.67174	0.77977	0.88943	1.04911	1.20214
11	0.36241	0.40608	0.45345	0.51457	0.58770	0.67282	0.77498	0.88766	1.04368	1.20667
12	0.36025	0.40878	0.45413	0.51708	0.58660	0.67417	0.77900	0.89647	1.03818	1.20193

Table A5.3: Acoustic properties data for diluted bitumen stock #2.

#	T (°C)	c_m (m/s)	$(\alpha_{int})_m$ 3.0 MHz	$(\alpha_{int})_m$ 3.7 MHz	$(\alpha_{int})_m$ 4.5 MHz	$(\alpha_{int})_m$ 5.6 MHz	$(\alpha_{int})_m$ 6.8 MHz	$(\alpha_{int})_m$ 8.4 MHz	$(\alpha_{int})_m$ 10.3 MHz	$(\alpha_{int})_m$ 12.7 MHz
13	20.8	1378.346	0.16274	0.16723	0.19591	0.21582	0.24144	0.25822	0.29006	0.32499
14	20.7	1378.445	0.16107	0.17639	0.19210	0.21229	0.23934	0.25093	0.29035	0.32528
15	20.7	1378.959	0.16066	0.17372	0.19468	0.21488	0.23787	0.25150	0.28982	0.32526
16	20.7	1378.966	0.15834	0.16335	0.19124	0.21191	0.24202	0.25497	0.28620	0.32583
17	20.7	1378.253	0.16576	0.16401	0.19417	0.21473	0.23901	0.25368	0.28909	0.32420
18	20.7	1377.985	0.15008	0.17312	0.19775	0.21535	0.24179	0.25438	0.28875	0.32528
19	20.7	1377.792	0.17089	0.16756	0.19181	0.21382	0.23821	0.25596	0.28947	0.32850
20	20.8	1378.296	0.15549	0.16754	0.19270	0.21468	0.23756	0.25494	0.28599	0.32667
21	20.7	1378.199	0.15259	0.16428	0.18869	0.21398	0.23543	0.25322	0.28788	0.32538
22	20.8	1378.007	0.16684	0.16237	0.19516	0.21558	0.23774	0.25798	0.28915	0.32465
23	20.8	1378.018	0.15257	0.16411	0.19216	0.21409	0.23647	0.25608	0.28771	0.32673
24	20.8	1378.000	0.16181	0.16890	0.19381	0.21708	0.23857	0.25537	0.28885	0.32543

#	$(\alpha_{int})_m$ 15.6 MHz	$(\alpha_{int})_m$ 19.2 MHz	$(\alpha_{int})_m$ 23.5 MHz	$(\alpha_{int})_m$ 28.9 MHz	$(\alpha_{int})_m$ 35.5 MHz	$(\alpha_{int})_m$ 43.7 MHz	$(\alpha_{int})_m$ 53.6 MHz	$(\alpha_{int})_m$ 65.9 MHz	$(\alpha_{int})_m$ 81.0 MHz	$(\alpha_{int})_m$ 99.5 MHz
13	0.36023	0.40556	0.45378	0.51499	0.58553	0.67298	0.77470	0.89688	1.02941	1.20142
14	0.36049	0.40781	0.45375	0.51620	0.58648	0.67366	0.77560	0.89253	1.03112	1.20652
15	0.36026	0.40617	0.45523	0.51559	0.58461	0.67309	0.77946	0.89770	1.02483	1.20658
16	0.36057	0.40753	0.45315	0.51438	0.58792	0.67308	0.77309	0.89733	1.03231	1.20077
17	0.36114	0.40811	0.45657	0.51563	0.58597	0.67168	0.77439	0.89656	1.02648	1.20349
18	0.36214	0.40445	0.45710	0.51602	0.58550	0.67352	0.77396	0.89799	1.02549	1.20369
19	0.36012	0.40474	0.45734	0.51439	0.58431	0.67044	0.77914	0.88518	1.02678	1.20349
20	0.36287	0.40606	0.45678	0.51547	0.58474	0.67153	0.77424	0.90135	1.02243	1.20382
21	0.36217	0.40455	0.45589	0.51460	0.58673	0.67309	0.77616	0.88988	1.02816	1.20397
22	0.36071	0.40500	0.45405	0.51353	0.58692	0.67261	0.77536	0.89955	1.02543	1.21053
23	0.35999	0.40552	0.45550	0.51300	0.58330	0.67044	0.77690	0.89316	1.02534	1.20267
24	0.35968	0.40631	0.45462	0.51198	0.58729	0.67196	0.77537	0.89324	1.02892	1.20228

Table A5.3: Acoustic properties data for diluted bitumen stock #2 (continuation).

#	T (°C)	c_m (m/s)	$(\alpha_{int})_m$ 3.0 MHz	$(\alpha_{int})_m$ 3.7 MHz	$(\alpha_{int})_m$ 4.5 MHz	$(\alpha_{int})_m$ 5.6 MHz	$(\alpha_{int})_m$ 6.8 MHz	$(\alpha_{int})_m$ 8.4 MHz	$(\alpha_{int})_m$ 10.3 MHz	$(\alpha_{int})_m$ 12.7 MHz
25	20.8	1378.054	0.16729	0.17297	0.19600	0.21919	0.23877	0.25520	0.29160	0.32472
26	20.8	1377.645	0.15958	0.17074	0.19615	0.22161	0.23964	0.25646	0.29227	0.32510
27	20.8	1377.812	0.15144	0.17574	0.19828	0.21878	0.24044	0.25634	0.28984	0.32402
28	20.8	1377.583	0.19431	0.17202	0.19517	0.21851	0.23846	0.25395	0.28804	0.32404
29	20.7	1378.386	0.18029	0.18321	0.19034	0.22285	0.24523	0.25829	0.29134	0.32638
30	20.7	1377.31	0.16273	0.17030	0.19718	0.22052	0.23881	0.25504	0.28876	0.32586
31	20.7	1377.89	0.17643	0.17553	0.19756	0.22300	0.24095	0.25733	0.28915	0.32505
32	20.7	1377.431	0.17323	0.16424	0.19194	0.21979	0.23744	0.25414	0.28878	0.32470
33	20.7	1377.98	0.17333	0.17212	0.19872	0.21463	0.23899	0.25545	0.28885	0.32544
34	20.7	1377.857	0.15796	0.15573	0.19215	0.21781	0.24151	0.25435	0.28905	0.32562
35	20.7	1377.907	0.16679	0.16553	0.19943	0.21618	0.24490	0.25729	0.28991	0.32509
36	20.7	1378.808	0.16405	0.17950	0.19845	0.22058	0.24135	0.26182	0.29138	0.32839

#	$(\alpha_{int})_m$ 15.6 MHz	$(\alpha_{int})_m$ 19.2 MHz	$(\alpha_{int})_m$ 23.5 MHz	$(\alpha_{int})_m$ 28.9 MHz	$(\alpha_{int})_m$ 35.5 MHz	$(\alpha_{int})_m$ 43.7 MHz	$(\alpha_{int})_m$ 53.6 MHz	$(\alpha_{int})_m$ 65.9 MHz	$(\alpha_{int})_m$ 81.0 MHz	$(\alpha_{int})_m$ 99.5 MHz
25	0.36016	0.40506	0.45546	0.51305	0.58807	0.67426	0.77387	0.89865	1.02575	1.20176
26	0.36052	0.40640	0.45567	0.51072	0.58533	0.67124	0.77606	0.90108	1.03060	1.20202
27	0.35962	0.40543	0.45655	0.51105	0.58462	0.67278	0.77345	0.89747	1.03100	1.19994
28	0.35948	0.40573	0.45493	0.51010	0.58344	0.67146	0.77403	0.89923	1.03522	1.19682
29	0.36105	0.40619	0.45585	0.51143	0.58532	0.67202	0.77370	0.90076	1.03178	1.19985
30	0.36094	0.40598	0.45454	0.51147	0.58303	0.67112	0.76975	0.89803	1.02817	1.20071
31	0.35823	0.40404	0.45432	0.51081	0.58333	0.67027	0.77399	0.89381	1.02311	1.20307
32	0.35937	0.40376	0.45448	0.51105	0.58413	0.66901	0.76894	0.89459	1.02512	1.20361
33	0.35958	0.40450	0.45391	0.51086	0.58327	0.67020	0.76967	0.89115	1.02787	1.20285
34	0.36085	0.40459	0.45329	0.51085	0.58355	0.66900	0.77349	0.89235	1.02404	1.20214
35	0.35951	0.40396	0.45178	0.51040	0.58033	0.66829	0.77003	0.88869	1.01972	1.20087
36	0.35709	0.40475	0.45346	0.51262	0.57913	0.66645	0.76616	0.89276	1.02363	1.19221

Table A5.3: Acoustic properties data for diluted bitumen stock #2 (continuation).

Appendix 6

Measurement of diluted bitumen electroacoustic properties

The diluted bitumen CVC signal magnitude and phase (CVC_{measured}) was measured for each of the two stock diluted bitumen samples (section 3.5.2). 36 measurements were performed for each stock sample. 99% interval of confidence on the mean are calculated (Table A6.1). The experimental data for each stock sample is also presented (Tables A6.2 and A6.3).

The diluted bitumen subtracted CVC signal (CVC) is also calculated. The magnitude of CVC is very important because it establishes the noise level of the CVC signal for any emulsion experiment. CVC is obtained from Equation 3.13, where $CVC_{\text{background}}$ is taken as the averaged CVC_{measured} of diluted bitumen.

Property	Stock 1	Stock 2	Overall
CVC_{measured} (magnitude)	$(168 \pm 3) \cdot 10^2$	$(160 \pm 4) \cdot 10^2$	$(164 \pm 3) \cdot 10^2$
CVC_{measured} (phase)	141 ± 5	143 ± 6	142 ± 4
CVC (magnitude)	$(35 \pm 2) \cdot 10^2$	$(38 \pm 2) \cdot 10^2$	$(36 \pm 2) \cdot 10^2$

Table A6.1: Electroacoustic properties of diluted bitumen (99% interval of confidence on the mean)

#	CVC _{measured} (magnitude)	CVC _{measured} (phase)	CVC (magnitude)
1	17204	129.9	4092
2	18278	130.9	4155
3	17005	132.4	3322
4	16369	154.2	3087
5	16768	134.1	2799
6	16242	153.4	2872
7	16578	133.4	2997
8	15327	156.1	3796
9	16627	131.6	3519
10	17077	129.6	4156
11	16767	133.6	2945
12	16793	130.5	3852
13	16676	129.4	4161
14	16329	130.6	3803
15	16441	156.3	3686
16	17325	132.6	3326
17	17056	131.4	3624
18	16573	157	3891
19	16892	132.6	3249
20	17042	154.7	3267
21	16097	154.2	3115
22	17365	153.1	2865
23	17629	130.7	3967
24	16909	130.3	3924
25	18085	130.3	4245
26	16748	153.8	2971
27	16178	154.4	3160
28	16709	152.8	2678
29	16062	153.9	3037
30	17382	129.2	4338
31	16187	152.4	2600
32	17079	130.2	3980
33	16913	128.6	4421
34	15910	153.2	2877
35	17454	130.2	4063
36	15591	154.1	3202

Table A6.2: Electroacoustic properties data for diluted bitumen stock #1.

#	CVC _{measured} (magnitude)	CVC _{measured} (phase)	CVC (magnitude)
1	14961	159.6	4697
2	15942	155.6	3612
3	17159	128.9	4122
4	17544	129.9	4013
5	16137	154	3188
6	16155	130	3545
7	16052	157.3	4096
8	16016	156.5	3870
9	15179	155.3	3549
10	17334	128.7	4247
11	15593	157.9	4225
12	15403	157.5	4117
13	16243	155.7	3678
14	16706	128.7	4027
15	16598	130.2	3578
16	17189	129.3	4023
17	14875	154.3	3350
18	15919	152.9	2862
19	15692	156.7	3901
20	17413	130.1	3898
21	14090	157.3	4306
22	15995	153.2	2950
23	16966	129	4024
24	15100	153.6	3120
25	16101	129.7	3621
26	16595	125.8	4809
27	15243	156	3726
28	15565	126.9	4352
29	14998	157.7	4199
30	17094	128.8	4125
31	16035	131.1	3224
32	16279	128	4123
33	15190	155.4	3574
34	15494	158.4	4359
35	16260	130.9	3309
36	16344	133.1	2708

Table A6.3: Electroacoustic properties data for diluted bitumen stock #2.

Appendix 7

Measurement of diluted bitumen electric conductivity

The conductivity was measured after the preparation of the two stock diluted bitumen samples (section 3.5.2). The experimental data is presented in Table A7.1 (conductivities are expressed in $\text{S}\cdot\text{m}^{-1}$ units). The average diluted bitumen conductivity is $(9.37 \pm 0.04)\cdot 10^{-7} \text{ S}\cdot\text{m}^{-1}$ (from overall data with 99% interval of confidence on the mean).

#	Stock 1	Stock 2
1	$9.27\cdot 10^{-7}$	$9.31\cdot 10^{-7}$
2	$9.35\cdot 10^{-7}$	$9.42\cdot 10^{-7}$
3	$9.37\cdot 10^{-7}$	$9.40\cdot 10^{-7}$
4	$9.35\cdot 10^{-7}$	$9.40\cdot 10^{-7}$
5	$9.37\cdot 10^{-7}$	$9.42\cdot 10^{-7}$
6	$9.37\cdot 10^{-7}$	$9.42\cdot 10^{-7}$
7		$9.39\cdot 10^{-7}$
8		$9.37\cdot 10^{-7}$

Table A7.1: Diluted bitumen electric conductivity data.

Appendix 8

Measurement of heavy water acoustic properties

The intrinsic attenuation coefficient ($(\alpha_{int})_m$) and sound speed (c_m) were measured for heavy water. 31 measurements were performed. 99% interval of confidence on the mean are calculated (Table A8.1). The experimental data is also presented in Table A8.2. The attenuation coefficient is expressed in dB·cm·MHz units.

Property	Stock 1
c_p (m/s)	1386.6 ± 0.2
$(\alpha_{int})_p$ 3.0 MHz	0.028 ± 0.006
$(\alpha_{int})_p$ 3.7 MHz	0.015 ± 0.004
$(\alpha_{int})_p$ 4.5 MHz	0.004 ± 0.003
$(\alpha_{int})_p$ 5.6 MHz	0.013 ± 0.003
$(\alpha_{int})_p$ 6.8 MHz	0.025 ± 0.003
$(\alpha_{int})_p$ 8.4 MHz	0.028 ± 0.002
$(\alpha_{int})_p$ 10.3 MHz	0.033 ± 0.002
$(\alpha_{int})_p$ 12.7 MHz	0.041 ± 0.001
$(\alpha_{int})_p$ 15.6 MHz	0.049 ± 0.001
$(\alpha_{int})_p$ 19.2 MHz	0.0606 ± 0.0005
$(\alpha_{int})_p$ 23.5 MHz	0.0714 ± 0.0004
$(\alpha_{int})_p$ 28.9 MHz	0.0880 ± 0.0003
$(\alpha_{int})_p$ 35.5 MHz	0.1069 ± 0.0003
$(\alpha_{int})_p$ 43.7 MHz	0.1321 ± 0.0004
$(\alpha_{int})_p$ 53.6 MHz	0.1625 ± 0.0005
$(\alpha_{int})_p$ 65.9 MHz	0.1975 ± 0.0004
$(\alpha_{int})_p$ 81.0 MHz	0.2455 ± 0.0004
$(\alpha_{int})_p$ 99.5 MHz	0.301 ± 0.001

Table A8.1: Acoustic properties of heavy water (99% interval of confidence on the mean)

#	T (°C)	c_m (m/s)	$(\alpha_{int})_m$ 3.0 MHz	$(\alpha_{int})_m$ 3.7 MHz	$(\alpha_{int})_m$ 4.5 MHz	$(\alpha_{int})_m$ 5.6 MHz	$(\alpha_{int})_m$ 6.8 MHz	$(\alpha_{int})_m$ 8.4 MHz	$(\alpha_{int})_m$ 10.3 MHz	$(\alpha_{int})_m$ 12.7 MHz
1	20.8	1386.923	0.01948	0.00938	0.00145	0.01169	0.02191	0.02723	0.03371	0.04083
2	20.8	1386.802	0.03544	0.01339	0.00432	0.01257	0.02219	0.02662	0.02990	0.03946
3	20.8	1386.437	0.03857	0.01678	0.00757	0.01175	0.02166	0.02756	0.03152	0.04046
4	20.8	1386.793	0.02377	0.01596	0.00375	0.01593	0.01910	0.02720	0.03288	0.04029
5	20.8	1386.624	0.02377	0.01551	0.00396	0.01207	0.02293	0.02460	0.03137	0.03952
6	20.8	1386.762	0.01276	0.01620	0.00045	0.01127	0.02784	0.02615	0.03258	0.04107
7	20.8	1386.161	0.02763	0.01043	0.00440	0.01300	0.02307	0.02958	0.03439	0.04074
8	20.8	1386.791	0.01933	0.01195	0.00764	0.01260	0.02478	0.02404	0.03100	0.04042
9	20.8	1386.737	0.03544	0.02193	0.00834	0.01699	0.02790	0.02908	0.03430	0.04120
10	20.8	1386.846	0.03472	0.01285	0.00457	0.01091	0.02369	0.02478	0.03169	0.04215
11	20.8	1387.533	0.01123	0.01789	0.00809	0.01540	0.02371	0.02491	0.03259	0.04076
12	20.8	1386.778	0.02634	0.01759	0.00262	0.01036	0.02822	0.03044	0.03103	0.04067

#	$(\alpha_{int})_m$ 15.6 MHz	$(\alpha_{int})_m$ 19.2 MHz	$(\alpha_{int})_m$ 23.5 MHz	$(\alpha_{int})_m$ 28.9 MHz	$(\alpha_{int})_m$ 35.5 MHz	$(\alpha_{int})_m$ 43.7 MHz	$(\alpha_{int})_m$ 53.6 MHz	$(\alpha_{int})_m$ 65.9 MHz	$(\alpha_{int})_m$ 81.0 MHz	$(\alpha_{int})_m$ 99.5 MHz
1	0.04977	0.06168	0.07188	0.08748	0.10664	0.13153	0.16199	0.19864	0.24590	0.30059
2	0.04867	0.06183	0.07201	0.08724	0.10724	0.13064	0.16246	0.19491	0.24606	0.29999
3	0.04800	0.05887	0.07127	0.08723	0.10653	0.13144	0.16301	0.19729	0.24562	0.30092
4	0.04918	0.06075	0.07226	0.08822	0.10612	0.13268	0.16189	0.19845	0.24616	0.30020
5	0.04852	0.05992	0.07062	0.08776	0.10610	0.13290	0.16236	0.19751	0.24561	0.29993
6	0.04926	0.06175	0.07186	0.08796	0.10708	0.13155	0.16156	0.19672	0.24551	0.29916
7	0.05123	0.06024	0.07193	0.08855	0.10645	0.13126	0.16163	0.19919	0.24659	0.30011
8	0.05099	0.06100	0.07192	0.08750	0.10633	0.13237	0.16239	0.19748	0.24465	0.30002
9	0.04988	0.06115	0.07297	0.08833	0.10703	0.13173	0.16223	0.19618	0.24492	0.30093
10	0.04822	0.05990	0.07132	0.08804	0.10609	0.13204	0.16169	0.19735	0.24612	0.30115
11	0.04845	0.06075	0.07146	0.08855	0.10664	0.13134	0.16260	0.19750	0.24535	0.30136
12	0.05105	0.06019	0.07131	0.08810	0.10536	0.13155	0.16074	0.19806	0.24536	0.30087

Table A8.2: Acoustic properties data for heavy water.

#	T (°C)	c_m (m/s)	$(\alpha_{int})_m$ 3.0 MHz	$(\alpha_{int})_m$ 3.7 MHz	$(\alpha_{int})_m$ 4.5 MHz	$(\alpha_{int})_m$ 5.6 MHz	$(\alpha_{int})_m$ 6.8 MHz	$(\alpha_{int})_m$ 8.4 MHz	$(\alpha_{int})_m$ 10.3 MHz	$(\alpha_{int})_m$ 12.7 MHz
13	20.7	1386.597	0.03444	0.01182	0.00163	0.01115	0.02551	0.02915	0.03327	0.03991
14	20.8	1386.976	0.02306	0.01324	0.00202	0.00961	0.02089	0.02965	0.02988	0.04063
15	20.8	1386.869	0.02755	0.01318	0.00729	0.01056	0.02654	0.02847	0.03187	0.04087
16	20.7	1386.609	0.02638	0.00799	0.00208	0.01080	0.02348	0.02937	0.03150	0.03968
17	20.7	1387.321	0.02793	0.00971	0.00015	0.01078	0.02426	0.02709	0.03236	0.04116
18	20.8	1386.484	0.02658	0.01218	0.00222	0.01216	0.02336	0.02565	0.03423	0.04192
19	20.8	1385.918	0.01689	0.01236	0.00080	0.00784	0.02289	0.02737	0.03008	0.04038
20	20.8	1386.469	0.03252	0.01269	0.00154	0.01011	0.02210	0.02424	0.03183	0.04140
21	20.8	1387.031	0.03140	0.01968	0.00457	0.01397	0.03467	0.03181	0.03481	0.04294
22	20.7	1386.566	0.01542	0.00265	0.00342	0.00906	0.02260	0.02542	0.02829	0.04024
23	20.7	1386.478	0.00091	0.01342	0.00087	0.01395	0.02511	0.03106	0.03207	0.04145
24	20.8	1386.018	0.02152	0.01244	0.00628	0.00928	0.01715	0.02805	0.03129	0.04008

#	$(\alpha_{int})_m$ 15.6 MHz	$(\alpha_{int})_m$ 19.2 MHz	$(\alpha_{int})_m$ 23.5 MHz	$(\alpha_{int})_m$ 28.9 MHz	$(\alpha_{int})_m$ 35.5 MHz	$(\alpha_{int})_m$ 43.7 MHz	$(\alpha_{int})_m$ 53.6 MHz	$(\alpha_{int})_m$ 65.9 MHz	$(\alpha_{int})_m$ 81.0 MHz	$(\alpha_{int})_m$ 99.5 MHz
13	0.04952	0.06054	0.07183	0.08813	0.10739	0.13348	0.16322	0.19817	0.24635	0.29969
14	0.04977	0.05966	0.07098	0.08847	0.10675	0.13242	0.16189	0.19771	0.24433	0.30335
15	0.04786	0.06008	0.07112	0.08739	0.10756	0.13150	0.16214	0.19748	0.24482	0.30177
16	0.05030	0.05972	0.07051	0.08738	0.10639	0.13264	0.16354	0.19771	0.24553	0.30275
17	0.04874	0.06101	0.07093	0.08811	0.10712	0.13174	0.16277	0.19780	0.24682	0.30217
18	0.04983	0.06057	0.07161	0.08866	0.10758	0.13273	0.16410	0.19667	0.24504	0.30124
19	0.04807	0.05951	0.07065	0.08925	0.10585	0.13290	0.16231	0.19751	0.24553	0.30083
20	0.04877	0.06142	0.07115	0.08808	0.10695	0.13352	0.16212	0.19712	0.24511	0.29956
21	0.05102	0.06309	0.07353	0.08975	0.10769	0.13402	0.16486	0.19883	0.24659	0.30066
22	0.04882	0.06155	0.07057	0.08865	0.10786	0.13173	0.16224	0.19688	0.24629	0.30021
23	0.04881	0.05995	0.07065	0.08860	0.10659	0.13171	0.16198	0.19716	0.24535	0.29990
24	0.04809	0.06070	0.07105	0.08818	0.10670	0.13169	0.16172	0.19763	0.24624	0.30133

Table A8.2: Acoustic properties data for heavy water (continuation).

#	T (°C)	c_m (m/s)	$(\alpha_{int})_m$ 3.0 MHz	$(\alpha_{int})_m$ 3.7 MHz	$(\alpha_{int})_m$ 4.5 MHz	$(\alpha_{int})_m$ 5.6 MHz	$(\alpha_{int})_m$ 6.8 MHz	$(\alpha_{int})_m$ 8.4 MHz	$(\alpha_{int})_m$ 10.3 MHz	$(\alpha_{int})_m$ 12.7 MHz
25	20.8	1386.781	0.02915	0.00996	0.00177	0.01404	0.02496	0.03038	0.03259	0.04088
26	20.8	1386.354	0.03380	0.00956	0.00115	0.01037	0.02845	0.02645	0.03354	0.04317
27	20.8	1386.276	0.02452	0.01254	0.00135	0.00927	0.02415	0.02894	0.03166	0.03930
28	20.7	1386.526	0.02486	0.01147	0.00303	0.01267	0.02623	0.03159	0.03386	0.04301
29	20.7	1385.865	0.06290	0.01970	-0.00359	0.00924	0.02484	0.02825	0.03443	0.04030
30	20.7	1385.225	0.02804	0.01623	0.01357	0.00944	0.01974	0.02556	0.03039	0.03886
31	20.7	1385.86	0.06885	0.04923	0.03047	0.03877	0.04618	0.04692	0.04806	0.04156

#	$(\alpha_{int})_m$ 15.6 MHz	$(\alpha_{int})_m$ 19.2 MHz	$(\alpha_{int})_m$ 23.5 MHz	$(\alpha_{int})_m$ 28.9 MHz	$(\alpha_{int})_m$ 35.5 MHz	$(\alpha_{int})_m$ 43.7 MHz	$(\alpha_{int})_m$ 53.6 MHz	$(\alpha_{int})_m$ 65.9 MHz	$(\alpha_{int})_m$ 81.0 MHz	$(\alpha_{int})_m$ 99.5 MHz
25	0.04901	0.06034	0.07081	0.08848	0.10753	0.13187	0.16423	0.19791	0.24580	0.29982
26	0.04850	0.06049	0.07115	0.08819	0.10746	0.13091	0.16396	0.19824	0.24482	0.30085
27	0.04771	0.05927	0.07045	0.08724	0.10756	0.13252	0.16214	0.19701	0.24397	0.29906
28	0.04744	0.06143	0.07163	0.08729	0.10710	0.13188	0.16257	0.19601	0.24535	0.30289
29	0.04846	0.06073	0.07077	0.08722	0.10834	0.13352	0.16316	0.19709	0.24551	0.30137
30	0.04758	0.05892	0.07103	0.08750	0.10658	0.13156	0.16150	0.19776	0.24426	0.30036
31	0.04786	0.06048	0.07168	0.08746	0.10653	0.13236	0.16179	0.19769	0.24536	0.29919

Table A8.2: Acoustic properties data for heavy water (continuation).